Novel Techniques for Spatial Orientation in Natural Orifice Translumenal Endoscopic Surgery (NOTES)

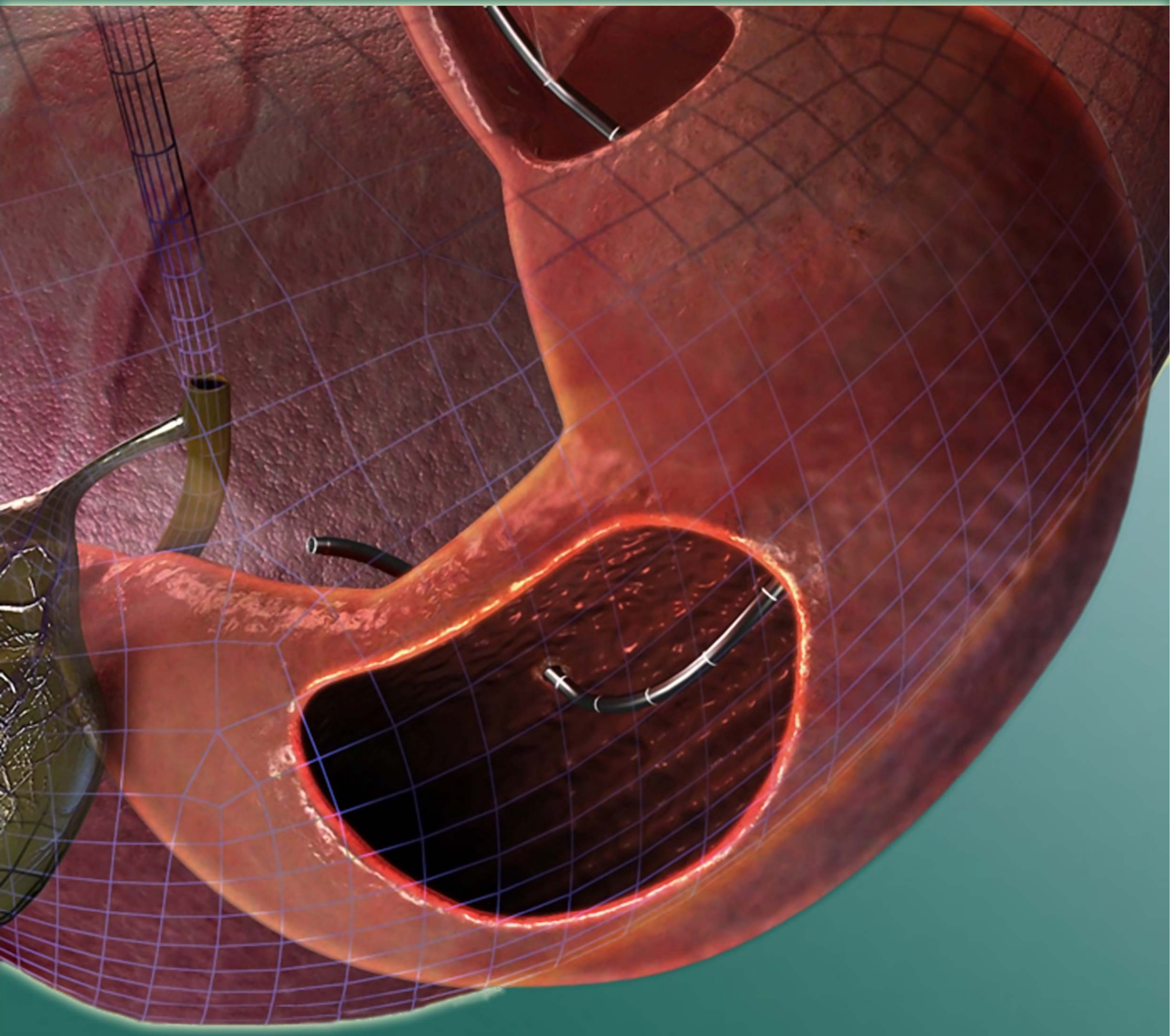

Kurt Höller

Novel Techniques for Spatial Orientation in Natural Orifice Translumenal Endoscopic Surgery (NOTES)

Submitted to

Technische Fakultät der
Universität Erlangen-Nürnberg

in partial fulfillment of the requirements for
the degree of

DOKTOR-INGENIEUR

of

Kurt Höller

Erlangen — 2010

As dissertation accepted by
Technische Fakultät der
Universität Erlangen-Nürnberg

Date of submission:	10/08/2010
Date of doctorate:	11/25/2010
Dean:	Prof. Dr.-Ing. Reinhard German
Reviewer:	Prof. Dr.-Ing. Joachim Hornegger
	Prof. Dr. med. Hubertus Feußner
	Prof. Dr. Gregory D. Hager

Neue Ansätze für räumliche Orientierung in der endoskopischen Chirurgie durch natürliche Körperöffnungen (NOTES)

Der Technischen Fakultät der
Universität Erlangen–Nürnberg

zur Erlangung des Grades

DOKTOR–INGENIEUR

vorgelegt von

Kurt Höller

Erlangen — 2010

Als Dissertation genehmigt von der
Technischen Fakultät der
Universität Erlangen-Nürnberg

Tag der Einreichung:	08.10.2010
Tag der Promotion:	25.11.2010
Dekan:	Prof. Dr.-Ing. Reinhard German
Berichterstatter:	Prof. Dr.-Ing. Joachim Hornegger
	Prof. Dr. med. Hubertus Feußner
	Prof. Dr. Gregory D. Hager

Abstract

With a novel approach abdominal surgery can be performed without skin incisions. The natural orifices provide the entry point with a following incision in stomach, colon, vagina or bladder. "Natural Orifice Translumenal Endoscopic Surgery" (NOTES) is assumed to offer significant benefits to patients such as less pain and reduced traumata as well as reduced collateral damages, faster recovery, and better cosmesis. Particular improvement can be reached even for obesity and burn injury patients and children. But the potential advantages of this new technology can only be exploited through safe and standardized operation methods. Several barriers identified for the clinical practicability in flexible intra-abdominal endoscopy can be solved with computer-assisted surgical systems. In order to assist the surgeon during the intervention and to enhance his visual perception, some of these systems are able to additionally provide 3-D information of the intervention site, for others 3-D information is even mandatory.

In this context, the question whether on-line 3-D information can be obtained in real-time had to be answered. One approach in this work to face this challenge is the acquisition of 3-D information directly via the endoscope with a hybrid imaging system. Parallel to the CCD camera a Time-of-Flight (ToF) system is integrated. ToF cameras illuminate the scene actively with an optical reference signal with intensity modulation. For each ToF pixel a distance value depending on the modulation phase shift of the reflected optical wave and the electrical reference signal is estimated. To compensate the high optical attenuation of endoscopic systems, a much more efficient illumination unit with laser diodes was designed. The 3-D depth information obtained by this "MuSToF endoscope" can furthermore be registered with preoperative acquired 3-D volumetric datasets like CT or MRI. These enhanced or augmented 3-D data volumes could then be used to find the transgastric, transcolonic, transvaginal, transurethral or transvesical entry point to the abdomen. Furthermore, such acquired endoscopic depth data can be used to provide better orientation within the abdomen. Moreover, it can also be used to prevent intra-operative collisions and provide an optimized field of view with the possibility for off-axis viewing.

Furthermore, providing a stable horizon on video-endoscopic images especially within non-rigid endoscopic surgery scenarios (particularly within NOTES) is still an open issue. Hence, this work's "ENDOrientation" approach for automated image orientation rectification contributes to a great extent to advance the clinical establishment of NOTES. It works with a tiny MEMS tri-axial inertial sensor that is placed on the distal tip of an endoscope. By measuring the impact of gravity on each of the three orthogonal axes and filtering the data using several subsequent algorithms the rotation angle can be estimated out of these three acceleration values. The result can be used to automatically rectify the endoscopic images using image processing methods. The achievable repetition rate is above the usual endoscopic video frame rate of 30Hz, accuracy is about one degree. The image rotation is performed by rotating digitally a capture of the endoscopic analog video signal, which can be realized in real-time. Improvements and benefits have been

evaluated in animal studies: Coordination of different instruments and estimation of tissue behavior regarding gravity related deformation and movement was considered to be much more intuitive having a stable horizon within endoscopic images.

Having additional 3-D data or a fixed horizon will not be an unalterable precondition for performing NOTES. But it will help to utilize robotic devices and to support surgeons, who are novices in the field of flexible endoscopy. Since gastroenterologists and surgeons are still not absolutely familiar with the NOTES approach, they will benefit from new technologies and appreciate them.

Zusammenfassung

Mit einem neuartigen Ansatz können chirurgische Eingriffe im Bauchraum auch ohne Schnitte in der Bauchdecke durchgeführt werden. Dazu wird der Zugang über natürliche Körperöffnungen mit einem anschließenden Schnitt in Magen, Darm, Vagina oder Blase gewählt. Von diesem Verfahren mit der Bezeichnung "Natural Orifice Translumenal Endoscopic Surgery" (NOTES) werden erhebliche Vorteile für die Patienten erwartet. Neben einer Reduktion von Schmerzen und Traumata sollen auch Kollateralschäden vermindert werden. Zudem sollen schnellere Genesung und bessere kosmetische Ergebnisse erreicht werden. Insbesondere die Einschränkungen bei der Behandlung von adipösen Patienten, Verbrennungsopfern und Kindern lassen sich mit NOTES lösen. Diese möglichen Vorteile des neuen Verfahrens sind jedoch nur in sichereren und standardisierten Operationsmethoden nutzbar. Einige Hürden, die für die klinische Anwendbarkeit in der flexiblen intra-abdominalen Endoskopie identifiziert wurden, können durch computergestützte chirurgische Systeme gelöst werden. Um den Chirurgen während des Eingriffs zu unterstützen und seine visuelle Wahrnehmung zu verbessern, bieten einige dieser Systeme unterstützende 3-D-Informationen vom örtlichen Eingriff, für andere Systeme sind diese sogar Voraussetzung.

In diesem Zusammenhang muss die Frage gelöst werden, ob direkte 3-D-Informationen in Echtzeit ermittelt werden können. Ein Ansatz dieser Arbeit ist es, 3-D-Informationen direkt über das Endoskop mit einem hybriden Bildgebungs-System zu erhalten. Parallel zur CCD-Kamera ist ein Time-of-Flight (TOF) System integriert. TOF-Kameras beleuchten den betrachteten Bereich kontinuierlich mit einem optischen Referenzsignal mit Intensitätsmodulation. Für jeden ToF-Pixel wird ein Entfernungswert in Abhängigkeit zur Modulations-Phasenverschiebung der reflektierten optischen Welle und des elektrischen Referenzsignals berechnet. Um die hohe optische Dämpfung von endoskopischen Systemen auszugleichen, wurde eine wesentlich effizientere Beleuchtungseinheit mit einer Laserdiode entwickelt. Die 3-D Tiefeninformation, die über das "MuSToF-Endoskop" ermittelt werden, können anschließend mit präoperativ akquirierten 3-D-Volumen-Daten aus CT- oder MR-Modalitäten registriert werden. Diese erweiterten 3-D-Volumen-Daten können dann verwendet werden, um zum transgastrischen, transkolonischen, transvaginalen, transurethralen oder transvesikalen Zugang zu navigieren und darüber den Bauchraum zu eröffnen. Darüber hinaus können derart gewonnene endoskopische Tiefendaten eingesetzt werden, um eine bessere Orientierung im Bauchraum zu gewährleisten. Zudem lassen sich damit intraoperative Kollisionen vermeiden und ein optimiertes Sichtfeld mit der Möglichkeit zur Betrachtung außerhalb der optischen Achse bieten.

Ein weiteres noch ungelöstes Problem stellt die Bereitstellung eines stabilisierten Horizonts im Videobild flexibler Endoskope dar. Dies betrifft insbesondere den Bereich der Chirurgie mittels flexibler Endoskope (insbesondere NOTES). Somit trägt diese Arbeit mit dem "ENDOrientation"-Ansatz zur automatischen Rektifizierung der Bildausrichtung in bedeutender Weise dazu bei, die klinische Etablierung von NOTES zu fördern. Es basiert auf einem winzigen MEMS-basierten

triaxialen Inertialsensor, der auf der distalen Spitze eines Endoskops angebracht wird. Durch die Erfassung des Schwerkraft-Einflusses auf jede der drei orthogonalen Achsen und einer nachgeschalteten intelligenten Filterung kann der Drehwinkel aus diesen drei Beschleunigungswerten ermittelt werden. Mithilfe dieses Ergebnisses können die endoskopischen Bilder über Methoden der Bildverarbeitung automatisch rektifiziert werden. Die erreichbare Wiederholungsrate liegt oberhalb der üblichen endoskopischen Bildwiederholungsrate von 30 Hertz, die Genauigkeit beträgt etwa ein Grad. Die Bildrotation wird durch digitale Drehung des endoskopischen analogen Videosignals erzeugt, was in Echtzeit realisiert werden kann. Verbesserungen und Vorteile sind im Tierversuch evaluiert worden: Die Koordinierung der verschiedenen Instrumente und die Beurteilung von Gewebeverhalten in Bezug auf Deformation und Bewegung durch Schwerkraft wurde mit einem stabilisierten Horizont der endoskopischen Bilder als wesentlich intuitiver bewertet.

Weitere 3-D-Daten oder ein stabiler Horizont werden keine zwingende Voraussetzung für die Durchführung von NOTES sein. Aber sie werden hilfreich sein beim Einsatz chirurgischer Robotik und zur Unterstützung für Chirurgen, die noch keine Experten auf dem Gebiet der flexiblen Endoskopie sind. Da die meisten Gastroenterologen und Chirurgen nach wie vor nicht absolut mit NOTES vertraut sind, werden sie von neuen Technologien profitieren und sie aufgeschlossen annehmen.

Acknowledgment

This thesis is dedicated to my whole family, especially to my girlfriend who contributed several great photographies of my prototypes and had to be patient due to night-long work for uncountable times.

I also wish to thank my former Pattern Recognition Lab colleagues B. Eskofier, S. Hempel, J. Penne, P. Ritt and C. Schaller, for the teamwork and the jointly developed new ideas with the MuSToF endoscope as well as R. Engelbrecht, T. Schrauder and D. Tacke from the Chair of Microwave Engineering and High Frequency Technology, Friedrich-Alexander University Erlangen-Nuremberg, for their helpful support with developing the laser illumination unit of the MuSToF endoscope.

For the development of my ENDOSens prototype I got a lot of support by J. Guttierrez, J. Jahn, T. Wittenberg and other colleagues at the Fraunhofer-Institute for Integrated Circuits IIS, Erlangen.

I really liked my time with A. Schneider, S. Gillen and all my other colleagues at the Research Group for Minimally invasive Interdisciplinary Therapeutical Interventions (MITI), Klinikum rechts der Isar, Technische Universität München, where I performed all the animal studies and medical feasibility evaluations as a long-term visiting researcher. I also enjoyed the fruitful collaboration with L. Maier-Hein, A. Groch, A. Seitel and S. Mersmann from the Medical and Biological Informatics Division at Deutsches Krebsforschungszentrum (DKFZ) in Heidelberg.

And I am thankful to G. Hager, P. Kazanzides, R. Taylor, R. Kumar, D. Mirota and H. Girgis for their helpful suggestions and discussions regarding the ENDOSens algorithms during my research stay at the Engineering Research Center for Computer-Integrated Surgical Systems and Technology, The Johns Hopkins University, Baltimore, MD.

Several of this work's illustrations have been created by A. Balleis and her team. Thank you for the great realization enabling a better visual understanding!

Moreover, this work would not have been possible without the grant financing by the Hanns-Seidel-Foundation. I really want to thank H. Zehetmair, H-P. Niedermeier and R. Pfeifenrath.

Last but not least I'm honestly glad to have such helpful demanding and supporting doctoral advisors with professors J. Hornegger and H. Feußner. They both gave me the chance to work at a high level on a very interdisciplinary focus. In fact it was a great time.

K. Höller

Contents

Part I

Introduction

Chapter 1

Introduction

1.1 Overview

Translumenal techniques in endoscopic surgery require an interdisciplinary collaboration not only between surgeons and gastroenterologists but also with engineers, who are requested to provide better imaging systems, medical robots, and endoscopic instruments to support the physician's coordination within interventions with increasing complexity. In this field it became apparent that technical developments are necessary for further medical progress. Therefore, physicians are highly encouraged to cooperate with engineers and to apply new technologies.

1.2 Open Research Questions

There are several approaches developed for 3-D measurements in combination with endoscopic devices to overcome existing restrictions. Additionally to the intra-operative color images and pre-operative abdominal CT or MRI volumes, augmented reality needs reliable information on position and deformation of the observed surface or tissue. For robotic devices it is important to provide distance measurement for collision avoidance and automated positioning. Metric information may help to get a better spatial impression of the operation area and to determine the size of suspect tissue. This generates a lot of open questions: Which approach is the best to provide intra-operative 3-D data? Is it possible to provide this data within real-time? How many surface frames can be required in real-time? How many measurement points can be delivered? Which modifications are required for the use with endoscopes for medical interventions? Will the obtainable spatial resolution meet the accuracy required for medical purposes?

A major problem for surgeons working with non-rigid endoscopes is the loss of a stable horizon in endoscopic images. They are used to rigid laparoscopes, where they have the possibility to rectify the image themselves at any time by rotating their hand. With flexible endoscopes it is not possible to do this manually. This opens the question if that could be done automatically by image processing. Is it possible to provide reliable information on the endoscopes orientation and which approach is the best? Is it possible to provide this data within real-time? Is it verifiable that the surgeon's spatial orientation is improved?

1.3 Contribution to the Progress of Research

Hybrid endoscopic imaging with an additional Time-of-Flight camera for surface measurement will provide great opportunities in modern medicine. No other 3-D measurement approach can provide that many measurement points in such a high frequency and without the need of detectable feature points. Within this work the following problems were solved:

- The benefits of additional 3-D data especially for NOTES procedures were identified
- Specific ToF camera parameters for this application were analyzed
- Algorithms for parameter adaption were created
- An illumination unit especially for the needs of endoscopic devices was developed
- First prototype images were generated and evaluated

Furthermore, an important contribution for providing a stable horizon in flexible endoscopy is presented. The measurement is highly reliable and needs no external reference setup like a magnetic field or a line of sight to the observing cameras. It can be integrated into the tip of a flexible endoscope and uses only gravity as reference. Clinical evaluations showed that the surgeon's spatial orientation can be improved significantly. Within this work the following steps were fulfilled:

- The benefits of a stable horizon especially for NOTES procedures were identified
- The new method using a MEMS accelerometer fixed on the tip of an endoscope for orientation correction was invented
- Algorithms for orientation determination based on acceleration measurements were developed
- Algorithms for data down sampling and movement filtering were developed
- Several hardware prototypes were developed
- Clinical evaluations were planned, performed and analyzed

Therefore both technologies have been developed and improved within the author's research and will be an important contribution for making special medical procedures safer and more convenient for patients and surgeons.

To make these methods and results available for a wider technical and medical community, they have been published by the author in journal articles [Holl 10b, Holl 10c] and abstracts [Holl 10d], contributions to conferences [Holl 08a, Holl 09b, Holl 09c, Holl 09a] and workshops [Holl 08c, Holl 08b, Holl 10a] as well as in several co-authored similar publications. Furthermore, the research focus of 3-D extensions for endoscopic surgery was placed and enforced in special sessions and their co-editored conference [Horn 07] and workshops [Horn 08, Horn 10] proceedings. Two patents have been applied [Guti 10b, Guti 10a].

1.4 Structure of this Work

The first chapter describes the field of endoscopic surgery including the history, the impact and the expectations of the special field of translumenal endoscopic surgery. The following chapter gives an overview of existing 3-D techniques in endoscopy. It points out technologies for 3-D vision and visualization. Within the third chapter on technical background the relevant sensor technologies will be explained regarding the following application purpose. The next two chapters incorporate the original work during the author's research. One main topic represents the improvements that are obtained with the integration of a 3-D ToF camera. With this camera an additional image of the observed surface can be gained and used for several enhancements. There are several parameters which can be optimized for hybrid imaging and the use of an endoscope. Especially illumination has to be improved for better results as shown in the experimental evaluation. The second fundamental contribution is a tiny sensor fixed on the tip of an arbitrary flexible endoscope for measuring the orientation of the endoscopic image. Special filtering algorithms and hardware prototypes are proposed. As shown in the evaluation a stable orientation of the endoscopic image is accomplished in real-time, which is an important postulation for safe endoscopic surgery. In the seventh chapter the impact of the described techniques on medical challenges especially regarding navigation and assessment will be discussed. Finally, the work is summarized and a short technical and medical outlook are given.

Part II

Medical and Technical Background

Chapter 2

Medical Background on Endoscopic Surgery

2.1 Development of Endoscopic Devices

Even though already Hippocrates described the use of a rectal speculum about 400 years before Christ [Adam 91], endoscopy was very unusual until Dr. Bozzini presented the "Lichtleiter" (light conductor) in 1806 as shown in fig. 2.1. Adding a candle as a light source and a reflecting mirror, the urethra could be observed through a double-lumen cannula [Bozz 06]. Unfortunately, the importance of his invention was not understood at that time. He was ridiculed, when he presented it to the Faculty of Medicine in Vienna [Shah 02].

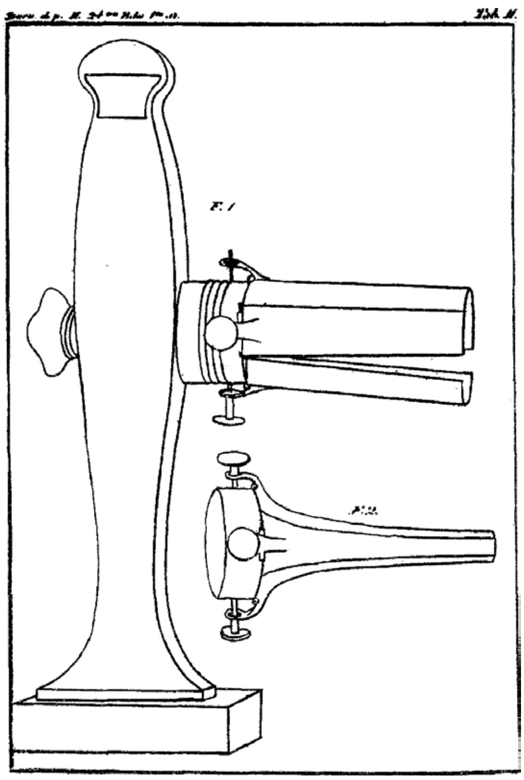

Figure 2.1: Bozzini's "Lichtleiter" with a wax candle and a reflecting mirror inside to observe the urethra through a double-lumen cannula [Bozz 06] (reprinted with kind permission of the International Nitze-Leiter Research Society for Endoscopy, Vienna, Austria).

With the invention of electric light by Edison in 1880, Dr. Nitze was finally able to develop operating cystoscopes in the following years [Davi 92]. In 1954 a non-rigid type of endoscopes, the so-called "fiberscope", with a coherent bundle of fibers having a corresponding order at the two ends of the bundle, was described by the physicist Dr. Hopkins and his student Kapany [Hopk 54]. Unfortunately, they had insufficient financial support to produce it themselves. Therefore, Dr. Hirschowitz, who met them in Britain, had the chance to develop the first clinically useful fiberscope and to publish his first cases of gastroscopy as shown in fig. 2.2 [Hirs 61].

Hopkins also introduced a rod lens system using glass spaces and air lenses instead of air spaces and glass lenses for improved transmission. After that, he used an incoherent bundle of fibers as an additional illumination channel. Therefore, he was the

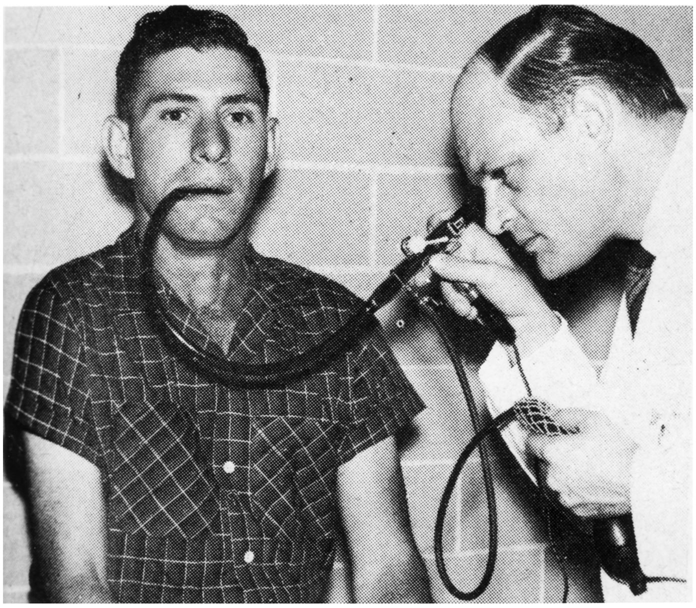

Figure 2.2: Hirschowitz using his flexible "fiberscope" with a coherent bundle of fibers having a corresponding order at the two ends of the bundle [Hirs 61] (reprinted with kind permission of Dittrick Medical History Center, Case Western Reserve University, Cleveland, Ohio).

first who managed the placement of the light source not at the distal but at the proximal end of the endoscope. But again, nobody in the UK and abroad was interested in financing and producing this new concept. Having an invited speech in Germany, Hopkins met Karl Storz, who was attending the lecture. Storz agreed to manufacture a rod lens system with an external light source transmitted through attached incoherent glass fibers [Gow 98]. In 1973, Dres. Classen and Demling, two internists at the Clinic of Internal Medicine at the University of Erlangen, performed an endoscopic papillotomy using their own device called "Erlanger Papillotom". Dr. Erich Mühe, an assistant at the Surgical Clinic in Erlangen at this time, reported the Erlangen surgeons' respect and proud on the internists' pioneering work [Lity 98]. In 1975, Dr. Frühmorgen's group from the University of Erlangen-Nuremberg Medicine Department reported the first endoscopic laser coagulation in two patients, one with a colonic hemangioma, and the other with an acute gastric stress ulcer [Morg 07]. An important technical step was the assembly of a video chip camera at the proximal end of the endoscope in the 1980s to make the video image visible on a video screen for all members of the team allowing them participation and interaction. By positioning the CCD chip at the distal end of the endoscope the quality could be improved again in the 1990s [Pelo 93].

2.2 Minimally Invasive Surgery

Due to the technological progress endoscopy got more and more usable for diagnostic purposes and first interventional approaches. Subsequently, surgery sustainably changed by the introduction of minimally invasive procedures in the late 80s [Rola 07].

At that time, the gynecologist Dr. Kurt Semm from the University of Kiel, Germany, performed an unorthodox procedure on a patient. After anesthesia, Dr. Semm insufflated the patient's abdomen with carbon dioxide, made several small incisions into his abdomen and removed his appendix with the help of laparoscopes. In response, he was requested by the president of the German Surgical Society to be suspended from medical practice. Finally, his paper that described the world's first laparoscopic appendectomy had been rejected. The procedure was considered to be unethical [Fran 07]. Nevertheless, this pneumoperitoneum procedure, based on Semm's new automatic abdominal insufflator and pressure monitor as shown in figures 2.3 and 2.4, was published in the Journal of Endoscopy [Semm 83a] and the Austrian "Wiener klinische Wochenschrift" [Semm 83b].

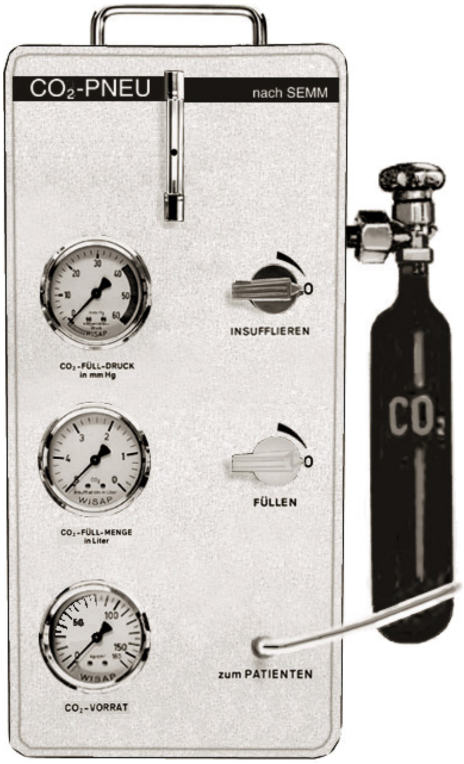

Figure 2.3: First Automatic abdominal insufflator and pressure monitor to establish an automated pneumoperitoneum according to Semm, 1964 (reproduced with kind permission of Dr. I. Semm, WISAP Gesellschaft für wissenschaftlichen Apparatebau mbH, Sauerlach, Germany).

In 1985, Mühe combined his fascination for Erlangen endoscopists' success and Semm's technique [Lity 98, Harr 05]. He performed the world's first laparoscopic cholecystectomy using his "Galloscope" as shown in fig. 2.5 after having established a continuous pneumoperitoneum [Muhe 92]. Growing interest in this new method led to an increasing number of similar interventions and publications. Even though Mühe was not a member of any endoscopic society, his work had an important impact on the introduction of laparoscopy into surgical practice [Lity 98]. Unparalleled in the history of surgery it took only a few years for this new technique with the title "minimally invasive surgery" (MIS) to be practiced all over the world.

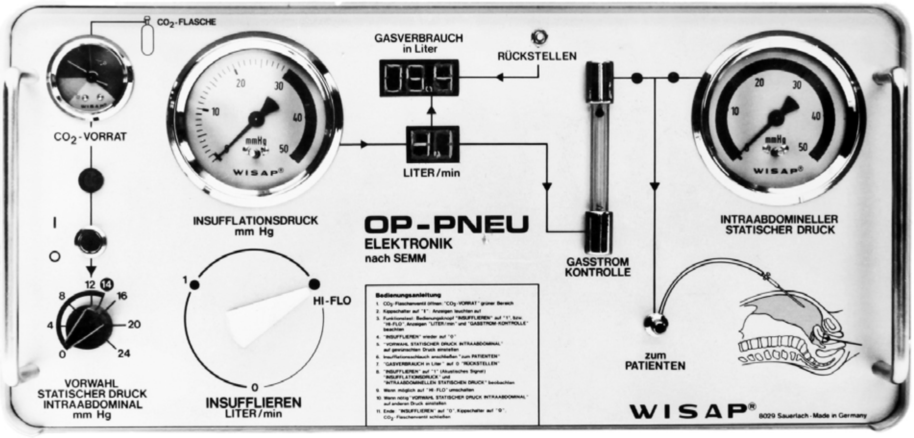

Figure 2.4: Automatic abdominal insufflator and pressure monitor to establish an automated pneumoperitoneum according to Semm, 1974 [Semm 83a] (reproduced with kind permission of Dr. I. Semm, WISAP Gesellschaft für wissenschaftlichen Apparatebau mbH, Sauerlach, Germany).

Figure 2.5: The "Galloscope" of Mühe, the first rigid operative laparoscope [Muhe 92] (reprinted with kind permission oft the Klinikum Sindelfingen-Böblingen, Klinikverbund Südwest, Sindelfingen, Germany).

2.3 Impact of NOTES

Now another revolution in surgery is on its way. The "dawn of a new era" [Hoch 05] started with Natural Orifice Translumenal Endoscopic Surgery (NOTES) at the beginning of this millennium. In the first years a real hype was perceptible. Publications with NOTES context increased rapidly. This topic had a fixed place at any considerable gastroenterologic or surgical journal or congress as illustrated with the NOTES publications numbers of the journals of Society of American Gastrointestinal and Endoscopic Surgeons (SAGES), American Society for Gastrointestinal Endoscopy (ASGE), European Society of Gastrointestinal Endoscopy (ESGE) and Digestive Disease Week (DDW) in fig. 2.6. NOTES is not only the most sophisticated but also the most fascinating form of endoscopic surgery.

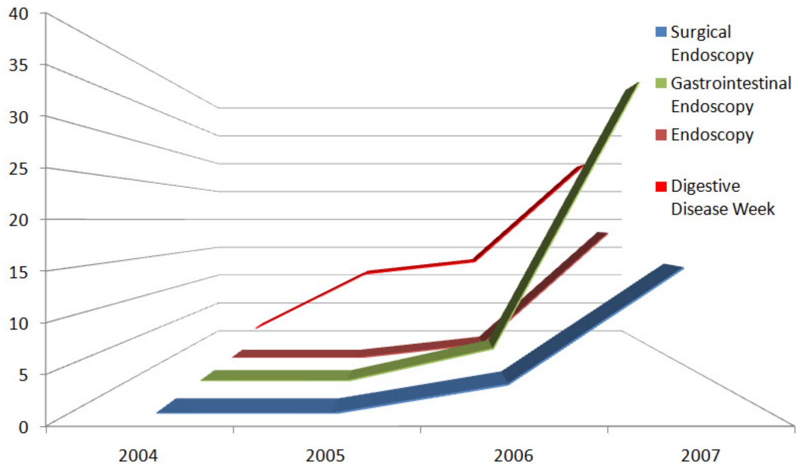

Figure 2.6: NOTES Publications increasing rapidly from 2004 to 2007 in Surg Endosc (SAGES), Gastrointest Endosc (ASGE), Endoscopy (ESGE) and DDW.

2.4 Concept of NOTES

The medical community is deeply stirred by a rapidly emerging, novel and innovative approach for abdominal surgery: Surgery can be performed through natural orifices of the human body avoiding any visible scars. In this particular type of surgery the peritoneal cavity is entered through mouth, rectum, vagina or urethra with a following translumenal incision in stomach, esophagus, colon, female posterior fornix or bladder. Apart from cosmetic reasons, the main justifications for NOTES are the ease of access and the reduction of anesthesia, trauma and discomfort [Wall 06, Swai 07a]. Additionally, reduced incidence of postoperative abdominal wall pain, fewer eventrations, herniations and adhesions [Fere 07] as well as less incision-related complications like post-operative wound infections [McGe 06] or visceral injuries by the use of a laparoscopic trocar [Bhoy 01] are assumed. The introduction of percutaneous endoscopic gastrostomy (PEG) by Gauderer, Ponsky et al. in 1980 [Gaud 80] established the principle that the lumen of the gastrointestinal tract could be safely violated with a flexible endoscope in order to perform a surgical procedure [Gee 07]. Gastric and colonic injuries heal quickly due to the good vascularization and perfusion of the gastrointestinal tract [Lama 06], so patients' hospital stays can be shortened significantly and more cost-effectiveness are expected [Gida 06]. Compared to conventional laparoscopy, a greater area of the peritoneal cavity can be visualized with flexible endoscopes [Sano 81]. Less pain, faster recovery, better cosmetic results [Kall 07b], and lower risks for some procedures [Swan 08] are advantages for the whole society. But there are also specific advantages: The absence of outward incisions has the further advantage that not in any case the whole operating room has to maintain sterile, but only the inserted instruments [Gida 10]. This opens up a new dimension of medical care, especially at the initial treatment on a battle field and an area-wide primary health care in developing countries. Less single-use devices and less equipment could reduce burden on the environment even in industrial countries [Fran 07]. Beyond this point, there will be better help for obese patients, where it is pretty difficult to find a way through the abdominal wall [Mali 06, Fuch 08]. Incisions through the affected skin of burn injuries can be avoided [Hage 07, Zhou 10] and growing children can be prevented from with-growing scars and the lifetime risk of incision-related complications [Swan 08].

2.5 History of NOTES

In the year 2000 the German physician Dr. Seifert was the first to successfully follow the transluminal path with human patients realizing a retroperitoneal endoscopic debridement for infected peripancreatic necrosis [Seif 00]. Four years later, two Indian surgeons at the Asian Institute of Gastroenterology in Hyderabad, Dres. Rao and Reddy [Rao 05, Redd 07], reported to have chosen the transgastric route to help humans with severe burn injuries [Baro 07], where external access was not possible.

And history seems to recur itself: 25 years earlier Dr. Semm was not allowed to publish his break-through, now the New England Journal of Medicine refused to publish the results of Dres. Rao and Reddy because the surgery was not conducted under the established professional guidelines. The lack of publication was compensated by many authors. They referenced personnel communication with Rao and Reddy in 2004 [Hoch 05].

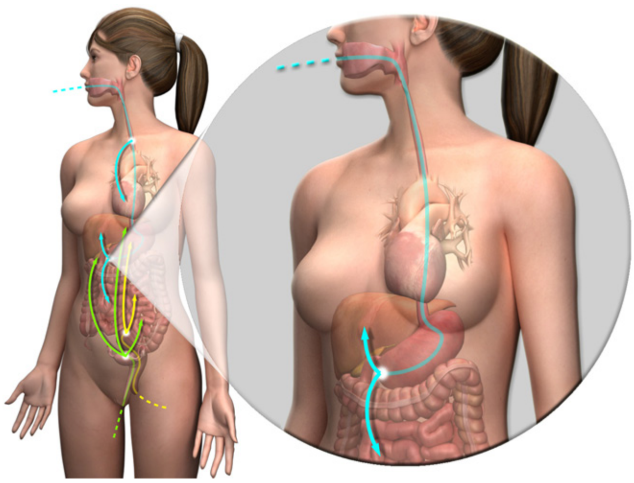

Figure 2.7: Scheme of a transgastric NOTES access through the mouth to the peritoneal cavity.

At the same time several peroral transgastric interventions (fig. 2.7) in porcine models were reported, for instance, peritoneoscopy [Kall 04], ligation of fallopian tubes [Jaga 05], cholecystectomy [Park 05, Feue 07], gastrojejunostomy [Kant 05, Mali 06], splenectomy [Kant 06], oophorectomy [Wagh 05], hepatic wedge resection [Fong 06], tubectomy [Wagh 06], hernia repair HU07 or diaphram pacing [Onde 07]. In 2006, Ponsky [Pons 06] pointed out human endoluminal procedures performed before 2006 and their impact for further NOTES procedures. In July 2005, the leading surgeons and gastroenterologists finally met in New York City to discuss further progressions. They founded the Natural Orifice Surgery Consortium for Assessment and Research (NOSCAR) and published a white paper. Therein they addressed fundamental chal-

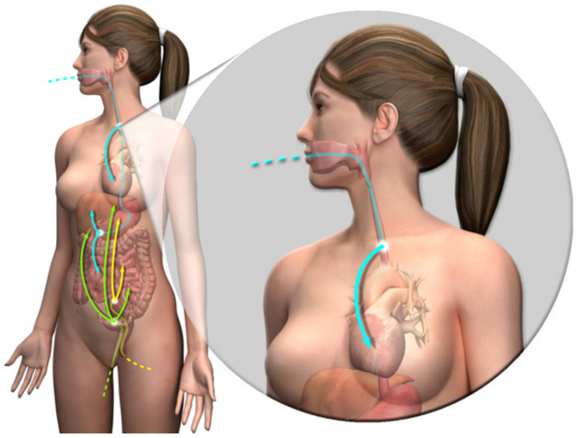

Figure 2.8: Scheme of a transesophageal NOTES access through the mouth to the heart.

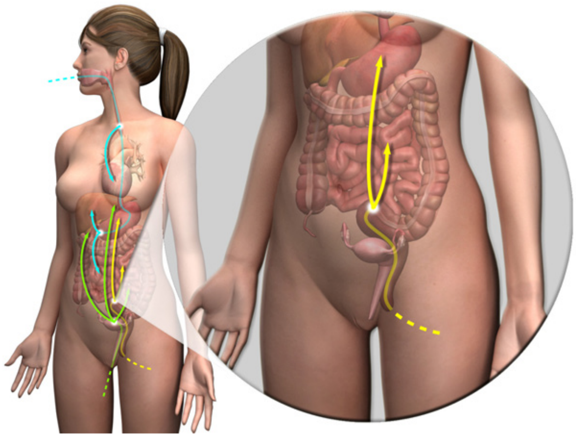

Figure 2.9: Scheme of a transcolonic NOTES access through the rectum to the peritoneal cavity.

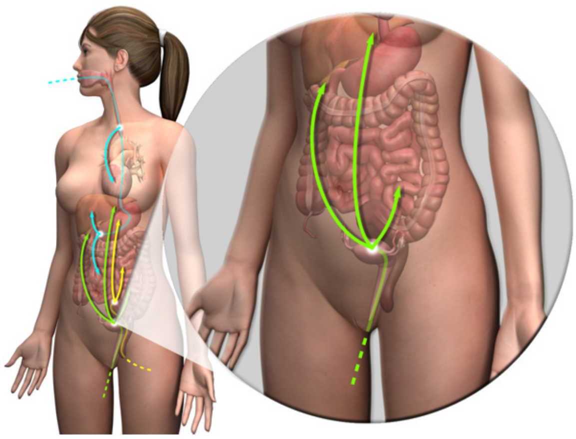

Figure 2.10: Scheme of a transvaginal NOTES access through the vagina to the peritoneal cavity.

lenges to the safe introduction of NOTES and discussed the following potential barriers [Ratt 06b, Ratt 06c, Bowm 06]:

Figure 2.11: Laparoscopic view on an endoscope in the peritoneal cavity introduced through the rectum (reprinted with kind permission of the Research Group for Minimally invasive Interdisciplinary Therapeutical Interventions (MITI), Klinikum rechts der Isar, Technische Universität München, Germany).

1. Access to peritoneal cavity
2. Gastric or intestinal closure
3. Prevention of infection
4. Development of suturing and anastomotic (nonsuturing) devices
5. Maintaining spatial orientation
6. Development of a multitasking platform
7. Management of intraperitoneal complications and hemorrhage
8. Physiologic untoward events
9. Training other providers

These challenges applied also to alternative translumenal routes for similar interventions that were found subsequently. By now the transcolonic route (fig. 2.9) especially for cholecystectomy [Pai 06] or the transesophageal access (fig. 2.8) to the mediastinum [Frit 07c] or the heart [Frit 07b] became quite common, too. The first published NOTES procedure in Europe was done in 2007 choosing the transvaginal route as shown in fig 2.10. The cholecystectomy of Zorron et al. in Strasbourg [Zorr 08] opened a long series of similar interventions as it is estimated to be the route with the lowest complication rate. Later, other routes like transvesical peritoneoscopy [Lima 07] or transvesically supported transgastric nephrectomy [Lima 07] were realized as well. Even though pure NOTES procedures might not be applicable for every indication, it could be useful to perform a rendezvous endoscopy with additional endoscopic or laparoscopic support as shown in fig. 2.11.

2.6 Instruments for NOTES

The procedure can be imagined as follows: The endoscope with at least one integrated working channel for the working instruments is inserted through a natural orifice. Then the entry point has to be identified for example by translumenal ultrasound. The access to the peritoneal cavity [Swan 05] is usually achieved with a needle knife incision [Berg 06]. Using a guidewire [Kant 07] the trocar or catheter [Deli 07a] can be inserted by additional cautery or balloon dilatation [Merr 06]. The endoscope then can be introduced through the trocar or placed over the guide wire [Mali 06]. Another approach is the innovative, safe and sterile sigmoid access (ISSA) for NOTES [Wilh 07, Mein 07]. The first step is keeping the bowel loops apart using a hydroperitoneum, which lifts them up as shown in fig. 2.12 l. The second step is encircing the entry point by a purse string suture as shown in fig. 2.12 r. In step three the sterilized trocar is inserted by perforating the area inside the purse string of the rectal wall as shown in fig. 2.13 l. In step four the endoscope is inserted through the trocar as shown in fig. 2.13 r. Even moving the endoscope forward and backwards will not contaminate the peritoneal cavity as there is a clean access through the trocar from the outside into the inner operation area. A pneumoperitoneum known from minimally invasive surgery [Neud 02] is applied in the same way and with similar effects [Deli 07b, McGe 07]. Finally, the purse string suture is immediately closed and an additional stapler line is placed over the incision after withdrawal of the trocar as shown in fig. 2.14.

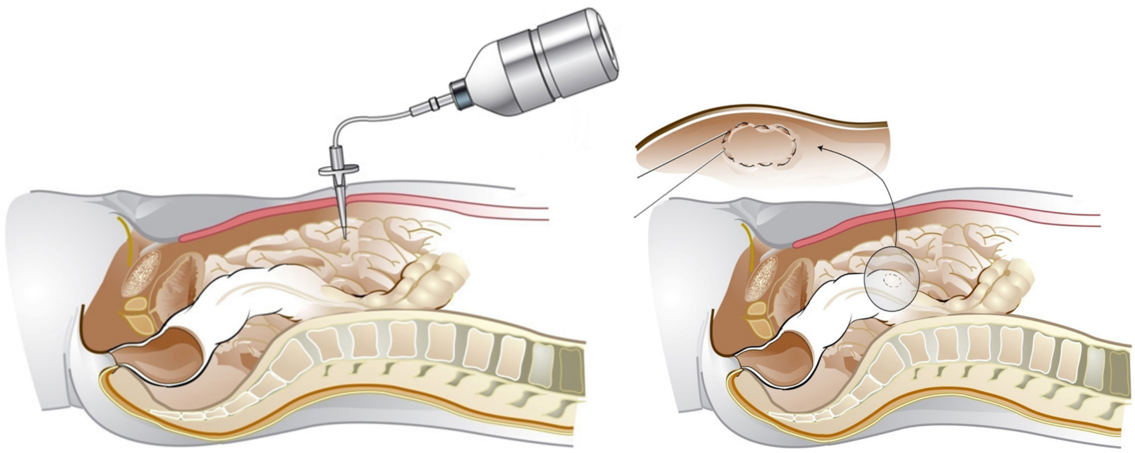

Figure 2.12: ISSA for transcolonic NOTES: Lifting the colon (l) and performing a purse string suture (r) [Wilh 07] (reprinted with kind permission of the Research Group for Minimally invasive Interdisciplinary Therapeutical Interventions (MITI), Klinikum rechts der Isar, Technische Universität München, Germany).

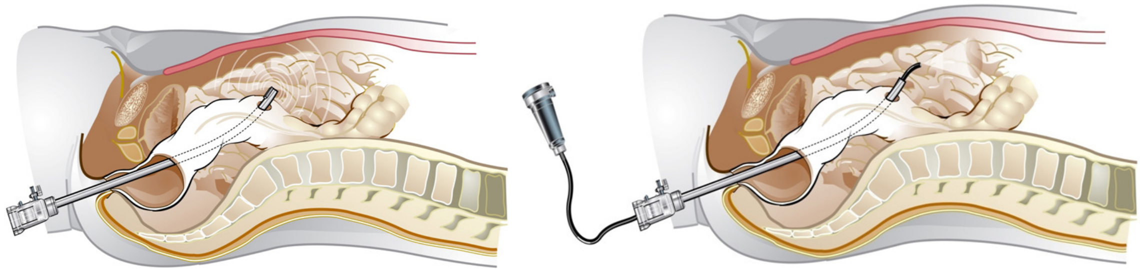

Figure 2.13: ISSA for transcolonic NOTES: Introducing the trocar through the perforated colon (l) and passing the flexible endoscope through the sterile interior of the trocar (r) [Wilh 07] (reprinted with kind permission of the Research Group for Minimally invasive Interdisciplinary Therapeutical Interventions (MITI), Klinikum rechts der Isar, Technische Universität München, Germany).

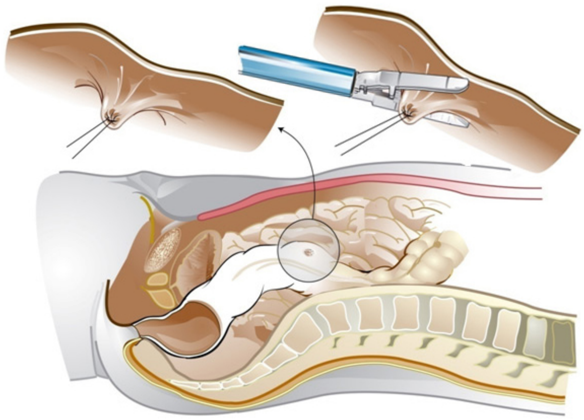

Figure 2.14: ISSA for transcolonic NOTES: Closing the purse string and placing a linear stapler on the intestinal wall line for safe closure [Wilh 07] (reprinted with kind permission of the Research Group for Minimally invasive Interdisciplinary Therapeutical Interventions (MITI), Klinikum rechts der Isar, Technische Universität München, Germany).

For leak-resistant closure of the incision [Ryou 07b], special stitching, sewing or suturing [Frit 04, Awan 02], stapling [Magn 07, Ryou 07a], clipping [Mais 08] and occluding [Perr 07] devices have to be developed [Scla 06, Arez 10]. They should be compatible to the work with flexible endoscopes by inserting them through the quite small working channels (fig. 2.17), fixing them on the endoscope's tip (fig. 2.16) or at least introducing them separately by guidance with the endoscopic guide wire (fig. 2.15). Instruments can be anchored and hold in place on the peritoneal surface using magnetic coupling via an external handheld magnet [Scot 07a, Scot 07b, Voer 07].

2.7 Challenges with NOTES

NOTES requires the skills of both, endoscopists, who are used to flexible endoscopes and surgeons, who are successful with laparoscopic abdominal surgery and intraabdominal complication management. They will only be able to perform NOTES in

Figure 2.15: ENDO GIA Universal 12 mm Auto Suture rigid stapling device with exchangeable tip, Covidien plc, Dublin, Ireland (reproduced courtesy of the Research Group for Minimally invasive Interdisciplinary Therapeutical Interventions (MITI), Klinikum rechts der Isar, Technische Universität München, Germany).

Figure 2.16: 'Eagle Claw' suturing device with a rigid distal part containing the curved needle itself, carrying the thread, and opposable jaws, which can be opened and closed by an outer handle, Olympus Medical Systems Corp., Tokyo [Chiu 08] (reproduced courtesy of the Research Group for Minimally invasive Interdisciplinary Therapeutical Interventions (MITI), Klinikum rechts der Isar, Technische Universität München, Germany).

close collaboration, so specialty lines will change [Pons 05] and a new subspecialty is needed [Hawe 07, Kall 07a]: A new interdisciplinary "surgical endoscopist" or "endoscopic surgeon" [Hoch 05] will be in demand. Not only the skills of physicians have to be trained [Gill 08] but also their instruments have to be enhanced [Koch 07] and require innovations in engineering. Since e.g. traction and retraction or locking in position for triangulation is hardly feasible with flexible endoscopes, current instruments are insufficient for complex intra-abdominal surgery [Lama 06]. It quickly

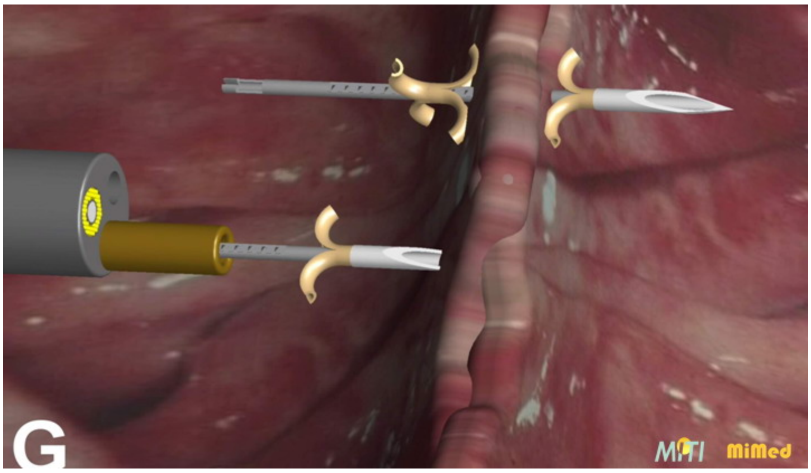

Figure 2.17: Closure of the gastric or colonic wall incision with Endorivet clips using dissolving magnesium spikes with self-opening barbed hooks and a linear reloading mechanism for multiple shots, MITI/MIMED, Technische Universität München, Germany (printed with kind permission of the Research Group for Minimally invasive Interdisciplinary Therapeutical Interventions (MITI), Klinikum rechts der Isar, Technische Universität München, Germany).

became clear that there has to be an interdisciplinary collaboration not only between surgeons and gastroenterologists [Pons 05] but also with engineers, who are requested to provide better imaging systems, medical robots and endoscopic instruments as proposed in [Ko 06] (visualized in fig. 2.18) .

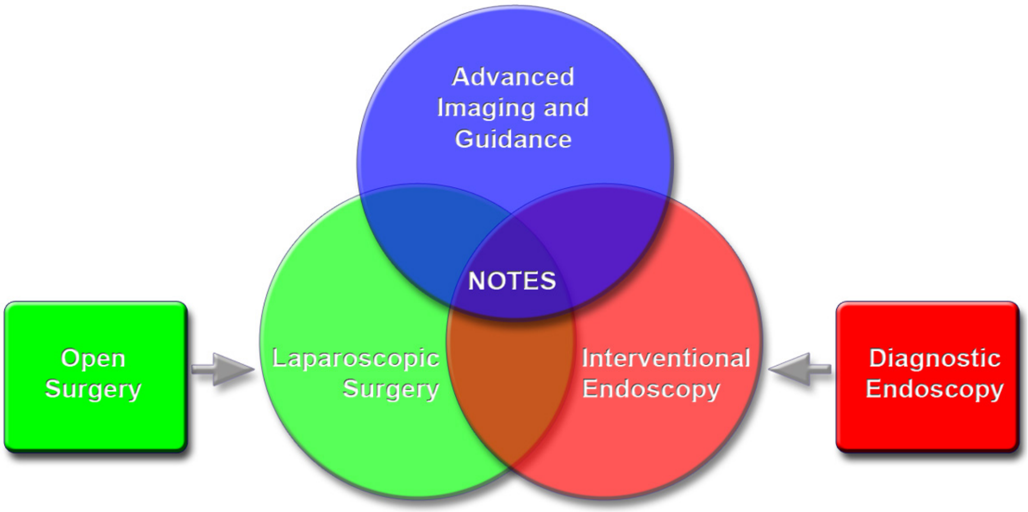

Figure 2.18: NOTES requires interdisciplinary collaboration not only between surgeons and gastroenterologists but also with engineers, who are requested to provide better imaging and guidance systems.

2.8 NOTES - "No longer if, but when"

Physicians of the NOTES community believe in their new technology. Richards and Rattner declared in 2005 that regarding NOTES the question is "No longer if, but when" [Rich 05]. Fritscher-Ravens describes transgastric endoscopy as "A new fashion, a new excitement" [Frit 07a]. Many popular magazines [Blec 07] and newspapers [Carm 08] presented this new method to the general public. According to a survey of Swanstrom [Swan 09] the majority of interviewed patients would prefer their cholecystectomy to be performed via NOTES as long as their surgeon is well trained and the inherent risks are not significantly greater than those associated with the conventional approaches. This is interpreted as an indication that physicians should keep an eye on developments related to NOTES since a rapid demand for these procedures may arise [Mali 06] once the possibility of NOTES reaches the attention of the public.

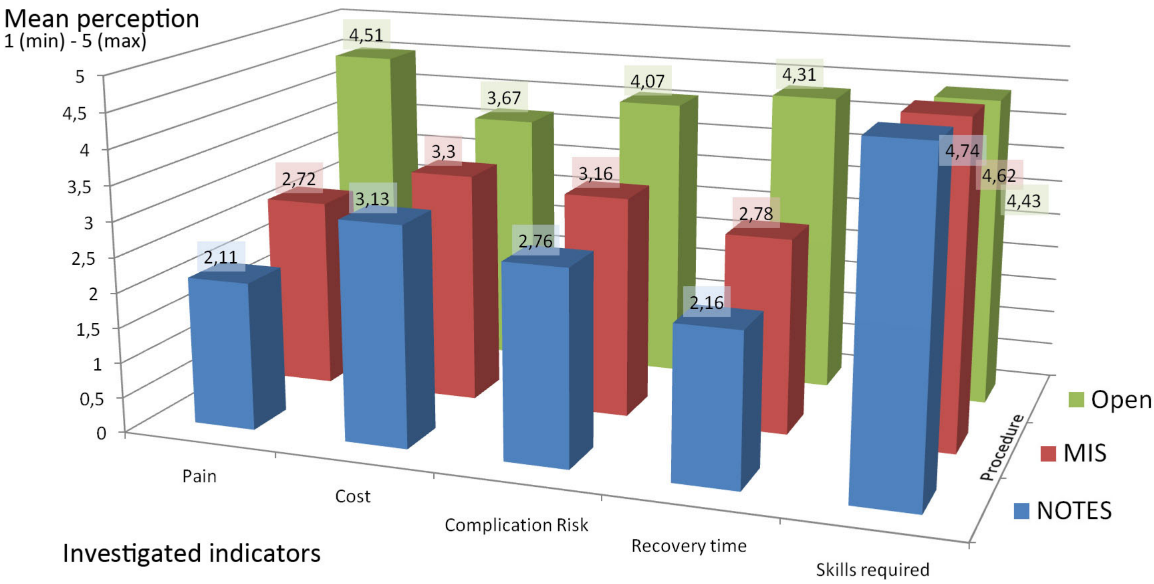

Figure 2.19: Patients would prefer NOTES if their surgeon meets its requisite skills [Swan 09].

At the same time not everyone in the community is so optimistic. Feußner et al. describe an extremely controversial debate, ranging from "euphoric visions to complete refusal" [Feus 09]. In fact there is only black or white for most of them. Those, who are not convinced of its success, decline it as a useless utopia. But even if NOTES itself will not become common standard for all peritoneal interventions, there will be a chance for the development of other new approaches like single port access [Fuch 08], hybrid interventions [Shih 07] or other new flexible instruments [Swan 05]. Thus, the medical and technical innovations and developments within this research enthusiasm will sustainably improve established methods and help thinking out of the surgeon's and gastroenterologist's box.

Chapter 3

Technical Background on Existing 3-D Enhancements in Endoscopy

3.1 3-D Measurement Technologies

Mainly, there are two different types of endoscopes: Rigid ones, which are called laparoscopes, and flexible ones. An endoscope consists not only of an image channel but also of an illumination channel and, especially with flexible endoscopes, optionally of one or two working channels. The image is transmitted via an optical lens system or optical fibers. With flexible endoscopes it is becoming common to transmit the images electrically having the camera chip on the distal end ("chip-on-the-tip"). Mechanically, flexible endoscopes can be controlled by small wheels integrated in the grip shaft.

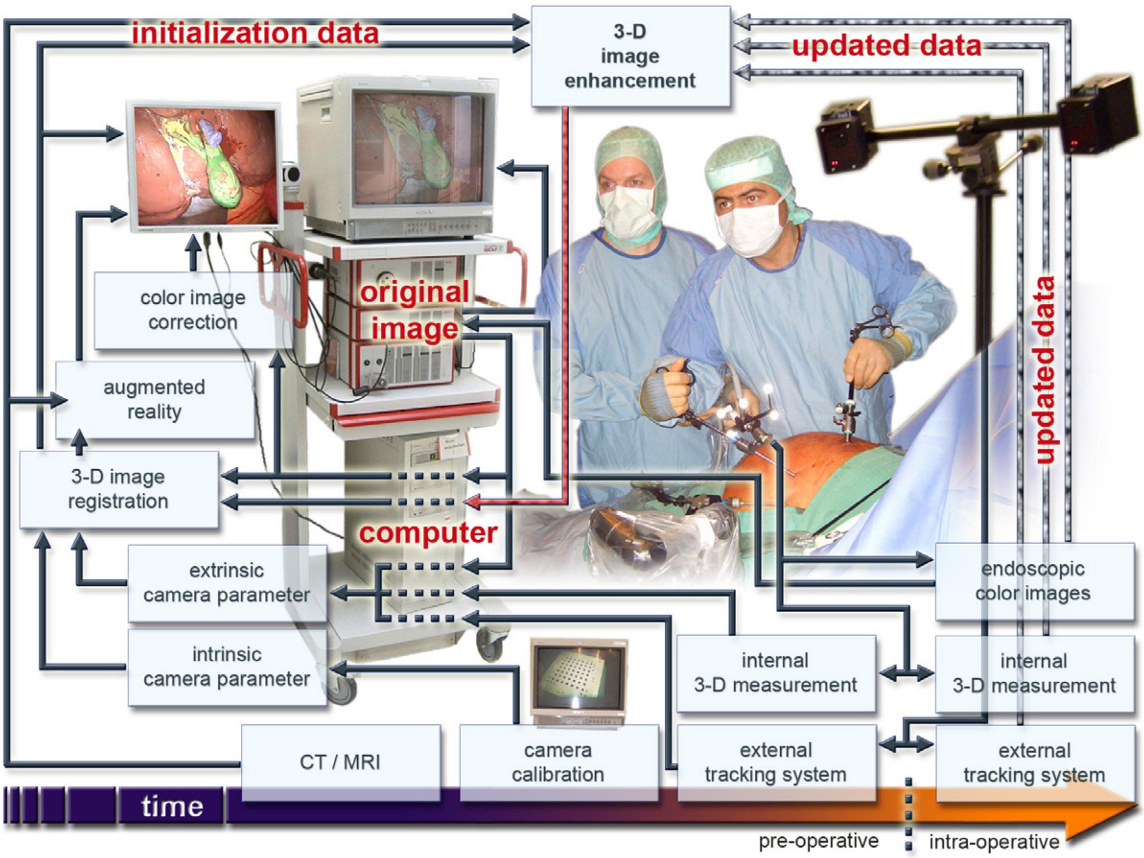

Figure 3.1: Internal and external 3-D data acquired in real time allow registration of endoscopic color images with pre-operatively acquired and segmented CT or MRI data to provide intra-operative augmented reality. Preconditions are calibration of cameras and tracking devices with intrinsic and extrinsic parameters. After an initialization process the 3-D image enhancement procedure requires permanently updated position and orientation data in addition to the endoscopic video stream.

Acquiring 3-D information from endoscopic images is often done during an off-line routine, i.e. an image sequence is recorded and subsequently processed to get the desired information about the operation area [Vogt 05a, Thor 01]. Some new approaches listed below aim to acquire 3-D data in real time. This is important to register pre-operatively acquired computer tomography (CT) or magnetic resonance imaging (MRI) 3-D data with preoperative data as shown in fig. 3.1 and subsequently to provide augmented reality (AR) [Milg 99, Vogt 05b, Olbr 05].

There are different optical, acoustical, inertial, and electro-magnetical approaches with passive or active methods to obtain 3-D information additionally to the conventionally acquired endoscopic color image. Some provide a whole depth or distance map of the observed area and some just determine additional parameters like position, movement or orientation. A good overview of the most important tracking technologies is given in [Welc 02].

3.1.1 Passive Optical Technologies

Stereo Endoscopy

Figure 3.2: Stereo endoscope with two equal image channels and one illumination channel (reprinted with kind permission of the Institut für Anthropomatik, Karlsruher Institut für Technologie (KIT), Germany).

Passive optical technologies like stereo endoscopes usually provide just a 3-D impression by separately showing only one of the two stereo images to each eye. They do not need any image processing effort but on the other hand they cannot provide any abstract or computable data. The distance between the optical elements in the laparoscope is not greater than 10mm apart and fixed, whereas the human interpupillary distance is greater than 60mm and can accommodate [Sata 93]. Due to this small distance between the two optical channels as shown in fig. 3.2 it is hard to apply optical triangulation like [Stoy 05]. But both images can be visualized separately in a manner that delivers a 3-D impression to the surgeon. A quite common stereo vision approach is described by [Berg 98].

Passive Monocular 3-D Endoscopy

Passive monocular 3-D endoscopy approaches are designed to estimate a 3-D surface by moving the observer position. To obtain higher-level information from a sequence of endoscopically acquired 2-D images, a 3-D reconstruction of the operation area from monocular endoscopic images is proposed. Such a reconstruction yields a triangulated mesh describing the surface of the observed area. The most convenient approaches are structure from motion (SfM) [Thor 01, Degu 96, Witt 06] and shape from shading (SFS) [Okat 96, Yeun 99]. Another issue here is the image-driven orientation correction ("rectification") to provide a stable horizon of endoscopic images. Different approaches for motion tracking have been suggested by [Welc 02] and [Kopp 04, Kopp 05]. They developed a passive approach to solve the rectification problem of monocular flexible endoscopes with varying orientation. They have proposed a three-step vision based approach, which tracks salient points in consecutive images, estimates the camera's extrinsic motion parameters, approximates the scene depth and finally infers the direction of an abstract 'head-up' vector in the camera's current reference frame [Kopp 01]. Therefore, at least eight trackable points have to be found. Additionally, this purely vision based approach entails high computational costs, which is not supposed to be realizable in real time.

3.1.2 Active Optical Technologies

Pattern Projection

Active optical technologies utilize certain effects with special illumination methods to increase accuracy and to decrease computational complexity. Nevertheless, they are supposed to gain the same 3-D surface information like the passive methods. This can be realized by pattern projection [Hase 02] and structured light [Albi 09] or consecutive illumination with varied colors from different directions [Fisc 08]. The endoscopic use of these methods is limited by the size of the projection assembly and the time required for computing.

Optical Tracking

Not only surface and distance information is important, but also position and orientation values are very useful additional 3-D enhancements for navigation and rectification. External optical tracking only works with rigid endoscopes since the transformation between marker and image coordinate system has to be constant. An optical reflecting target is mounted on a laparoscope and observed by at least two cameras (fig. 3.3). By triangulation of the two recorded images the position is computable. Orientation can be computed as well if the target consists of multiple reflecting points. A target is built from markers that can easily be identified in the captured pair of images. The use of infrared light simplifies marker detection additionally. The knowledge of the geometry of a target and its carrier laparoscope allows computing its pose after recognition of all visible individual markers [West 04].

Figure 3.3: Polaris Spectra with two cameras and illumination units for stereo vision optical tracking, Northern Digital Inc., Ontario, CA - photo taken at MICCAI 09, London, UK.

3.1.3 Active Magnetic Technologies

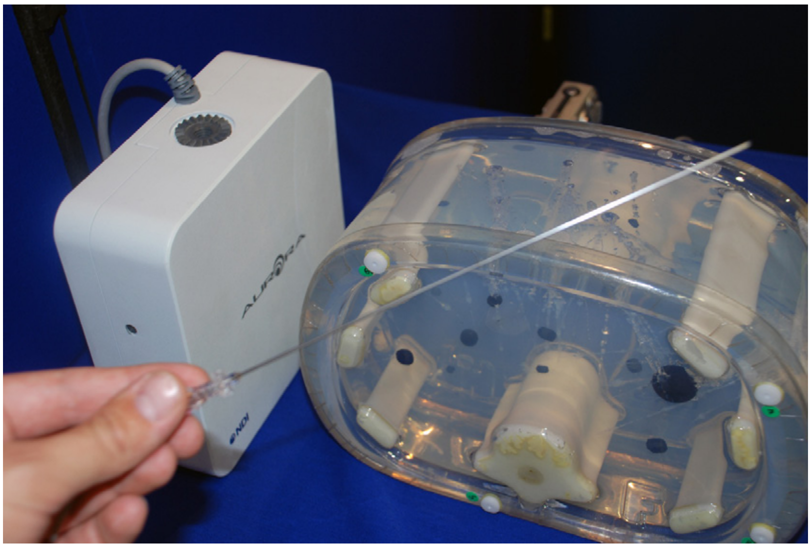

Figure 3.4: Aurora electro-magnetic tracking device with external field generator (l) and three tiny coils in the tip of the bar (r), Northern Digital Inc., Ontario, CA - photo taken at MICCAI 09, London, UK.

Similar to the previous optical tracking one can apply electro-magnetic tracking for measuring position and orientation. Since there is no need for a line of sight between reference source and target it can be used even with flexible endoscopes or directly in the abdomen. A magnetic tracking system always consists of a field generator and receivers consisting of coils. A 1-D sensor is made up of a single coil in the field transmitter and another coil in the receiver. Current applied to the coil in the generator leads to an electromagnetic field in which the receiver coil induces a voltage providing information about the distance to the field generator (fig. 3.4). Three separate coils mounted orthogonally in the field generator as well as in the receiver will then provide information about the position in x, y, and z direction. With this data additionally roll, pitch and yaw can be estimated. If more than one coil is used, the coils are activated serially. The main disadvantage of electromagnetic tracking are still existing distortions due to ferromagnetism [Humm 02]. They occur mainly with steel or iron instruments and objects which cannot be simply substituted without further costs or decreasing performance.

3.1.4 Active Acoustical Technologies

With endoscopic ultrasound (EUS) it is possible to visualize a slice of a 3-D volume orthogonal to the original endoscopic color image. However, it cannot be used to compute a surface, orientation or position. EUS is inserted or integrated in the tip of an endoscope. Its working principle is not different to common ultrasound devices. Endoscopic ultrasound is especially important e.g. with transesophageal access to the heart as described in [Frit 06].

3.2 3-D Visualization Technologies

In general, the surgeon's impression of the surgical scene using a laparoscope is not as good as in open surgery since the depth perception is reduced. Thus, any 3-D approach will help to improve this missing perception and to increase the surgeon's effort [Wenz 94].

3.2.1 Head Mounted Display

Head mounted displays (HMDs) are a pair of image display units mounted on a helmet or on the face in the form of glasses. By generating an individual image for each eye, an imaginary screen that appears to be positioned several meters in front of the viewer can be created. Either it is possible to record two different image streams with a fixed inter-space or they have to be calculated using 3-D data. The image can be superimposed on an external scene by means of see-through function. In any case, it is quite easy to make each image only visible for one eye [Shib 02].

3.2.2 Stereo Monitor

For visualization on monitors there are methods like passive stereo projection monitors and active stereo (auto-stereoscopic) monitors. Similar to the HMD approach it is intended to project a different image to each eye using these monitor technologies. Therefore, the passive stereo projection requires the use of anaglyph glasses with two different colors (typically red/green) [Dubo 01] or glasses with differently polarized filters [Kawa 02]. Another approach is to show high-frequent alternating images with synchronized active shutters in user's glasses [Volb 96]. Using an eye tracking camera, different stereo views can be provided. This allows viewing from different angles and furthermore, a three-dimensional visualization for more spectators. Active displays have a lens raster with a beam splitter placed on the LCD panel [Funk 07]. It splits the light of each pixel in different ways. A precondition to use these displays is a fixed position in front of the monitor. However, with a mounted beam splitter, 2-D information is no more displayable.

Both technologies have their advantages and disadvantages. Actually, techniques using glasses are more common and provide a better, less fatiguing way to display 3-D content. However, wearing these special glasses is difficult in some scenarios. For example, during surgery it could be useful to provide the surgeon three-dimensional planning data, i.e. resection margins during liver surgery. Since he is in a sterile area, it is not possible for him to put on and off the glasses frequently [Herr 99].

3.2.3 Virtual View

Other systems are not able to provide a real 3-D feeling, but a better 3-D impression can be gained. With a virtual view as used with so called light fields [Vogt 04], the observed object can be moved and rotated virtually and therewith provide the 3-D impression. But this requires the user to move the virtual object and to disturb the real or virtual alignment, or to move his head around the real objects, which is not always possible or practical.

3.2.4 Virtual Mirror

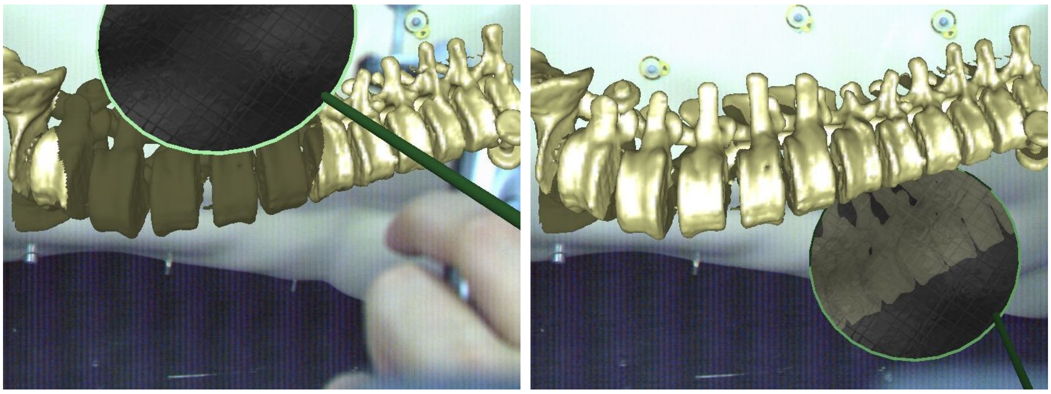

Figure 3.5: Virtual light effects like shadow (l) and reflection (r) cause visual cues to enhance information on relative position of objects in an AR scene. Here, a spinal column is registered and superimposed on a plastic thorax phantom [Bich 09] (reprinted with kind permission of C. Bichlmeier).

A virtual view is quite impractical when a single camera is used for augmentated images on a usual color display without 3-D enhancement, such as in augmented laparoscopic surgery. Navab et al. introduced an interaction and 3-D visualization method, which uses an interactive virtual mirror as shown in fig. 3.5 positioned into the augmented scene [Nava 07]. It allows easy and complete interactive visualization of 3-D virtual data without the need of moving the object or the point of view.

3.2.5 Projected and Semi-transparent Representation

Instead of providing a 3-D image or impression on a flat screen it is possible to integrate virtual 3-D data into real world perception. Therefore, virtual components can be projected onto the real world. Another approach is to project the virtual components onto the user's retina. An easier implementation of this idea can be realized by observing the real world through a semi-transparent display visualizing virtual components or other 3-D information [Nava 01].

3.3 3-D Enhanced Interventions

Since in clinical routine 3-D visualization is not a precondition, firstly the implementation is planned for special applications. During laparoscopic interventions, where a camera observes the instruments and organs in the abdominal cavity, creation of intra-operative real-time 3-D images is usually realized with stereo optics and direct 3-D visualization of this pair of images without further computation. Since the diameter of these telescopes with fibers for illumination is typically limited to 10mm, the use of stereo optics limits the useful lens diameter additionally. Also the difficulty of combining high-quality 3-D displays with maximum real color representation confines the use of 3-D in the surgical OR. The eye fatigue problem makes it inconvenient for every medical pioneer and thus the various prospects for the acquisition of additional 3-D data are not taken into account widely enough.

3.3.1 Prospective Intervention Planning

Planning of difficult surgeries can be done days before surgery. Especially liver resection planning is done right after imaging. After segmentation of the liver, resection margins can be planned, vessels and bile ducts can be set in relation [Numm 05]. Measurement of liver volume and hepatic functional reserve are important especially in resectional surgery for hepatic tumors as shown in fig. 3.6. For this application, pre-operative virtual 3-D data and measurement are very useful. The surgeon gets a better insight of the situation. Additionally, we do not have the eye fatigue problem since the pre-operative planning is not as time consuming as with real surgery.

3.3.2 Intra-operative Augmented Reality

It would be useful to combine both, the 3-D view and the planning methodology with knowledge on hidden areas and exact positions, orientations and distances. Therefore several new intra-operative approaches [Feue 07] with computer-assisted surgical systems [Hart 07a] require additional metric 3-D information. Registered with pre-operative CT or MRI data, it may provide information on position and orientation of the robotic device or endoscope. Hidden organs or vessels can be visualized by augmented reality (AR), i.e. a simultaneous view of pre- and intra-operative data

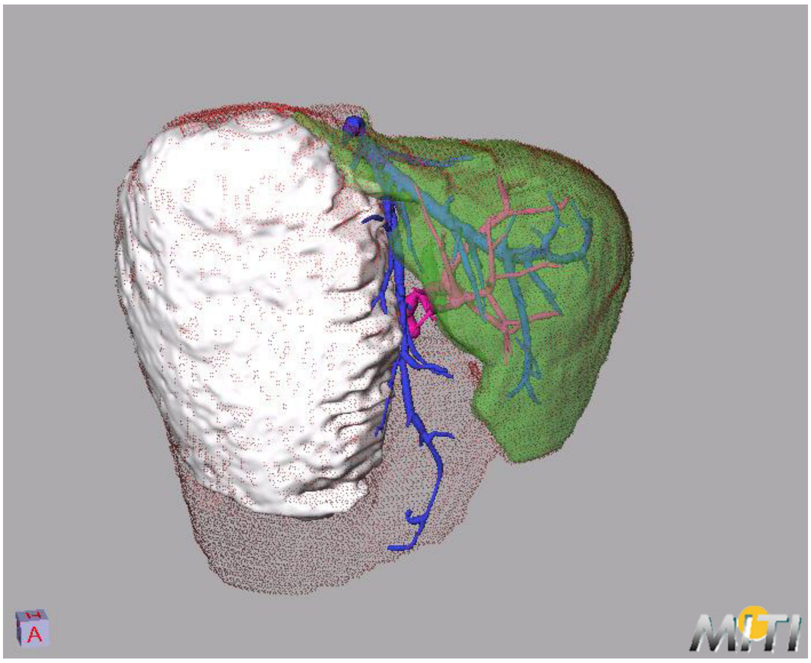

Figure 3.6: Measurement of liver volume and hepatic functional reserve in resectional surgery for hepatic tumors using pre-operative 3-D data for augmented reality (reprinted with kind permission of the Research Group for Minimal Invasive Surgery (MITI), Klinikum rechts der Isar, Technische Universität München, Germany).

[Feus 03, Sole 08]. There will be a possibility to virtually rotate the field of view for a stable horizon or an off-axis view. Building a greater map by stitching or mosaicking can extend the field of view and enable a more intuitive and reliable navigation.

3.3.3 Multitasking Platforms

Because some procedures require a team to manipulate instruments, devices with multiple ports are likely to be important. The role of robotics in this area seems promising, but a lot of development work remains to be done. Development should focus on manual tools that ultimately can be modified for robotic control [Ratt 06c].

In [Hart 07a] a questionnaire of the use of medical robots in Germany, Austria and Switzerland was performed with $n = 89$ participants. In $n = 67$ cases there was no use of robotic systems (75.3%). In $n = 6$ cases (6.7%) an experimental use of robotic systems was reported. $n = 19$ $(21, 3\%)$ hospitals reported the use of robotic systems in clinical routine. $n = 7$ (7.9%) of them used the AESOP (Automatic Endoscopic System for Optimal Positioning, Computer Motion Inc. [Oban 03], fig. 3.8) system, $n = 7$ (7.9%) the daVinci system (Intuitive Surgical Inc., fig. 3.7) and $n = 5$ (5.6%) applied other systems. In $n = 6$ cases (6.7%) the use of robotic devices, thereof $n = 5$ (5.6%) AESOP systems and $n = 1$ (1.1%) ROBODOC system (CUREXO Technology Corporation [Kaza 07, Kaza 08], fig. 3.9) has been discontinued. The average use per year was 20 cases with a wide range from $2 - 74$.

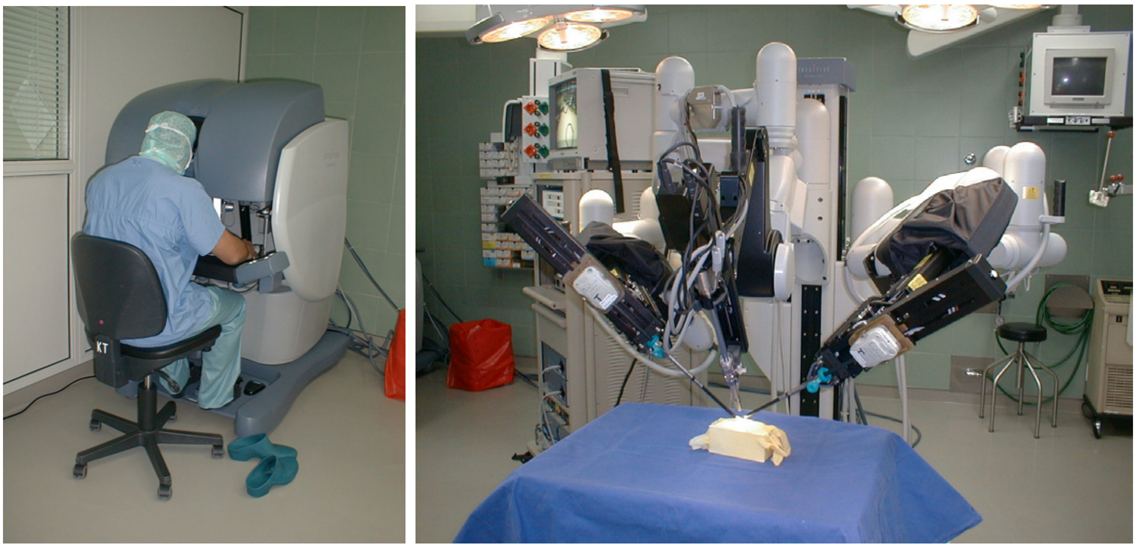

Figure 3.7: Robotic surgery at MITI with the DaVinci system using a controlling console (l) and a multi-arm manipulatior system (r), Intuitive Surgicals Inc., Sunnyvale, CA (reproduced courtesy of the Research Group for Minimal Invasive Surgery (MITI), Klinikum rechts der Isar, Technische Universität München, Germany).

Figure 3.8: Robotic surgery at MITI with the AESOP system, Computer Motion Inc., Goleta, CA (reproduced courtesy of the Research Group for Minimal Invasive Surgery (MITI), Klinikum rechts der Isar, Technische Universität München, Germany).

As reason for no application or discontinued application of robotic systems, the high costs played the major role in 50% of all answers , followed by lack of indications in 41%. Those, who use camera-guiding systems like AESOP or EndoAssist (Armstrong Healthcare Inc. [Gilb 09], fig. 3.10), approved a stable visual field, the absence

Figure 3.9: Robotic surgery with the RoboDoc system, CUREXO Technology Corporation, Fremont, CA [Kaza 08] (reprinted with kind permission of P. Kazanzides).

of exhaustion and the reduction of staff. They criticize uncomfortable handling, high operating costs and prolonged operating time.

The users of master-slave systems like daVinci point out as advantages the 3-D visualization, the precise movements and the ergonomic position of the surgeon at the console. On the other hand they criticize the high purchase and running costs, the long time for installation, the huge dimensions and weight and the reduced operating field. Telemanipulation systems are used in all surgical sections. For surgical purposes a system is preferable, which can assist the surgeon in several different ways, which does not obstruct visibility in the operation-field, which is as compact as possible, which is easily mountable and removable in clinical routine and can furthermore be controlled intuitively by the surgeon.
For secure work with computer assisted robotic systems especially collision prevention, motion compensation and automatic positioning of surgery tools are big issues that can be solved using additional 3-D data. For the planning of the setup with robotic devices a complete pre-operative planning is very useful, too [Adha 00]. There are specific robotic manipulators for special tasks [Ho 07], so some steps like suturing could be carried out automatically.

3.4 3-D Enhancements in Endoscopy

3-D measurement technologies with passive and active approaches as proposed in section 3.1 assist the surgeon for better orientation and coordination during the intervention. This is important especially for endoscopic surgery since in contrast to open surgery there is no direct view to the intervention site and the surgeon is not able

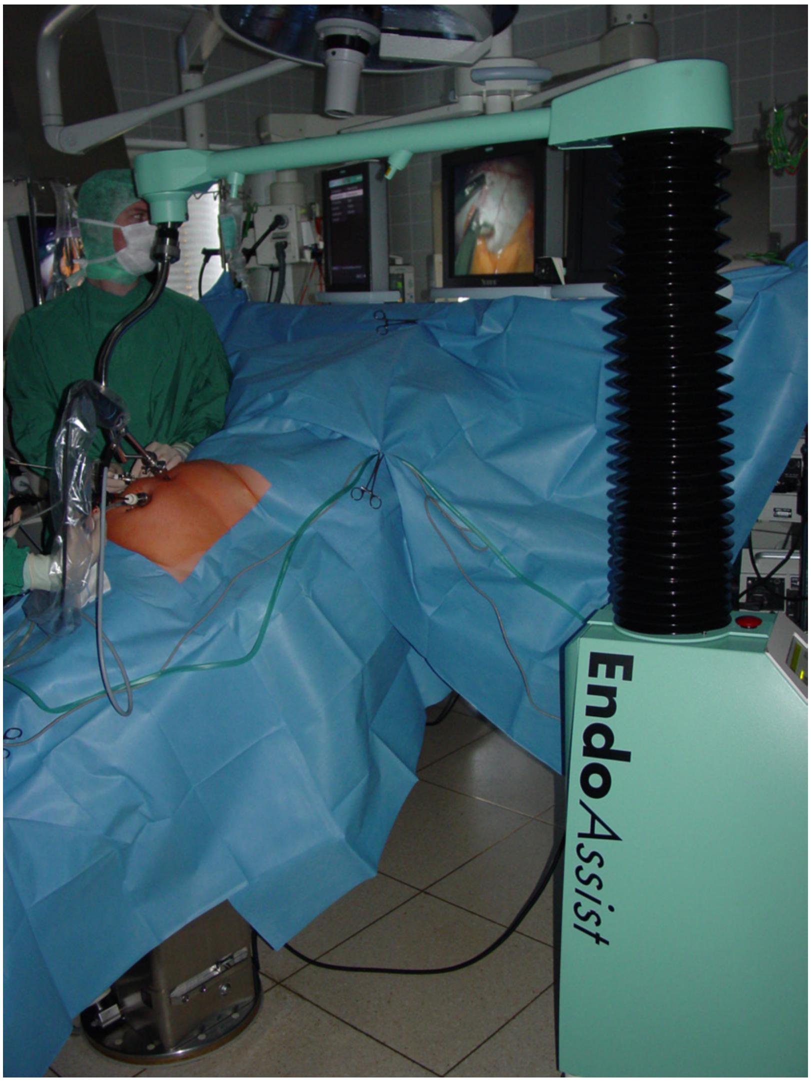

Figure 3.10: Robotic surgery at MITI with the EndoAssist system, Armstrong Healthcare Inc., Dallas, TX (reproduced courtesy of the Research Group for Minimal Invasive Surgery (MITI), Klinikum rechts der Isar, Technische Universität München, Germany).

to use his own eyes to get a spatial impression. Therefore these data have to be prepared and visualized for example with HMD devices or stereo monitors as proposed in section 3.2. Common displays can be used with virtual visualization methods. With these techniques prospective intervention planning as shown in section 3.3 can be realized. Projection and semi-transparent representation can be used to combine real world view and virtual data. This is helpful especially for intra-operative augmented reality. Metric data can also be used for better coordination with multitasking platforms and robotic devices. Therefore 3-D enhancements in endoscopy have a great impact for laparoscopic and endoscopic surgery with and without robotic assistance.

Chapter 4

Novel Sensor Technologies for Endoscopic Image Extension

4.1 ToF Basics

Time-of-Flight (ToF) sensors are special imaging chips used for measuring 3-D surfaces. They play a major role for the approach proposed in section 5.3. Therefore, in this section the basic idea, the measurement principle and various models will be proposed.

4.1.1 ToF Principle

A very obvious approach for optical distance measurement would be to send an infrared (IR) light pulse and to measure the time till its reflection can be observed by a photo diode (PD) as visualized in fig. 4.1. As light has a speed of $c = 3 \cdot 10^8$m/s, this delay τ_d is very short: an object $d = 0.5$m away will delay the light by:

$$\tau_d = 2 \cdot \frac{d}{c} = 2 \cdot \frac{0.5m}{3 \cdot 10^8 \text{m/s}} = 0.000000003333s = 3.333\text{ns} \tag{4.1}$$

For our purposes the distances and therefore the delay time are too small to measure τ_d and calculate the distance using the speed of light c.

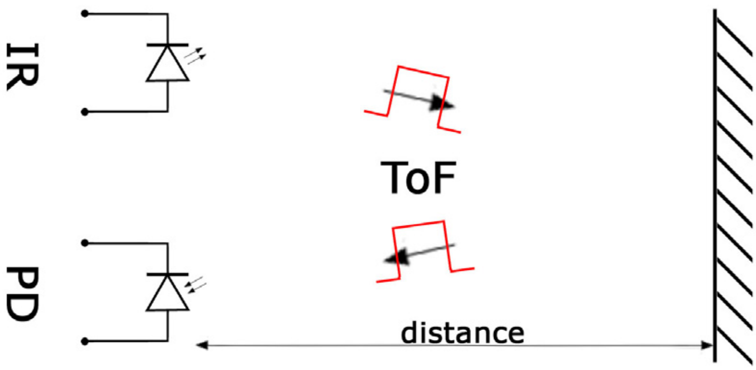

Figure 4.1: Principle of an emitted and rejected infrared pulse with distance depending time of flight from IR emitter to the object and back to the photo diode.

Thus commercially available ToF cameras based on the photonic mixing device principle (PMD) provide active amplitude modulated illumination with the modulation frequency f_{mod} and corresponding modulation wavelength $\lambda_{mod} = \frac{c}{f_{mod}}$. Frequency f_{ir} and wavelength λ_{ir} of the carrying light are independent of the modulation dimensions and are not relevant for the functional principle. Nevertheless, usually infrared (IR) light is emitted to facilitate the suppression of background illumination by optical filters. The light is scattered by the object and received again by the photonic mixing device (PMD) after a time of flight τ_d (fig. 4.2).

The camera measures the phase difference φ_d between the sent signal $g(t)$ with the phase φ_T and the reflected and received wave $s_d(t) \sim g_k(t - \tau_d)$ with phase φ_R.

$$\varphi_d = \varphi_R - \varphi_T = 2\pi f_{mod} \tau_d \tag{4.2}$$

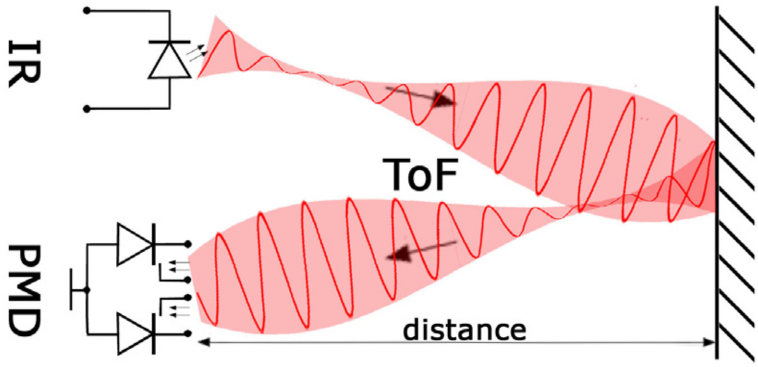

Figure 4.2: ToF principle using emitted and rejected intensity modulated IR carrier wave. Distance depends on the time of flight from IR emitter to object and back to the photonic mixing device. The resulting modulation phase shift between emitted and received signal can be measured and depends only on modulation frequency and time of flight.

With the constant speed of light c, the distance d can be determined according to [Hein 01] by:

$$d = \frac{c \cdot \varphi_d}{4\pi \cdot f_{mod}} \tag{4.3}$$

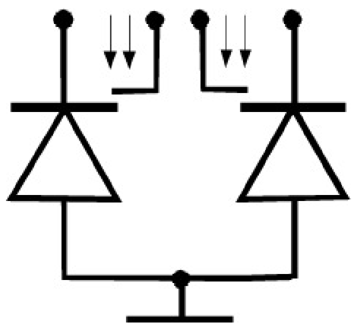

Figure 4.3: Electrical symbol of ToF distance sensors [Luan 01].

The received wave generates electrons in the photoactive zone of each pixel. The phase difference for each ToF pixel (symbol shown in fig. 4.3) is measured by sampling the received signal $s_d(t)$ at $N \geq 3$ (commonly 4) equidistant measurement cycles with a certain duration τ_{int} (integration time). This can be realized by mixing it in a charging swing (”Ladungsschaukel”, fig. 4.4) with an electrical reference signal. Initially it is mixed at the moment of emission in phase with the sent signal $g(t)$ and subsequently with the stepwise increased phase shift resulting from angular velocity $\bar{\omega}$ and shifting time τ_k resulting in the reference signal $g_k(t + \tau_k)$ [Luan 01]:

$$\bar{\omega}\tau_k = \frac{2\pi}{N} \cdot (k-1) \quad \text{with} \quad k = 1, 2, .., N \tag{4.4}$$

For usually applied $N = 4$ within a period of 360° this means an iterative phase shift by 90° with $\bar{\omega}\tau_1 = 0°$ and $\bar{\omega}\tau_4 = 270°$ for the reference signal $g_k(t+\tau_k)$ while mixing it with the received and transformed signal $s_d(t)$.

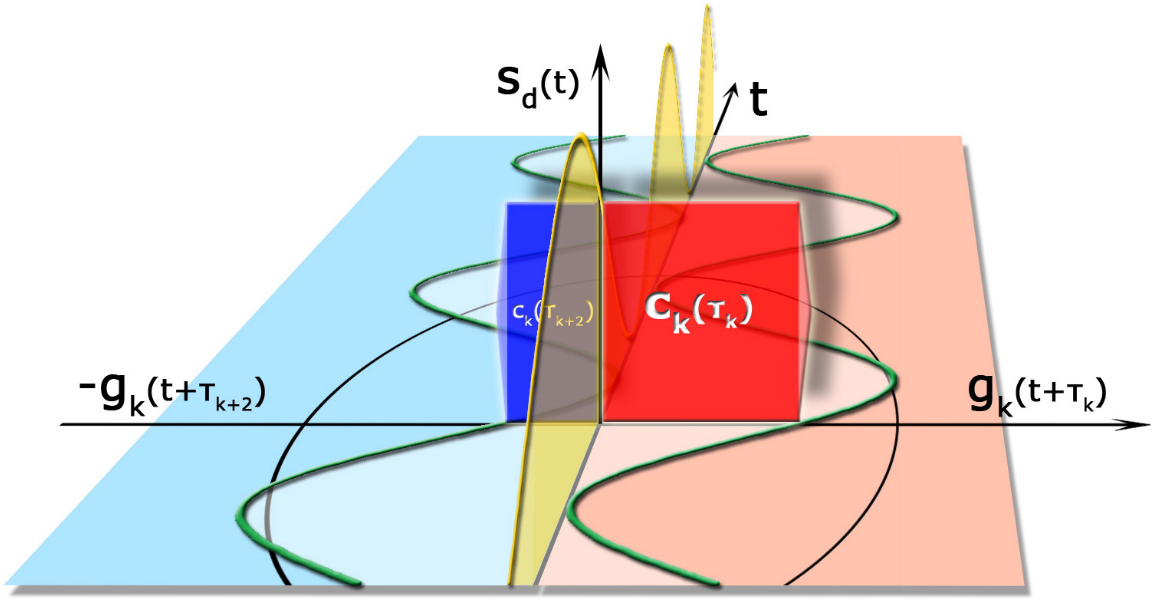

Figure 4.4: In the charging swing principle, the charge distribution depends on the phase shift between the optical light intensity $s_d(t)$ generating electrons in the photo-active zone (corresponding to the phase of the received wave, indicated by the yellow curve) and the electrical reference signal $g_k(t+\tau_k)$ resp. complementary $-g_k(t+\tau_{k+2})$ inducing an electrical field below the photo-active zone (corresponding to the phase of the emitted wave, indicated by the green curve). The resulting charge distribution (indicated by the red and blue area) depends on the correlation function $c(\tau_k)$ resp. $c(\tau_{k+2})$ and induces a potential between both sides of the semiconductor.

The correlation function $c(\tau_k) \sim s_d(t) \otimes g_k(t+\tau_k)$ scaled with amplitude a_p for the light amplitude is approximated according to [Lang 00] as:

$$c(\tau_k) = \frac{a_p}{2} \cdot \cos(\varphi_d + \bar{\omega}\tau_k) \tag{4.5}$$

The voltages U_k measured at the electrodes with overlaying offset and background illumination influence b and the electrical amplitude a resulting from a_p lead to:

$$U_k = b + 2\frac{a}{a_p}c(\tau_k) \tag{4.6}$$

Using eq. 4.5 and 4.6 the resulting voltages U_k for $N = 4$ can be computed as

$$\begin{aligned} U_1 &= b + a \cdot \cos(\varphi_d), \quad U_2 = b - a \cdot \sin(\varphi_d), \\ U_3 &= b - a \cdot \cos(\varphi_d), \quad U_4 = b + a \cdot \sin(\varphi_d) \end{aligned} \tag{4.7}$$

Thus, a pair of phase shift depending voltage differences ΔU_{24} and ΔU_{31} can be built. These potentials can be measured directly by using two electrodes:

$$\begin{aligned}\Delta U_{24} &= U_2 - U_4 = -2a \cdot \sin(\varphi_d)\\ \Delta U_{31} &= U_3 - U_1 = -2a \cdot \cos(\varphi_d)\end{aligned} \tag{4.8}$$

The relation of these two voltage differences is depending on φ:

$$\frac{\Delta U_{24}}{\Delta U_{31}} = \tan(\varphi_d) \tag{4.9}$$

But without knowledge of the unit circle quadrant the common arctangent function is not sufficient to compute φ unambiguously for the range of values between 0 and 2π. To handle the ambiguity, the two-argument function atan2 visualized in fig. 4.5 is used. This takes into account the signs of both vector components, and places the angle in the correct quadrant:

$$\text{atan2}(y, x) = 2 \arctan \frac{y}{\sqrt{x^2 + y^2} + x} \tag{4.10}$$

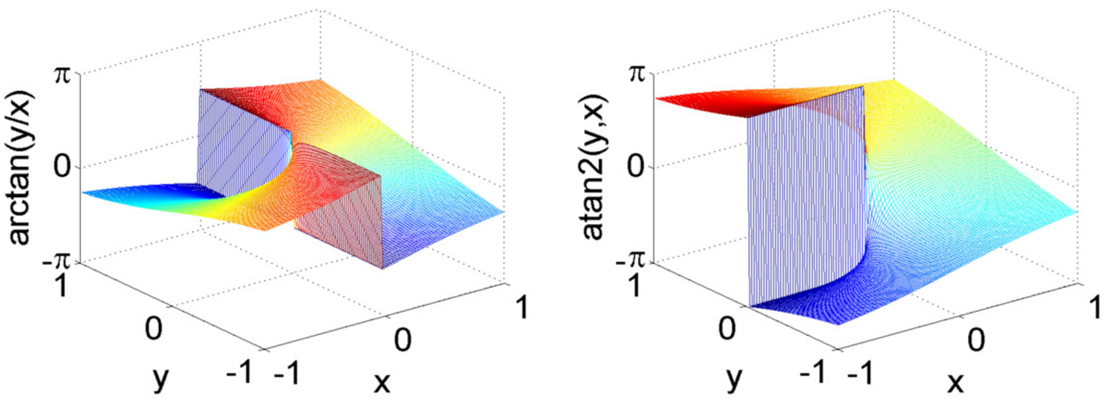

Figure 4.5: The arctan(y/x) function (l) has two discontinuities between quadrant 1 and 2 as well as 3 and 4 and ambiguities due to the symmetric shape. The atan2(y, x) function (r) has no ambiguities and a discontinuity only between quadrant 2 and 3.

Shifting the results from a range of $[-\pi ... \pi]$ back to $[0 ... 2\pi]$ one finally can compute the phase shift φ_d:

$$\varphi_d = \text{atan2}\left(\Delta U_{24}, \Delta U_{31}\right) + \pi \tag{4.11}$$

Amplitude a depends as well on ΔU_{24} and ΔU_{31}

$$a = \frac{\sqrt{\Delta U_{24}^2 + \Delta U_{31}^2}}{2} \tag{4.12}$$

Offset b can be computed with voltages $U_1 ... U_4$

$$b = \frac{U_1 + U_2 + U_3 + U_4}{4} \tag{4.13}$$

4.1.2 Resolution Dependencies

As for unambiguous measurements at maximum only one period has to be spanned from the illumination unit to the scene and back to the sensor, this range d_{max} depends on the modulation wavelength which is fixed by its frequency f_{mod}:

$$d_{max} = \frac{c}{2f_{mod}} \tag{4.14}$$

In [Gokt 04] the limiting parameters for resolution d_{res} are given as:

$$d_{res} = \frac{c}{2f_{mod}} \sqrt{\frac{P_{mod} + P_{amb}}{P_{mod}^2} \frac{A_{illum}}{k_{opt} \cdot q_e(\lambda_{ir}) \cdot r \cdot \tau_{int}}} \tag{4.15}$$

with

P_{mod}:	power of modulated signal
P_{amb}:	power of ambient light
A_{illum}:	illuminated area
k_{opt}:	optical system constant
$q_e(\lambda_{ir})$:	quantum efficiency
r:	target reflectivity

This shows that resolution can be improved by higher modulation frequency, more power for the modulation signal, reduction of ambient light, downsizing of the illuminated area, highest possible target reflectivity and long integration time. To achieve this resolution for an arbitrary distance d the required optical power P_{emitt} of the emitter [Lang 00] has to be at least:

$$P_{emitt} = \frac{N_e \cdot \dfrac{A_{image}}{A_{pix}} \cdot \hbar \cdot c}{r \cdot \left(\dfrac{D}{2d}\right)^2 \cdot k_{opt} \cdot q_e(\lambda_{ir}) \cdot \lambda_{ir} \cdot \tau_{int}} \tag{4.16}$$

with

N_e:	number of electrons per pixel
A_{image}:	image area in sensor plane
A_{pix}:	light sensitive area of pixel
$\hbar$:	Planck's constant
D:	aperture of lens

For the power of the modulated signal and ambient light, the sensitivity of the sensor for the concerning wavelength provided in [Hein 01] as shown in fig. 4.6 has to be considered. With additional IR filters the relevant spectrum can be narrowed additionally.

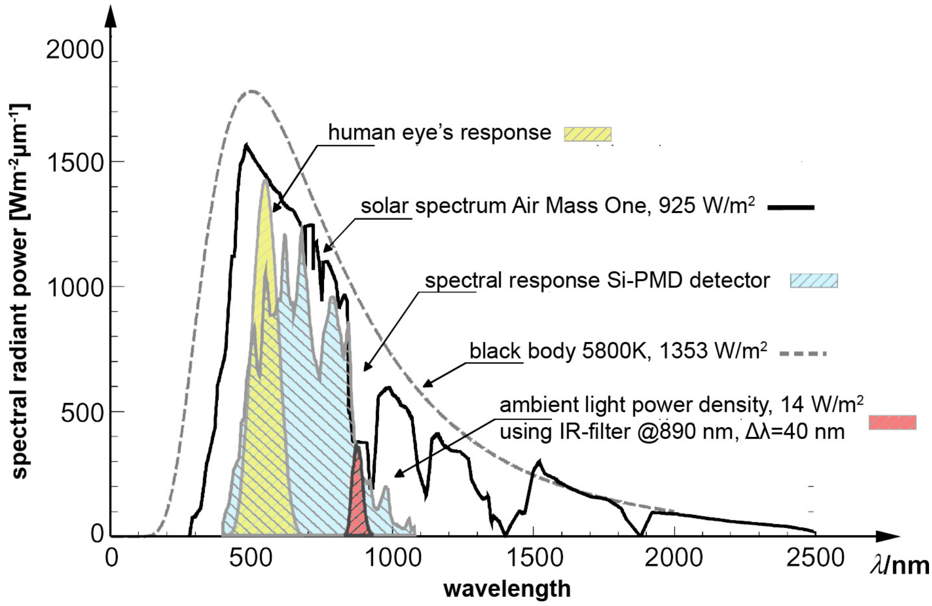

Figure 4.6: The comparison of the ToF frequency spectrum with spectra of sun light, visible light and infrared light help to choose the ideal frequency in the infrared range [Hein 01].

4.1.3 Actual ToF Cameras

There are several ToF cameras on the market that have to be taken into consideration. The development since the first publication of the ToF approach in 1999 [Lang 99, Schw 99] was rather fast. The first experiments with a commercial system started with a Mesa Imaging Swiss Ranger 3000 (table 4.1 [Oggi 05]) shown in fig. 4.7:

Table 4.1: Characteristics Swiss Ranger ToF camera, MESA Imaging AG, Zuerich, Switzerland [MESA 06, MESA 09].

Model	3000	3100	4000
Lateral resolution:		176 × 144 pixel	
Depth resolution:	2.5mm	2.5mm	2mm
Wavelength:		850nm	
Pixel dimension:		40µm × 40µm	
Modulation frequency:	20MHz	10 − 30MHz	29 − 31MHz
Non ambiguity range:	7.5m	15 − 5.0m	5.2 − 4.8m
Frame rate:	12 − 29fps	≤ 29fps	≤ 54fps
Modulation shape:		sine	
Year of introduction:	2005		2008

Compared to other cameras used at this time this system has a good performance but the small housing has no possibility to mount other adapters. In addition, it is not possible to grip the modulation signal. Therefore, we chose the German PMDvision 3k-S and 19k shown in fig. 4.8, which has a C-mount for the optics (the thread is nominally 1 inch in diameter, with 32 threads per inch) and makes it possible to

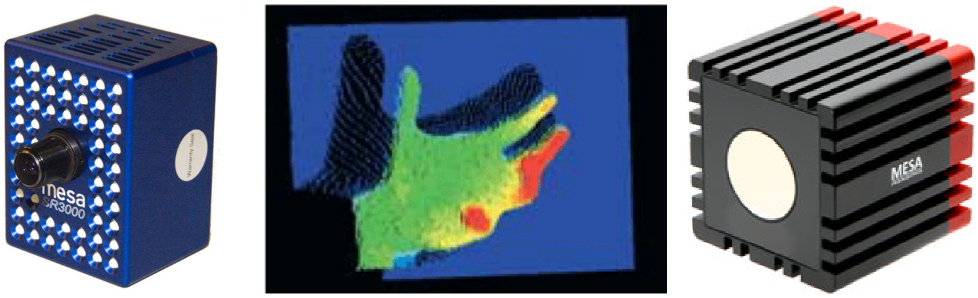

Figure 4.7: Swiss Ranger SR3000 (l) and SR4000 (r) ToF-camera and example images (m) [MESA 06, MESA 09]. Reprinted with kind permission of MESA Imaging AG, Zuerich, Switzerland.

access the modulation signal as there are external illumination units. The 3k-S has lower resolution (table 4.2) but an additional circuit for the suppression of backlight illumination (SBI):

Table 4.2: Characteristics PMD-3kS and PMD-19k ToF cameras, PMDTechnologies GmbH, Siegen, Germany [PMDv 05b, PMDv 05a].

Model	3k-S	19k
Lateral resolution:	64×48	160×120 pixel
Depth resolution:	6mm	
Wavelength:	870nm	
Pixel dimension:	$100\mu m \times 100\mu m$	$40\mu m \times 40\mu m$
Modulation frequency:	$10 - 30$MHz	
Non ambiguity range:	$15 - 5.0$m	
Frame rate:	≤ 25fps	≤ 15fps
Modulation shape:	rectangle	
Year of introduction:	2004	

Figure 4.8: 3k-S ToF-camera (l) and resulting distance (m) and intensity (r) example image [PMDv 05b, PMDv 05a]. Reprinted with kind permission of PMDTechnologies GmbH, Siegen, Germany.

In the United States, Canesta developed a similar sensor [Cane 08] that is called Jaguar [Gokt 04]. This chip (table 4.3) is used for example for the Fotonic C70 sensor system as shown in fig. 4.9:

Table 4.3: Characteristics Jaguar ToF camera, Canesta Inc., Sunnyvale, CA [Gokt 04].

Model	Jaguar
Lateral resolution:	160×120 pixel
Depth resolution:	3mm
Wavelength:	808nm
Pixel dimension:	$50\mu m \times 50\mu m$
Modulation frequency:	$44 - 50$MHz
Non ambiguity range:	$3.4 - 3.0$m
Frame rate:	$50 - 75$fps
Modulation shape:	rectangle
Year of introduction:	2008

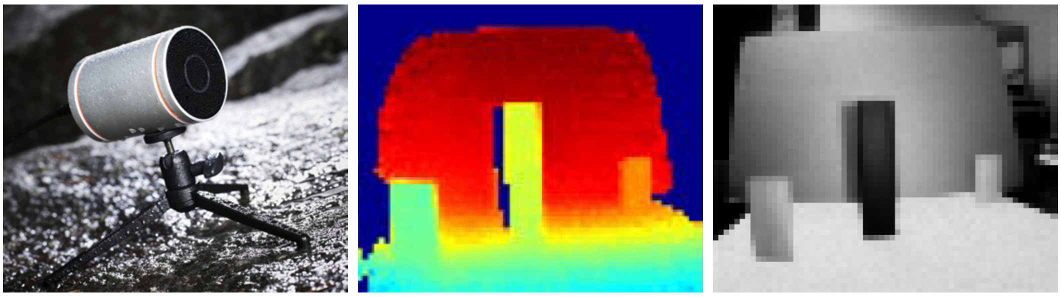

Figure 4.9: Fotonic C70 [FOTO 10] sensor based on Canesta Jaguar chip with distance (m) and intensity (r) example images [Gokt 04]. Reprinted with kind permission of Fotonic, Stockholm, Sweden, and Canesta Inc., Sunnyvale, CA .

For our latest research the PMDvision CamCube 2.0 (table 4.4, fig. 4.10) was utilized. It still provides a C-mount adapter and external illumination units but smaller size and higher lateral resolution.

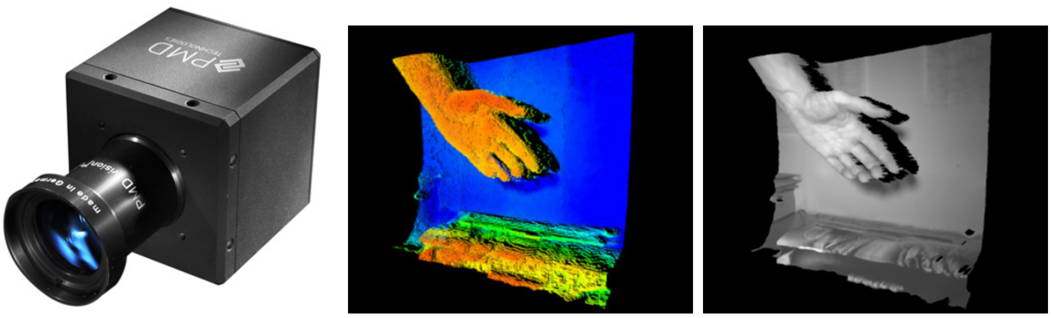

Figure 4.10: CamCube ToF-camera with distance (m) and intensity (r) example images. Reprinted with kind permission of PMDTechnologies GmbH, Siegen, Germany [PMDv 09b, PMDv 09a, PMDv 10].

Table 4.4: Characteristics CamCube ToF camera, PMDTechnologies GmbH, Siegen, Germany, CamCube [PMDv 09b, PMDv 09a, PMDv 10].

Model	1.0	2.0	3.0
Lateral resolution:	204×204 pixel		200×200 pixel
Depth resolution:	3mm		
Wavelength:	870nm		
Pixel dimension:	$40\mu m \times 40\mu m$		
Modulation frequency:	$20 - 40$MHz		
Non ambiguity range:	$7.5 - 3.75$m		
Frame rate:	≤ 25fps		≤ 40fps
Modulation shape:	rectangle		
Year of introduction:	2009		2010

4.2 Existing Medical ToF Applications

There already are some ToF applications addressing problems in the medical environment. Two of them are quite promising and will be presented below.

4.2.1 ToF Sensor for Respiratory Motion Gating

Current methods to account for respiratory motion use 1-D surrogate signals to determine respiratory phases [Tart 06]. Using this information, it is possible to either reconstruct 4-D computer tomography (CT) volumes or to apply tumor tracking or gating procedures for cancer treatment based on the surrogate signal [Sepp 07]. The ToF sensor's high lateral resolution allows to define multiple regions of interest to compute an anatomy-adaptive multidimensional respiratory signal from 3-D surface measurements without the use of markers. The setup is quite easy as can be seen in fig. 4.11.

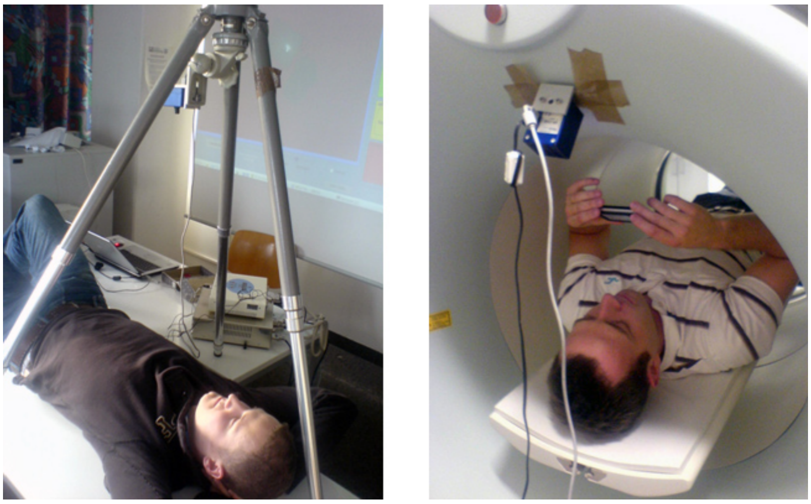

Figure 4.11: Example setup in the Lab (l) and in a positron emitting tomography scanner (r) with a ToF camera fixed above the patient for respiratory motion gating using ToF.

It is possible to compute a respiratory signal for both the thorax and the abdomen (fig. 4.12) in real-time ($\sim$ 15fps) with a standard PC hardware (Pentium M 1.0 GHz). Comparing a ToF based respiratory signal with the signal acquired by a commercially available external respiratory gating system (ANZAI Medical Co.), the respiratory peaks can be recognized at the same position [Scha 08, Holl 08b].

4.2.2 Patient Positioning using 3-D Surface Registration

Patient positioning is a crucial issue in the field of radiotherapy. In a common work flow, a CT scan of the patient is acquired a few days before therapy in order to plan the treatment. Right before the therapy starts, the patient has to be positioned accurately in the same way like for acquiring the planning data to ensure that the treatment plan can be applied correctly [Brah 08]. With the ToF technology a patient's position can

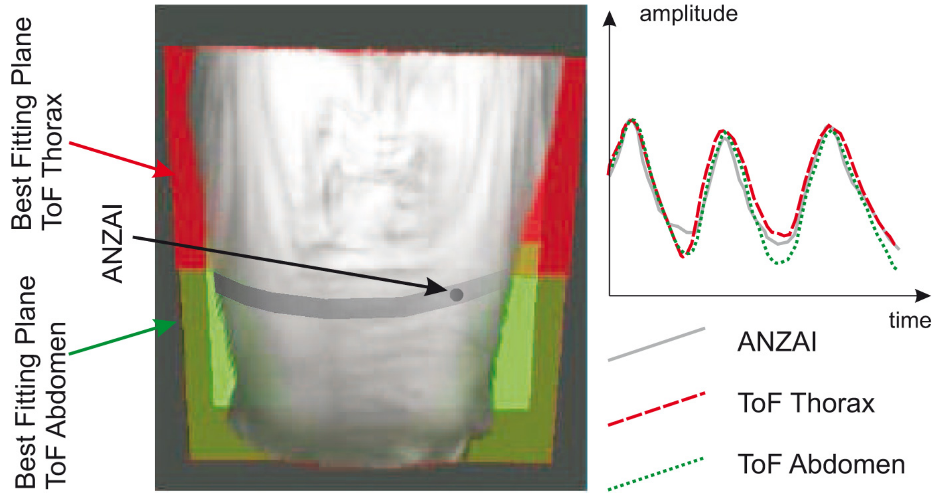

Figure 4.12: 3-D model of the automatically segmented upper part of the body of a patient. The colored planes are regression planes used to determine two independent respiratory signals (gray: ANZAI reference, red: chest, green: abdomen) [Scha 08]. Reprinted with kind permission of Metrilus GmbH, Erlangen, Germany.

be corrected by acquiring body surfaces. The surface measurement of the patient's body during the planning CT scan is followed by a second one performed right before or even repeatedly during the treatment session. Using 3-D surface registration, the patient's misalignment can be identified and corrected. The surface matching process is divided into segmentation and registration processes. Before the two point sets are registered, the patient's body has to be separated from the background. After this preprocessing step an iterative closest point (ICP) algorithm is applied to the datasets in order to determine translation and rotation parameters to correct the position of the patient as shown in fig. 4.13 [Scha 09].

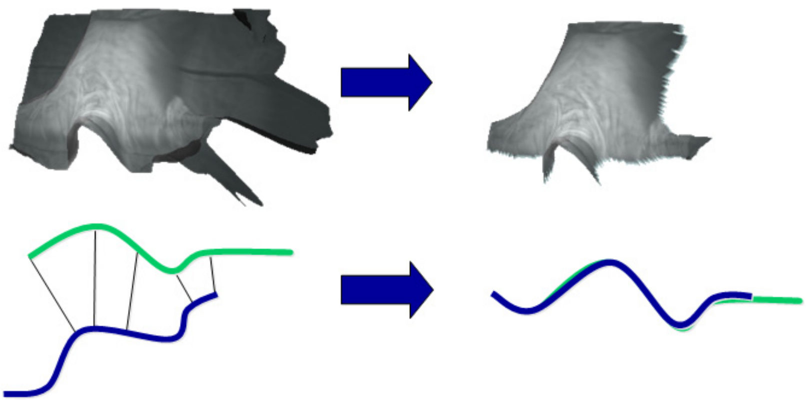

Figure 4.13: Body-backgound segmentation with ToF data and following ICP body registration. Reprinted with kind permission of Metrilus GmbH, Erlangen, Germany.

Fig. 4.14 shows an error image between a reference surface and a moving surface. Green colors indicate an error of 0mm, whereas red indicates an error of more than ±10mm [Holl 08b].

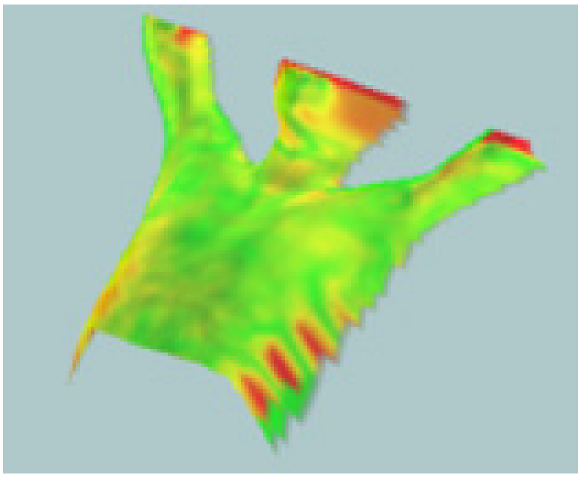

Figure 4.14: Evaluation of patient positioning with green for an error of 0mm and red for an error of more than 10mm [Holl 08b]. Reprinted with kind permission of Metrilus GmbH, Erlangen, Germany.

4.2.3 ToF Application Discussion

ToF cameras are off-the-shelf technology. Since automotive and consumer electronics industry are heavily interested in this emerging technology a lot of research investment is allocated to improve the chip design. Currently, a typical ToF camera is available for about 5,000 EUR. But if automotive and consumer applications enable large-scale production, prices will rapidly fall and innovation cycles can be expected to be quite short. Although prices are too high for the consumer market at the moment, there are several medical applications and auspicious approaches to improve health care in a simple but helpful way.

4.3 Inertial Sensor Basics

Inertial sensors play a major role for the approach proposed in section 6.1. Therefore their characteristics will be explained briefly below.

4.3.1 Inertial Measurement

There are two main types of inertial sensors: accelerometers and gyroscopes. Accelerometers are able to measure linear accelerations, Gyroscopes can measure angular velocities. For inertial navigation in a 3-D space there are three degrees of freedom for linear acceleration and another three degrees of freedom for rotation. Therefore, an Inertial Measurement Unit (IMU) for navigation purposes needs not only a three-axis accelerometer but also three gyroscopes. Movements are always defined with respect to a reference system which can be e.g. the world coordinate system or the board coordinate system. With a gimbaled system the sensors have to be held in their original position using a feedback loop control system, whereas the carrying platform is moving. The orientation with respect to the reference coordinate system remains. The platform position change has to be calculated by double-integrating the acceleration values to get the velocity and the position. The gravity-related offset has to be compensated. With a strap down system the sensors are fixed rigidly on the carrying platform. The measured acceleration depends on the attitude towards the reference system and changes according to angular velocities measured by gyroscopes. Therefore the acceleration measures have to be corrected with a rotation matrix while applying the double-integration. An important advantage is the immediate availability of the rotation angles in the board coordinate system.

4.3.2 Accelerometer Functional Principle

In the simplest form an accelerometer is a seismic proof mass moving only in one direction and held in a mid-position by a spring. The higher the acceleration the higher the deflection of the mass from its neutral position. Therefore, the extension is a direct measure for the acceleration.

With Micro Electro-Mechanical Systems (MEMS) it is possible to integrate proof mass, spring and capacitor for reading out the dilatation in miniaturized silicon structures [Lott 98]. With changing accelerations in measurement direction a capacity variation between fixed and mobile electrodes (fingers) can be imagined in the model shown in fig. 4.15. MEMS accelerometers have a very small and thin package in a mm range. By adequate structure design they can detect three axes simultaneously (triaxial) and with a price of a few Dollars they are at very low cost due to high volume manufacturing.

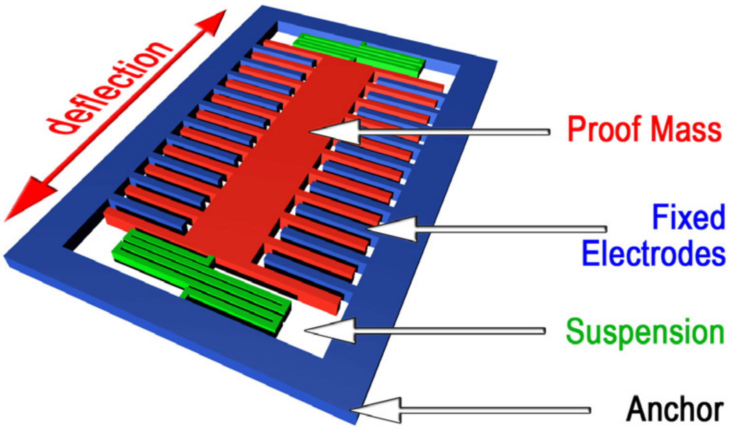

Figure 4.15: Model of the silicon mechanical structure of a 1-D accelerometer with proof mass (red), fixed electrodes (blue) and suspension springs (green). Acceleration along the deflection axis decreases the distance of the orthogonal fingers of the proof mass and the fixed electrodes. The capacity between fixed electrodes and proof mass depends on variations of their distance since their relevant area remains the same [Bais 08].

4.3.3 Inertial Sensor Parameters

Bias

The underlying constant deterministic offset is called bias. Since it is linear and stable the bias as shown in fig. 4.16 l. can be determined directly after fabrication. As it remains constant it can be eliminated just by adding that value.

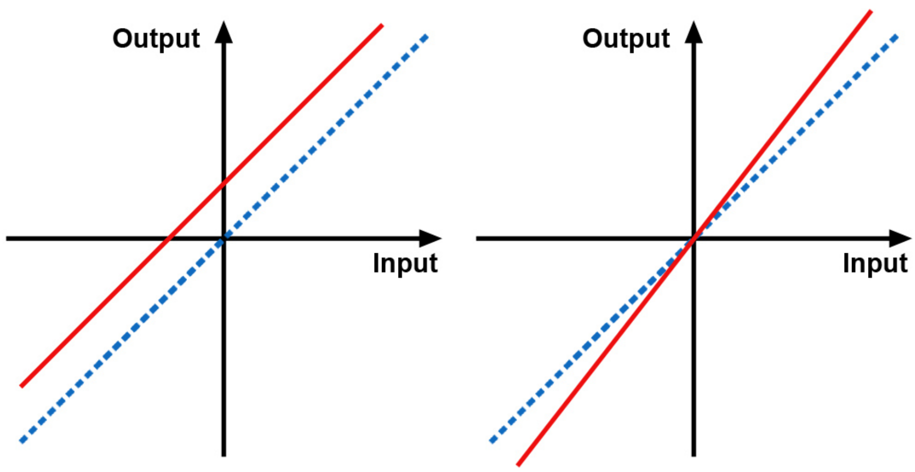

Figure 4.16: Schematic illustration of original acceleration (blue) and deviation caused by bias (l) and scaling error (r) with MEMS accelerometers.

Random Drift

The variable random offset is called drift. It looks exactly the same as the bias in fig. 4.16 l., but it is changing randomly and cannot be predicted.

Scaling factor and Misalignment

The scaling error results from an incorrect factor of one axis. The misalignment error results from imprecise mounting and crosstalk between the axes. An example for the scaling error on one axis is depicted in fig. 4.16 r. This has impact on all three axes. Each axis measures fractions of acceleration, which should be measured on another one. This causes a double error as not only the scaling of the respective axis is incorrect.

Nonlinearity

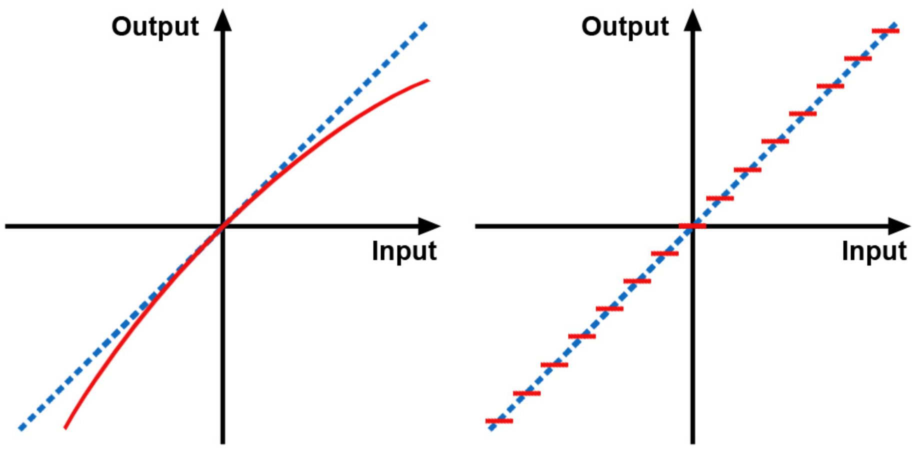

Figure 4.17: Schematic illustration of original acceleration (blue) and deviation caused by nonlinearity (l) and quantization error (r) with MEMS accelerometers.

A nonlinear scaling factor as shown in fig. 4.17 l.is hard to compensate. Usually there has to be inserted a nonlinear correction term or a look-up table, but in our case with ±0.5% of the measurement range [STM 08b, STM 09] it is an order lower than the other errors. Therefore, it is not essential to correct it.

Quantization Noise

The quantization error as shown in fig. 4.17 (r) occurs due to a low resolution analog-digital converter. For a converter with 8-bit quantization and a value range R this leads to an error F_q of:

$$F_q = \frac{R}{2^8} = 0.4\% \cdot R \tag{4.17}$$

This error can only be reduced applying a temporal filter using several subsequent samples. For our purposes the error is too low to play a major role.

Resulting Preprocessing Correction Matrix

Misalignment, scaling error and constant offset between original forces F_{x0}, F_{y0} and F_{z0} and measurements F_x, F_y and F_z can be analyzed and permanently corrected with a calibration matrix [Holl 05]:

$$\begin{pmatrix} F_x \\ F_y \\ F_z \end{pmatrix} = \begin{pmatrix} M_{11} & M_{12} & M_{13} & T_x \\ M_{21} & M_{22} & M_{23} & T_y \\ M_{31} & M_{32} & M_{33} & T_z \end{pmatrix} \cdot \begin{pmatrix} F_{x0} \\ F_{y0} \\ F_{z0} \\ 1 \end{pmatrix} \tag{4.18}$$

This correction matrix has to be quantified for each sensor once by recording a series of measurement values with known ground truth and a subsequent least square pseudo inverse. The resulting rotation parameters $M_{11}...M_{33}$ and translation parameters T_x, T_y and F_z which are only important if angular velocities are measured as well are stored for the permanent correction. While the use of newer sensors, especially supply voltage depending scaling errors and misalignment are protruding errors which have to be corrected necessarily.

Part III

Extensions for Endoscopic Imaging with NOTES

Chapter 5

Novel Endoscopic Image Extension by Time-of-Flight

5.1 ToF Parameters

For the use of ToF cameras it is important to know how environmental factors can affect the camera's parameters. Therefore the above proposed functional principle will be simulated and external factors will be analyzed either in the model or in real experiments partly presented in [Ritt 07a, Ritt 07b].

5.1.1 ToF Simulation

To understand the previously presented functional principle of Time-of-Flight distance measurement a simulation tool (sec. A fig. A.1) was created to show how the signals and their mixing products behave. The black line through the origin shows an ideal result for a modulation frequency of 75MHz, where a complete phase shift of 2π means a measured distance of 2m. The cyan line shows the reflected optical signal, whose photons generate electrons on the surface of the chip that yield a charge and therefore an electrical potential at the measuring electrodes. The blue line represents the electrical reference signal. This reference signal is varied subsequently with a stepwise (steps $k = 1...4$) increased phase shift resulting from angular velocity $\bar{\omega}$ and shifting time τ_k according to eq. 4.4 on p. 37. The first step with $k = 1$ is depicted in fig. 5.1. The reference signal is applied between the measuring electrodes and divides the charge generated by the incoming photons variably. In a simple example, the simulated amplitude of measuring and reference signal is $1V$ and the offset is $1.25V$. The green line represents this mixed signal of incoming and reference signal at the electrode with the higher potential with respect to the reference signal. In the simulation the resulting voltage is estimated via the correlation function of both. Using the atan2 function the distance can be estimated, the result is shown with the magenta line. The difference between this estimation and the black line through the origin symbolizing the ground truth is visualized with the red line of the bias. This line incorporates the offset phase shift which is $\frac{\pi}{4}$ in this simulation. Additionally, it is very important to know that there is a systematic estimation error, too. It is caused by the non-linearity of the estimation method which is only approximated for sine shaped signals. In a real system the modulation signal assumes other shapes. The effects will be shown in simulations. For each step of the reference signal shift there is a sine modulation on the left and a rectangle modulation with fast rise and fall time on the right to clarify the deviations for different shapes. In a second step the reference signal is shifted by $\frac{\pi}{2}$ for $k = 2$ according to eq. 4.4 on p. 37. This phase shift is simulated in fig. 5.2.

As the signal is symmetric, the following equation is true for $N = 4$ in eq. 4.5:

$$\cos(\varphi_d + \bar{\omega}\tau_{k+2}) = \sin(\varphi_d + \bar{\omega}\tau_k) \tag{5.1}$$

Instead of shifting the reference signal again the second electrode in step one with $k = 1$ is used to get the voltage of the mixed signal for $k = 3$. The result is illustrated in fig. 5.3. Similar to $k = 3$ the second electrode in step two with $k = 2$ is used to get the potential of $k = 4$ visible in fig. 5.4. Using the advantage of two electrodes it is possible to reduce the phase shifts to only $k = 2$ after the original $k = 1$. As for

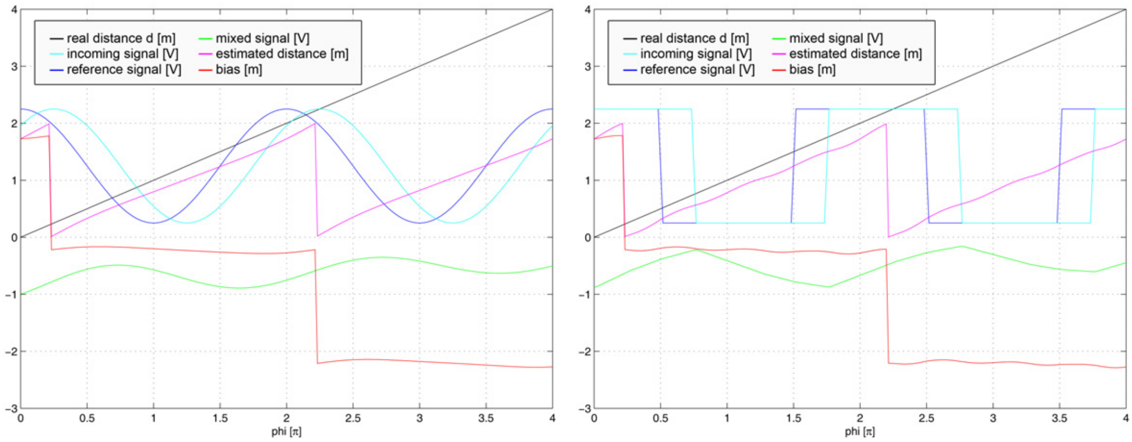

Figure 5.1: Reference signal (l: sine, r: rectangle) for k=1. Real distance (black), estimated distance (magenta) and bias (red) are indicated by [m], incoming signal (cyan), reference signal (blue) and mixed signal (green) are indicated by [V].

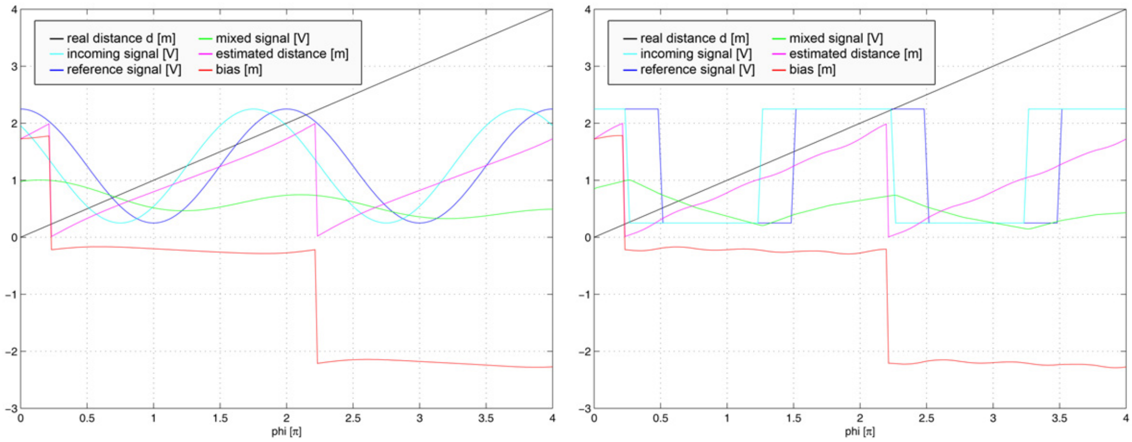

Figure 5.2: Stepwise increasing shift of the reference signal (l: sine, r: rectangle) with k=2. Real distance (black), estimated distance (magenta) and bias (red) are indicated by [m], incoming signal (cyan), reference signal (blue) and mixed signal (green) are indicated by [V].

eq. 4.2 and eq. 4.12 just the difference of the potential on both electrodes at $k = 1$ and $k = 2$ is required. The procedure can be simplified again by measuring the potential between the two electrodes without regarding the potential to the ground. Only the offset cannot be determined that way. Having a closer look on the modulation signal shape a shape-dependend non-linearity can be detected. The real signal lies between sine or cosine modulation and rectangle modulation, depending on the manufacturer and the applied system. The PMD 3kS uses a noisy rectangle signal as can be seen in the oscilloscope plot of the electrical reference signal in fig. 5.5. Therefore the deviation has to be corrected. Using the measurement setup in fig. 5.6 it is possible to determine the shape of an emitted optical PMD 3k-S modulation signal:

According to fig. 5.7 the PMD modulation signal is not a perfect rectangle but rather a rectangle than a sine. Nevertheless it converges slightly to a sine with higher frequencies as shown more detailed later in section 5.4.5 on p. 87.

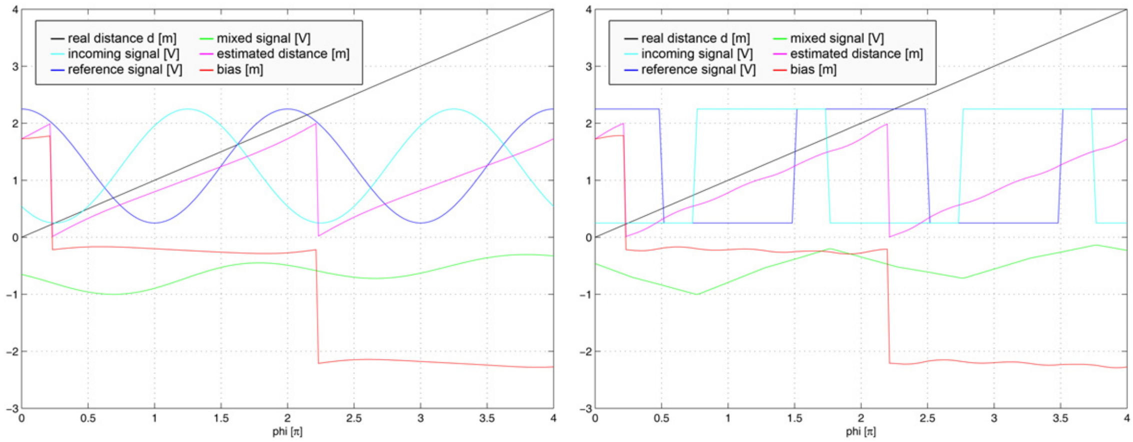

Figure 5.3: Stepwise increasing shift of the reference signal (l: sine, r: rectangle) with k=3. Real distance (black), estimated distance (magenta) and bias (red) are indicated by [m], incoming signal (cyan), reference signal (blue) and mixed signal (green) are indicated by [V].

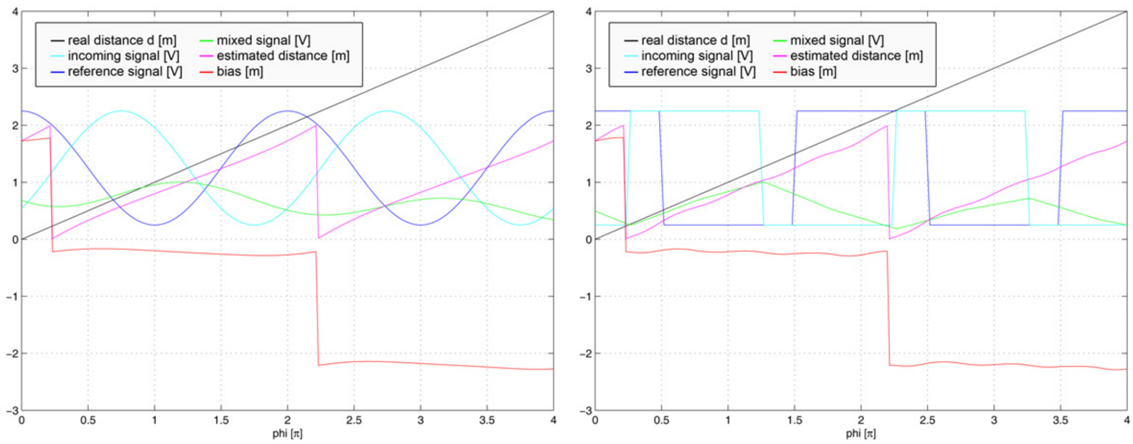

Figure 5.4: Stepwise increasing shift of the reference signal (l: sine, r: rectangle) with k=4. Real distance (black), estimated distance (magenta) and bias (red) are indicated by [m], incoming signal (cyan), reference signal (blue) and mixed signal (green) are indicated by [V].

The magnified simulated signal in fig. 5.8 shows different distance estimations and corresponding a different bias depending on the used modulation shape. Therefore every special shape needs a calibration with a lookup table to correct that specific error. That is the main challenge for ToF manufacturers to achieve better results. For their specific illumination unit they have to measure with known distances and to record the correction terms over the whole range given by the modulation frequency f_{mod} as shown in eq. 4.14 on p. 40 .

5.1.2 Color and Reflectivity

Other parameters that influence the measured distance are color and reflectivity of the surface that the ToF camera points at. This is due to amplitude variations in

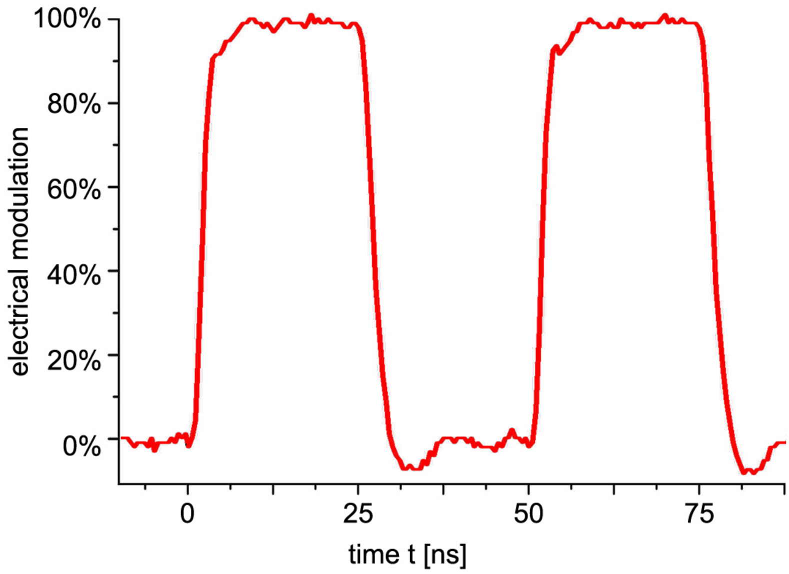

Figure 5.5: Electrical PMD 3k-S modulation signal with a frequency of 20MHz and rectangle shape.

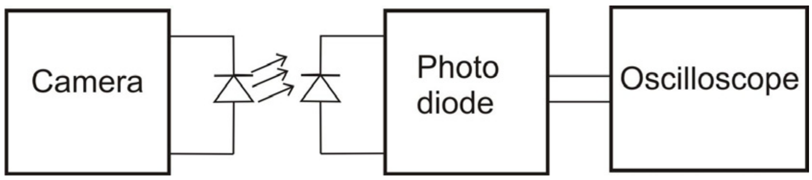

Figure 5.6: Measurement setup for the determination of the optical LED modulation shape.

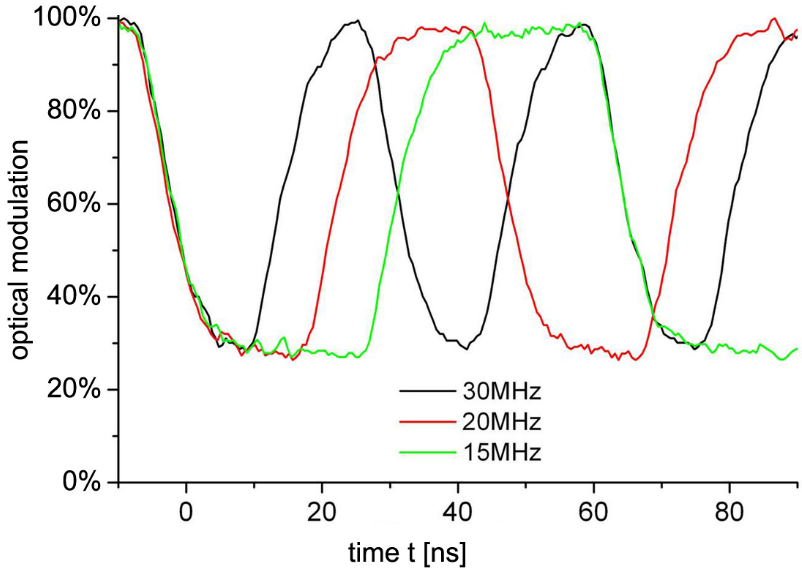

Figure 5.7: Results of the optical LED modulation shape measurement.

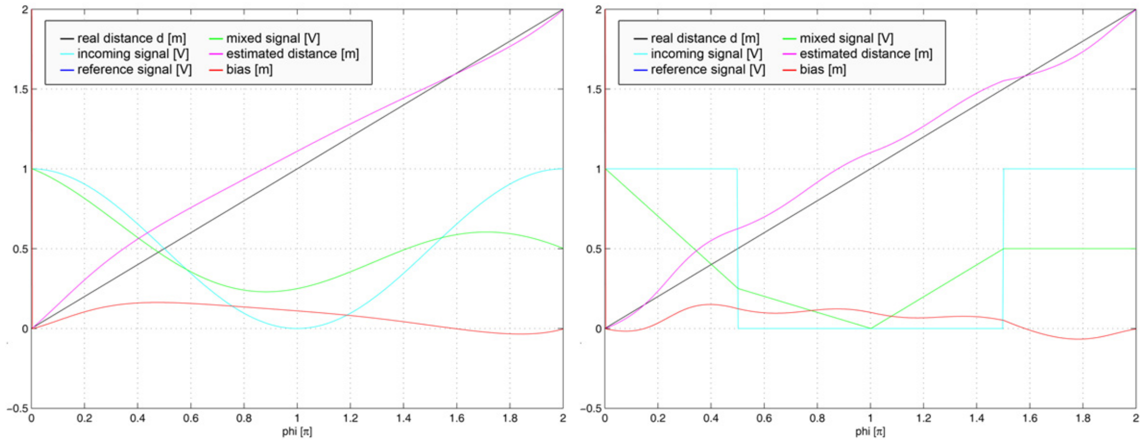

Figure 5.8: Simulated wave shape dependency (l: sinus, r: rectangle). Real distance (black), estimated distance (magenta) and bias (red) are indicated by [m], incoming signal (cyan), reference signal (blue) and mixed signal (green) are indicated by [V].

the measured electrical signal since less reflected light means a higher portion of unmodulated ambient light, especially during the observation of black objects. In order to quantitatively assess the variations that are caused by surface color and reflectivity, the test pattern shown in fig. 5.9 was created according to the standard PTV Circle television test pattern.

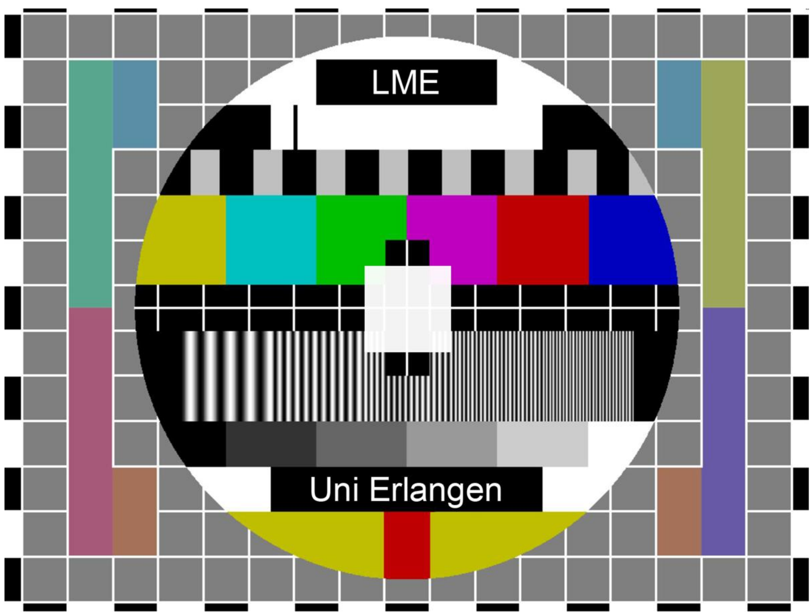

Figure 5.9: LME test pattern for the analysis of color and reflectivity depending errors according to the standard PTV Circle television test pattern.

The camera was pointed at the test pattern and a gray-scale amplitude image with corresponding distance image was recorded. The obtained distance image supplied by the used ToF shown in fig. 5.11 depends on color and reflectivity. On the gray-coded distance image it is not observable that the depicted object is planar although it is just printed on a paperboard hardcopy. The red pixels symbolize that the distance cannot be determined at all. The amplitude image supplied by the used ToF shown in fig. 5.10 represents the amount of reflected light and depends not only on the color and reflectivity of the observed object, but also on the illumination shape.

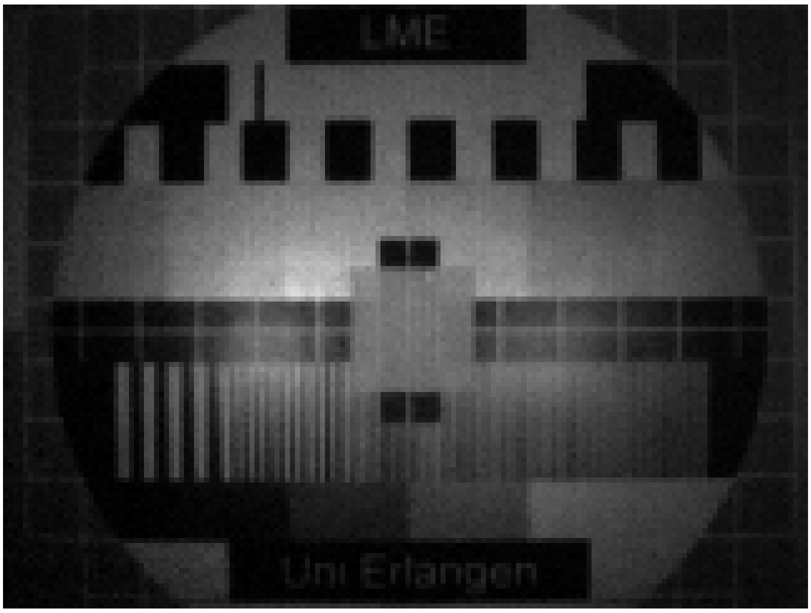

Figure 5.10: Amplitude image recorded by the used ToF camera depending on color and reflectivity. Bright pixels represent high reflectivity with sufficient illumination whereas dark pixels represent low reflectivity and/or less illumination.

It is clearly visible that the reflected amplitudes have a considerable influence on the measured distances. Obviously the combination of illumination and reflectance is the decisive factor whether sufficient light for estimation reaches the sensor.

5.1.3 Temperature Variation

Whenever the camera is started from a cold state, a variation of the measured distance data within the first 1000 frames and above can be observed as shown in the measurement of a single pixel in a still scene visible in fig. 5.12. That indicates a significant temperature dependency of ToF-cameras until a constant operating temperature is reached.

To get reliable information on this phenomenon, a fixed distance in a climatic chamber was measured under varying temperature conditions as shown in fig. 5.13. The magenta curve shows the temperature in the climate chamber and the green curve shows the temperature of the ToF camera cooling air. Due to slow heat dissipation the cooling air temperature is always a little bit above the surrounding air. Changes of the ToF temperature are identifiable some minutes after the temperature within the climate chamber has changed.

Comparing the temperature change and the distance error, a significant correlation as shown in fig. 5.14 is detected. If the temperature goes below a boundary of about 24°C there is nearly no influence, but above there is a high correlation.

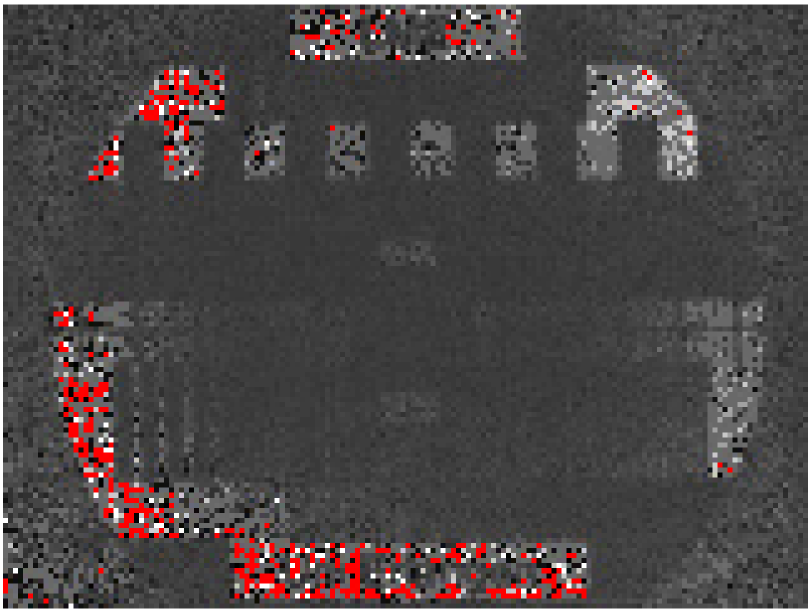

Figure 5.11: Distance image depending on color and reflectivity. Bright pixels represent short distances whereas dark pixels represent longer distances. For red pixels no distance value could be determined.

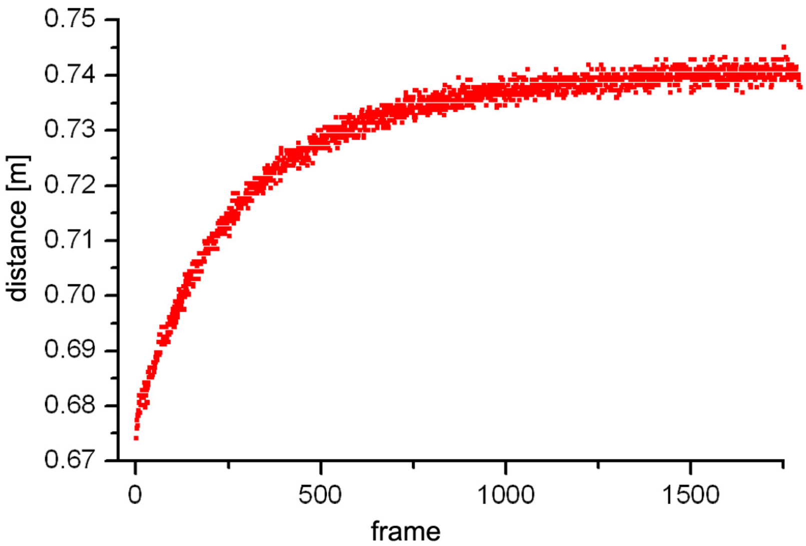

Figure 5.12: Increasing temperature after turning the camera on results in a temperature depending error which is called ”drift”.

To compensate this temperature depending error, a black-box identification method using a time-discrete first order state-space model estimation of the response on an arbitrary input signal as shown in fig. 5.15 can be used [Holl 05].

The deterministic identification for a memory afflicted system as shown in fig. 5.16 can be done by determining its transmission parameters A, B, C, and D. The transmission is modeled by tracking the input temperature u directly via D

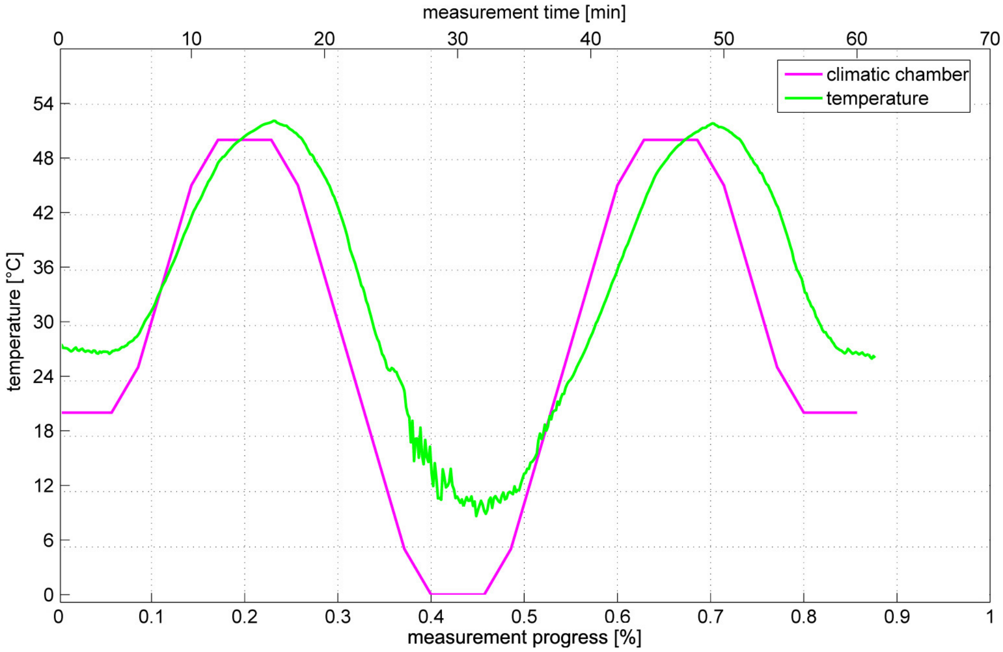

Figure 5.13: Temperature variation (magenta) in a climatic chamber leads to a following camera temperature variation (green).

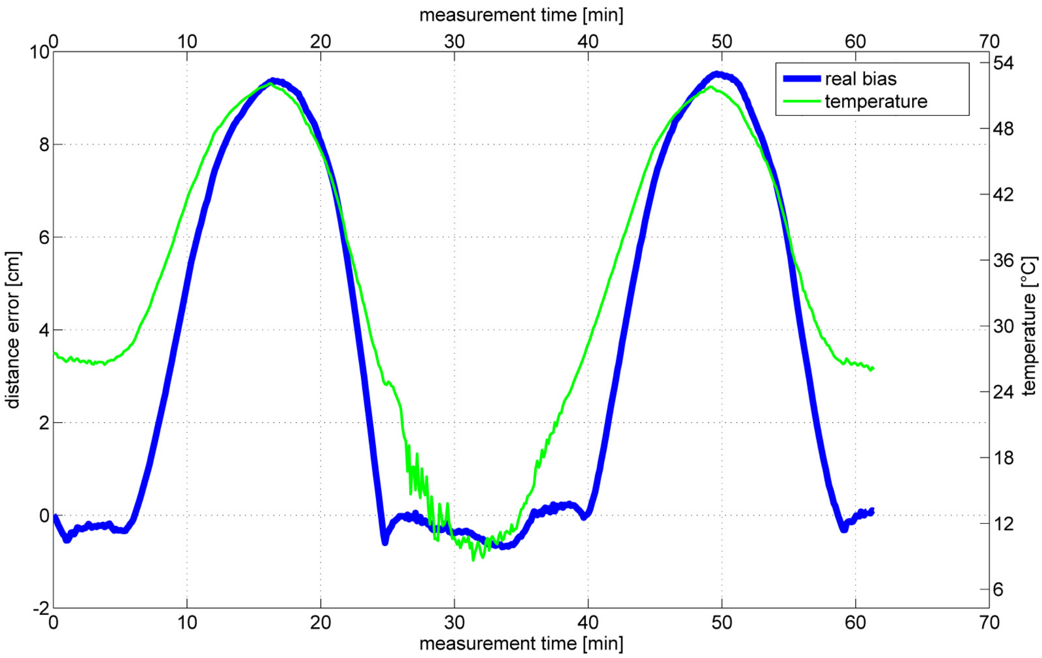

Figure 5.14: Temperature variation (green) of the camera leads to a following bias of the distance measurements (blue).

to the output error y and via B to the differentiated state space value z which is continuously fed back via A and also contributes to the output error y via C as pointed out in eq. 5.2, eq. 5.3 and eq. 5.4.

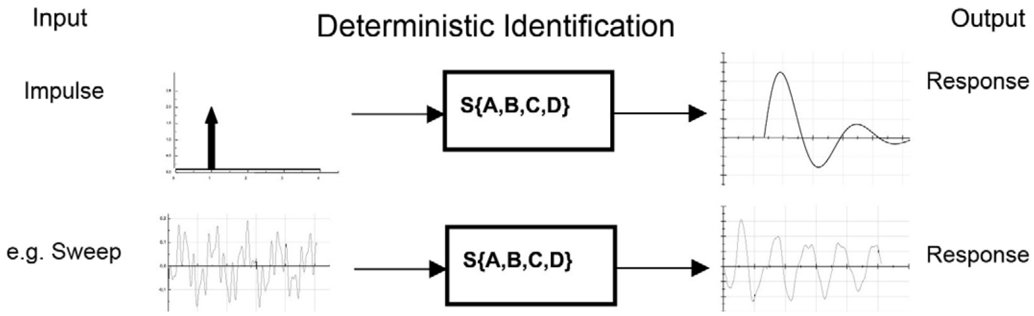

Figure 5.15: Black-box identification method of a system S with unknown transmission parameters A, B, C and D [Holl 05].

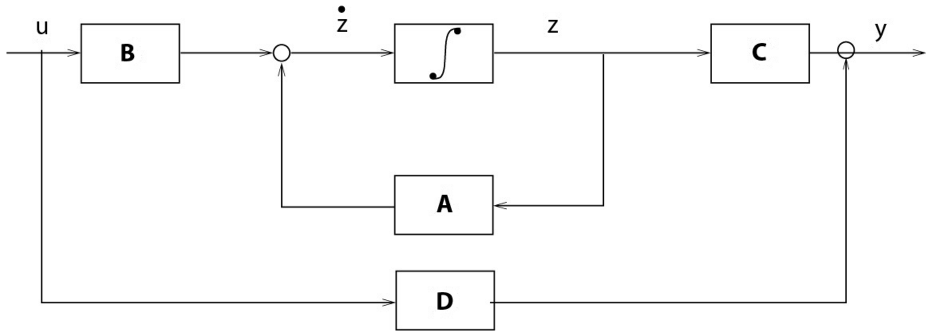

Figure 5.16: Deterministic identification of a system with input u, output y, and unknown transmission parameters A, B, C and D using a time-discrete first order state-space model [Holl 05].

$$z_{k+1} = Az_k + Bu_k \tag{5.2}$$

$$y_k = Cz_k + Du_k \tag{5.3}$$

$$z_0 = u_0 = 0 \tag{5.4}$$

with

u_k: input (temperature)
y_k: output (bias)
z_k: state space value

After recording the measurement values and representing them as shown in eq. 5.5, the system parameters A, B, C, and D are estimated with the Matlab system identification toolbox [Holl 05].

$$\begin{pmatrix} y_1 \\ \vdots \\ y_k \end{pmatrix} = C \cdot \begin{pmatrix} z_0 & u_0 \\ \vdots & \vdots \\ z_{k-1} & u_{k-1} \end{pmatrix} \cdot \begin{pmatrix} A \\ B \end{pmatrix} + D \cdot \begin{pmatrix} u_1 \\ \vdots \\ u_k \end{pmatrix} \tag{5.5}$$

Once these state space parameters have been determined, the estimation of the future bias for correction purposes is easily done as shown in fig. 5.17 as long as the temperature is known.

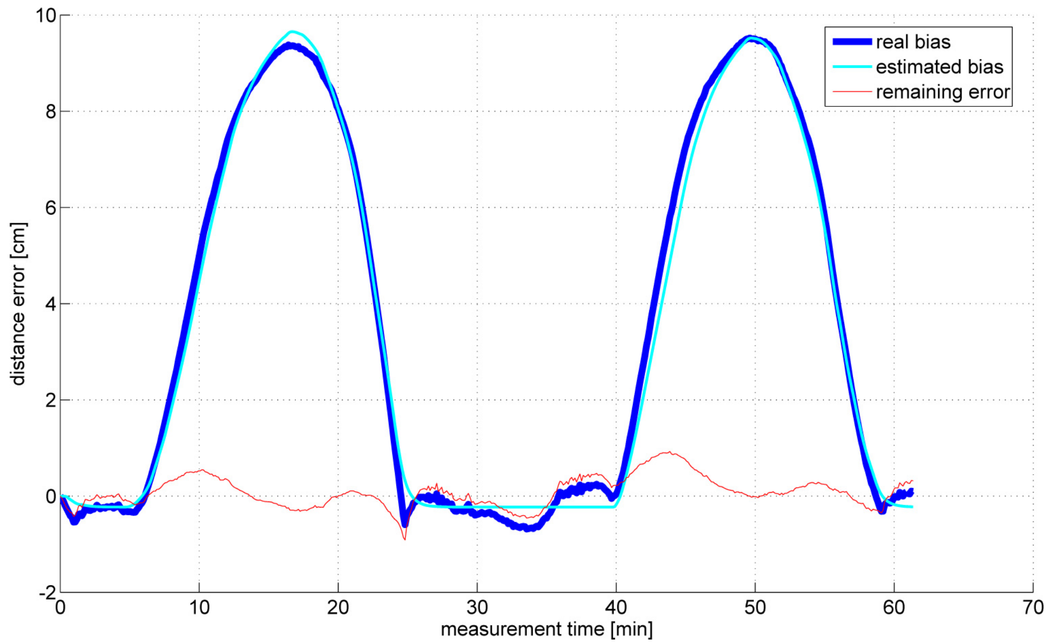

Figure 5.17: Bias correction results with real bias (blue), estimated bias (bright blue) and remaining error (red).

5.1.4 Modulation Frequency

The modulation frequency f_{mod} has an influence on the non-ambiguity range as shown in eq. 4.14 on p. 40. Further measurements showed that the standard deviation is increased with lower modulation frequencies as shown in fig. 5.18. Thus, it is not only important to have a frequency depending calibration but also to use the highest possible modulation frequency.

5.1.5 Integration Time

Each measurement cycle of the ToF camera has a defined constant duration, which is called integration time. During this integration time a charge is accumulated at the two measuring electrodes. Each measurement step with increasing phase shift is repeated for the same integration time. The longer the integration time the higher is the accumulated charge for each step. This results in a higher amplitude of the mixed signal according to eq. 4.12 on p. 39 and is shown in the measurement illustrated in fig. 5.19 [Ritt 07a].

In further measurements it could be shown that by varying the integration time a slight bias can be recognized and corrected as shown in fig. 5.20. A low integration time results in a high uncertainty with a high standard deviation. This is caused by statistical effects of the electron-generation and photon-absorption process [Lang 99].

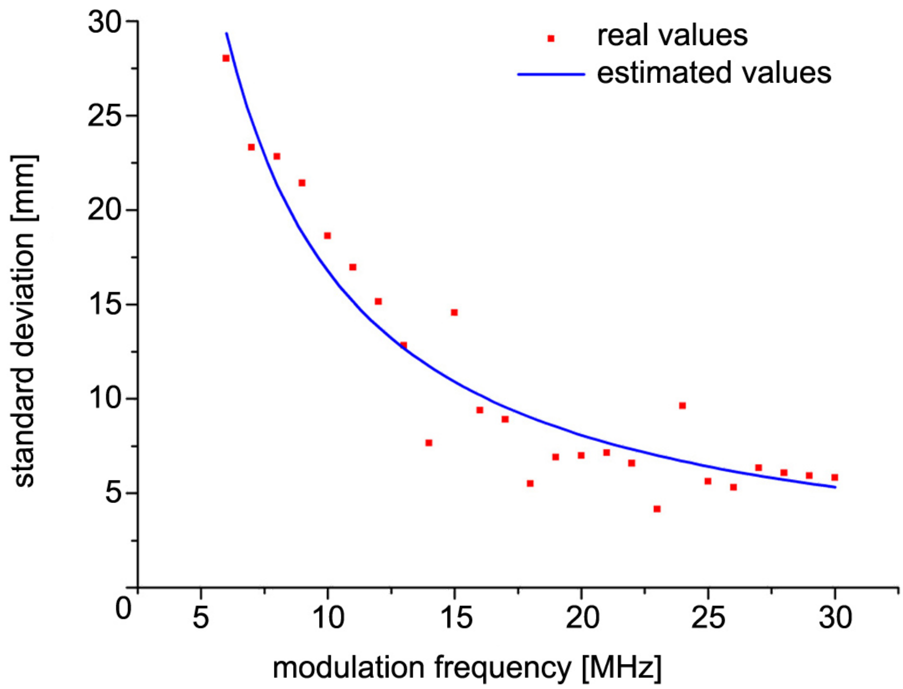

Figure 5.18: Standard deviation variation due to modulation frequency changes within a still scene. Single measurement points are approximated by a best fitting line.

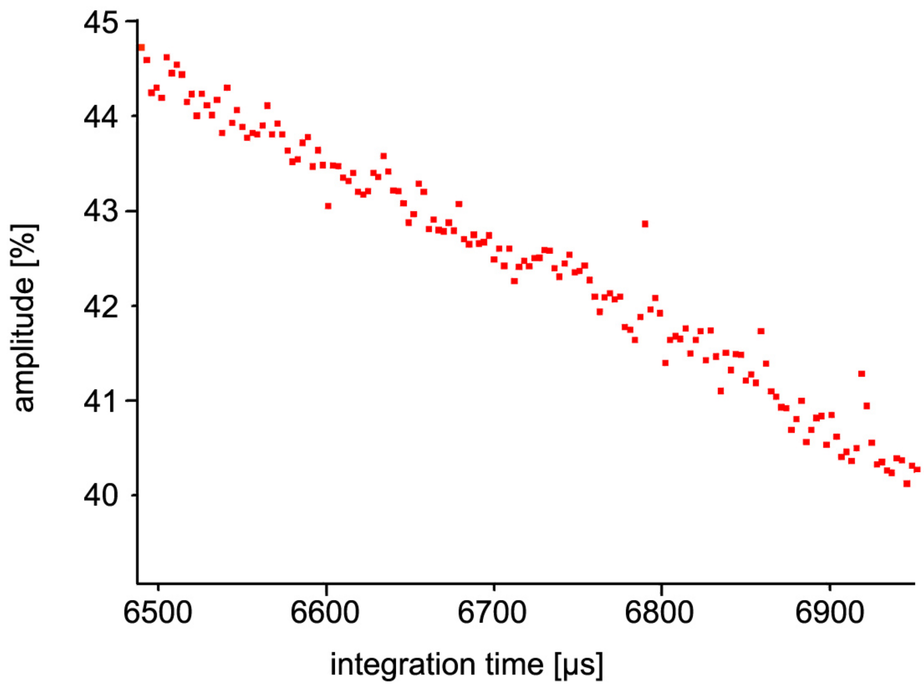

Figure 5.19: Amplitude depending on a varying integration time for a brown carton with a distance of 50cm.

From a special point a too high integration time leads to high uncertainty caused by saturation effects, too [Albr 07]. The pixels are only able to store a certain amount

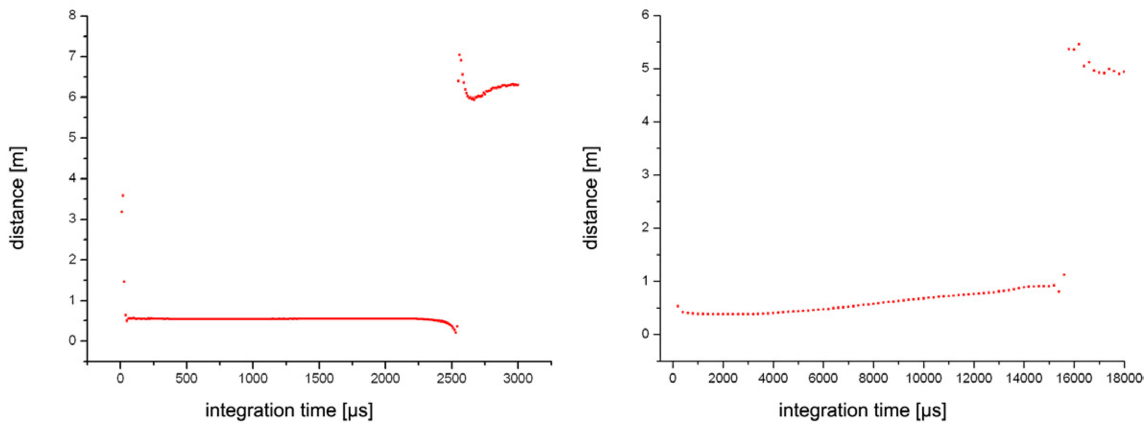

Figure 5.20: Measured distances are influenced by erroneous drift for a too high integration time (l: pmd, r: mesa).

of charge, which means a limited amount of electrons. The electrons themselves are generated by the photons (photo-effect). In eq. 4.2 on p. 36, voltage differences are used to calculate the distance. For the case of having the same charge on the constant electrode's capacity, these differences become nearly zero and no distance can be measured. If the differences are very small, the output distance becomes very sensitive to slight variations according to eq. 4.9 on p. 39 and therefore the distance value has a high uncertainty. The region of 'correct' integration time varies with distance and reflectivity of the observed object. For less reflectivity or distant objects, this region is shifted to higher values, which results in longer integration time. For higher reflectivity and closer objects this region shifts to lower values, which means shorter integration time (fig. 5.21). Therefore, it is necessary to find the right integration time for any observed object. When adjusting the integration time the real time data acquisition requirement has to be considered, too. Manually adjusting the integration time has major drawbacks. As it takes between $5 - 10$s to adjust it manually, we need another reliable way to decide which integration time would be the best. With fast automated integration time adaption, confusions and inconveniences for the surgeon and the medical staff caused by unstable images can be avoided.

During the experiments it turned out that the amplitude image supplied by the used ToF cameras is a good indication of the reliability of the distance values as shown in fig. 5.22. There it can be seen that the curves for different reflectivities or distances are congruent. Therefore, a certain range of the amplitudes resulting from the mixed signal can be interpreted as an indicator for accuracy independently from the observed object. Basically the amplitude a depends on the measured values according to eq. 4.12 on p. 39 but the scaling is different for each camera model. Thus, an amplitude range that offers a good reliability has to be measured for every camera model.

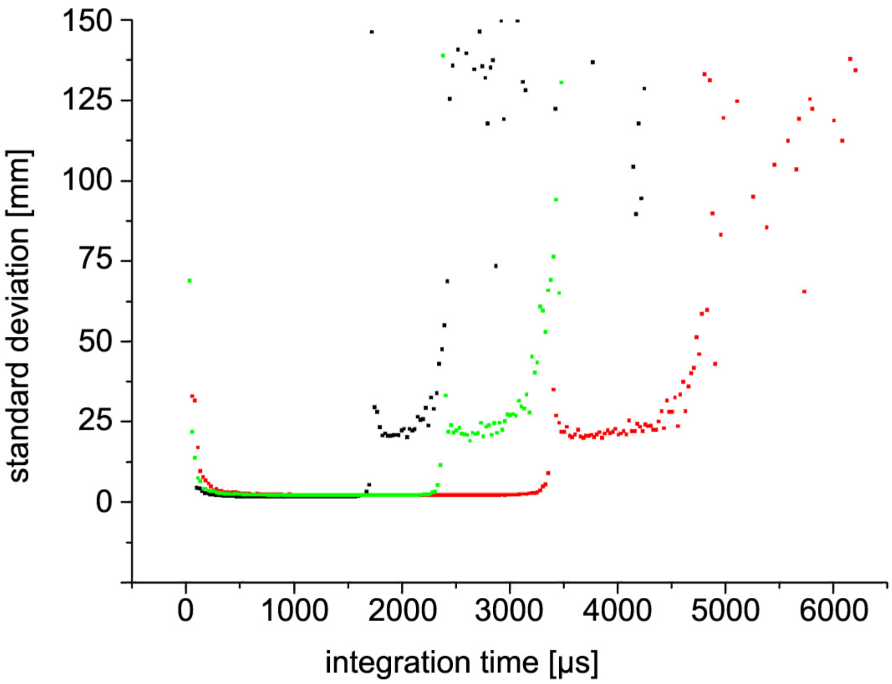

Figure 5.21: Standard deviation rises high at an upper limit of integration time for varying distances/reflectivities (black: brown target at 40cm, red: brown target at 60cm, green: white target at 60 cm).

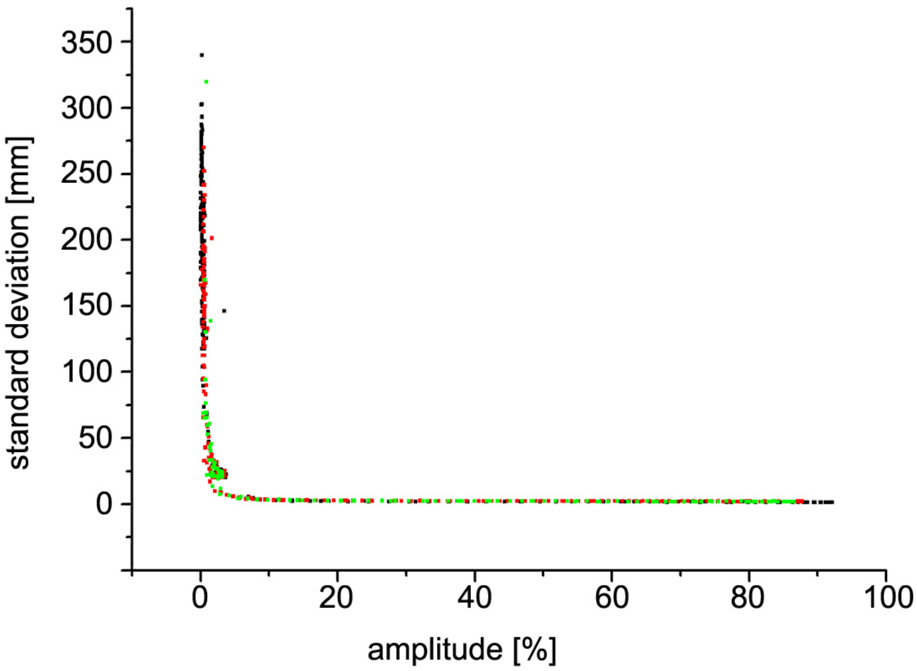

Figure 5.22: Standard deviation rises high at an lower limit of amplitude for varying distances/reflectivities (black: brown target at 40cm, red: brown target at 60cm, green: white target at 60 cm).

In order to obtain a minimum standard deviation in distance measurement it has to be made sure, that the amplitude has to be within the range depicted in fig. 5.23 by continuously adapting the integration time.

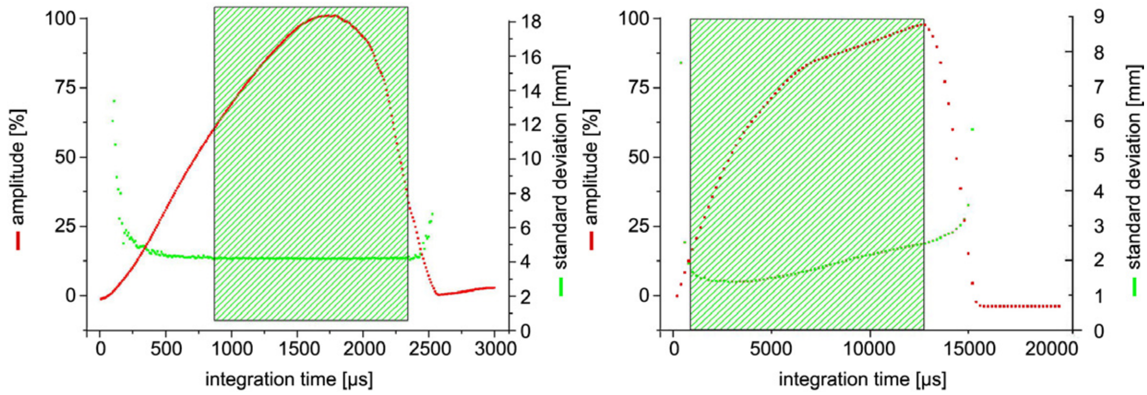

Figure 5.23: Changes of integration time affect amplitude and standard deviation (l: pmd, r: mesa).

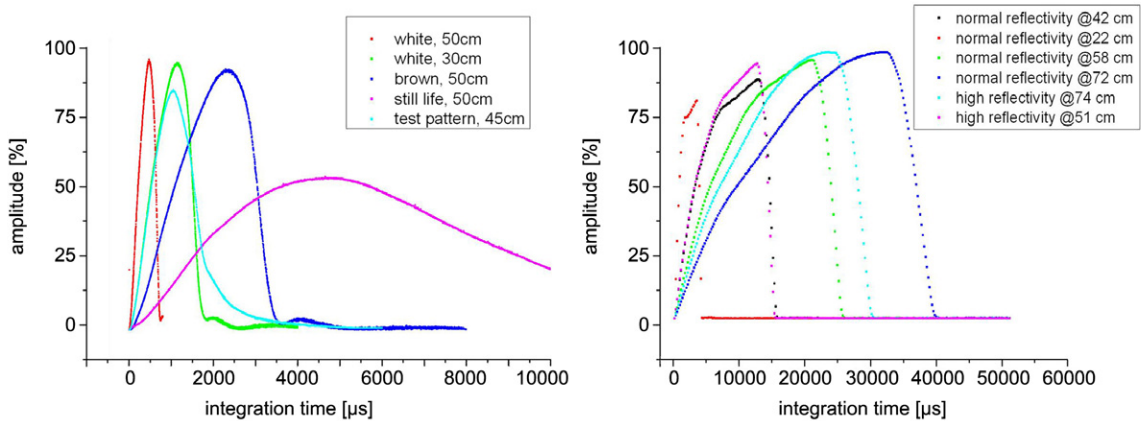

Figure 5.24: Even for the same integration time the amplitude curves vary for different distances or reflectivities (l: pmd, r: mesa).

For changing environments usually the integration time is changed by fixed steps until the best adjustment is found. This approach had two major drawbacks:
Firstly it is not clear for changed amplitudes if the measured value is on the left rising or on the right falling arm of the amplitude curve. Therefore the changes could have the wrong direction and would need several changes before the image gets better. Secondly a precise manual adjustment is quite slow, as the curves for low reflectivity or high distance are flat compared to high reflectivity or short distances as shown in fig. 5.24. It would take many steps for low reflectivities or high distances to reach the desired region of amplitudes. Consequently, the next approach involves slopes to estimate as fast as possible the size of consecutive steps for a good amplitude and to determine on which side (positive slope/negative slope) of the curve the actual amplitude is right now. A lot of measurement points are

needed to calculate a reliable slope. This gets clear with a detailed view on the integration time - amplitude curve in fig. 5.24. The points are scattered, therefore it is not possible to calculate a reliable slope out of points less than round about 10, where every point is one frame. Even if a reliable slope could be found, this could only give a coarse clue for the position on the curve due to the different shapes for different reflectivities and distances as shown in fig. 5.24.

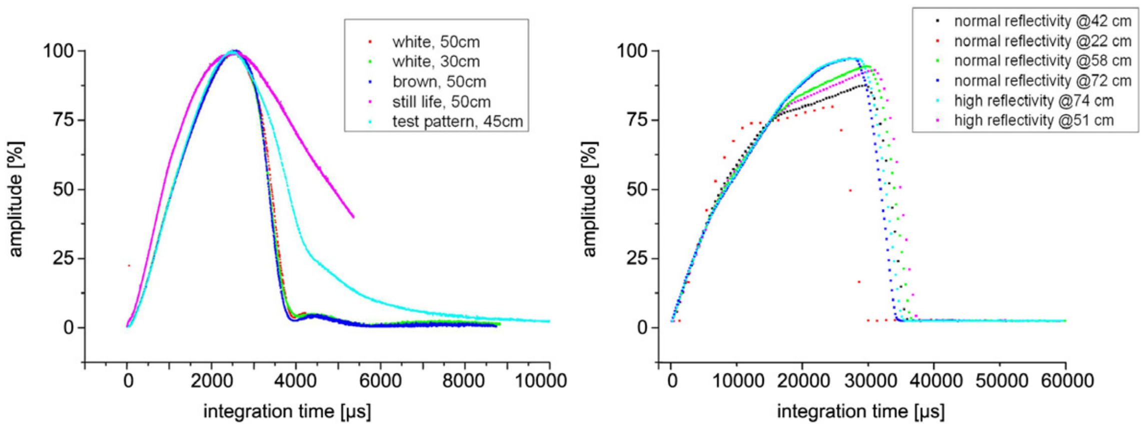

Figure 5.25: Although the amplitude - integration time curves vary for different distances or reflectivities they can be normalized by rescaling (l: pmd, r: mesa).

It is visible that the curves for different reflectivities or distances look similar. The curves in fig. 5.24 are linearly scaled on the integration time axis up to a certain degree. If the curves are rescaled to a reference curve they are nearly congruent as shown in fig. 5.25. This can be used for adjusting the integration time. The proposed algorithm takes the following steps to calculate the correct integration time [Ritt 07b]:

1. Before starting a reference curve is needed. The camera has to be directed to a static scene (typically similar to the later mapped scene) and the amplitude values for consecutive integration time values (for example, 100µs, 200µs, 300µs...) have to be recorded. For a reliable curve, a few frames for every integration time are measured and the mean value of the amplitude data is calculated. In the end there is a curve with n (typically a few hundred) pairs with

$$(\tau_x; a_x), 0 < x \leq n \tag{5.6}$$

   where τ_x is the integration time and a_x the corresponding amplitude. This is our reference curve. The maximum amplitude a_t out of a_x is our target amplitude which should be reached after automatic integration time adjustment. The integration time belonging to the target amplitude is our reference integration time τ_r

2. In the auto gain process a reliable data pair on the unknown curve, which consists of an integration time τ_m and the measured amplitude a_m is needed. This is done by averaging some subsequent amplitude measures at a constant integration time τ_m. If a_m is below a critical threshold amplitude, which indicates

unreliable results, this measurement is repeated with adapted integration time. This is necessary because the curve has got a very low slope for low amplitudes, so the uncertainty of the amplitude measurement measuring only $3-5$ frames would not deliver a reliable data pair.

3. If a following measurement with increased integration time leads to a higher amplitude, it is clarified that the first value is on the left arm of the curve and therefore unambiguous.

4. Next, the amplitude a_m of the data pair is compared to the amplitudes a_x with $0 < x \leq n$ of the reference curve. The amplitude a_x with $x = b$ that matches the measured amplitude best is identified and the corresponding integration time τ_b is read out.

5. The scaling factor s_τ is calculated. It is the ratio of the integration time τ_m used for the measurement and the integration time τ_b that is read out:

$$s_\tau = \frac{\tau_m}{\tau_b} \tag{5.7}$$

6. Now, the target amplitude a_t can be reached by using the target integration time τ_t according to:

$$\tau_t = s_\tau \cdot \tau_r \tag{5.8}$$

The knowledge of the scaling factor s_τ allows to directly compute the appropriate integration time τ_t, without having any intermediate steps. The reference curve usually needs only to be obtained once for every camera setup.
With the help of the described procedure it is possible to speed up the auto gain process. Instead of $5-10$s for manual adaption, this method normally takes $1-3$s or even less for good conditions.

5.2 MuSToF Hybrid Imaging

An important step is the design of a hybrid imaging system for the simultaneous acquisition of color and 3-D images. For each CCD color image pixel a distance value measured with the ToF technology is determined. This can be realized by putting both cameras beneath each other or by using a beam splitter for the same field of view. For this hybrid system the name "Multi-Sensor Time-of-Flight" (MuSToF) is chosen [Krug 06]. To handle the simultaneous use of two different types of cameras an algorithmic framework for the handling of this multi-sensor system is required. In this section, the needed algorithms for basic requirements like calibration and registration are proposed.

5.2.1 Multi-Sensor Imaging Model

Penne et al. presented in 2007 a model of the multi-sensor system [Penn 07b]:
The amplitude value acquired with a ToF chip at pixel (i, j) is denominated with $a_{i,j}$. The corresponding distance value is denominated with $d_{i,j}$. The average color value of the CCD image corresponding to position (i, j) is denominated with $p_{i,j}$. ToF camera and CCD camera are considered as pinhole cameras. The focal length f and the sensor coordinates principal point $(c_x,\ c_y)$ are preconditioned intrinsic parameters, rotation matrix $\mathbf{R} \in \mathbb{R}^{3\times3}$ and translation vector $\mathbf{t} \in \mathbb{R}^3$ are extrinsic parameters that have to be measured for the ToF camera and, primed with a $'$, for the CCD camera. p_x, p_y and p'_x, p'_y represent the physical size of a sensor element of the ToF or CCD camera.

A 3-D point $\mathbf{q}$ is projected to the ToF camera pixel P using homogeneous coordinates indicated by underlining:

$$P = \mathbf{K}[\mathbf{R}|\mathbf{t}]\underline{\mathbf{q}} \tag{5.9}$$

It is projected to the CCD camera pixel P' in the same way:

$$P' = \mathbf{K}'[\mathbf{R}'|\mathbf{t}']\underline{\mathbf{q}} \tag{5.10}$$

where $\mathbf{K}$ is the 3×3 calibration matrix containing the intrinsic camera parameters according to [Tsai 87]. $\mathbf{R}$ and $\mathbf{t}$ are estimated by the method that is explained in section 5.2.2. For a pixel with the index i, j the horizontal and vertical distances d_x and d_y of the pixel from the principal point can be determined as

$$d_x = (i - c_x)p_x \tag{5.11}$$

$$d_y = (j - c_y)p_y \tag{5.12}$$

Accordingly, the distance d_z of the optical center to the pixel can be determined as

$$d_z = \sqrt{d_x^2 + d_y^2 + f^2} \tag{5.13}$$

The corresponding 3-D point $\mathbf{q} = (q_x, q_y, q_z)^T$ may be computed using the measured distance $d_{i,j}$ by

$$q_x = \frac{d_x d_{i,j}}{d_z},\ q_y = \frac{d_y d_{i,j}}{d_z},\ q_z = \frac{f}{d_z} \tag{5.14}$$

5.2.2 Multi-Sensor Calibration Method

For distance calibration a plane with defined pattern in both views, usually a checkerboard, is taken. It is used to calibrate both cameras to each other which means the extrinsic parameters, but also to compensate the intrinsic parameters like lens distortions [Hart 07b]. The color of an observed point on a plane is not affected by the pinhole camera model irrespective of the distance. But beyond that, another issue has to be handled especially with 3-D cameras: After lens distortion correction, the pinhole camera model represents a plane still as a plane independent from its pixel position. Instead of that with the 3-D camera the measured distance of a plane differs for each pixel and leads to a curved plane with ostensible longer distances at outer regions as shown in fig. 5.26. The pretended deformation depends on the focal length f', the physical pixel size $p'_x \times p'_y$, the positioning angles α, β and γ and the distance d between chip and object as shown in fig. 5.27.

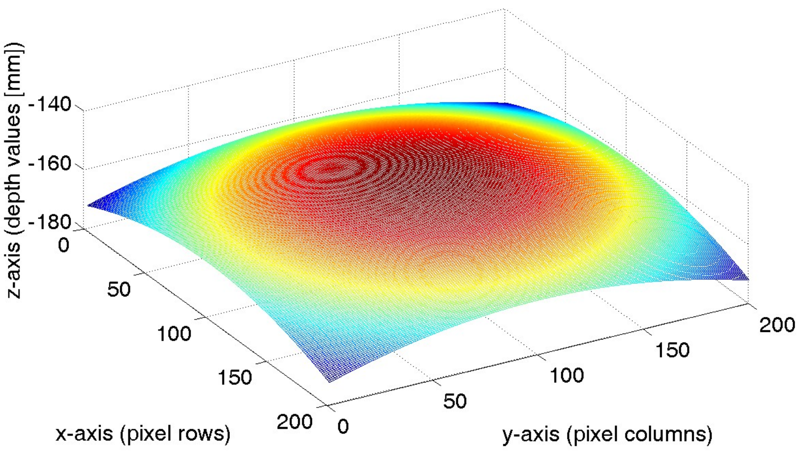

Figure 5.26: In the camera coordinate system, the measured distances for a plane without calibration represent a curved plane with ostensible longer distances at outer regions.

After calibration of intrinsic parameters, the sensor coordinates' principal point (c'_x, c'_y) corresponds to the half of the number of pixels per row and column.

For each pixel i, j the measured distance $d_{i,j}$ can be calculated using eq. 5.15 with equations 5.11, 5.12 and 5.13. The inverse of the distance matrix for $\alpha = \beta = 90°$ and $\gamma = 0°$ helps to correct this error.

$$d_{i,j} = \frac{\cos(\alpha)d_x + \cos(\beta)d_y - d}{\cos(\alpha)d_x + \cos(\beta)d_y - \cos(\gamma)f} \cdot d_z \tag{5.15}$$

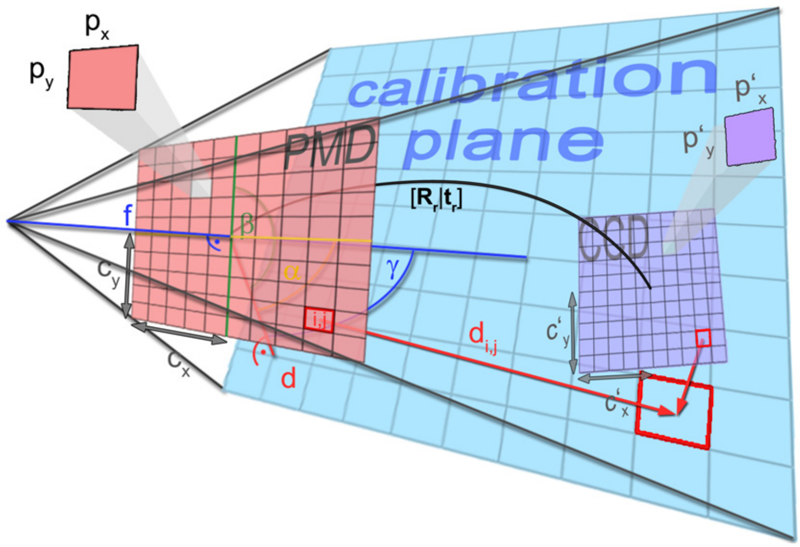

Figure 5.27: Model of ToF and CCD parameters and measured distances using a plane for calibration. For a pixel (i, j) on the ToF chip the measured distance is defined by the ToF chip's orientation and distance to the calibration plane. The physical size of the pixel, the number of pixels per column and row and the focal length have a contribution as well. With known relative rotation and translation parameters between ToF and CCD principal point also the color image information can be assigned.

Assuming that both cameras are rigidly mounted, the spatial relation between the optical centers of ToF and CCD camera can be described by a relative rotation $\mathbf{R_r} \in \mathbb{R}^{3\times3}$ and translation $\mathbf{t_r} \in \mathbb{R}^3$, with

$$\mathbf{R_r} = \mathbf{R}\mathbf{R}'^{-1}, \;\; \mathbf{t_r} = \mathbf{t} - \mathbf{R_r}\mathbf{t}' \tag{5.16}$$

$\mathbf{R}$, $\mathbf{R}'$, $\mathbf{t}$ and $\mathbf{t}'$ describe the pose of the corresponding camera in a common world coordinate system.

In [Penn 07b] the following method for the calibration of both cameras was proposed:

1. Capturing of an image of the calibration pattern as shown in fig. 5.28 with N calibration points.

2. Determination of 2-D calibration points $C_n,\ n \in 1, 2, ..., N$.

3. Assigning of 3-D world points $W_n,\ n \in 1, 2, ..., N$ to 2-D calibration points.

4. Estimation of intrinsic $(\mathbf{K})$ and extrinsic $(\mathbf{R}, \mathbf{t})$ camera parameters applying Levenberg-Marquardt non-linear optimization [Denn 83].

For calibration of the ToF camera the standard algorithm is modified. The low lateral resolution of the ToF cameras leads to an unspecific localization of the points

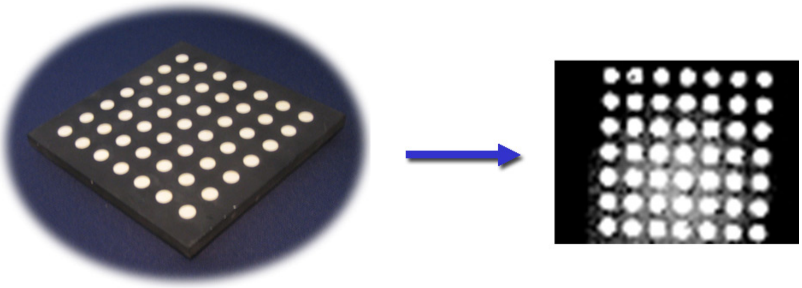

Figure 5.28: For the use of a calibration pattern with 7×7 points (l) the ToF camera's intensity image (r) has to be used since the distance image ideally should represent a plane.

of the calibration pattern in the acquired data. The non-linear optimization usually aims at minimizing the squared backprojection error

$$\sum_{n=1}^{N} \|C_n - proj(W_n, \mathbf{K}, \mathbf{R}, \mathbf{t})\|^2 \tag{5.17}$$

where $proj(W_n, \mathbf{K}, \mathbf{R}, \mathbf{t})$ is the projection of the world point W_n into the image plane specified by $\mathbf{K}$, $\mathbf{R}$ and $\mathbf{t}$. This was extended by a term, which describes the deviation of the 3-D reconstructed calibration points from the plane. Let $\hat{C}_n$ be the 3-D point reconstructed from C_n specified in world coordinates (of the calibration pattern) using the distance information available from the ToF camera and the extrinsic parameters. Furthermore, ϵ_C denominates the regression plane calculated using all $\hat{C}_n,\ n \in 1, 2, ..., N$. The extended formula, which is minimized in the calibration routine for the ToF camera, is

$$\sum_{n=1}^{N} \|C_n - proj(W_n, \mathbf{K}, \mathbf{R}, \mathbf{t})\|^2 + \kappa\|\hat{C}_n - W_n\| + \nu d(\hat{C}_n, \epsilon_C) \tag{5.18}$$

where $d(\hat{C}_n, \epsilon_C)$ is the distance of $\hat{C}_n$ to the regression plane ϵ_C and $\kappa,\ \nu$ are scaling parameters for the impact of intrinsic and extrinsic camera parameter errors. The term $\|\hat{C}_n - W_n\|^2$ penalizes wrong intrinsic and extrinsic camera parameters, which lead to a wrong registration of the calibration points. The term $d(\hat{C}_n, \epsilon_C)$ only penalizes wrong intrinsic camera parameters as only those are relevant for the reconstruction of all $\hat{C}_n$ on a plane. Wrong extrinsic parameters only imply a rotation and translation of the plane [Penn 07a].

5.2.3 Multi-Sensor Registration Method

The CCD and the ToF camera have to be registered as it is necessary for medical applications to relate the acquired 3-D information with the acquired color information of the operation area. In [Penn 07b] the following method was proposed:
Using the calibration routine described above the extrinsic parameters ($\mathbf{R}'$,$\mathbf{t}'$,$\mathbf{R}$,$\mathbf{t}$) and intrinsic parameters ($\mathbf{K}$,$\mathbf{K}'$) are known for each camera when capturing simultaneously an image of the calibration pattern. This enables the calculation of $\mathbf{R_r}$

and $\mathbf{t_r}$ as described by eq. 5.16. For a parallel acquisition of data the assignment of color information to 3-D points can be realized without high computational costs: by using eq. 5.14 a 3-D surface specified in the ToF camera coordinate system can be reconstructed. By applying eq. 5.9 the color image is projected onto that ToF surface. Vice versa it is possible to find out the 3-D position of a point pictured on the CCD camera image plane using eq. 5.10.

5.3 MuSToF Endoscopy

So far the presented Multi-Sensor Time-of-Flight hybrid system had low medical impact. In the next step this system will be attached to endoscopes to provide a 3-D view into closed cavities.

5.3.1 Hardware Approach

Time-of-Flight and CCD camera are attached on parallel standard fiber-endoscope (not a chip-on-the-tip endoscope!) as shown in fig. 5.29. All modifications are done at the distal endings and thus, they do not entail problems concerning the sterilizeability. In the next step a beam splitter enables the attachment of both cameras at only one rigid endoscope as shown in fig. 5.30. Replacing the rigid laparoscope by a flexible endoscope as shown in fig. 5.31 extends the usability for translumenal surgery like NOTES.

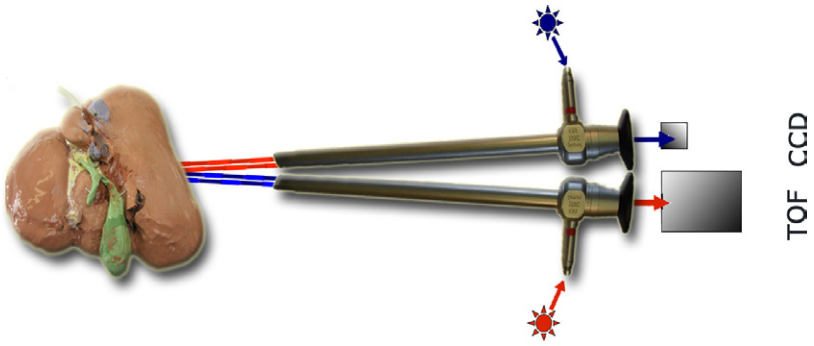

Figure 5.29: Schematic depiction of endoscopic hybrid imaging. The real world scene (l) is looked at with ToF and CCD cameras (r) attached onto two rigid laparoscopes (m) for reconstruction of the scene. Illumination with visible (blue) and infrared (red) light is carried out separately.

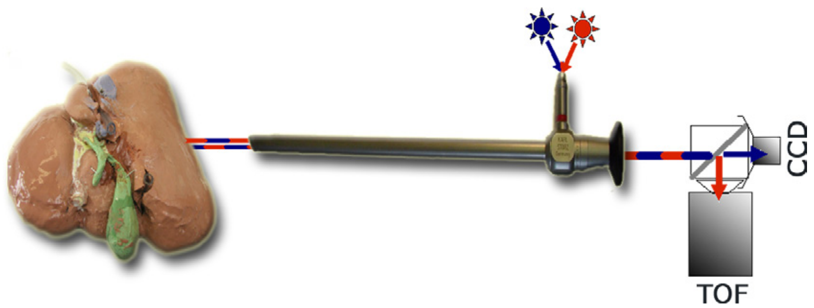

Figure 5.30: Schematic depiction of endoscopic hybrid imaging. The real world scene (l) is looked at with ToF and CCD cameras (r) attached onto only one rigid laparoscope (m) for reconstruction of the scene. Illumination with visible (blue) and infrared (red) light is carried out jointly.

The image acquisition technique applied in endoscopes fits the requirements for a ToF based distance measurement. The near-infrared optical reference signal through

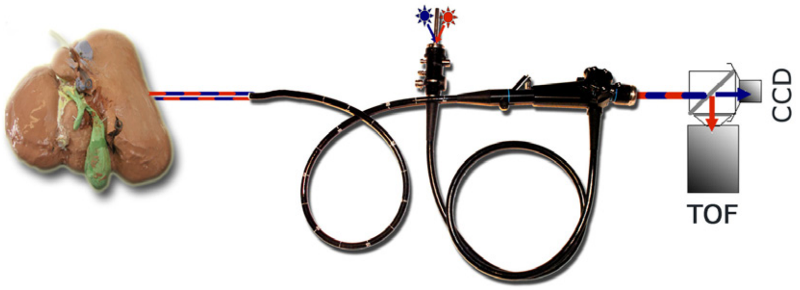

Figure 5.31: Schematic depiction of endoscopic hybrid imaging. The real world scene (l) is looked at with ToF and CCD cameras (r) attached onto only one flexible endoscope (m) for reconstruction of the scene. Illumination with visible (blue) and infrared (red) light is carried out jointly.

the illumination channel can be transmitted together with the visible light of the normal endoscopic system. Using a beam splitter, the ToF chip can be mounted distally together with the CCD chip. Therefore, the parallel acquisition of image and distance data is possible. The very first prototype in fig. 5.32 was presented by [Penn 06]. But as there are high attenuations and distortions the methods described in this section could not be transferred easily to this proof of concept hardware. Especially the illumination method had to be adapted completely new and will be discussed in section 5.4.

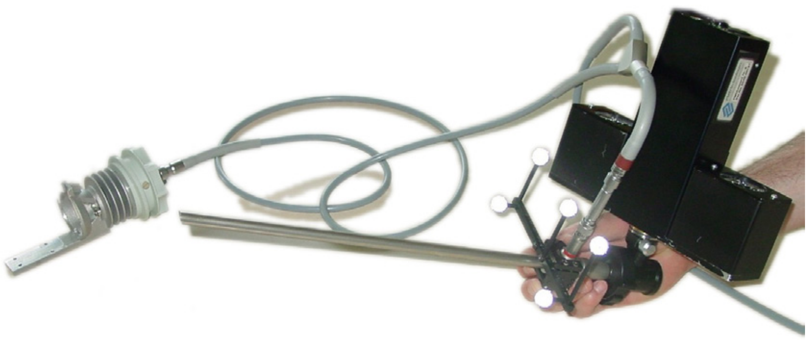

Figure 5.32: Very first prototype of a MuSToF-Endoscope presented in Moscow 2006. The still attached original light sources of the ToF-camera are to be replaced by the external visible and infrared reference light source integrated by the Y-shaped illumination cable (l). It leads to the illumination channel of a rigid laparoscope (m). Using a beamsplitter, a PMD 3k-S ToF camera (r) is attached to the laparoscope. An additional target for optical tracking (m) should provide reliable position and movement information for evaluation.

5.3.2 Distance Offset and Scaling

The distance value computed by a pixel of the ToF sensor does not initially represent exactly the distance from the endoscope tip to the operation area [Penn 09]. First, the light has to pass the way from the laser diode through the optical fiber to the illumination channel of the endoscope until it leaves the endoscope's tip after the constant starting illumination path length d_{il}. After the free-air path length of two times the distance d to the reflecting object, it re-enters the endoscopic image channel through the front lens with a path length $d_{il} + 2d$. After passing the image channel and the following camera optics the measured distance is increased by d_{im}. Therefore, it reaches the ToF chip after an overall path length $d_{il} + 2d + d_{im}$. That means that every distance measurement is biased by a constant offset resulting from the sum of the illumination offset d_{il} and the image channel offset d_{im}:

$$d_e = d_{il} + d_{im} \tag{5.19}$$

This error may differ for each pixel due to slight differences in the transmission way through the illumination channel and the endoscopic optic. Thus, the computation of a distance error map may be useful in a later step. But unless we do not have an uniformly distributed illumination of the scene, we confine ourselves to just one calibration value d_e for all pixels. As in outer regions the image quality decreases, only a frame of 10×10 pixels in the center of the distance image is used. To determine the offset d_e, erroneously the idea of fixing a plane with distance $d = 0$ right in front of the lens may look like a useful approach. But due to the fact that illumination channel and image channel are conducted separately no reflection can be measured off a plane placed directly in front of the tip.

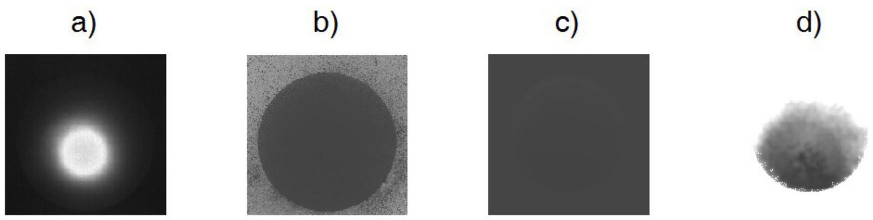

Figure 5.33: Rawdata of a calibration plane at a distance of 50mm with a) intensity image, b) original distance image, c) filtered image and d) narrowed range.

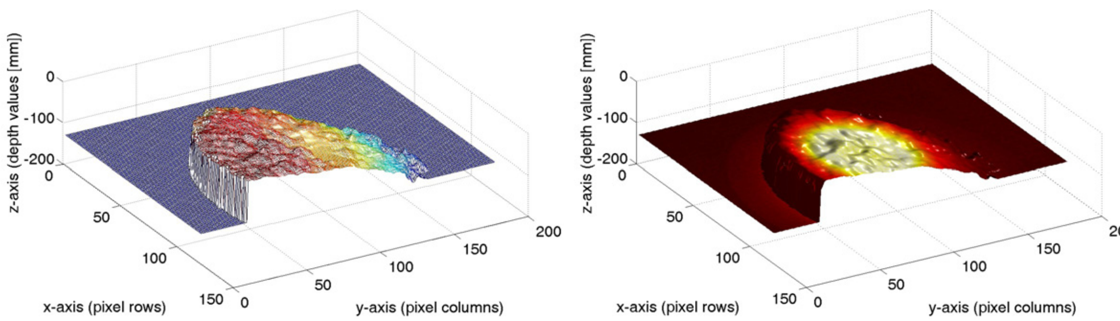

Figure 5.34: Filtered (l: median, r: bilateral) 3-D representation of a calibration plane at a distance of 50mm with colored mesh (l) and reflectivity mapped surface (r) representation.

To solve the distance calibration problem, a new approach is proposed instead: A white calibration plane is fixed with a known calibration distance d_c orthogonal

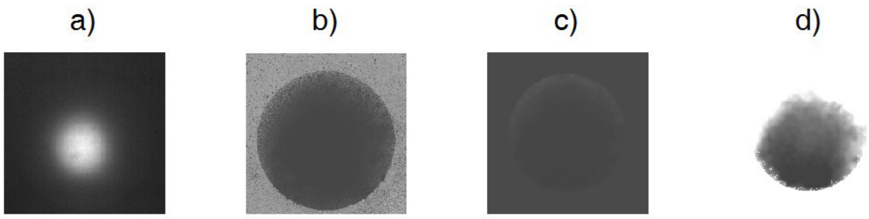

Figure 5.35: Rawdata of a calibration plane at a distance of 100mm with a) intensity image, b) original distance image, c) filtered image and d) narrowed range.

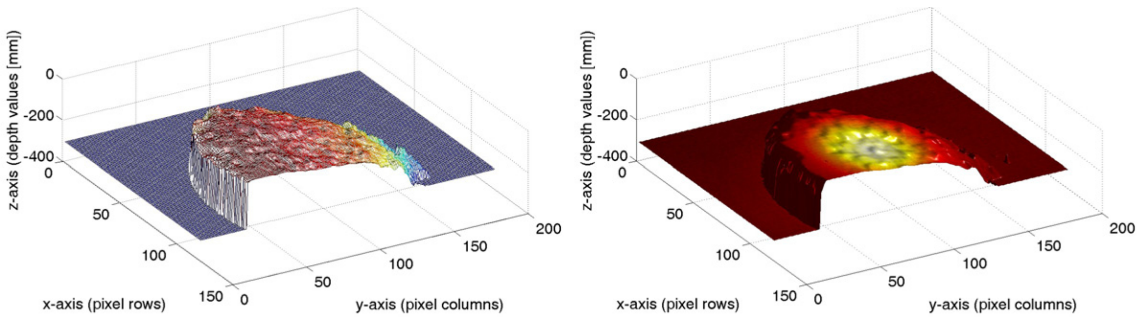

Figure 5.36: Filtered (l: median, r: bilateral) 3-D representation of a calibration plane at a distance of 10mm with colored mesh (l) and reflectivity mapped surface (r) representation.

in front of the endoscope as visualized in figs. 5.33 and 5.34. The measured distance d_1 now is $d_1 = 2d_c + d_e$. In the next step, the distance between endoscope and calibration plane is doubled as shown in figs. 5.35 and 5.36. The measured distance now is $d_2 = 4d_c + d_e$. Subsequently, the distance error d_e measured in each pixel corresponds to:

$$d_e = 2d_1 - d_2 \tag{5.20}$$

Subtracting the computed distance error from the acquired distances for each pixel and bisecting the obtained values leads to the offset-corrected distances d between the tip of the endoscope and the observed points.

With known calibration distance d_c the scaling factor s can be determined as well:

$$s = \frac{d_c}{d_1 - d_e} = \frac{2d_c}{d_2 - d_e} \tag{5.21}$$

However, if there can be assumed equidistant quantization of the distances encoded in the original distance images by n-bit grayscales as shown in sub-images b), another method would be preferable: With a given frequency f_{mod} the scaling factor s can just mathematically be derived by:

$$s = \frac{3 \cdot 10^8 \mathrm{m/s}}{2 \cdot 2^n \cdot f_{mod}} \tag{5.22}$$

5.4 MuSToF Illumination

The evaluations pointed out in section 5.5 on p. 90 bared disappointing results for our initial prototype shown in fig. 5.32 on p. 78. Rapidly it got clear that illumination will be one of the key steps for a working MuSToF endoscope.

5.4.1 Illumination Power Requirements

For the ToF principle the light source has to be modulated with a very high frequency. As this modulation frequency f_{mod} is in a range of 10MHz to 100MHz a mechanical modulation of the light beam by a rotating chopper wheel is not possible. Also, thermal light sources like halogen or xenon lamps typically used for endoscope illumination cannot be modulated that fast by the electrical current. Therefore, usually light emitting diodes (LEDs) are used to build a high intensity illumination unit. LEDs can be modulated up to 100MHz. However, to generate a sufficient light intensity to overcome the high attenuation of a fiber-endoscopic system, many LEDs are required in parallel. Consequently, the LED illumination is impractical for coupling to the fiber guide of an endoscope since the uniform amplitude modulation of the carrier wave is disturbed. Due to different distances between LED and in-coupling lens the modulation uniformity gets lost as shown in fig. 5.37. Since uniform modulation is necessary for the photonic mixer functional principle, a point light source is required for that measurement principle as shown in fig. 5.38.

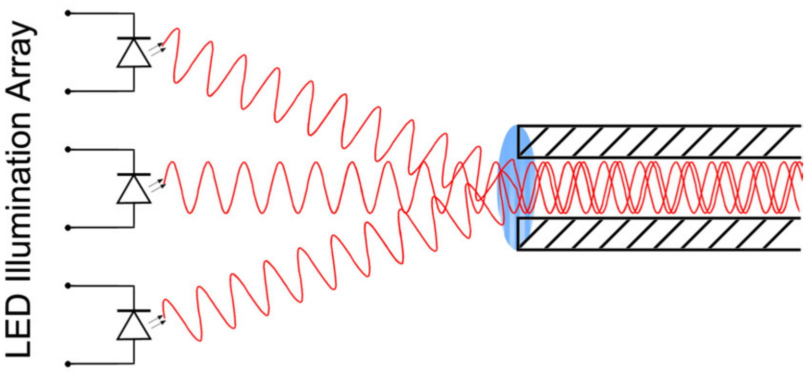

Figure 5.37: Different distances between multiple LEDs of the illumination array and the in-coupling lens disturb the modulation uniformity.

For this work, several single fiber-coupled high-power laser diodes have been tested with the endoscope. The most important factor was the ability of modulation capacity as high as the LEDs with a frequency f_{mod}. The second important factor was the high optical power P_{opt} emitted from a single 200µm diameter optical fiber. The laser diode chosen, OSRAM SPL 2F81-2S, can be coupled to the endoscope easily and provides sufficient light power to overcome the transmission loss of the endoscopic illumination fibers and image guides for a good signal-to-noise ratio at the ToF sensor. Last but not least the narrow-band characteristics enable that ambient light with power P_{amb} can be suppressed by using a dichroitic beam splitter. Hereby, the resolution defined in eq. 4.15 on p. 40 can be increased very efficiently.

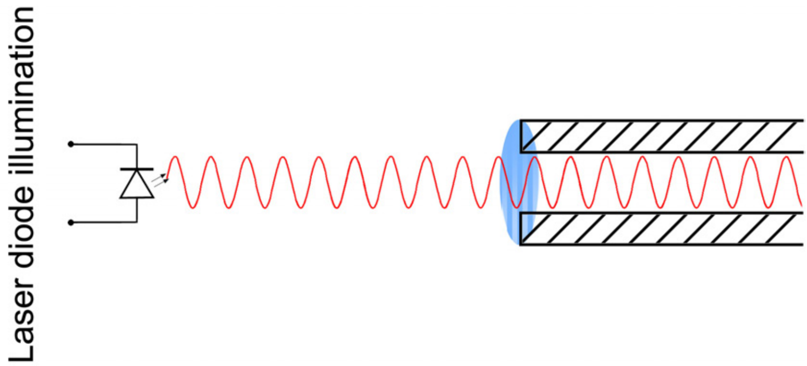

Figure 5.38: Using a laser diode preserves modulation uniformity even with high power.

5.4.2 Illumination Frequency Spectra Requirements

Regarding the light spectrum, it was important to find laser diodes, whose spectrum characteristics fulfill both, the specifications of a ToF camera and those of an arbitrary endoscope. To characterize the ToF camera illumination, a spectral measurement setup as shown in fig. 5.39 was designed. The reference spectrum of the original LED illumination with ToF cameras was identified as shown in fig. 5.40.

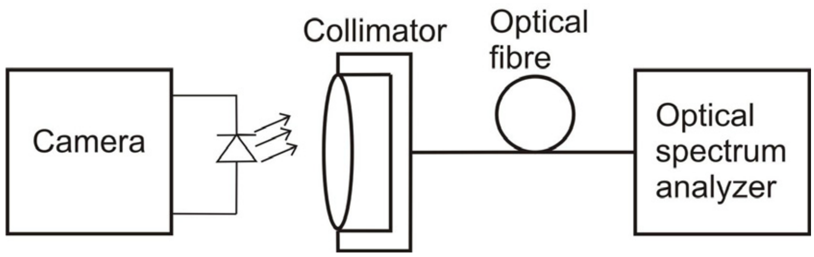

Figure 5.39: Measurement setup for the determination of the ToF camera LED illumination spectrum with ToF camera (l), collimator and transmitting fiber (m) and optical spectrum analyzer (r).

To characterize the laparoscopic transmission behavior, a spectral measurement setup as shown in fig. 5.41 was designed. The transmission characteristics of a usual laparoscope with an image channel and an illumination channel was recorded as shown in fig. 5.42. The lowest attenuation in the image channel is recorded between 800nm and 900nm. The attenuation of the illumination channel decreases slightly with longer wavelengths.

5.4.3 Choice of Laser Diodes

The high-frequency characteristics of the laser diode have been studied thoroughly to design the required high-speed driver electronics. First the Thorlabs L808P030, L850P030 and L808P200 laser diodes [L808 09] were used [Tack 08], in a second step

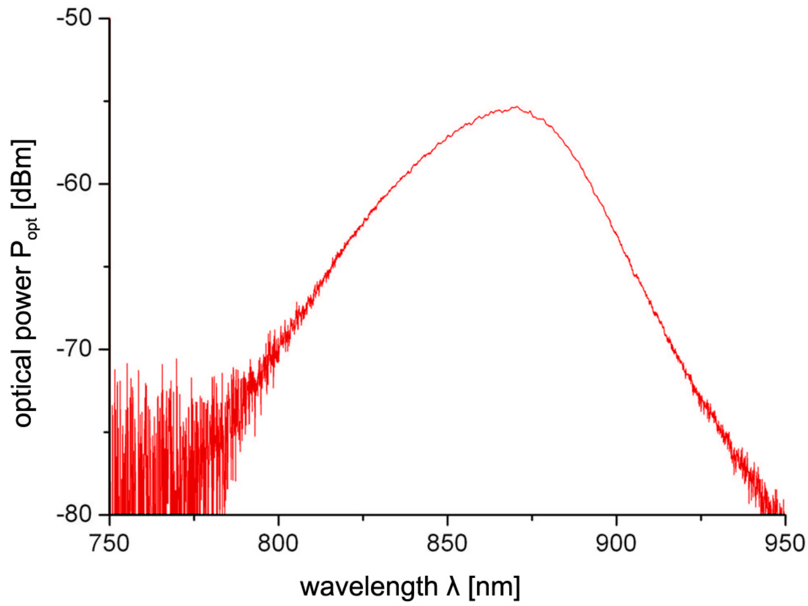

Figure 5.40: Visualization of the illumination spectrum of the LED array used in the PMD 3k-S ToF camera. A peak at a wavelength of 875nm is recognizeable.

Figure 5.41: Measurement setup for the determination of the laparoscope transmission spectrum with white light source, fiber and collimator (l), laparoscope (m), collimator and transmitting fiber and optical spectrum analyzer (r).

Table 5.1: Used Laser Diodes for MuSToF illumination [Tack 08, Schr 08].

Type	L850P030	L808P030	L808P200	SPL 2F81-2S
Wavelength in nm	850	808	808	808
Optical power in mW	30	30	200	1500
V_{CC} in V	2.0	2.0	2.0	2.0
Threshold current in mA	20	50	80	600
Operating current in mA	65	100	260	2500

they were replaced by the OSRAM SPL 2F81-2S laser diode [OSRA 05, Schr 08] shown in fig. 5.43 and table 5.1.

To characterize the laser diodes, a spectral measurement setup as shown in fig. 5.44 was designed. In fig. 5.45 and 5.46 the spectrum of each laser diode is shown. The Thorlabs L808P200 and the Osram SPL 2F81-2S exhibit the most narrow peak in their spectra. In combination with a narrow-band dichroitic beam splitter both would fulfill the requirements. But regarding the illumination power they differ by a factor

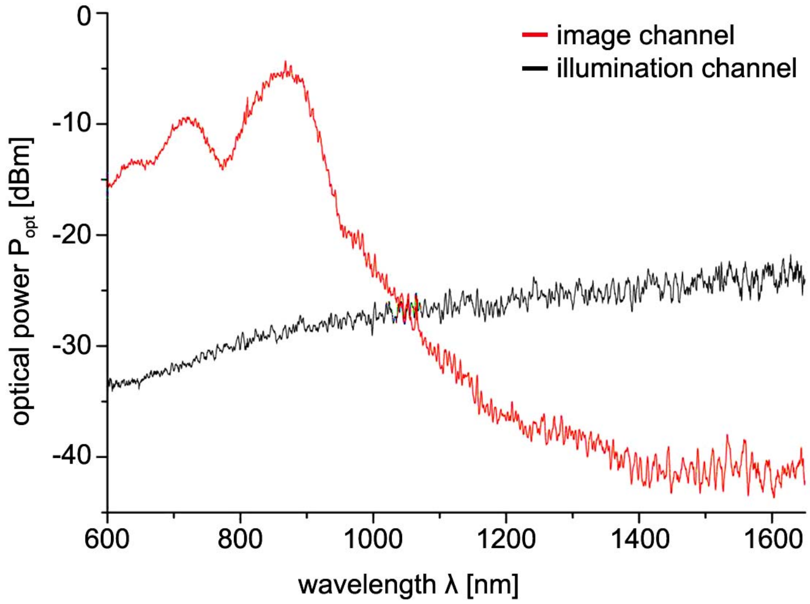

Figure 5.42: Visualization of the laparoscopic transmission spectrum with a minimum at a wavelength of 870nm is recognizable.

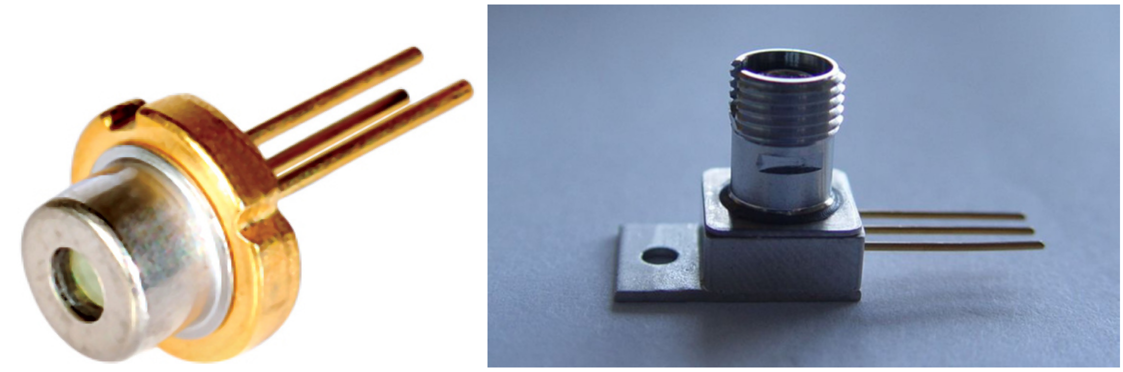

Figure 5.43: Housings of chosen laser diodes by Thorlabs L808P200 [L808 09] (l, reprinted with kind permission of Thorlabs GmbH, Dachau, Germany) and Osram SPL 2F81-2S [OSRA 05] (r, reprinted with kind permission of OSRAM Opto Semiconductors GmbH, Regensburg, Germany).

of 7.5, so the replacement of the Thorlabs L808P200 with the Osram SPL 2F81-2S was an important step for adequate illumination.

5.4.4 Modulation coupling Bias Tee

In fig. 5.47 it can be seen that laser diodes do not have a completely linear modulation behavior. First there is an unactive range until the threshold current I_{th} is reached. Then the gradient rises connotatively and turns in a linear modulation phase reaching to the maximum. For modulation it is important to stay in this range between threshold current I_{th} and maximum current I_{max}. Therefore the characteristic curves

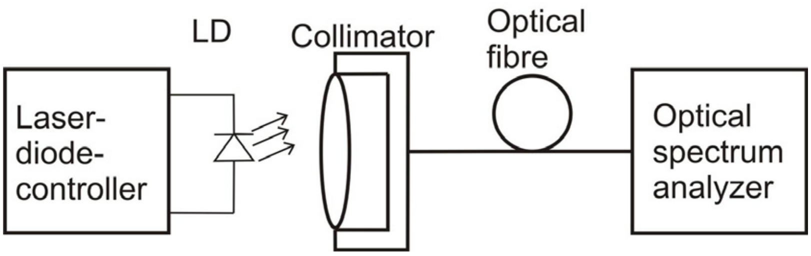

Figure 5.44: Measurement setup for the determination of the Laser illumination spectra with laser controller and laser diode (l), collimator and transmitting fiber (m) and optical spectrum analyzer (r).

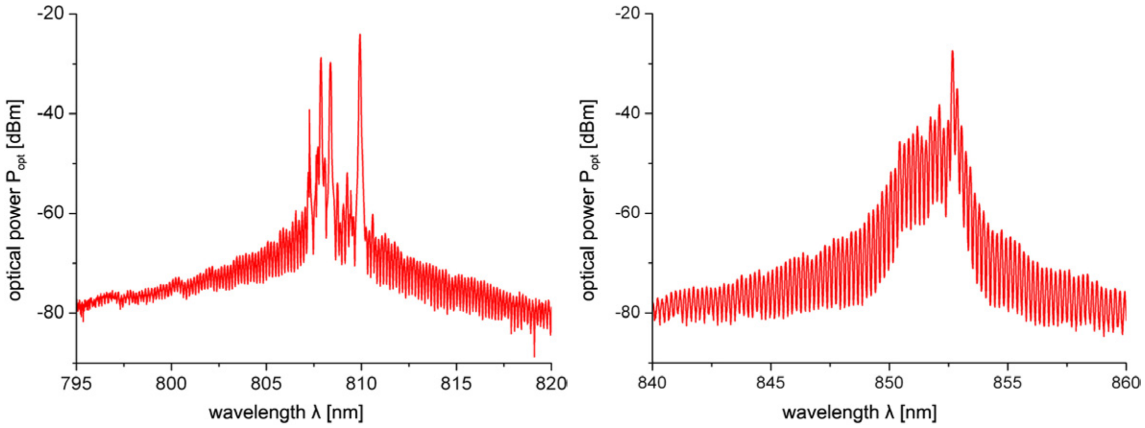

Figure 5.45: Laser illumination spectra of Thorlabs L808P030 (l) and L850P030 (r) laser diode with peaks between 808nm and 812nm resp. 850nm and 854nm.

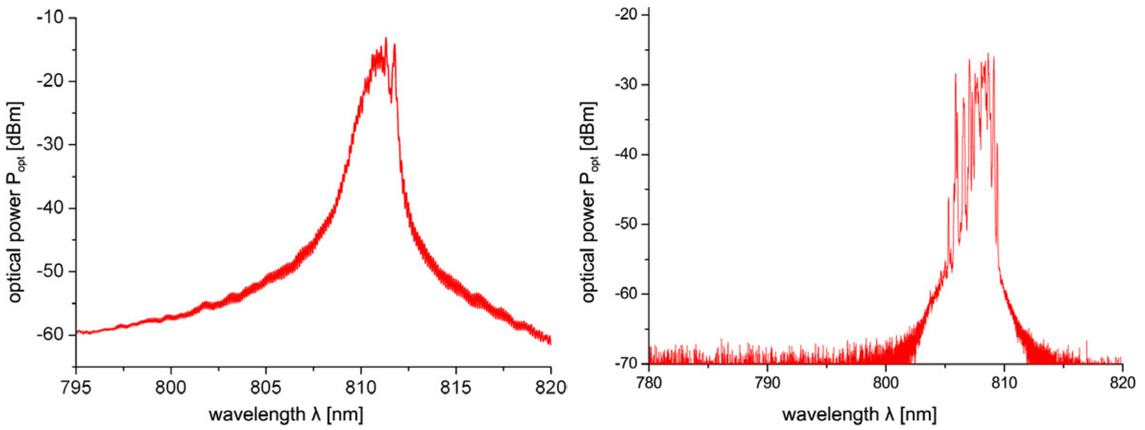

Figure 5.46: Laser illumination spectra of Thorlabs L808P200 (l) and OSRAM SPL2F81 (r) laser diode with sharp peaks between 808nm and 812nm resp. 805nm and 809nm.

of the used laser diodes shown in fig. 5.48 and 5.49 shed light on the modulation width and the modulation linearity.

To generate the modulation current I_{LD} as shown in fig. 5.47 out of the modulation signal balanced to ground a so-called bias tee as shown in fig. 5.50 is used. With the

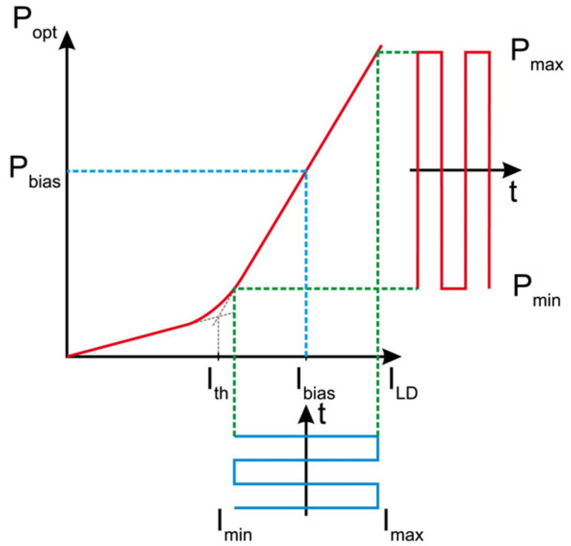

Figure 5.47: Laser diode modulation principle with an unactive range below the turning point with the threshold current I_{th} and a quasi-linear behavior between I_{min} and I_{max} with $I_{min} \geq I_{th}$. Current modulation in the quasi-linear range is transformed to optical illumination power P_{min} and P_{max}.

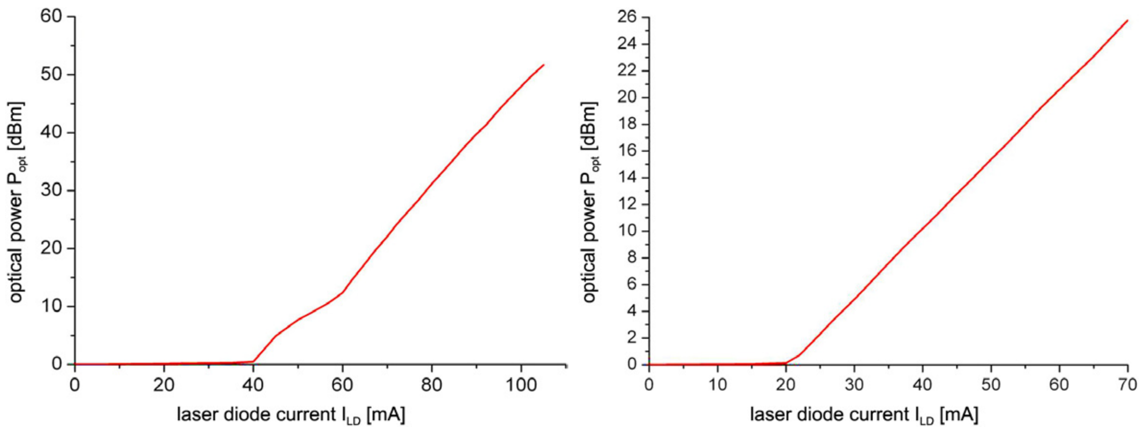

Figure 5.48: Characteristic curve of Thorlabs L808P030 (l) and L850P030 (r) laser diodes with threshold current I_{th} at 40mA resp. 20mA.

continuous current I_{bias} the operating point of the laser diode is regulated. The transconductance amplifier on the left generates an alternating current I_{mod} with the frequency and the shape of the modulation signal U_{mod}. Ideally, the alternating current I_{mod} passes through the capacitor to the laser diode and the continuous current I_{bias} passes through the inductor to the laser, too. Both cannot pass to the other path as the inductor limits the alternating current and the capacitor the continuous current. Both add up to the laser diode current I_{LD} that is generating the optical laser emission. With real signals and circuits, the passing and blocking behavior of passive components differs from ideal properties.

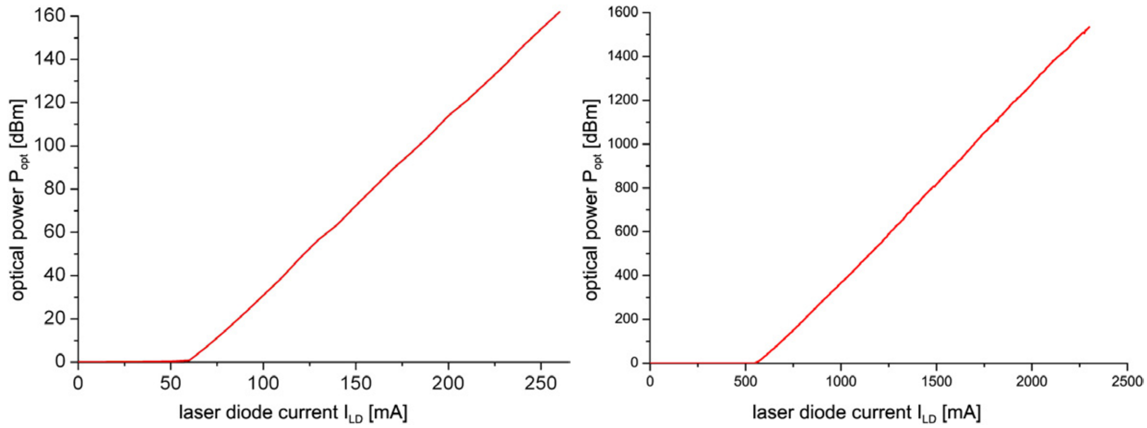

Figure 5.49: Characteristic curve of Thorlabs L808P200 (l) and OSRAM SPL2F81 (r) laser diodes with threshold current I_{th} at 60mA resp. 600mA.

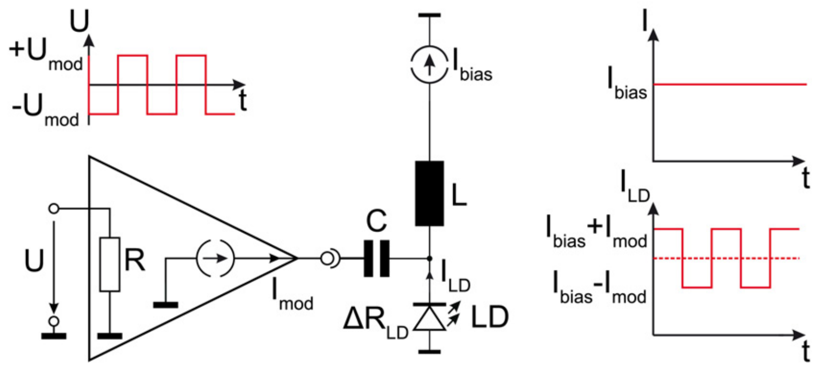

Figure 5.50: The incoming modulation signal is amplified using a RFMOSFET (l). With a so called "Bias Tee" circuit (m) the amplified signal $\pm I_{mod}$ with high frequency passes the capacitor and adds up with the conductor passing continuous bias current I_{bias} to the laser diode current $I_{LD} \geq I_{bias} - I_{mod}$ (r). This is required as I_{LD} only behaves linearly above the threshold current I_{th}.

5.4.5 Illumination Power Amplifier

A big issue with this circuit design is the high current in combination with the very high modulation frequency. As normally only one of these points has to be taken into account, a new amplifier with the same principle but components with higher power capability had to be designed. By a single RFMOSFET transistor the modulation of the laser diode up to frequencies of 50MHz with potential to reach 100MHz for future ToF sensors was enabled [Schr 08]. By use of this technology the high power modulation of the diode can be synchronized with the low power, but high frequency ToF reference signal for accurate phase-delay measurements. Thus, a powerful and versatile illumination light source for adopting standard 3-D ToF sensors to endoscopes was realized as shown in fig. 5.51.

To prove and evaluate the quality of the bias tee and the input amplifier a measurement setup for the transmission characteristics from modulation signal to optical modulation was build as shown in fig. 5.52. The modulation frequency was increased

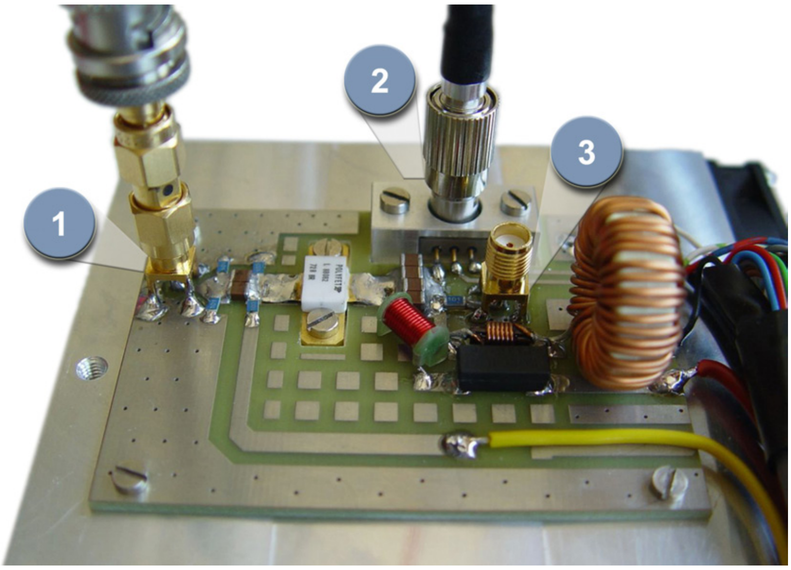

Figure 5.51: The incoming modulation signal (1) is amplified and passes through the bias tee, where the bias current is added, to the laser diode (2). The bias tee components are initially calibrated using the calibration adapter (3) [Schr 08].

stepwise from 10MHz up to 50MHz as shown in figs. 5.53, 5.54 and 5.55. The comparison between the LED signal deformation with the original ToF illumination shows a major improvement even with 50MHz.

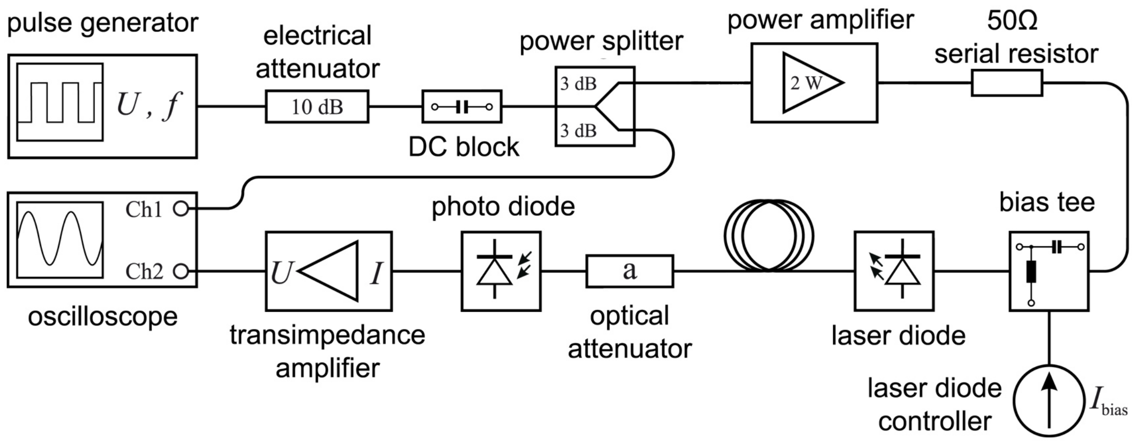

Figure 5.52: The transmission characteristics from modulation signal to optical modulation are measured by generating an electrical pulse signal which is adapted, amplified and transformed to a infrared laser beam. Using a photo diode this laser beam is transformed to an electrical signal that can be compared with the originally generated pulse signal in the oscilloscope.

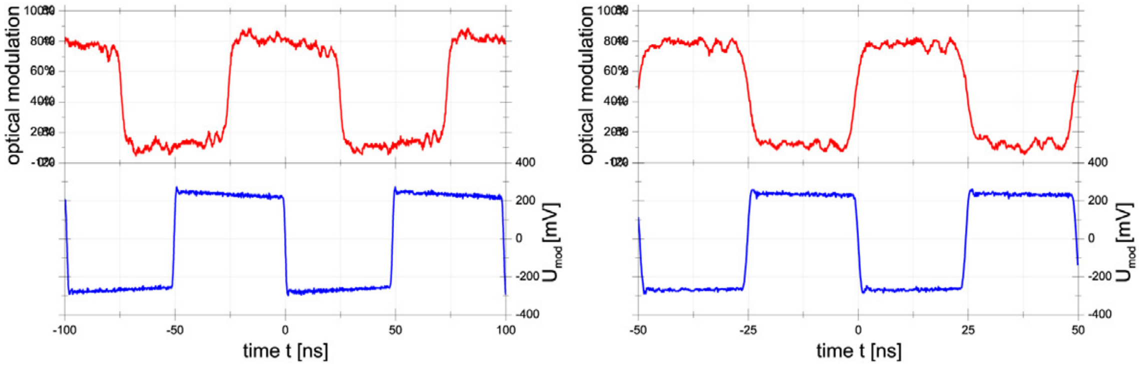

Figure 5.53: Transmission characteristics of the modulation signal to the optical modulation with 10MHz (l) and 20MHz (r) using the measurement setup according to fig. 5.52. The shape of both signals is still nearly a rectangle shape.

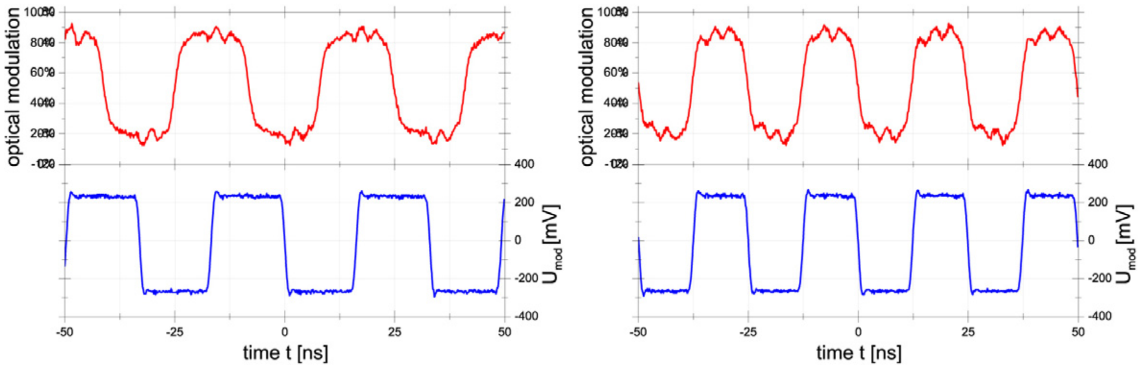

Figure 5.54: Transmission characteristics of the modulation signal to the optical modulation with 30MHz (l) and 40MHz (r) using the measurement setup according to fig. 5.52. The shape of both signals gets farther away from an rectangle shape.

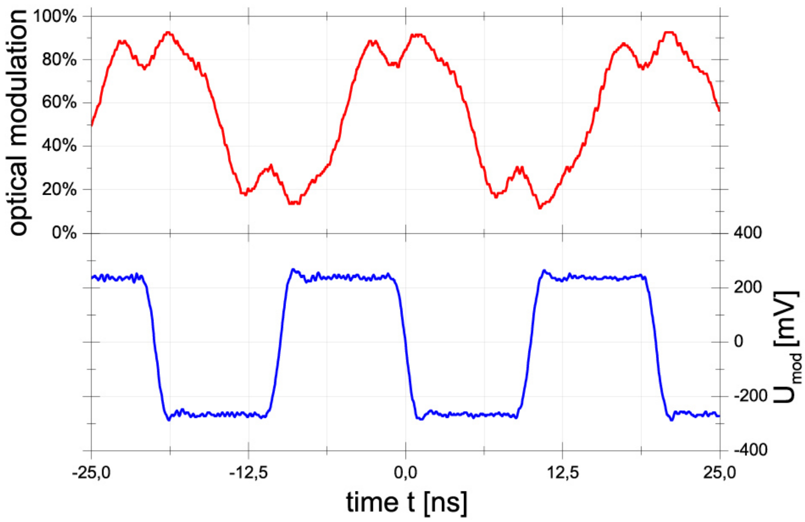

Figure 5.55: Transmission characteristics of the modulation signal to the optical modulation with 50MHz using the measurement setup according to fig. 5.52. The shape of the signals is rather a sine than a rectangle shape.

5.5 Experimental Laboratory Evaluation

With our fist prototype shown in fig. 5.32 on p. 78 absolutely nothing could be observed. Due to the use of uncalibrated components without optimization and tuning not any infrared light reached the ToF chip. The first idea for improvement was the use of a laser diode. Therefore it was possible to couple the infrared light directly from a point source into the endoscopic illumination channel guiding the light to the tip of the endoscope. Nevertheless, the first setup with laser illumination (Thorlabs L808P030) was not powerful enough to overcome the high endoscopic attenuation. Due to its increased attenuation the beam splitter was omitted subsequently. Without a beam splitter and the more powerful Thorlabs L808P200 laser diode, it finally was possible to enable the first endoscopic 3-D view on a liver model as depicted in fig. 5.56.

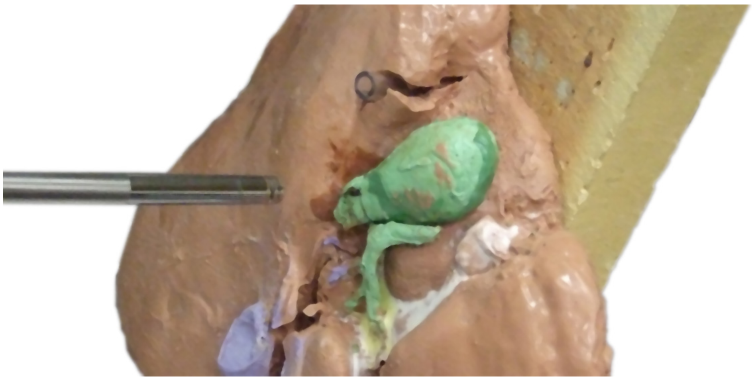

Figure 5.56: Measurement setup with a silicon model of the liver with gall bladder.

With extensive filtering it was possible to get acceptable results at least for short distances as shown in fig. 5.57.

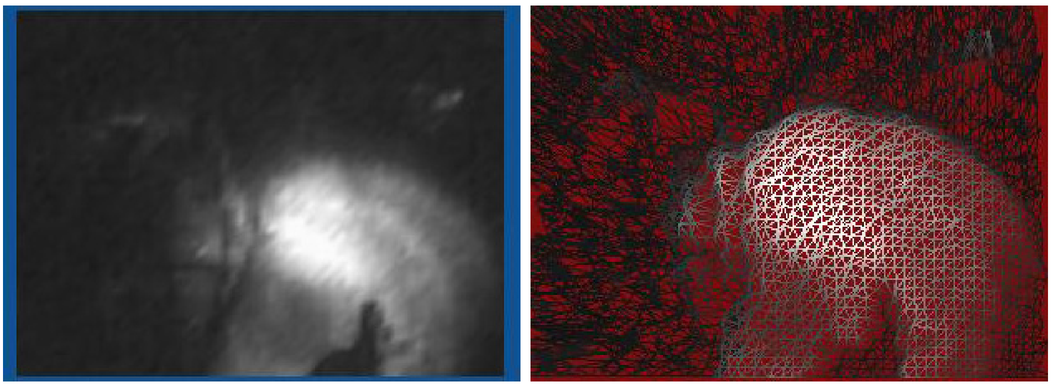

Figure 5.57: Experimental results with amplitude (l) and distance (l) image recorded with the ToF endoscope using the Thorlabs L808P200 laser diode for illumination [Tack 08].

Nevertheless, the high integration time and the short measurement range have been an indication that the illumination power had to be increased significantly. After the replacement of the Thorlabs laser diode by the even more powerful one from OSRAM and the design of a new amplifier and bias tee with more powerful components, better results could be achieved with the same PMD 3k-S ToF camera attached to an endoscope. The newly integrated illumination unit was evaluated to demonstrate the improvement compared to the results obtained with a simple LED. To assess this new design, two plastic cubes each of size $15 \times 15 \times 15$mm were inserted into an empty porcine stomach. Then it was manually insufflated with air. The ToF endoscope was inserted through the remaining parts of the esophagus as shown in fig. 5.58.

Figure 5.58: Measurement setup with a ToF camera mounted on a laparoscope and illumination using an OSRAM SPL2F81 laser diode. The laparoscope was introduced in an insufflated porcine stomach with two cubes of known size inside.

As the attenuation of the system with integration of the beam splitter was still too high, two combined laparoscopes were used for parallel acquisition of 3-D and color image as shown in fig. 5.59 instead.

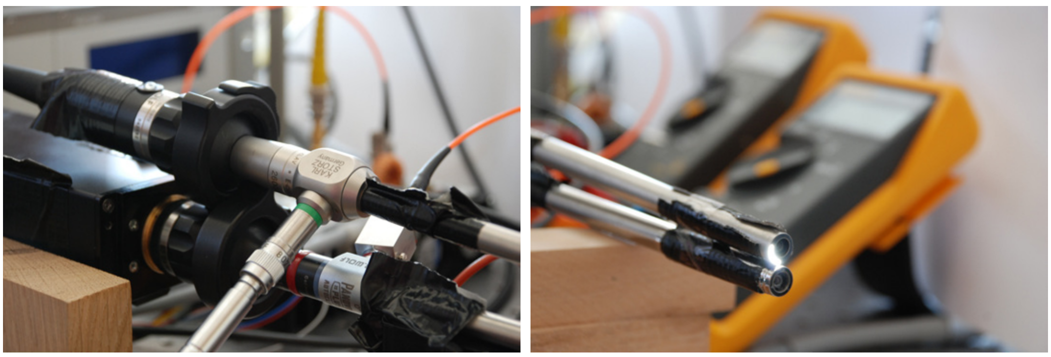

Figure 5.59: ToF and CCD camera with visible resp. laser illumination (l) attached to two parallel fixed endoscopes with uniformly oriented tips (r) to acquire 3-D and color images separately.

With that modified experimental setup it was possible to observe the cubes. They were taken as 3-D objects of known size and shape to assess the accuracy (fig. 5.60). Determination of the cube size was possible with an average error precision of $\mu =$ 0.89mm based on 100 acquired distance maps [Penn 09].

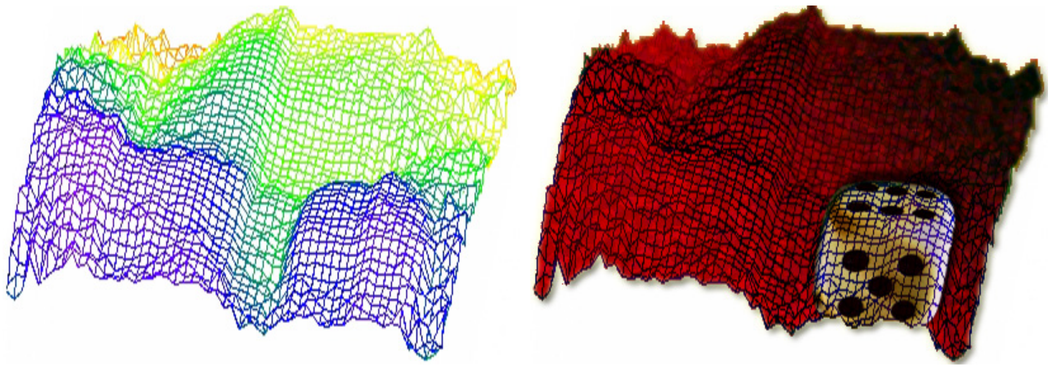

Figure 5.60: Colored 3-D mesh (l) of a cube with known size inside a porcine stomach (r).

In a next step the new MuSToF version with the PMD CamCube 2.0 was used. For a start the beam splitter and the CCD camera were omitted. The modulated laser illumination beam is rather narrowed as shown in fig. 5.61 l., where the emitted infrared light is made visible using an adapted IR sensor card. This provides important indications for further investigations and hardware designs conducting illumination fibers through the working channel to decrease the coupling attenuations. A terminating optical diffuser could provide a more equally distributed illumination field.

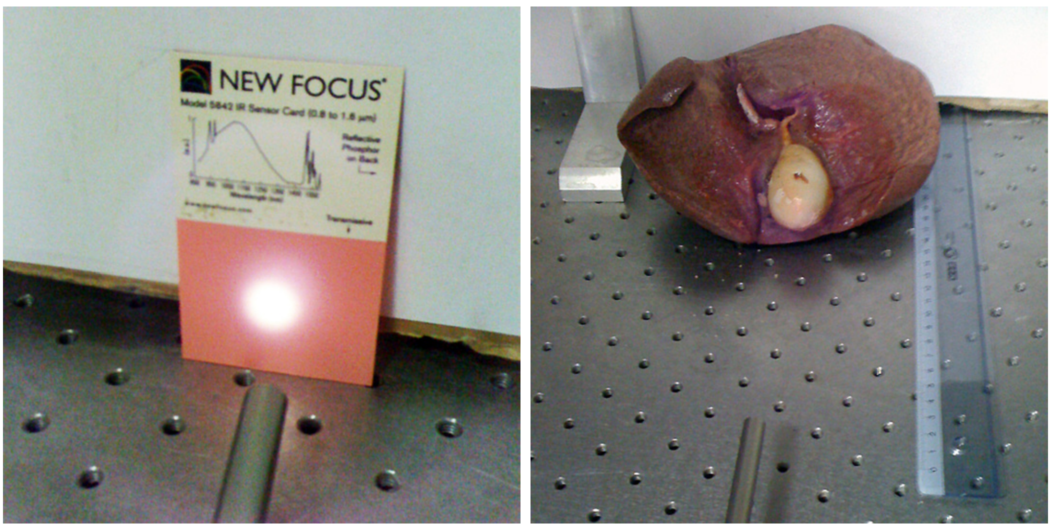

Figure 5.61: Evaluation setup to determine the laser illumination beam size and spread.

To qualitatively evaluate the results with the new hardware setup, a gelatine liver model as shown in fig. 5.61 r. was used for explorations. Looking into the raw data distance images in fig. 5.62 a) and the 3-D representation in fig. 5.63, high noise is visible. After averaging $N = 10$ subsequent image frames and applying a 5×5 median filter and a trimming vignette, the results look much better as shown in fig. 5.64. The results can even be optimized using a bilateral filter [Toma 98] with half-width $w = 5$ and standard deviations for a geometric spread of $\sigma_d = 3$ and a photometric spread of $\sigma_r = 0.3$. The noise can be eliminated and the observed structures get recognizable as shown in fig. 5.65. The protruding gall bladder is well detectable.

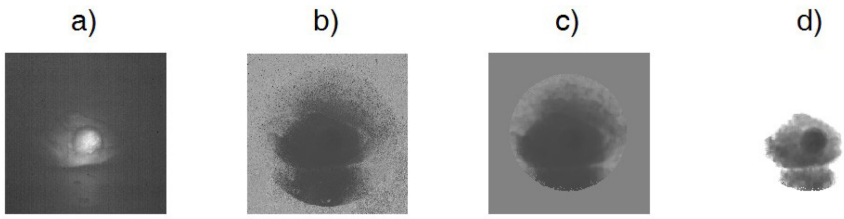

Figure 5.62: Rawdata of a liver model record with a) intensity image, b) original distance image, c) filtered image and d) narrowed range.

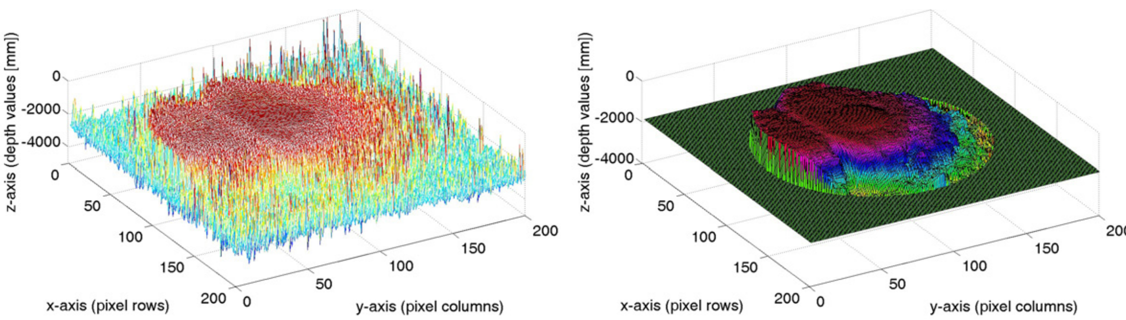

Figure 5.63: 3-D representation of unfiltered (l) and unconfined (r) data of a liver model with a protruding gall bladder.

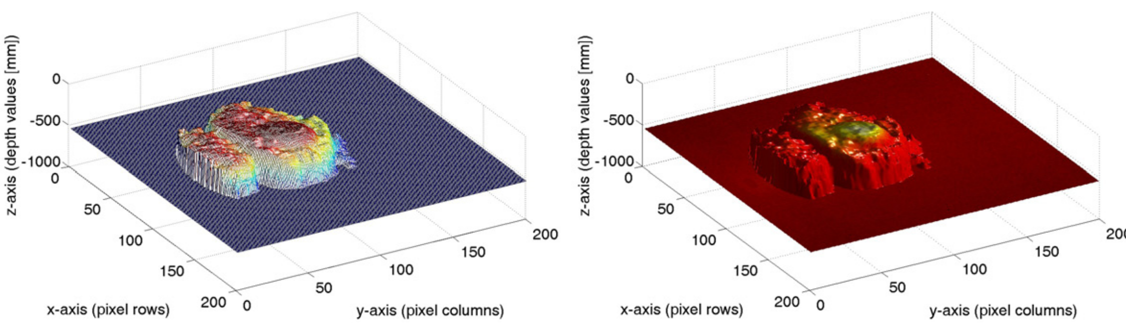

Figure 5.64: 3-D representation of median filtered liver model data with colored mesh (l) and reflectivity mapped surface (r) representation.

The same procedure was repeated with a colon model as shown in fig. 5.66, fig. 5.67, fig. 5.68 and fig. 5.69. In the midrange the structures can be captured much better than in the outer areas. Calibrating the plane deformation produces a more realistic view for the outer regions visible in fig. 5.69.

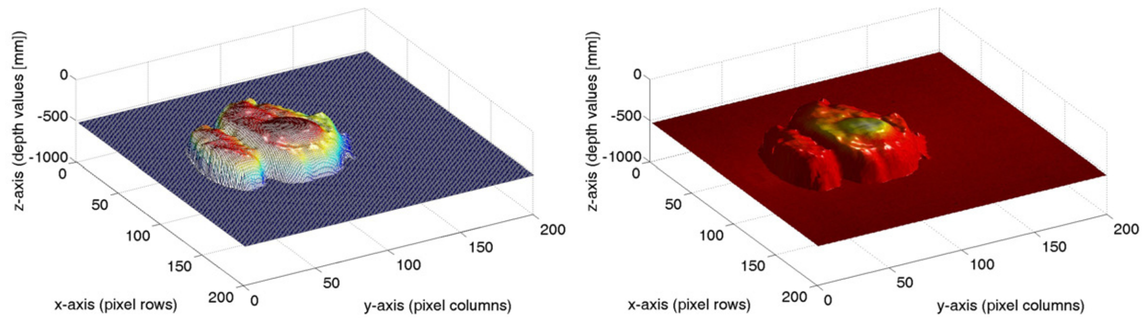

Figure 5.65: 3-D representation of bilateral filtered liver model data with colored mesh (l) and reflectivity mapped surface (r) representation.

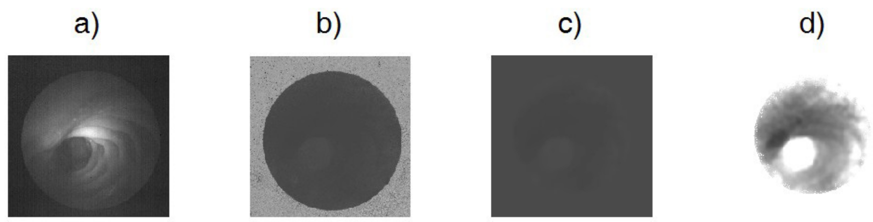

Figure 5.66: Rawdata of a colon model record with a) intensity image, b) original distance image, c) filtered image and d) narrowed range.

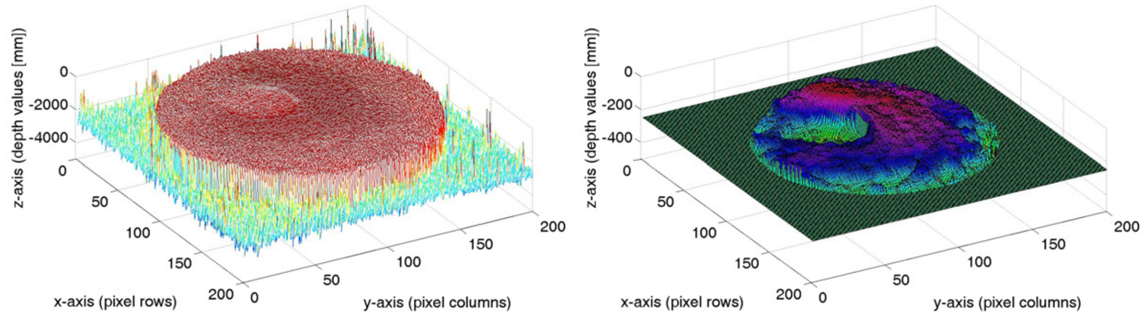

Figure 5.67: 3-D representation of unfiltered (l) and unconfined (r) colon model data with colored mesh (l) and colored surface (r) representation.

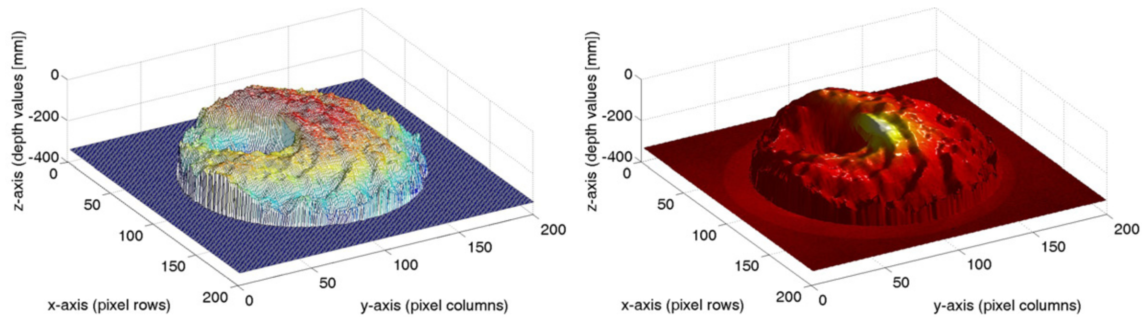

Figure 5.68: 3-D representation of filtered (l: median, r: bilateral) colon model data with colored mesh (l) and reflectivity mapped surface (r) representation.

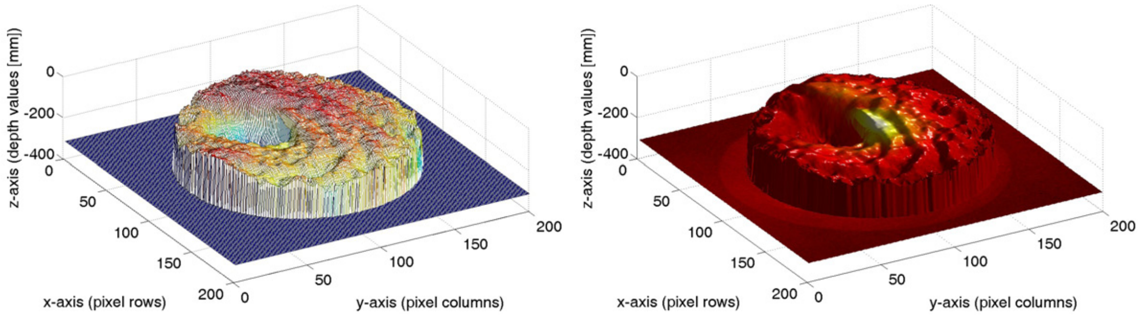

Figure 5.69: 3-D representation of plane calibrated and median resp. bilateral filtered colon model data with colored mesh (l) and reflectivity mapped surface (r) representation.

To have a visual comparison to the evaluation in [Penn 09], the third measurement comprehended a cube in a stomach model as shown in fig. 5.70, fig. 5.71, fig. 5.72 and fig. 5.73.

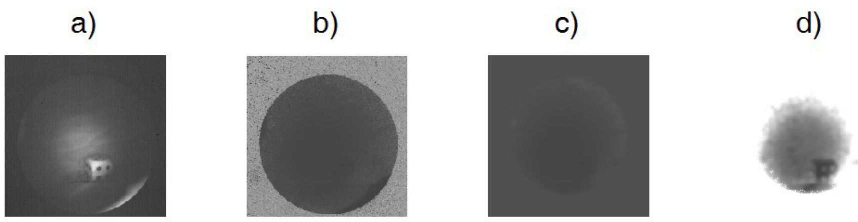

Figure 5.70: Rawdata of a cube inside a stomach model with a) intensity image, b) original distance image, c) filtered image and d) narrowed range.

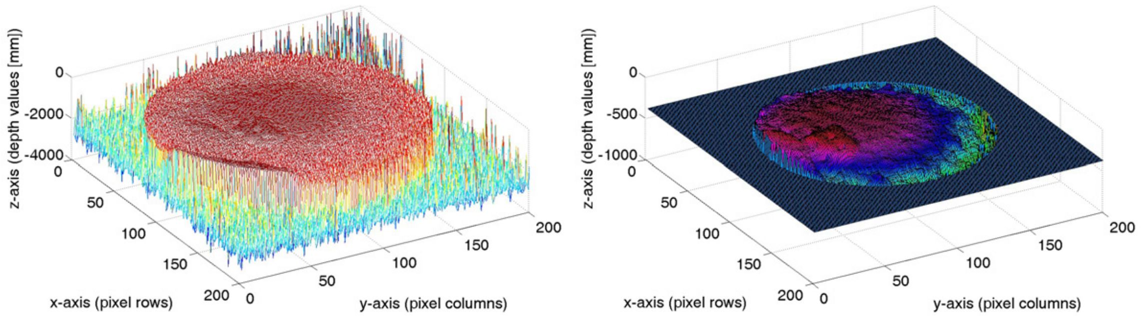

Figure 5.71: 3-D representation of unfiltered (l) and unconfined (r) stomach model data with cube inside with colored mesh (l) and colored surface (r) representation.

To have a visual impression on reflectivity dependency of ToF distance data as discussed in section 5.1.2, finally a checkerboard calibration pattern as shown in fig. 5.74, fig. 5.75, fig. 5.76 and fig. 5.77 is presented.

The black squares of the checkerboard seem to be several centimeters behind the white ones. In general, objects with poor reflectivity appear to be farther away than material with excellent reflectivity even when their actual distance is the same. This makes clear that within the next development steps the illumination distribution has

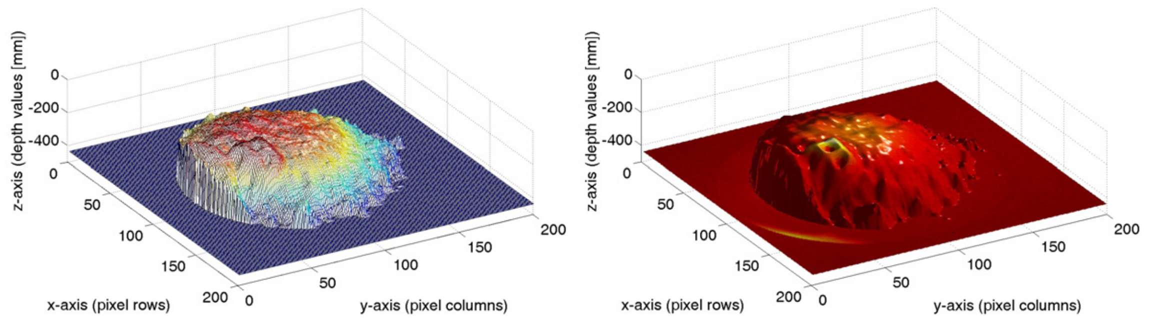

Figure 5.72: Filtered (l: median, r: bilateral) 3-D representation of a cube inside a stomach model with colored mesh (l) and reflectivity mapped surface (r) representation.

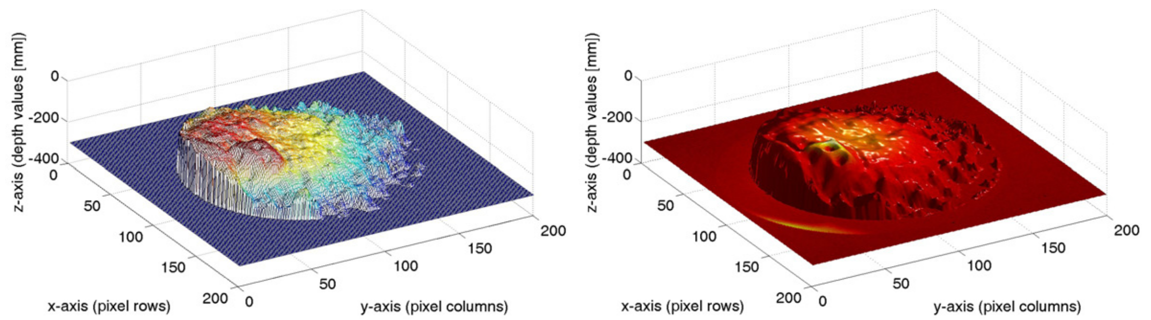

Figure 5.73: Plane calibrated and filtered (l: median, r: bilateral) 3-D representation of a cube inside a stomach model with colored mesh (l) and reflectivity mapped surface (r) representation.

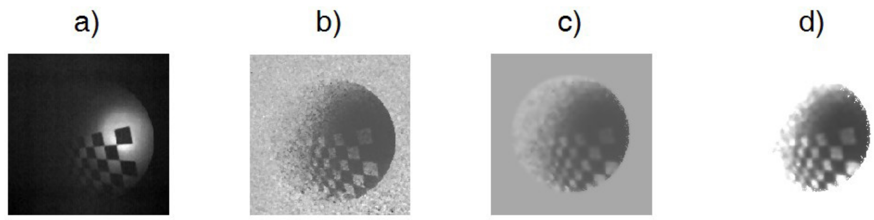

Figure 5.74: Rawdata of a checkerboard calibration pattern record with a) intensity image, b) original distance image, c) filtered image and d) narrowed range.

to be improved and additional calibration for measured distances depending on the intensity and amplitude values is needed.

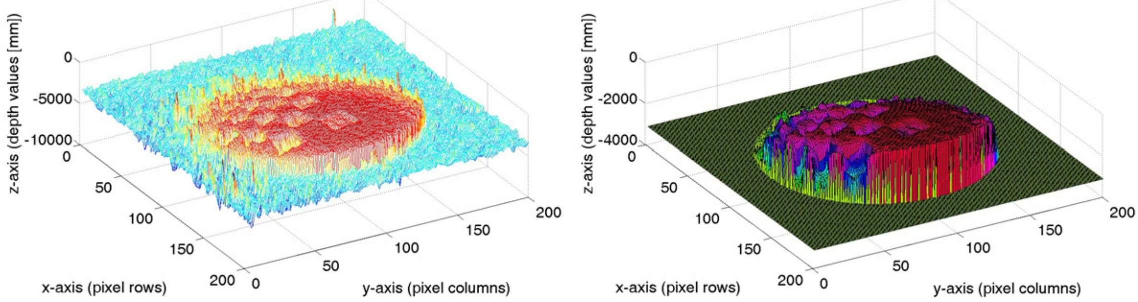

Figure 5.75: 3-D representation of unfiltered (l) and unconfined (r) checkerboard calibration pattern data with colored mesh (l) and colored surface (r) representation.

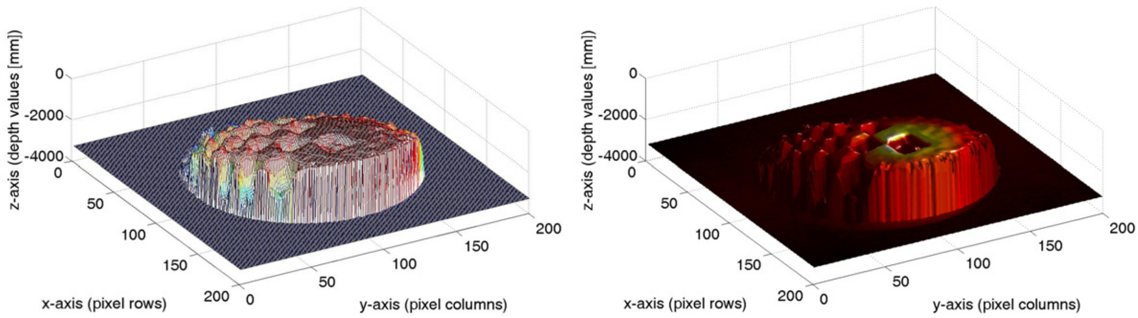

Figure 5.76: Filtered (l: median, r: bilateral) 3-D representation of a checkerboard calibration pattern with colored mesh (l) and reflectivity mapped surface (r) representation.

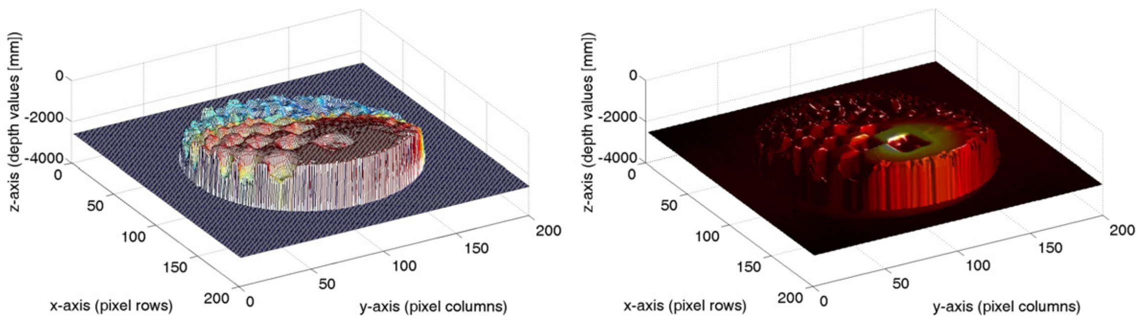

Figure 5.77: Plane calibrated and filtered (l: median, r: bilateral) 3-D representation of a checkerboard calibration pattern with colored mesh (l) and reflectivity mapped surface (r) representation.

5.6 Summary

First the parameters of the used ToF cameras had to be analyzed as described in section 5.1. For some common ToF requirements like temperature compensation or integration time adaption new algorithms were proposed. In section 5.2 an imaging model for the use of two rigidly mounted cameras, a calibration method and a registration method for multi-sensor imaging was proposed. In section 5.3 several hardware approaches with endoscopic devices fixed on the hybrid system were described. Distance and offset scaling methods were proposed. Requirements on illumination power and frequency spectra were discussed in section 5.4. The choice of the used laser diodes, the modulation coupling bias tee and the illumination power amplifier were described as well. In section 5.5 the experimental laboratory evaluation with liver, stomach and colon models showed satisfactory results.

Chapter 6

Novel Endoscopic Image Extension by Gravity based Rectification

6.1 Stable Endoscopic Horizon

Gastroenterologists have been trained and accustomed to navigate through the lumen of the colon, stomach or esophagus by pushing, pulling and rotating the flexible video-endoscope (fig. 6.1), regardless of orientation, rotation and pitch of the endoscope's tip inside the patient and the image orientation displayed on the monitor. Surgeons, on the other hand, are used to a fixed relation between the tip of the endoscope and the inside of the patient. As the currently practiced NOTES interventions require flexible endoscopes to access the abdominal cavity as well as the rigid surgical instruments to perform the actual intervention, both disciplines and technologies are needed. Mismatches in the spatial orientation between the visual display space and the physical workspace lead to a reduced surgical performance [Hold 99, Cao 00].
Hence, in order to assist surgeons interpreting and reading images from flexible video-endoscopy, an automated image rectification or re-orientation according to a pre-defined main axis is desirable [Kopp 01]. A stable horizon of the image is even more important in hybrid NOTES procedures, where an additional micro instrument is inserted through the abdominal wall for exposition during complex interventions. In the past, different approaches have been suggested for motion tracking [Welc 02], manual [Tang 08] and automated image rectification [Kopp 05, Eile 10]. But real-time computation of registration parameters between endoscopic image and secondary referencing 3-D systems is still a challenge [Miro 09] especially since colon or stomach surfaces do not provide clear feature points. Approaches that apply electro-magnetic tracking for endoscopic interventions require not only an additional sensor in the endoscope's tip but also an external magnetic field. The disturbance by metallic instruments is immense and leads to several further restrictions [Humm 02]. All the different approaches to solve the orientation problem have major restriction and thus a clinically acceptable solution is required to establish NOTES in the OR. A new approach, aiming to enhance the orientation during NOTES interventions, is presented in this work. It measures the orientation angle of the endoscope with a integrated Micro Electro-Mechanical System (MEMS) based inertial sensor device in the endoscope's tip. Gravity and other influencing forces as changes in movement are measured in three orthogonal directions (fig. 6.1). While prior trials just thought around putting an accelerometer at the end on an rigid laparoscope [Kara 94, Matt 00, Gree 02, Chat 05, Scha 05, Hoeg 05, Chat 06, Scha 06, Adam 07, Chat 07, Wiit 08, Dunk 08] it is now possible to integrate the sensor in the tip of a flexible endoscope [Holl 09b, Holl 10d]. If the endoscope is not moving, only the acceleration of gravity has an effect on the three axes as shown in fig. 6.1.

6.1.1 Technical Approach

To describe the orientation of the endoscope, an Cartesian "endoscopic board navigation system" with axes $\mathbf{x}$, $\mathbf{y}$ and $\mathbf{z}$ (according to the DIN 9300 aeronautical standard [DIN 90]) is used as body reference frame [Titt 04]. The tip points in $\mathbf{x}$-direction, which is the boresight, the image bottom is in $\mathbf{z}$-direction and the $\mathbf{y}$-axis is orthogonal to both in horizontal image direction to the right. Rotations about these axes are called roll Φ (around $\mathbf{x}$), pitch Θ (around $\mathbf{y}$) and yaw Ψ (around $\mathbf{z}$). Image rotation

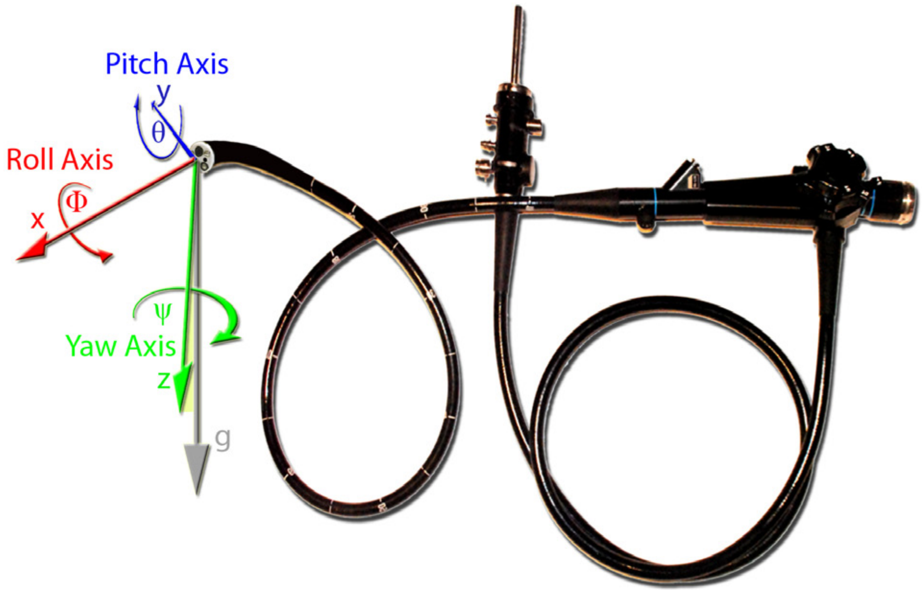

Figure 6.1: Roll, pitch and yaw description for endoscopic orientation.

has only to be performed about the optical axis **x**, which is orthogonal to the image plane. Gravity **g** is considered as an external independent vector. Since there is no explicit angle information, only the impact of gravity on each axis can be used to correct the image orientation. Equation (6.1) shows, how rotation parameters Φ, Θ and Ψ of the IMU (Inertial Measurement Unit) have to be chosen for measured accelerations F_x, F_y and F_z in order to obtain a corrected spatial orientation which means that **z** is parallel to **g**:

$$\begin{pmatrix} F_x \\ F_y \\ F_z \end{pmatrix} = \begin{pmatrix} 1 & 0 & 0 \\ 0 & \cos(\Phi) & \sin(\Phi) \\ 0 & -\sin(\Phi) & \cos(\Phi) \end{pmatrix} \cdot \begin{pmatrix} \cos(\Theta) & 0 & -\sin(\Theta) \\ 0 & 1 & 0 \\ \sin(\Theta) & 0 & \cos(\Theta) \end{pmatrix} \cdot$$
$$\cdot \begin{pmatrix} \cos(\Psi) & \sin(\Psi) & 0 \\ -\sin(\Psi) & \cos(\Psi) & 0 \\ 0 & 0 & 1 \end{pmatrix} \cdot \begin{pmatrix} 0 \\ 0 \\ g \end{pmatrix} = \begin{pmatrix} -\sin(\Theta)g \\ \sin(\Phi)\cos(\Theta)g \\ \cos(\Phi)\cos(\Theta)g \end{pmatrix} \tag{6.1}$$

Using the two-argument function atan2 to handle the atan ambiguity within a range of $\pm\pi$ one finally can compute roll Φ for $F_x \neq \pm g$ and pitch Θ for all values:

$$\Phi = atan2(F_y, F_z) \tag{6.2}$$

$$\Theta = \arcsin\left(\frac{-F_x}{g}\right) \tag{6.3}$$

As **g** determines just 2 degrees of freedom with this approach yaw Ψ cannot be computed. For $F_x = \pm |\mathbf{g}|$ ($\rightarrow$ $\Theta = \pm\pi$ $\rightarrow$ $F_y = F_z = 0$) roll Φ is not determinable either. To avoid movement influence, correction is only applied if superposed acceleration additional to gravity **g** is below a boundary value ΔF_{absmax}:

$$|\sqrt{F_x^2 + F_y^2 + F_z^2} - g| < \Delta F_{absmax} \tag{6.4}$$

6.2 Filtering the Measurement Data

With the employed sensor there is a uniform quantization of 8 bit for a range of $\pm 2.3 \cdot |\mathbf{g}|$ for each axis. This implies a quantization accuracy of $0.018 \cdot |\mathbf{g}|$ per step or 110 steps for the focused range of $\pm|\mathbf{g}|$. This is high enough to achieve a durable accuracy even to one degree within relatively calm movements. This is possible as roll angle Φ is calculated out of inverse trigonometric values of two orthogonal axes. Acceleration occurs only in the short moment of changing movement's velocity or direction. For the special case of acceleration with the same order of magnitude as gravity, the upper acceleration limit can be chosen small enough to suppress calculation and to freeze the angle for this short period of time. By choosing a longer delay line for the smoothing Hann filter and a higher minimum variation threshold on each axis, correction may be delayed by fractions of a second but will be stable even during fast movements.
Video rate is 25 frames per second. Accelerometer values are refreshed every 2.5ms, which is equivalent to a rate of 400 values per second.

A peak elimination is the result of down sampling the measuring frequency, which is 16 times higher than the image frame rate (up to 400Hz vs. 30Hz).

For each image just one angle value is needed for image rectification. This means that the rate for angle calculation should be synchronized with the video frame rate (fig. 6.2).

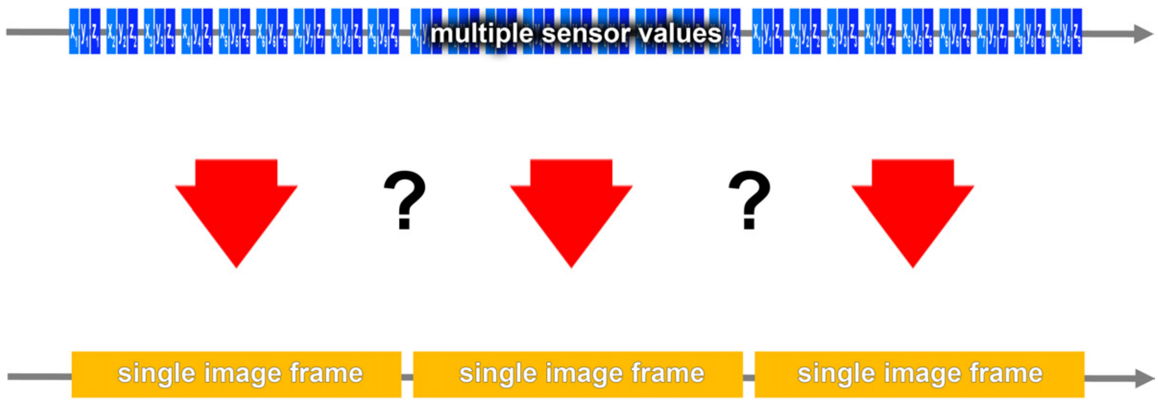

Figure 6.2: There are different possible approaches for the down sampling by a factor of 16 from the sensor measurement frequency to the image frame rate.

The down sampling procedure for accelerometer values can be realized by different approaches, which will be explained in the following steps:

6.2.1 Using Last Triple

Using the last triple (fig. 6.3) is the easiest way. It uses the newest sensor value. But unfortunately, the noise reduction was not sufficient. Especially, if the considered value is not appropriate, there is a high movement influence.

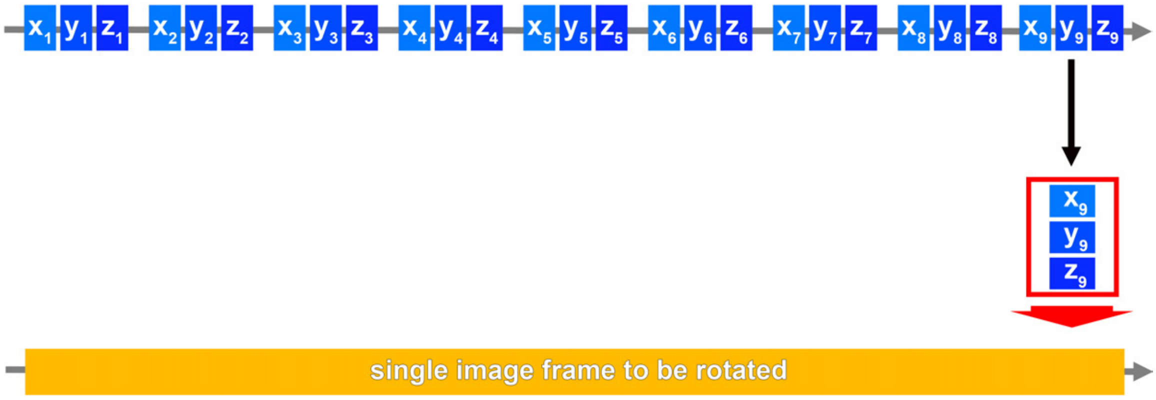

Figure 6.3: Down sampling from the sensor measurement frequency to the image frame rate can be realized by choosing the last triple value to rotate the new image frame.

6.2.2 Using Mean Values

$$\begin{pmatrix} F_x \\ F_y \\ F_z \end{pmatrix} = \frac{1}{n} \cdot \sum_{i=1}^{n} \begin{pmatrix} F_{x_i} \\ F_{y_i} \\ F_{z_i} \end{pmatrix} \tag{6.5}$$

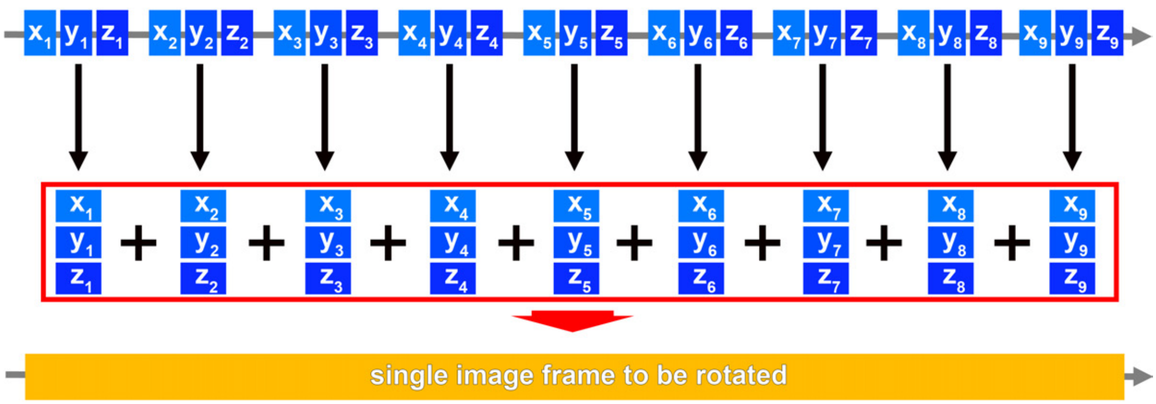

Figure 6.4: Down sampling from the sensor measurement frequency to the image frame rate can be realized by averaging all sensor triples to rotate the new image frame.

Using mean values (eq. 6.5, fig. 6.4) is a simple but efficient way. It provides noise reduction, but there still is some movement influence, as every value has the same impact without regarding its quality.

6.2.3 Using Median

Not very different to the mean value is the median. If all recorded values are sorted for each axis separately one can determine a new triple by taking the individual median values F_{x_i}, F_{y_j} and F_{z_k}.

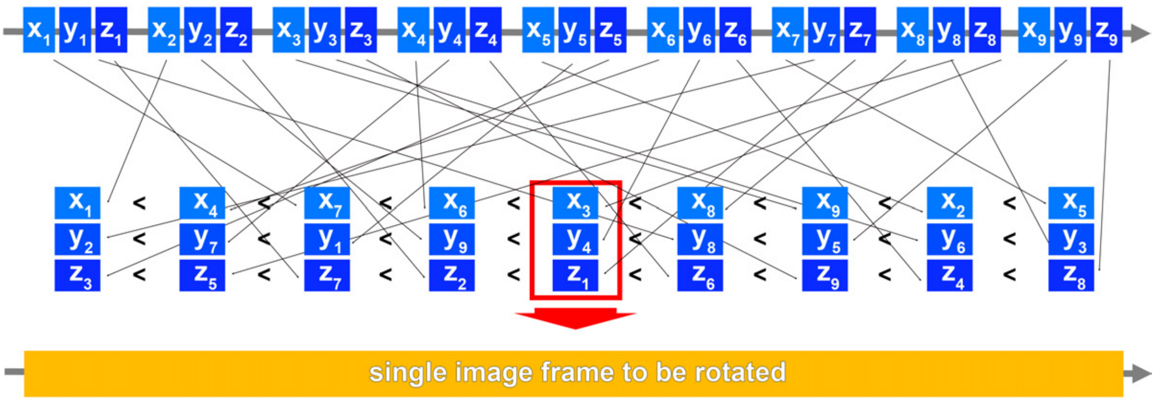

Figure 6.5: Down sampling from the sensor measurement frequency to the image frame rate can be realized by choosing the median of each sensor axis to rotate the new image frame.

The median is not taken of the angle but of each axis (fig. 6.5). It provides even better noise reduction, but there still is some distortion left due to the fact that those values are recorded at different times.

6.2.4 Using Best Triple

If the magnitude of all three axes is taken into account, one can choose the triple F_{x_i}, F_{y_i} and F_{z_i} with the minimum superposed force, which means the magnitude of $\mathbf{F_i}$ nearest to the magnitude of gravity $\mathbf{g}$.

$$|\mathbf{F_i}| = \sqrt{F_{x_i}^2 + F_{y_i}^2 + F_{z_i}^2} \tag{6.6}$$

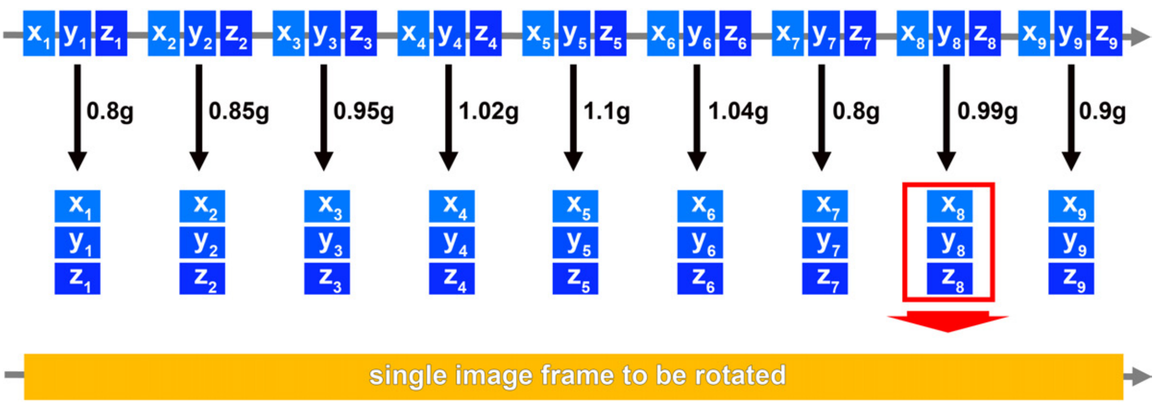

Figure 6.6: Down sampling from the sensor measurement frequency to the image frame rate can be realized by choosing the best triple to rotate the new image frame.

Taking the best triple (eq. 6.6, fig. 6.6) provides values with least movement influence. But as there is no averaging there is no noise reduction.

6.2.5 Using Weighted Sum

A combination of all different approaches is to sum up separately all $i = 1, ..., n$ sensor values F_{x_i}, F_{y_i} and F_{z_i} within an image frame and weight them with a weighting factor w_i with maximal weight w_0:

$$w_i = \frac{1}{\frac{1}{w_0} + |\sqrt{F_{x_i}^2 + F_{y_i}^2 + F_{z_i}^2} - |\mathbf{g}||} \tag{6.7}$$

Afterwards the sum has to be normalized by the sum of all weighting factors w_i:

$$\begin{pmatrix} F_x \\ F_y \\ F_z \end{pmatrix} = \sum_{i=1}^{n} (\begin{pmatrix} F_{x_i} \\ F_{y_i} \\ F_{z_i} \end{pmatrix} \cdot w_i) \cdot \sum_{i=1}^{n} (w_i)^{-1} \tag{6.8}$$

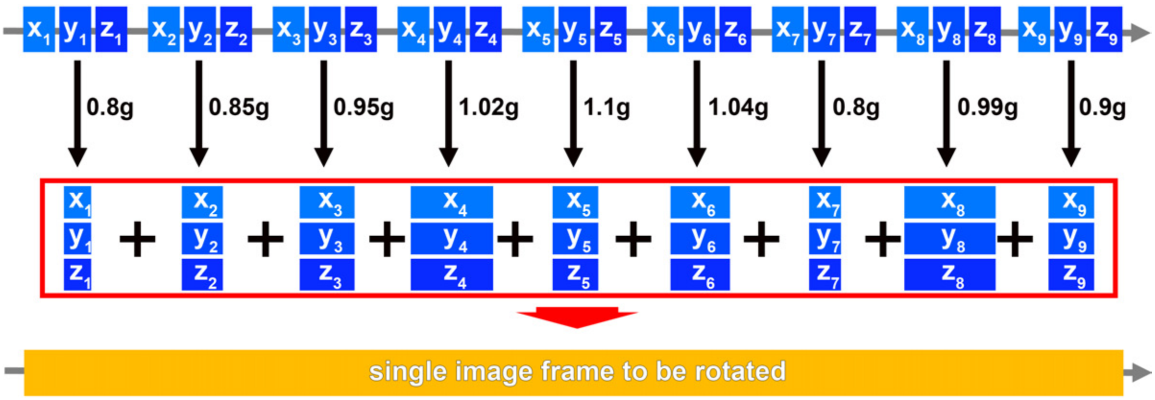

Figure 6.7: Down sampling from the sensor measurement frequency to the image frame rate can be realized by summing up weighted values to rotate the new image frame.

Using the weighted sum (eq. 6.8, fig. 6.7) provides less movement influence with quite good noise reduction [Holl 09a].

6.3 Algorithm Processing

To realize measurement, down sampling and filtering an effective software and hardware architecture had to be designed. The sensor implementation, filtering, communication and image rotation concept will be explained below.

6.3.1 Algorithm Implementation

The "ENDOrientation" algorithm shown in fig. 6.8 is divided into two parts. One part running on a small 8-Bit microcontroller and one part running as an application on a workstation.

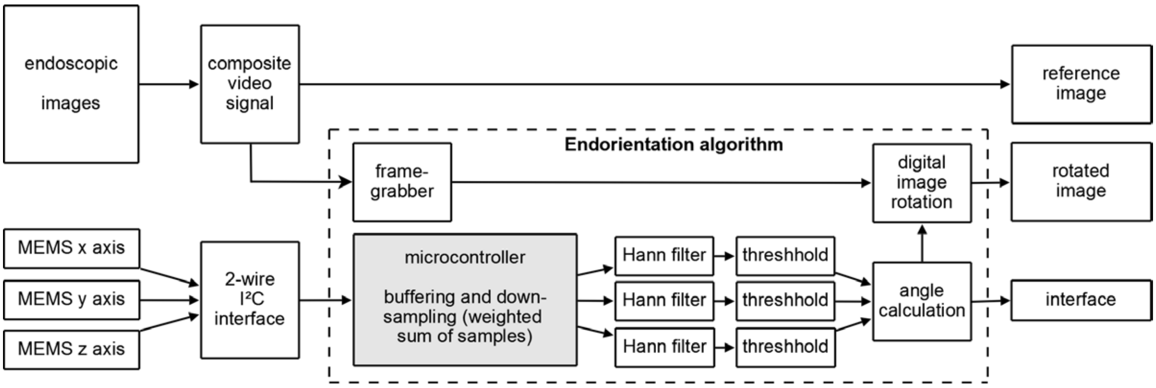

Figure 6.8: Block diagram of rotation correction with the "ENDOrientation" algorithm devided into two parts: One running on a microcontroller and one running on a workstation.

One main aspect in choosing the appropriate filter algorithm for rotation angle computation is the implementation characteristic of the target platform. In this approach, acquisition of acceleration measurements, filtering and down sampling is done on a small $8-bit$ microcontroller as shown in fig. 6.9.

Figure 6.9: ENDOSens controller box for the acquisition, filtering and down sampling of the acceleration measurements.

First, it had to be taken into account if it is useful to synchronize the measurements with the frame acquisition. To keep the hardware design simple a not synchronized free running data acquisition was used instead. All calculations are done with fixed-point numbers to avoid unneeded computational complexity. Squaring the acceleration vector components for magnitude calculation is done fast with the available hardware multiplier. The square root calculation is done with dedicated integer math like a CORDIC (COordinate Rotation DIgital Computer) implementation. At a first step the magnitude of an incoming acceleration vector and the weighting factor for the weighted sum method has to be calculated. The data storage itself is realized with a ring buffer structure. To avoid the need of synchronization, the outgoing value is calculated on demand. The calculation of eq. 6.8 on p. 106 is done every time the capture device acquires a new frame and the software running on the workstation requests the actual acceleration values from the software on the microcontroller.

Then all remaining calculations are done on the workstation only once per frame. First, a preceded 3×3 calibration matrix, which incorporates misalignment and scaling errors [Doro 99, Holl 05], has to be retrieved by initial measurements and applied. To avoid bouncing or jittering images as a result of the angle correction, additional filtering is necessary. Hence, prior to angle calculation, each axis is filtered with a Hann filter to smooth angle changes and with a minimum variation threshold ΔF_{axmin} to suppress dithering. As long as superposed acceleration calculated in eq. 6.4 remains below the boundary value ΔF_{absmax}, roll Φ and pitch Θ can be calculated using equations 6.2 and 6.3. Otherwise they are frozen until ΔF_{absmax} is reached again. If these boundaries are chosen correctly, the results will be continuous and reliable since nearly all superposed movements within usual surgery will not discontinue or distort angle estimation.

6.3.2 Sensor Communication

As visualized in fig. 6.10 the measurement data is transferred as a digital signal via a two-wire I^2C interface from the accelerometer fixed at the distal end along the flexible endoscope tube to the controller box fixed at the proximal end. This has three major advantages: The minimum number of wires needed for any communication is used, communication anyway is quite robust and permanent communication has to be done only by the controller box. The workstation only has to communicate if a new image frame is acquired. The communication between the controller box and the workstation is realized via the common universal serial bus (USB). For potential use with other devices the calculated angle also is transmitted to an external communication interface at the workstation.

6.3.3 Image Rotation

The endoscopic video signal is digitalized via a frame grabber or video capture device with a usual resolution of 720×480 with a frame rate of 30fps (NTSC) respectively a resolution of 720×576 and a frame rate of 25fps (PAL) to provide the highest

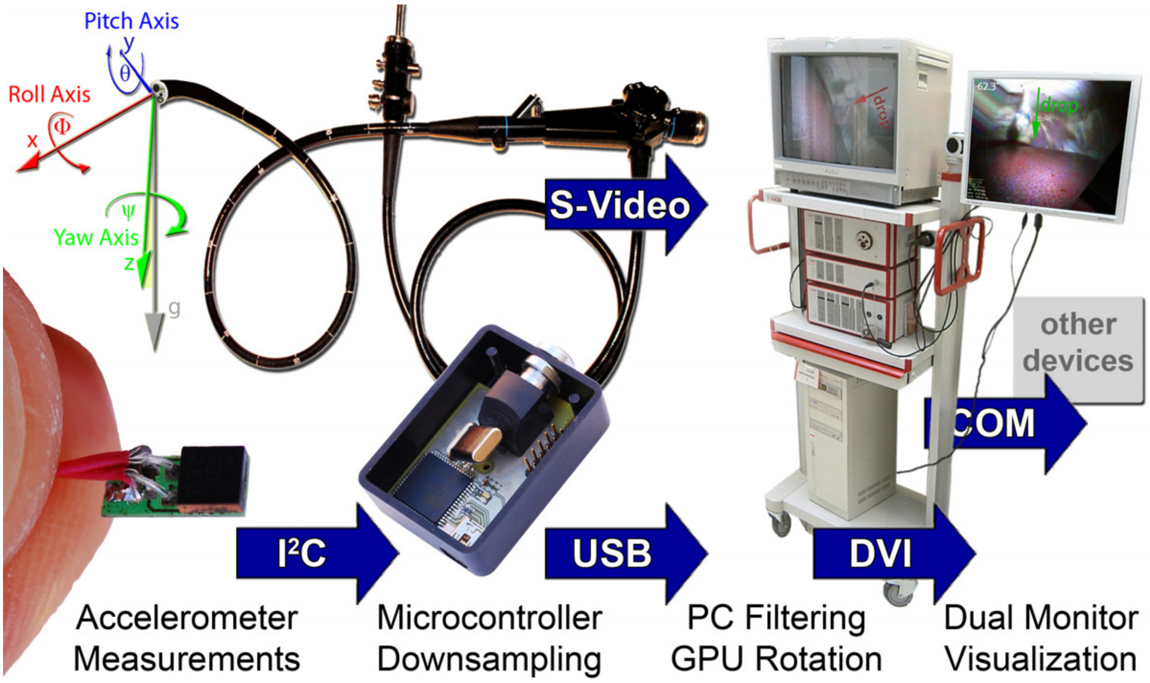

Figure 6.10: ENDOrientation communication concept between sensor, microcontroller, workstation and display.

quality to the operator. Even fullHD with a resolution of 1920×1080 and a frame rate of 30fps should be realizable. The rotation angle is calculated according to the previously presented equations. The rotation of the frame as shown in fig. 6.11 is performed via the OpenGL library GLUT [Kilg 96]. The advantage of this concept is the easy handling of time-critical tasks in the software. The sensor's sample rate of 400Hz can be used doing some filtering without getting into trouble with the scheduler granularity of the workstation OS, which mainly has to perform the angle calculation and the image rotation once per image frame. The information of the endoscope tip attitude is available within less than 30ms. The "ENDOrientation" algorithms including the image rotation can be performed in real-time on any off-the-shelf Linux or Windows XP/Vista workstation.

6.3.4 ENDOsens Hardware Prototypes

A first prototype of a 12×18mm circuit board with a 3-axis MEMS chip for acceleration measurement, SMD capacitors for power supply HF denoising and a two-wire I^{2}C communication interface was already build with this approach (table 6.1, fig. 6.12). By the use of a better MEMS sensor reduced the size to 5×8mm (table 6.2, fig. 6.13 l). In the next step, a new design using the same components but an improved layout reduced the size to 3×7mm (table 6.2, fig. 6.13 r). With a fourth sensor design and the use of the newest sensor generation, the resolution could be improved from 8bit to at least 12bit as shown in table 6.3. A fifth design is currently in development. The width of the sensor board will be reduced to 2mm as shown in table 6.4.

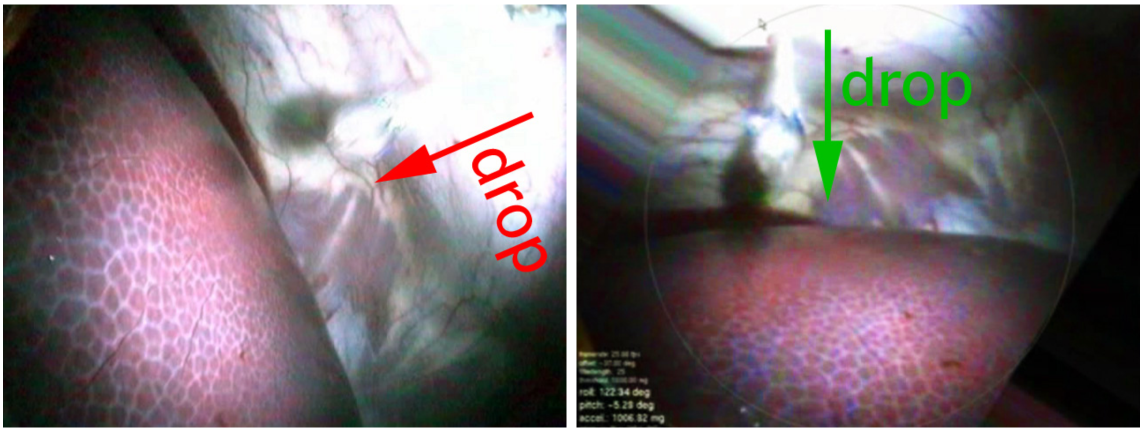

Figure 6.11: Screenshots of unrotated (l) and rotated (r) images with a falling drop injected through the abdominal wall above the liver during a porcine animal study. In the original video sequence it is visible that the drops of the unrotated image seem to move in any direction due to endoscope rotations whereas the drops on the right image are moving permanently vertically from up to down.

Table 6.1: First ENDOSens Prototype

Parameter	ENDOSens 1
Sensor model:	STM AIS326DQ [STM 08a]
Sensor type:	3-axis MEMS accelerometer
Measurement range:	$\pm 2 \cdot \lvert\mathbf{g}\rvert$
Resolution:	12bit
Data rate:	640Hz
Interface:	two-wire I^2C
Capacitors:	10µF + 100nF SMD 0603
Resistors:	2 × 4k7 SMD 0402
Overall size:	12mm × 18mm

Table 6.2: Second and third ENDOSens Prototype

Parameter	ENDOSens 2	ENDOSens 3
Sensor model:	STM LIS331DL [STM 08b]	
Sensor type:	3-axis MEMS accelerometer	
Measurement range:	$\pm 2.3 \cdot \lvert\mathbf{g}\rvert$	
Resolution:	8bit	
Data rate:	400Hz	
Interface:	two-wire I^2C	
Capacitors:	10µF + 100nF SMD 0603	
Resistors:	2 × 4k7 SMD 0402	
Overall size:	5mm × 8mm	3mm × 7mm

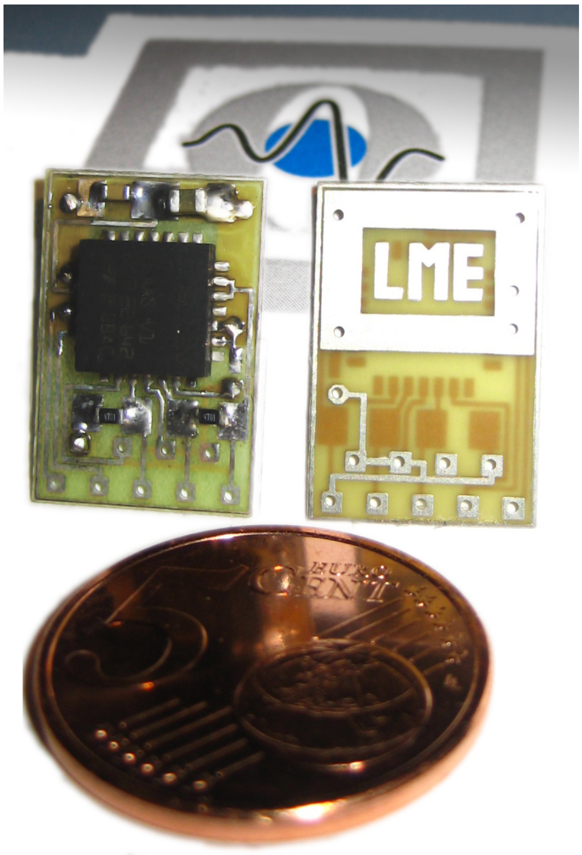

Figure 6.12: First ENDOSens prototype with STM AIS326DQ MEMS accelerometer and SMD capacitors and resistors.

Table 6.3: Fourth ENDOSens Prototype

Parameter	ENDOSens 4
Sensor model:	STM LIS331DLH [STM 09]
Sensor type:	3-axis MEMS accelerometer
Measurement range:	$\pm 2.3 \cdot \lvert\mathbf{g}\rvert$
Resolution:	12bit
Data rate:	1kHz
Interface:	two-wire I^2C
Capacitors:	10µF + 100nF SMD 0402
Resistors:	-
Overall size:	3mm × 7mm

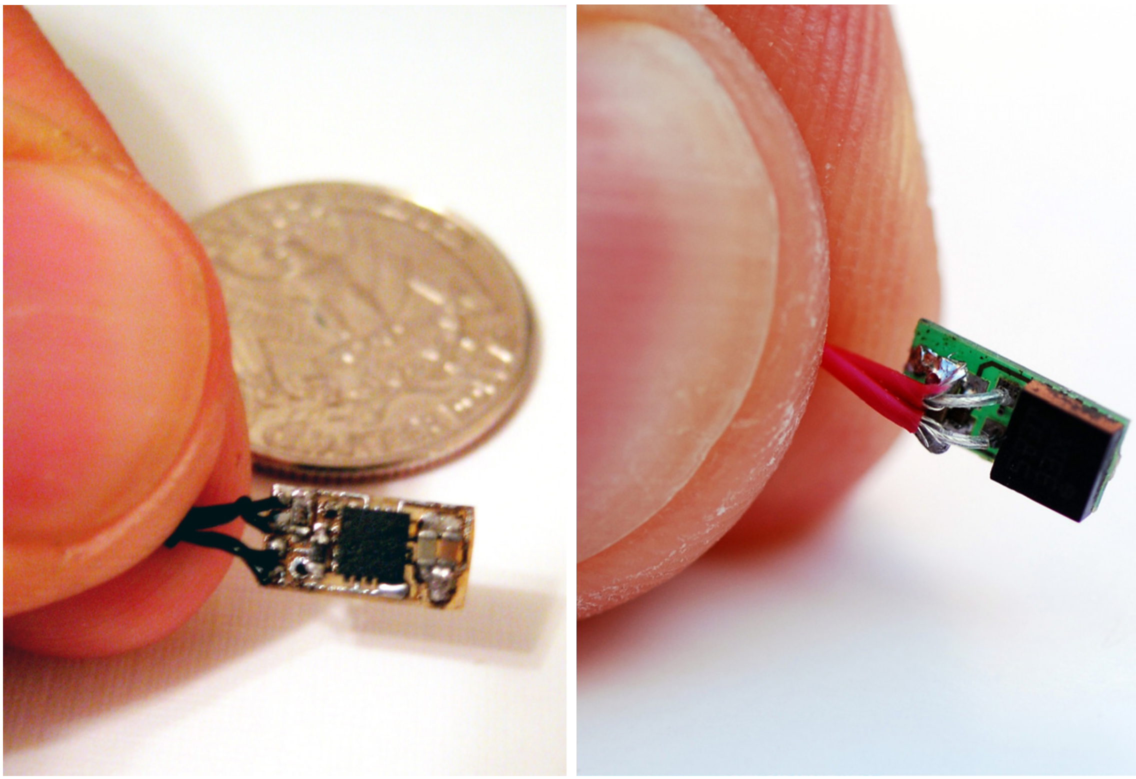

Figure 6.13: Second (l) and third (r) ENDOSens prototype with STM LIS331DL accelerometer and SMD capacitors and resistors.

Table 6.4: Fifth ENDOSens Prototype

Parameter	ENDOSens 5
Sensor model:	Bosch BMA220 [BMA2]
Sensor type:	3-axis MEMS accelerometer
Measurement range:	$\pm 2 \cdot \|\mathbf{g}\|$
Resolution:	6bit
Data rate:	1kHz
Interface:	two-wire I^2C
Capacitors:	10µF + 100nF SMD 0402
Resistors:	-
Overall size:	2mm × 6mm

6.4 Experimental Clinical Evaluation

To evaluate the benefit of rectified images for endoscopic surgery as well as the quality of the proposed ENDOrientation system for this purpose, an experimental clinical evaluation was performed.

6.4.1 Experimental Setup

During a porcine animal study approved by the Regierung von Oberbayern and shown in fig. 6.14, the navigation complexity with and without automated image rotation during a NOTES peritoneoscopy via the trans-sigmoidal access route [Wilh 07] was compared [Holl 09c].

Figure 6.14: Porcine animal study for experimental evaluation of automated image rectification using the ENDOrientation approach with multiple displays for original and rectified image and electromagnetic tracking of the surgeon's hand movements guiding the rigid instrument.

The endoscopic inertial measurement unit was fixed on the tip of a flexible endoscope as shown in fig. 6.15. Additionally, Ascension's "Flock of Birds", a pulsed DC magnetic tracking sensor with a resolution of 0.5mm and an accuracy of ±1.75mm, was fixed on a hybrid instrument to record the position of the surgeon's hands. To evaluate the benefit of automated real-time MEMS based image rectification, four different needle markers were inserted through the abdominal wall to the upper right, lower right, lower left and upper left quadrants. These four needle markers had to be grasped with a trans-abdominal introduced endoscopic needle holder under standardized conditions [Holl 09c].

First, only the original endoscopic view was presented to the surgeons, navigating the transcutaneous inserted rigid instrument. In a second run, the image view with the automatically corrected image horizon was displayed on a control monitor, while the surgeons performed the grasping of the needles again. The order was changed randomly for 50% of the probands, in order to avoid falsification of the study resulting

Figure 6.15: Prototyping with an external MEMS sensor on the endoscope's distal tip.

from learning effects. The turn with the original view still took longer time. During the study an unmanipulated image was available exclusively for the endoscopist who had to navigate the flexible scope which was not part of the evaluation focus. The time required for navigation of the surgical instrument to the four markers was recorded and statistically evaluated. The participating test persons were surgeons with different levels of surgical experience and expertise, including beginners, well-trained surgeons and one expert. All of them considered the automated image rectification to be very useful to navigate the transcutaneous inserted instrument towards the needle markers (fig. 6.16).

6.4.2 Time Comparison

In the performed experiments, it could clearly be shown that grasping a needle marker with an automatically rectified image is faster than with the originally rotated endoscopic view (Fig. 6.17). To accomplish the grasping task $n = 20$ times without image correction, the mean time of $\mu_{\text{orig}} = 53.95$s with a standard deviation of $\sigma_{\text{orig}} = 41.55$s has been observed. For the same operational task ($n = 20$) using the proposed image correction scheme a mean procedure time of $\mu_{\text{rect}} = 29.65$s with a standard deviation of $\sigma_{\text{rect}} = 21.15$s could be achieved.

More detailed analysis of the specific tasks separating in the four abdominal quadrants, shows that the highest benefit of image rectification could be achieved during manipulations in the lower abdomen (fig. 6.18). Grasping the needle in the upper right abdomen takes a mean time of $\mu = 72.00$s (± 67.13s) *without* image manipulation versus a mean grasping time of $\mu = 38.8$s (± 23.27s) with correction of the image horizon. In the lower right abdomen quadrant the grasping procedure took 62.2s (± 40.54s) vs. 24.6s (± 12.05s). On the left patient side the task could be accomplished in the lower abdomen with the original (unrectified) image in 38.8s

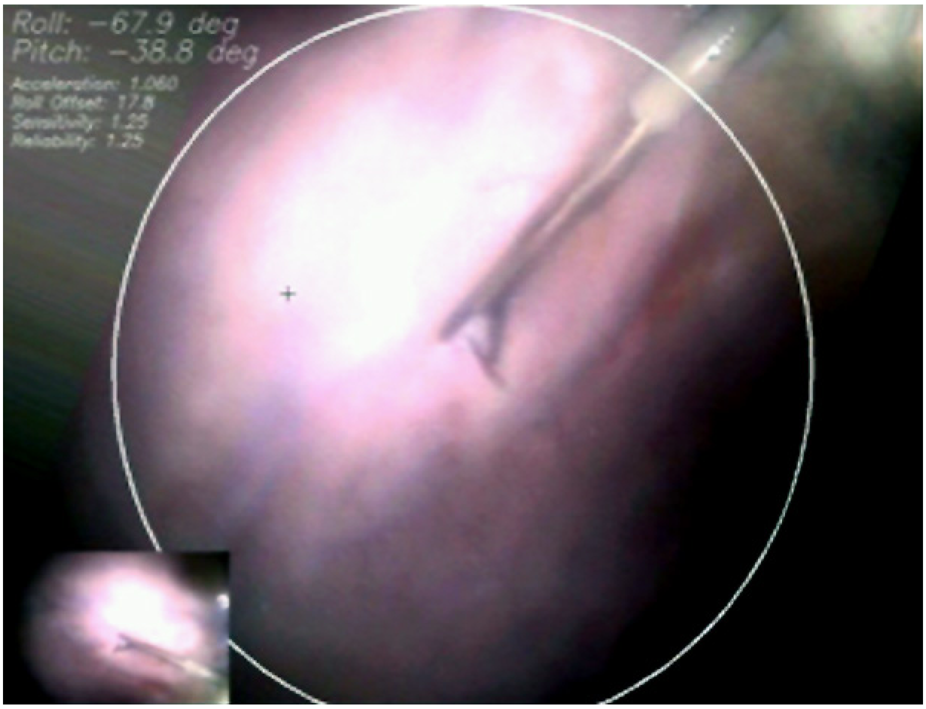

Figure 6.16: Screen shot of a rectified image produced by the ENDOrientation software while grasping a needle with a needle holder.

(±22.25s) vs. 15s (±9.41s) with the modified image, respectively $42.8s(\pm 24.89s)$ vs. 40.2s (±28.38s) in the upper abdomen. Especially for the both needles in the lower abdomen image rectification enables better performance.

6.4.3 Movement Comparison

The tracked movements of the hybrid instrument holder with our MEMS device performed by a well-trained test person are displayed in a 3-D plot (fig. 6.19). Increased movement activities are visible at four distinct points. These movements are translated through the fixed point of the trocar to the rigid instrument's tip inside the peritoneal cavity. With these translated movements the needles in each quadrant had to be grasped.

In comparison to the procedure based on the original image the movements based on rectified images are significantly more accurate with from 1650cm to 805cm reduced path lengths as one can see in fig. 6.20. Obviously the two parameters duration and path length are strongly correlated and can be regarded as a significant measure for the complexity of surgical procedures. Since duration and path length are decreased with the application of image rectification, the complexity of the complete procedure can be reduced.

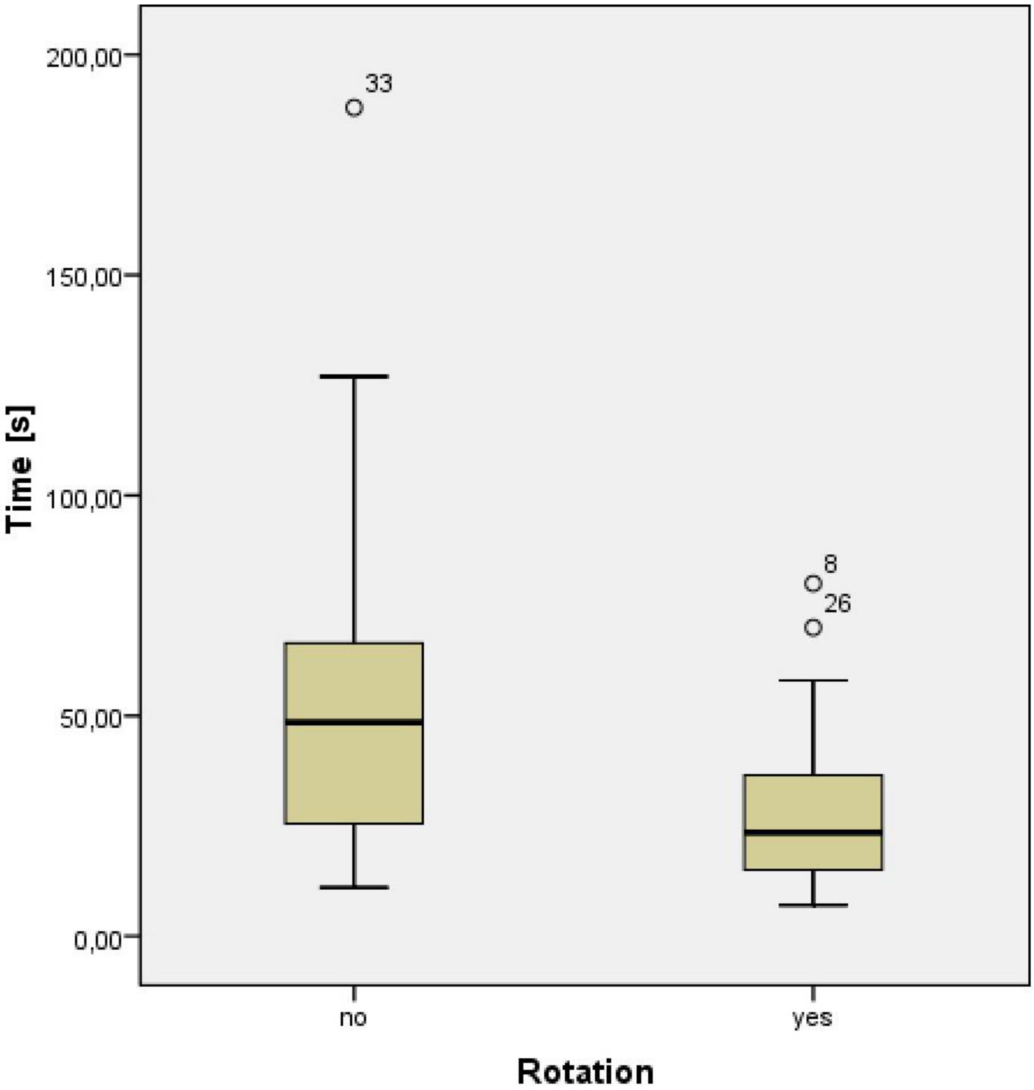

Figure 6.17: Box-and-Whisker-plot for the overall average time comparison without and with image rectification.

6.4.4 Technical Restrictions

As the test persons complained on the time delay correlated with the image rectification process, a simple method for measurement was found. Instead of an endoscopic image a video stream with 25fps showing the actual frame number was fed into the frame grabber and simultaneously shown on a display. On a second display the rotated video stream was depicted. Both displays were recorded with a camera. On a snapshot a delay of 10 frames could be observed. This means a time delay of 400ms.

In a new implementation with a new frame grabber, no delay could be observed any more. This is important for an intuitive coordination of the surgeon's movements.

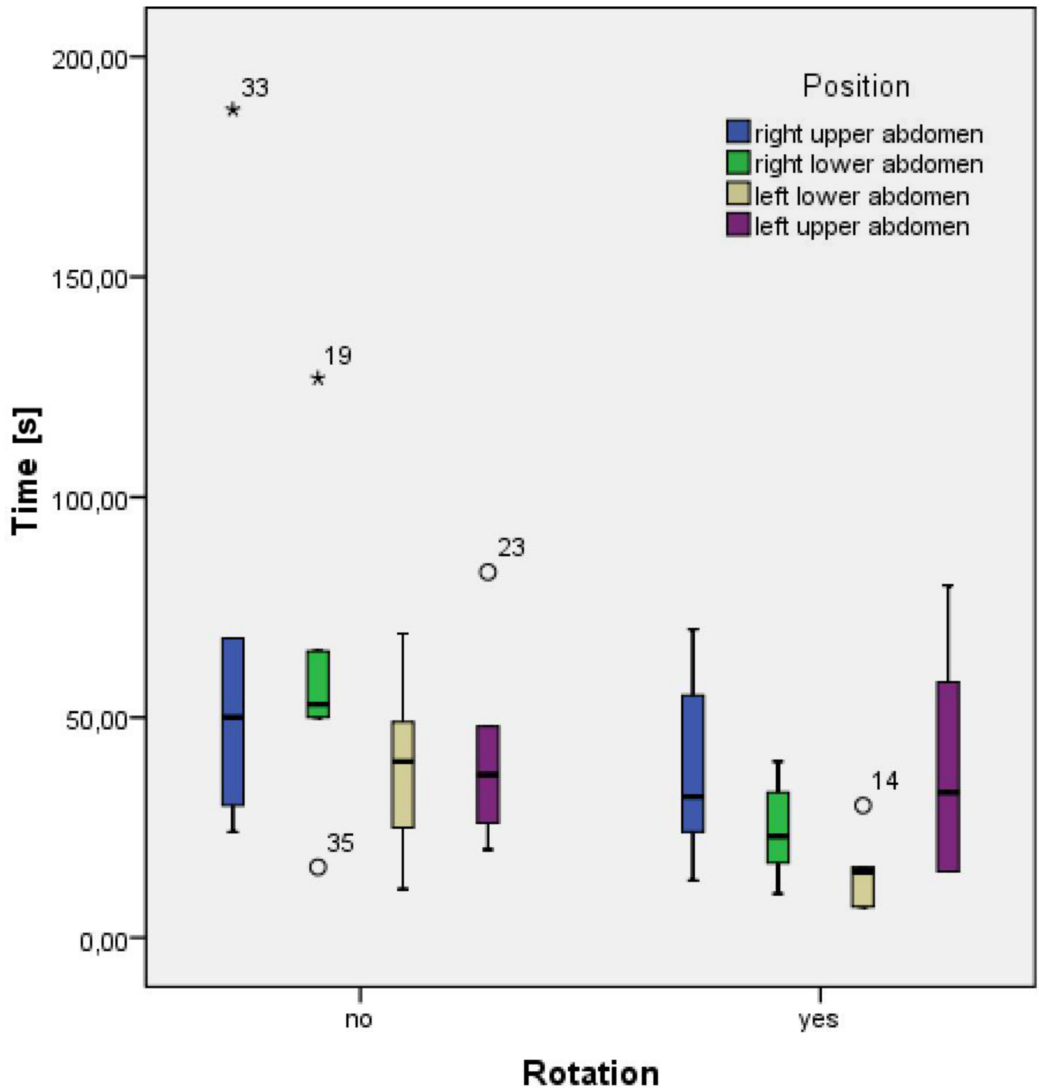

Figure 6.18: Box-and-Whisker-plot for the comparison of time needed to grasp the needle target in each of the four quadrants without and with the proposed image rectification scheme.

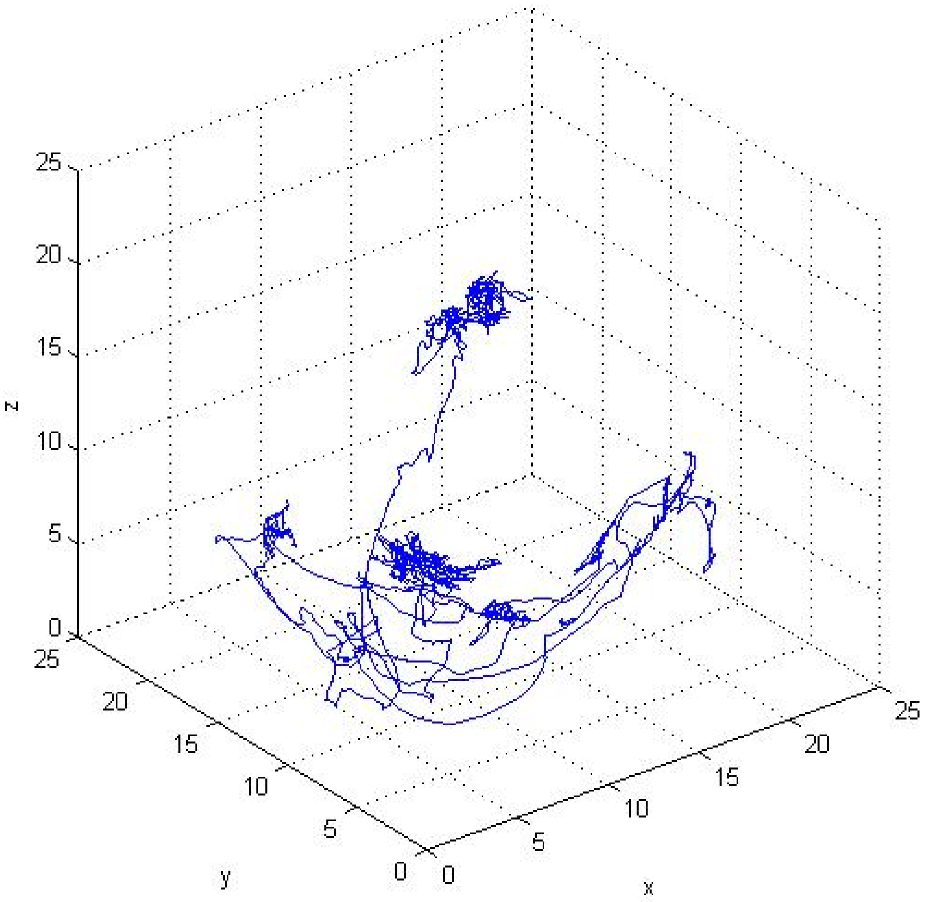

Figure 6.19: Original images cause movements with a total path length of 1650cm inches.

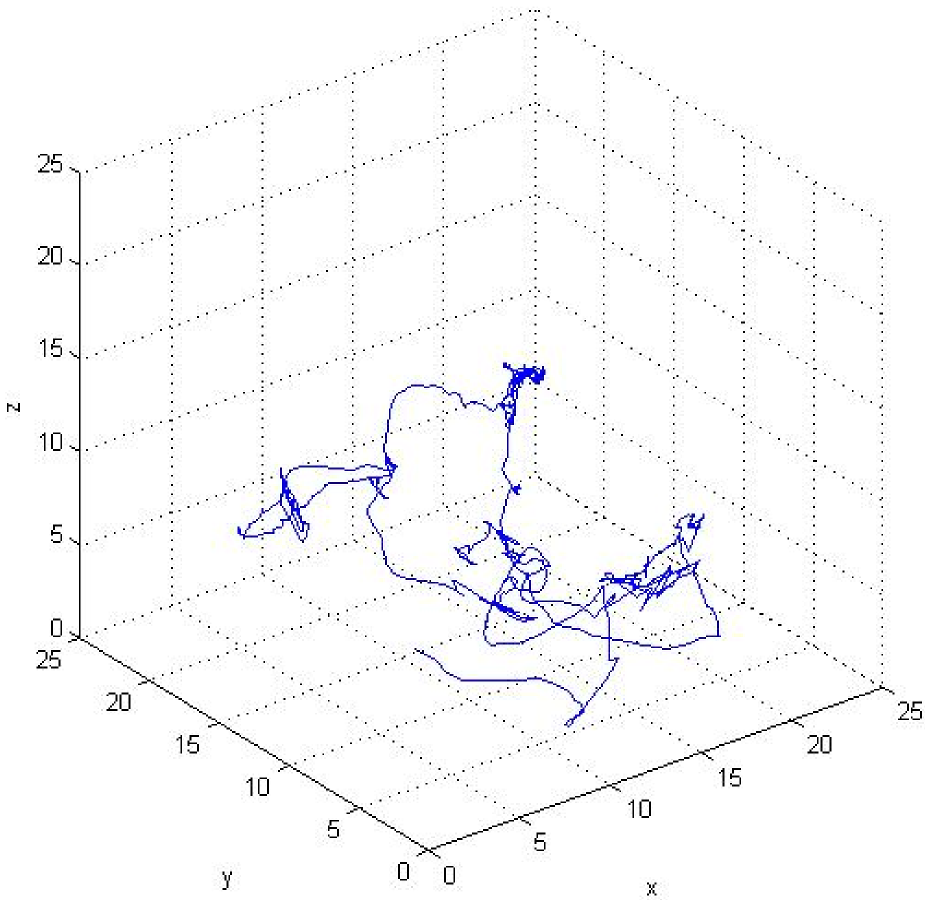

Figure 6.20: Rectified images cause movements with a total path length of 805cm. Obviously movements based on rectified images are significantly more accurate than having the original view.

6.5 Summary

The need of a stable horizon especially for flexible endoscopic surgery as well as an idea to solve this barrier by integrating an accelerometer in the tip of an endoscope is proposed in section 6.1. Since gravity is used as reference, only measurement values with low superposed acceleration should have an impact on the estimated orientation. Therefore, in section 6.2 different existing methods and a new derived weighted sum filter algorithm is proposed to combine the down sampling process with effective acceleration suppression. In section 6.3 the software and hardware architecture with a division in one part running on a small $8-$bit microcontroller and one part running as an application on a workstation is proposed. In section 6.4 an experimental clinical evaluation shows the benefit of rectified images for endoscopic surgery by decreasing the intervention time and the instrument path length by a factor of 2. The quality of the proposed ENDOrientation system is verified to be sufficient for this purpose.

Chapter 7

Discussion on Novel 3-D Image Extensions with NOTES

7.1 Notes Assessment Techniques

The introduction of NOTES procedures during the last years increased the amount of clinical studies in this new medical field. Actually, working groups all over the world establish new techniques and instruments. Today, clinical studies typically include the type of the intervention, operating time, infection rate and other clinical parameters. These data could be enhanced, if additionally technical parameters would be recorded. Objective evaluation and assessment is rarely done as there are no established methods with reliable measuring devices for exact navigation due to the surgeons' orientation abilities.

7.1.1 Time

The overall intervention time is an indicator for its complexity and quality. However, the training level of the surgeon, and moreover, the whole surgical team must be taken into account, too. If the intervention did not take much time with the same team it is likely to have been not to complex and well-done. But it is worth to have a closer look also on other NOTES evaluation parameters, currently existing techniques for the acquisition of spatial information, possible usages during an intervention and their post-operative evaluation contribution.

7.1.2 Path Length

To provide more information on the position and accumulated path length of the endoscope, electromagnetic tracking can be used. The actual position in a pre-operative volume, image or planning draft can be shown. Hereby the accuracy resp. unintended deviations of the surgical navigation can be verified intra-operatively. Alternatively to the tracking approaches intra-operative optical 3-D surface data can be registered with preoperative and pre-segmented CT or MR data. With those calculated transformation parameters, position and orientation can be determined, too. Therefore, it is possible for evaluation purposes to compare the actual path to the pre-operatively planned path.

7.1.3 Acceleration

Measurement of the acceleration could be used to classify the quality of the intervention performance and the experience of the physician. The lower the accelerations are, the better trained and experienced is the physician. A well-trained physician needs just one try to navigate to the position where he wants to go to or to cut where he wants. There is less forward-backward movement and a smoother control of the instrument. With the Fast Fourier Transformation (FFT) of the acceleration it is possible to visualize special individual frequency peaks for each physician. They are a measure for calm movements, constant velocity and steady direction.

7.2 Notes Navigation Techniques

As shown more detailed in section 3.1, additional information for medical applications beyond the 2-D color image can be acquired by endoscopic ultrasound, electromagnetic tracking or active optical approaches for distance and surface measurement. The last one is used with our MuSToF system proposed in section 5.3 and measures distance by Time-of-Flight (ToF), i.e. the phase shift between sent and recieved signal according to section 4.1.1. With a precondition of real-time ability and an accuracy of 1mm, some existing problems with NOTES like access to peritoneal cavity, maintaining spatial orientation or development of a multitasking platform according to section 2.5 on p. 17 can be solved. Especially the registration with pre-operative acquired CT or MRI volumes will provide numerous possibilities for improvement [Holl 08a]. Several points of the fundamental challenges to the safe introduction of NOTES and potential barriers discussed in the NOTES White Paper proposed in section 2.5 on p. 17 seem to be solvable with the on-line acquisition of additional 3-D data [Holl 10c].

7.2.1 Access to the Peritoneal Cavity

Translumenal surgery offers challenging possibilities for trauma reduction. Current investigations are mainly focused upon optimization of the access routes and its safe closure [Wilh 08]. Not only the route as shown in fig. 7.1, but above all the optimal entry point for the secure introduction of the instruments into the abdominal cavity is hard to find. Additional information is needed to avoid injuries during the penetration of the gastric or intestine wall without knowledge of structures behind the visible structures as shown in fig. 7.2. Reducing the risk of lacerations would be a great improvement.

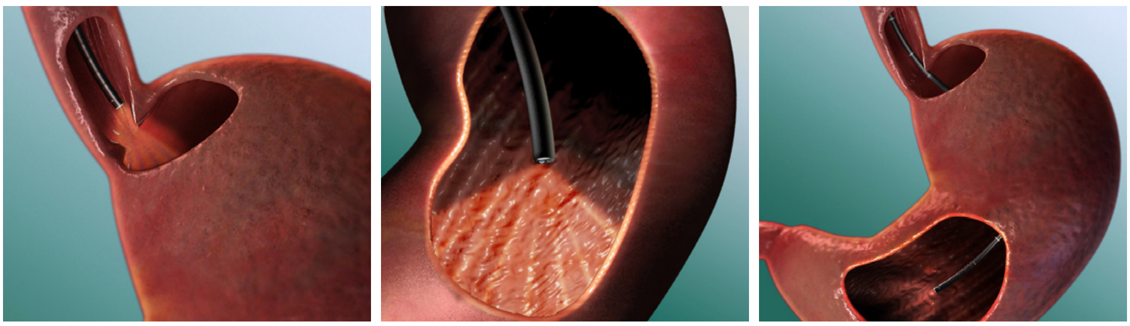

Figure 7.1: Virtual endoscopic route from the esophagus (l) to the stomach (m, r) in a virtual model.

Registration with preoperative MRI or CT volumes opens up lots of additional possibilities. The most promising one is to show hidden organs or vessels by augmented reality. They have to be segmented in the preoperative volumes and to be transformed by iteratively computed transformation parameters. Then these organs and vessels can be displayed by Augmented Reality (AR) [Vosb 07] as shown in fig. 7.3.

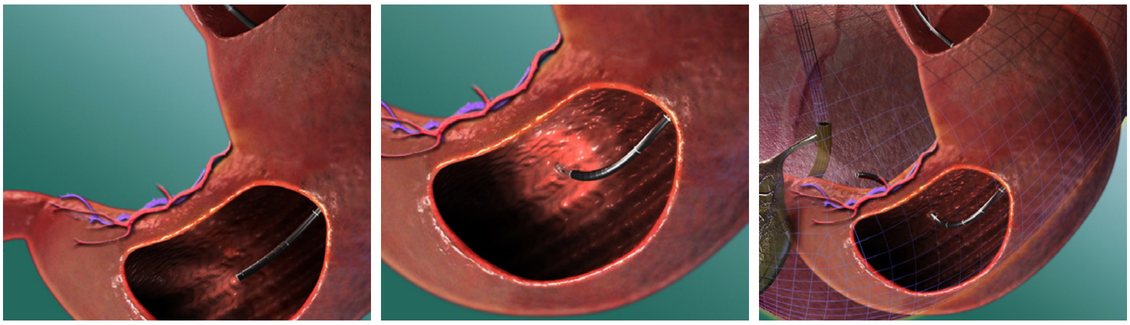

Figure 7.2: Augmented Reality (l), off-axis view (m) and distance measurement (r) in a virtual gastric model.

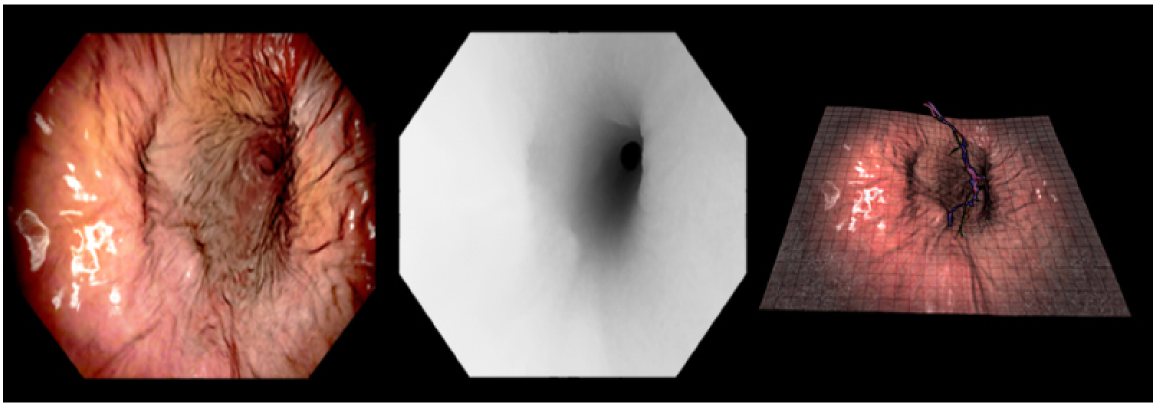

Figure 7.3: Virtual vessel visualization with conventional color image (l), depth values (m), and augmented 3-D image (r) for safer navigation inside the human body.

7.2.2 Enhanced Field of View

Endoscopic axis in-line view and loss of spatial orientation is especially for surgeons quite uncomfortable. To compensate this disadvantage, online 3-D surface knowledge can be used to extend and virtually rotate the field of view (fig. 7.4). Such a virtual off-axis view will provide the feeling of a rendezvous method with increased depth perception [Swai 07b] but without additional incisions. Using a 3-D mosaicking technique, the field of view can be extended additionally by a reconstruction of the operation area.

7.2.3 Distance Measurement

If for each color pixel in an image there is a corresponding distance value it is possible to determine the distance from the endoscope's tip to special selectable points (e.g. instruments, structures, organs) or even better to determine the distance between two freely selectable points (e.g. size of an organ) as shown in fig. 7.5.

With accurate distance measurement it will be possible to implement an automatic light intensity control to avoid glare for short distances with material of high reflectivity. Additionally, motion compensation enables to focus on the desired field of view and a visually stabilized surgical view even if the scene is moving [Stoy 08].

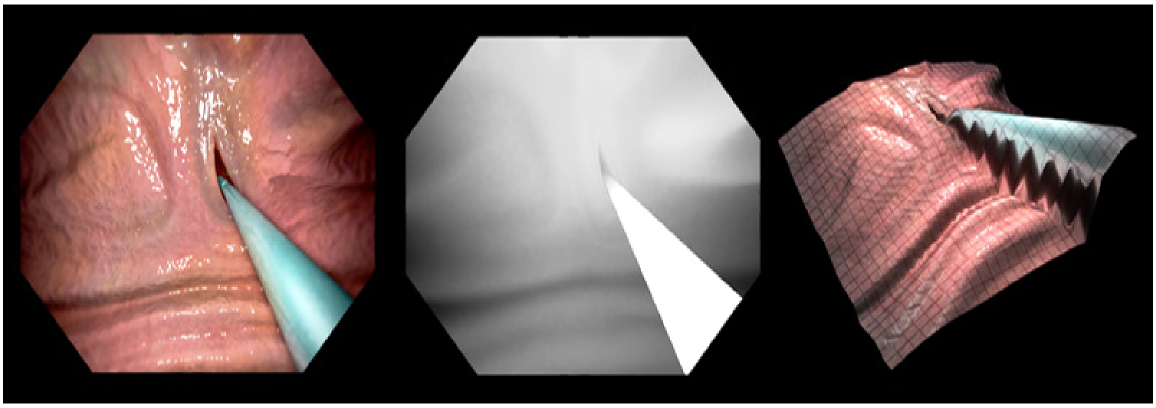

Figure 7.4: Virtual off-axis view with conventional color image (l), depth values (m) and off-axis view (r) for a better impression and depth perception with surgical scenes.

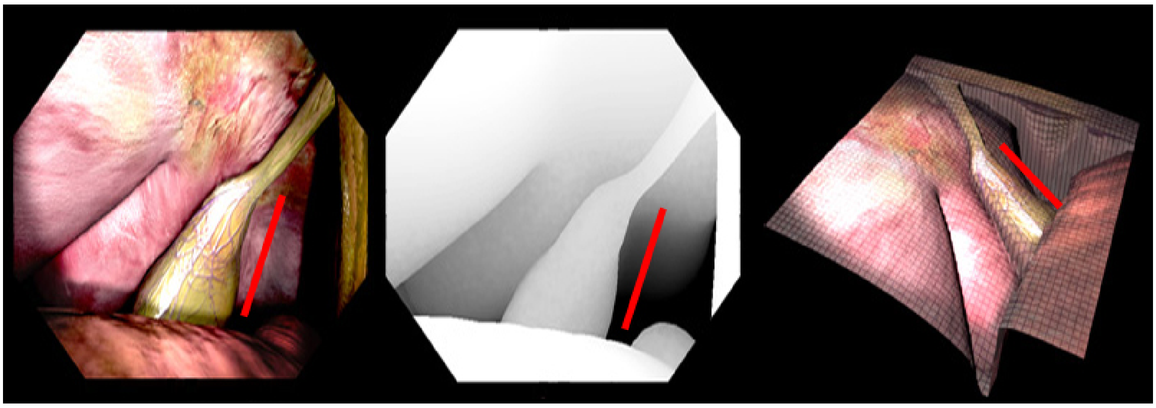

Figure 7.5: Distance measurement with conventional color image (l), depth values (m) and real distances (r) for verifiable distance measures within the surgical scene.

With knowledge on the physical dimensions and occurring variations also an automated instrument positioning is possible.

7.2.4 Collision Prevention

The increasing demand of robotic devices to control multiple instruments through only one flexible endoscope or a hybrid intervention needs additional control mechanisms to avoid unintentional injuries. To enable efficient collision prevention, real-time distance information is needed. Avoidance of impending collision of robotic multi-pivot instruments with tissue or other surgical devices will be especially important for higher safety within automated processes of upcoming robotic approaches.

can be realized as well as auto-positioning depending on respiration or other patient movements (fig. 7.6).

7.2.5 Dynamic Reconstruction

In many cases with limited view a virtual change of the point of view provides a better impression of the scene. This includes not only simulated views from other

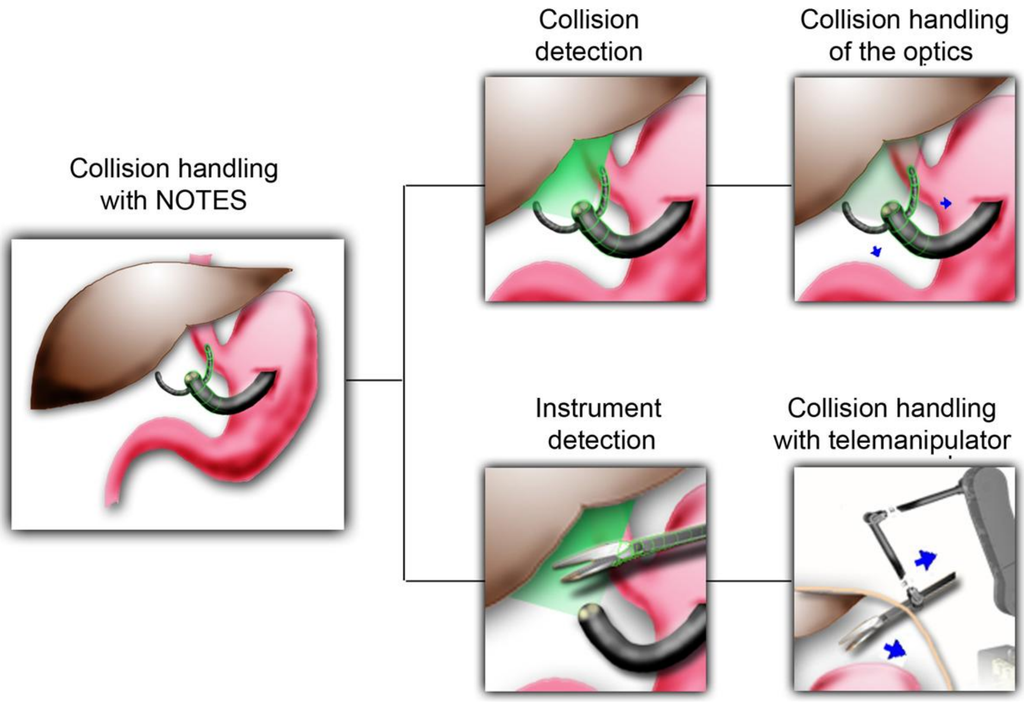

Figure 7.6: Methods for efficient real-time collision prevention with collision detection, collision handling with the optics as well as instrument detection and collision handling with the manipulator.

view angles as proposed in section 7.2.2 but also from an imaginary higher distance to get an overview on the scene. This reconstruction of an operation site has to be done in real-time. Simultaneous feature detection on the color image and on the 3-D surface increases the efficiency of stitching and mosaicking procedures (fig. 7.7). Furthermore, information on movement and orientations respectively acceleration and rotation can be provided by inertial sensors additionally and increase efficiency over again.

7.2.6 Maintaining Spatial Orientation

In contrast to gastroenterologists, who are accustomed to work in line with their camera and light source, laparoscopic surgeons normally use multiple instruments and access ports. According to the white paper [Ratt 06a] many NOTES procedures will be performed with the endoscope in a retroflexed position, where the image is upside down and an off-axis manipulation is required. Potential solutions to perform advanced procedures with two or more instruments and assistants include incorporating visualization systems and electronic image stabilization/inversion. If the principles learned in advanced laparoscopic operations are applicable also to NOTES, then basic surgical preconditions like orientation and triangulation will be fundamental requirements for any NOTES surgical system [Ratt 06c]. With the aid of calculated transformation parameters between intra-operative and pre-operative data, position and orientation can be represented, corrected and visualized. With direct approaches

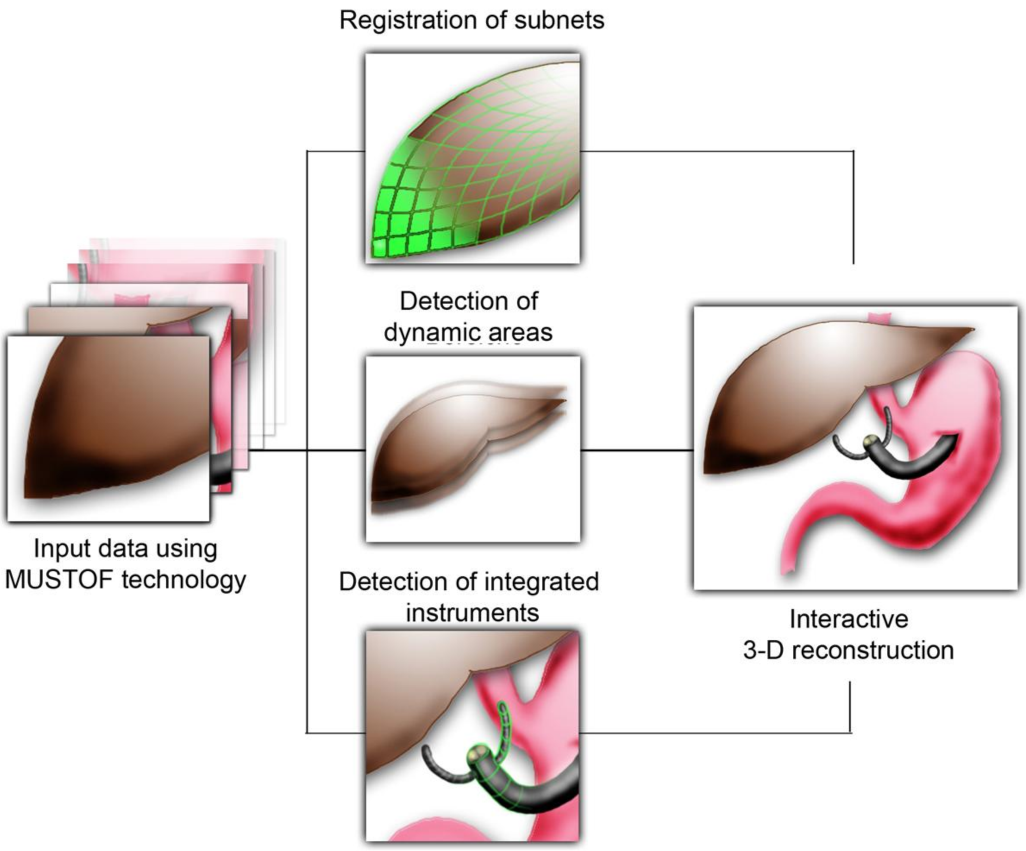

Figure 7.7: Methods for dynamic reconstruction with registration of subnets, detection of dynamic areas, detection of integrated instruments and interactive 3-D reconstruction using MuSToF input data.

like the ENDOrientation method proposed in section 6.1 the orientation can be measured directly to rectify endoscopic images [Holl 10b].

Part IV

Summary and Outlook

Chapter 8

Summary

In this work two new approaches were proposed to enhance endoscopic 2-D images with a third dimension. The MuSToF approach is technically more sophisticated than the ENDOrientation approach. It provides versatile possibilities for combination with conventional modalities. Additional 3-D data will not be an unalterable precondition for performing NOTES. But it will help especially for a safer introduction of robotic devices and improve the visualization for surgeons who are not satisfied with the in-line-view and loss of orientation with flexible endoscopy. Since gastroenterologists and surgeons are still not absolutely familiar with this new NOTES approach, they both will accept new technologies more likely than with established procedures.

8.1 Contribution to Augmented Reality

Augmented Reality is needed to avoid injuries, e.g. while finding the entry point to the peritoneal cavity or other situations, where an incision in unknown tissue has to be made without knowledge of the structures behind the visible wall. The registration with preoperative volumes opens up lots of additional possibilities. The most promising one is to show hidden organs and vessels or other virtual information additionally to the real world image. Therefore organs have to be segmented in the preoperative volumes and to be transformed by iteratively computed transformation parameters. The reliable intra-operative 3-D surface for transformation computation and actual position estimation can be gained by using a MuSToF endoscope.

8.2 Contribution to Enhanced Field of View

Endoscopic axis in-line view and loss of spatial orientation is especially for surgeons quite uncomfortable. To compensate this disadvantage, 3-D surface knowledge can be used to extend and enhance the field of view. ENDOrientation supports the reconstruction of the operation area by knowledge on the translation between subsequent images, whereas MuSToF provides an additional feature set for the registration. Using a 3-D mosaicking technique is especially useful if there are no features detectable in the color image. But another use of the real-time depth map could be much more important: Now a virtual rotation of the view on the introduced instruments can be performed orthogonal to the axis of the original line of sight. This allows a better intuitive estimation of the instruments' position and the distance to tissue or organs.

8.3 Contribution to Collision Prevention

The increasing demand of robotic devices to control multiple instruments through only one endoscope needs additional control mechanisms to avoid unintended injuries. To perform efficient collision prevention, real-time distance information is needed. Avoidance of impending tissue injury or collision with other instruments can be realized, as well as auto-positioning depending on respiration or other patient movements. For the field of endoscopic surgery there is an urgent demand to have a stable platform for secure movements and stabilization of tissue during the intervention.

8.4 Contribution to Spatial Orientation

To provide more information on position and orientation of the robotic device or the endoscope intraoperative 3-D data could be registered with preoperative CT or MR data. With the aid of the calculated transformation parameters, position and orientation can be visualized and corrected. Alternatively, the ENDOSens hardware is able to measure the rotation angle directly. The ENDOrientation approach is much less challenging, but it works reliable and addresses directly a still unsolved problem.

8.5 Use of Standard Components

The hardware for both approaches is based on off-the-shelf components. Since automotive and consumer electronics industries are heavily interested in this emerging technologies, lot of research investment is being allocated to improve the so far developed chip design. Currently a typical ToF camera is available for some 1.000 Euros. But if automotive and consumer applications enable large-scale production, prices will rapidly decline and innovation cycles will be quite short. Even if costs at the moment are too high to address the consumer market, the presented medical applications are auspicious approaches to improve actually provided health care. The ENDOSens hardware is even much cheaper by now. The whole hardware is a few payable 100 Euros for the obtained benefits. And integration of this tiny MEMS chip in a new endoscope is not a difficult technical task.

Chapter 9

Outlook

Even if NOTES may not get a common standard for surgery, it is quite obvious that many developments and inventions will help to improve minimally invasive surgery as well. The approaches of peritoneal single port access (SPA) surgery or trans-anal endoscopic microsurgery (TEM) deal with the same problems of access through only one incision using a special trocar. Missing triangulation, and difficulties with orientation and appropriate view on the operation area require technical support. On the other hand approaches like SPA and TEM are auspicious possibilities to achieve trauma reduction, too. Having reliable 3-D data in real-time is an issue for many related methods like augmented reality. With better visualization methods without the fatiguing and view-limiting restrictions, the approvement of this wide field of imaginable surgical assistance systems will increase rapidly. Robotic devices will increasingly support the physicians in sophisticated intervention concepts.

In future, the MuSToF endoscope will have the ToF chip combined with the CCD chip on its tip enabling higher resolution and requiring less illumination power. This will lead to a less dangerous illumination concept, which does not require the current restrictions of laser lab security. A modulated high-power white LED on the tip will provide enough illumination power for both, the color and the distance image.

The ENDOSens accelerometer for gravity based rectification will be fully integrated in every endoscope's tip and will provide an improved data transmission and image processing. For gastroenterologists only a little arrow will point in the direction of gravity. For surgeons the whole image will be rectified with a little arrow pointing in the direction of the endoscope's top. A little button enables to switch between those two modes. Anything else will be done fully automated with no second monitor.

Capsule endoscopy is a further step to make a diagnostic examination more convenient than performed with usual endoscopes. There the loss of orientation will be an even bigger restriction. Many medical pioneers assume that one day there will be gaggles of tiny robotic devices, which navigate autonomously through the human body and its lumenal paths and vessel structures. They could have some instruments like electro-cutting scalpels and electric staplers for closure to perform their own intervention processes after an inter-flight diagnosis. For orientation and intervention computation they could use highly miniaturized ToF and inertial sensors as well. In order to act autonomously, a wide set of sensors will be an unalterable precondition. Thereby inertial and 3-D sensors definitively will play a major role.

Part V

Appendix and Indices

Appendix A

Functional Principle Simulation Tool

MATLAB-based ToF simulation tool (source *Matlab/ToF-Simulation/modulation2.m*) illustrated in fig. A.1

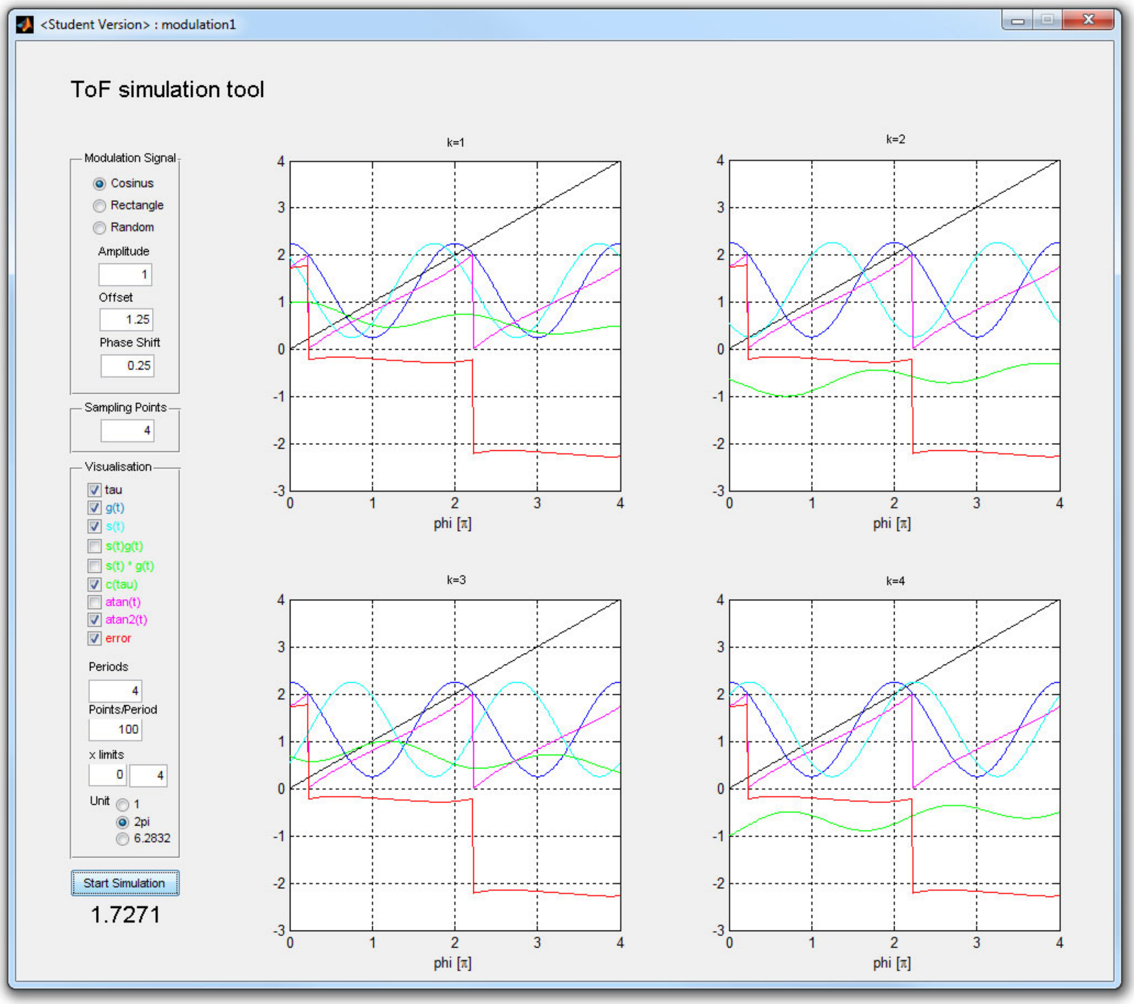

Figure A.1: MATLAB-based Tool for ToF simulation according to theory in section 4.1.1.

The MATLAB-based phase mixing simulation tool (source *Matlab/ToF-Simulation/Mixing-Demixing.m*) visible in fig. A.2 and fig. A.3 is used to gain a better understanding of mixing and demixing basic signals.

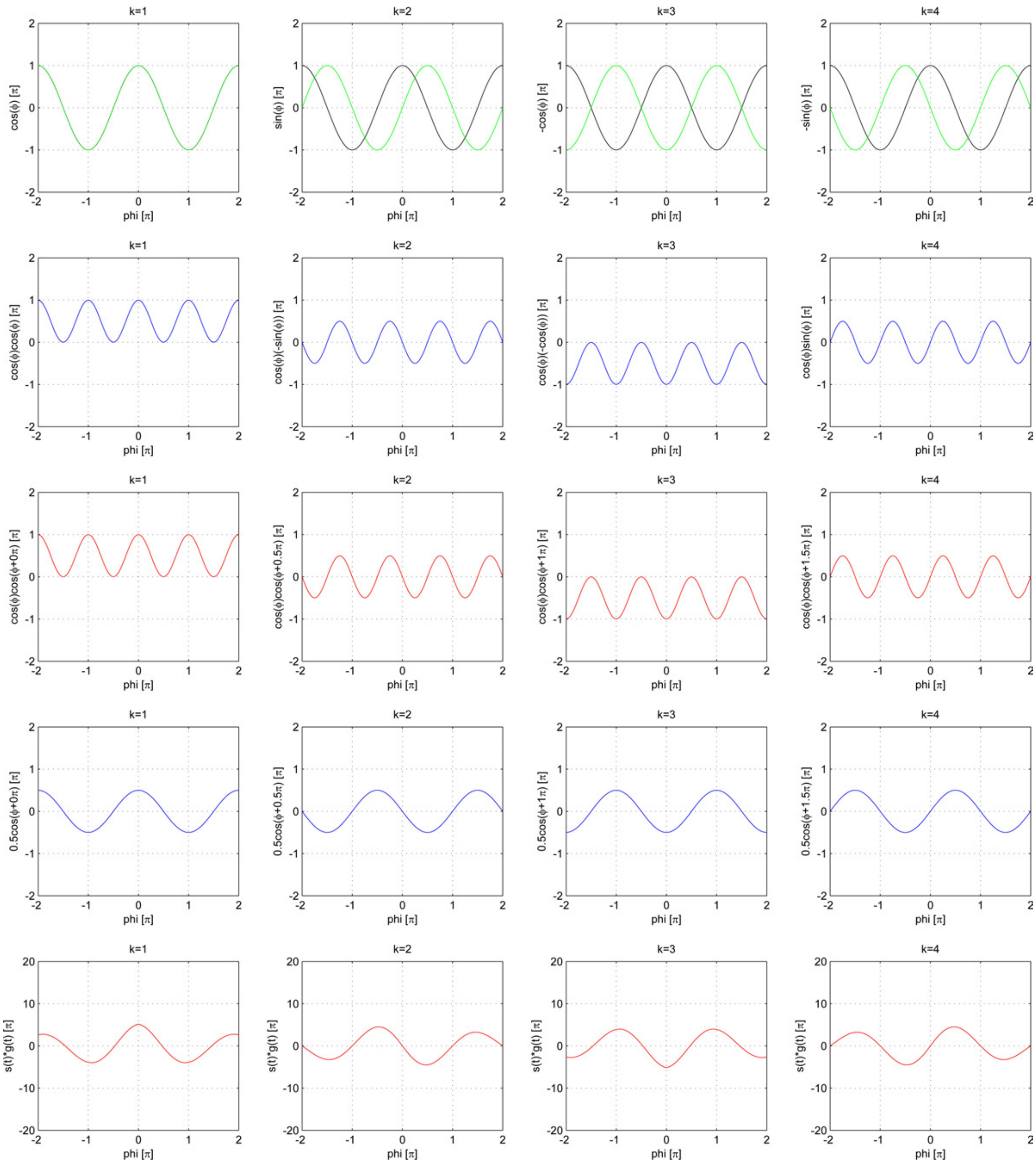

Figure A.2: MATLAB-based simulation for mixing two signals with different methods and increased phase shift.

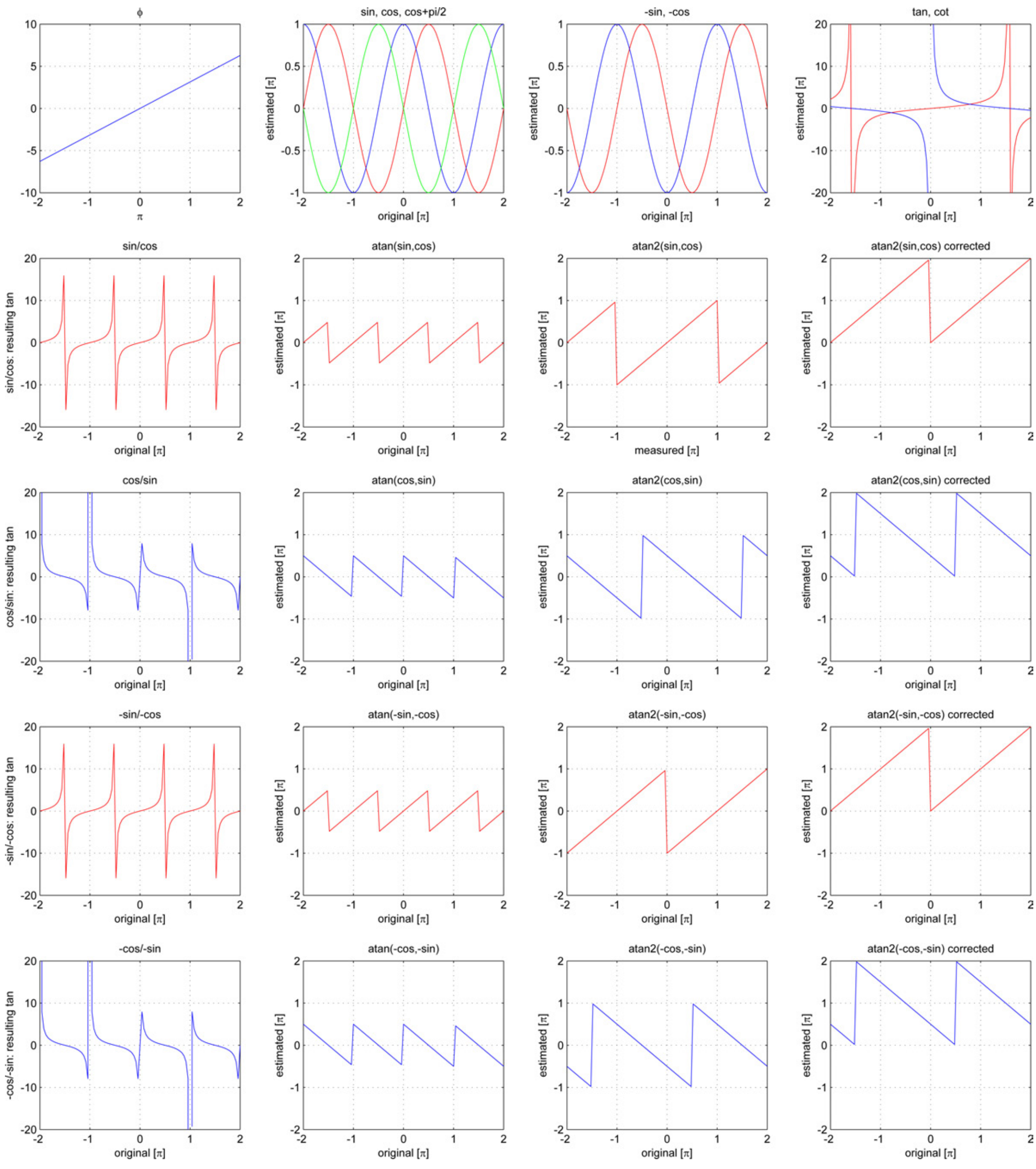

Figure A.3: MATLAB-based simulation for demixing varying signals with different methods.

Appendix B

Resolution Analysis Tool

The MATLAB-based Resolution tool (source *Matlab/ToF-Resolution/TOF_resolution.m*) visible in fig. B.1 uses a plane for calibration and allows the calibration of the Swiss Ranger 3000 ToF Camera.

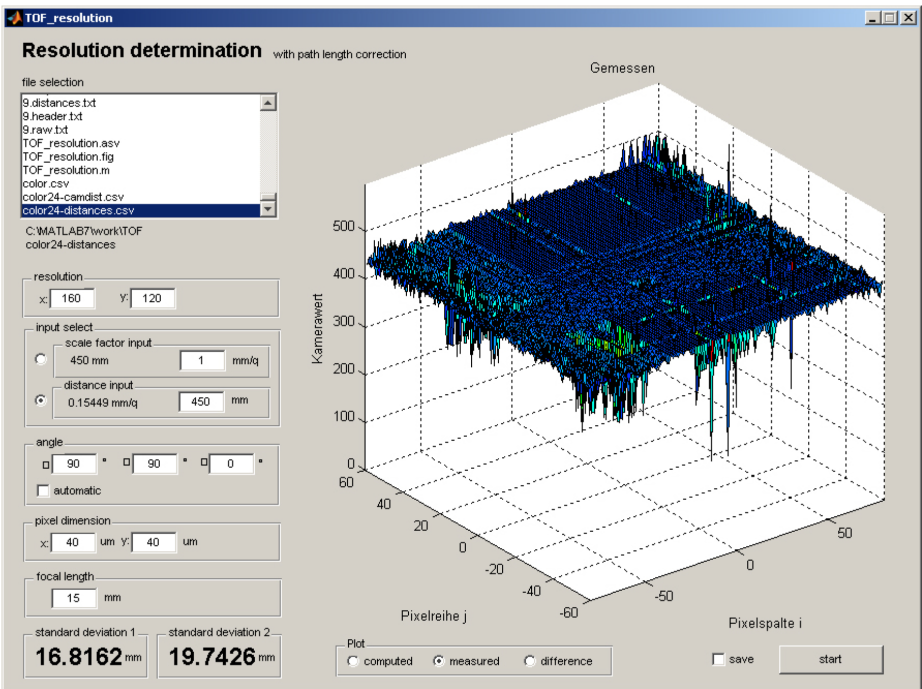

Figure B.1: MATLAB-based tool for resolution analysis using a plane for calibration.

Appendix C

Raw Data Analysis Tool

The MATLAB-based raw data analysis tool (source *Matlab/ToF-RawData/raw.m*) visible in fig. C.1 displays phase, amplitude, raw measurements at the electrodes and a 3-D distance plot of a Swiss Ranger 3000 ToF camera.

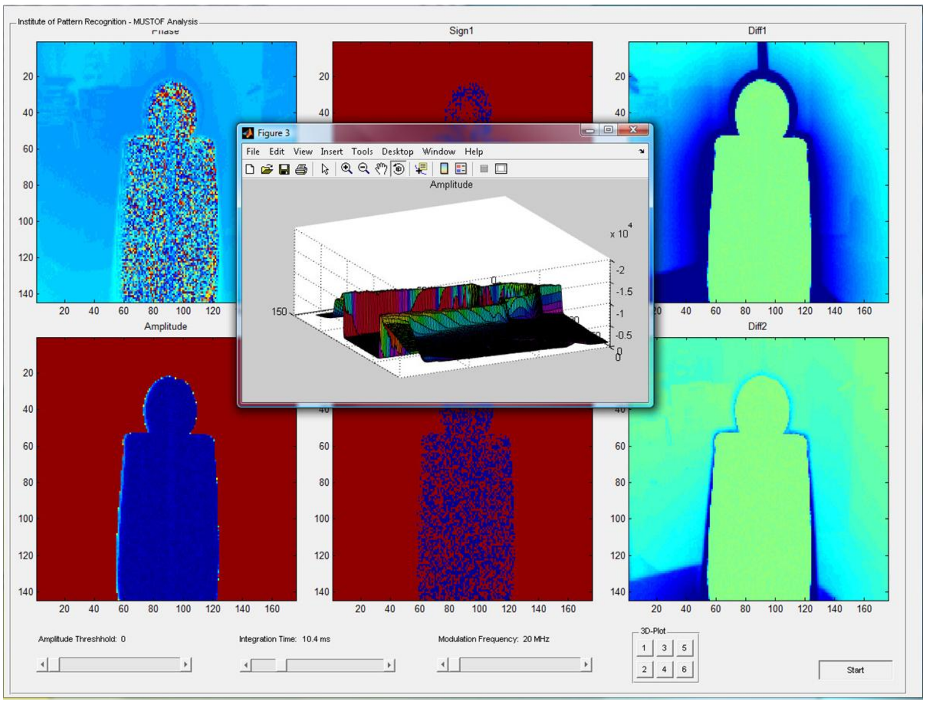

Figure C.1: MATLAB-based tool for raw data analysis.

Appendix D

MEMS Simulation Tool

MATLAB-based tool (source *Matlab/MEMS/MEMSgui2.m*) for the evaluation of MEMS sensor based orientation data as shown in fig. D.1. The first results with real-time rotation parameter detection encouraged to implement a real-time rectification tool using the OpenCV [Brad 00, Brad 08] libraries in C++ in cooperation with the Fraunhofer Institute for Integrated Circuits IIS.

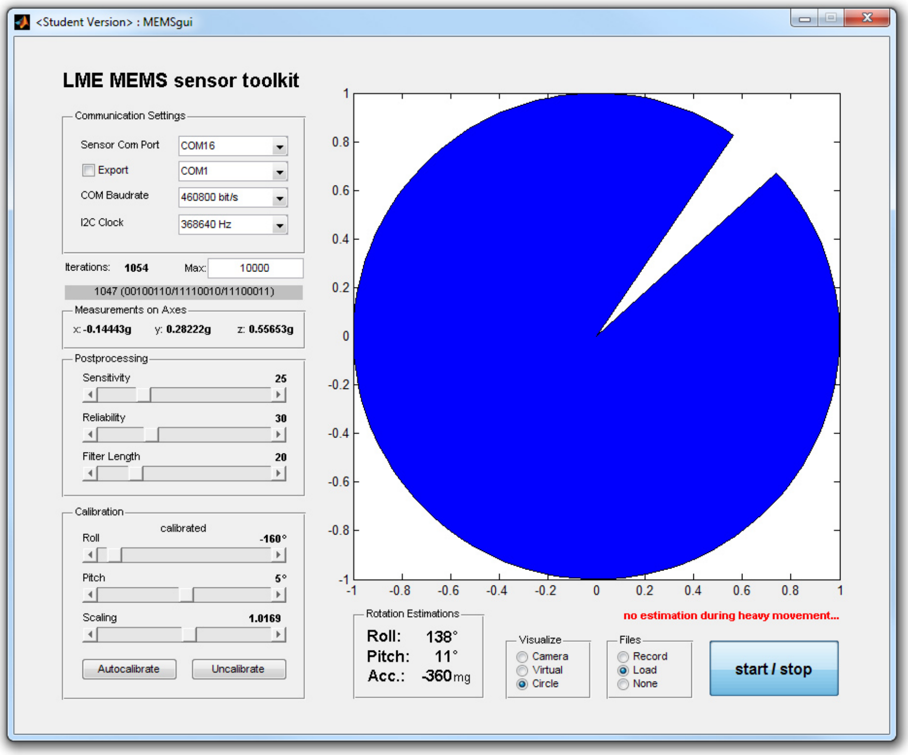

Figure D.1: MATLAB-based tool for MEMS sensor orientation measurement evaluation.

List of Figures

List of Tables

Bibliography

[Adam 07] M. Adameck, L. Büscher, and P. Claes. "Übertragung von Informationen im Bildsignal eines Kamerasystems". German Patent DE 102005042987 A1, March 2007.

[Adam 91] F. Adams. *The Genuine Works of Hippocrates.* Vol. 2, New York: William Wood and Company, 1891.

[Adha 00] L. Adhami, È. Coste-Manière, and J.-D. Boissonnat. "Planning and simulation of robotically assisted minimal invasive surgery". In: S. L. Delp, A. M. DiGioia, and B. Jaramaz, Eds., *Proc. 3rd International Conference on Medical Image Computing and Computer-Assisted Intervention (MICCAI'00), ISBN 3-540-41189-5*, pp. 624–633, Pittsburgh, Pennsylvania, USA, October 2000.

[Albi 09] C. Albitar, P. Graebling, and C. Doignon. "Fast 3D vision with robust structured light coding". In: M. I. Miga and K. H. Wong, Eds., *Proc. Medical Imaging 2009: Visualization, Image-Guided Procedures, and Modeling (SPIE'09), ISBN 978-081-9475-12-1*, pp. 726113.1–726113.8, Lake Buena Vista, FL, USA, February 2009.

[Albr 07] M. Albrecht. *Untersuchung von Photogate-PMD-Sensoren hinsichtlich qualifizierender Charakterisierungsparameter und -methoden.* PhD thesis, Department of Electrical Engineering and Computer Science at University of Siegen, August 2007.

[Arez 10] A. Arezzo and M. Morino. "Endoscopic closure of gastric access in perspective NOTES: an update on techniques and technologies". *Surgical Endoscopy, ISSN 0930-2794*, Vol. 24, No. 2, pp. 298–303, February 2010.

[Awan 02] A. N. Awan and C. P. Swain. "Endoscopic vertical band gastroplasty with an endoscopic sewing machine". *Gastrointestinal Endoscopy, ISSN 0016-5107*, Vol. 55, No. 2, pp. 254–256, February 2002.

[Bais 08] B. Bais and B. Y. Majlis. "Low-g area-changed MEMS accelerometer using bulk silicon technique". *American Journal of Applied Sciences, ISSN 1546-9239*, Vol. 5, No. 6, pp. 626–632, June 2008.

[Baro 07] T. H. Baron. "Natural orifice transluminal endoscopic surgery". *British Journal of Surgery, ISSN 0007-1323*, Vol. 94, No. 1, pp. 1–2, January 2007.

[Berg 06] M. Bergstrom, K. Ikeda, P. Swain, and P. O. Park. "Transgastric anastomosis by using flexible endoscopy in a porcine model (with video)". *Gastrointestinal Endoscopy, ISSN 0016-5107*, Vol. 63, No. 2, pp. 307–312, February 2006.

[Berg 98] P. van Bergen, W. Kunert, J. Bessell, and G. F. Bueß. "Comparative study of two-dimensional and three-dimensional vision systems for minimally invasive surgery". *Surgical Endoscopy, ISSN 0930-2794*, Vol. 12, No. 7, pp. 948–954, July 1998.

[Bhoy 01] S. Bhoyrul, M. A. Vierra, C. R. Nezhat, T. M. Krummel, and L. W. Way. "Trocar injuries in laparoscopic surgery". *Journal of the American College of Surgeons, ISSN 1072-7515*, Vol. 192, pp. 677–683, June 2001.

[Bich 09] C. Bichlmeier, S. M. Heining, M. Feuerstein, and N. Navab. "The Virtual Mirror: a new interaction paradigm for augmented reality environments". *IEEE Transactions on Medical Imaging, ISSN 0278-0062*, Vol. 28, No. 9, pp. 1498–1510, September 2009.

[Blec 07] J. Blech and V. Hackenbroch. "Schläuche in die Leiber". *Der Spiegel, ISSN 0038-7452*, Vol. 29, p. 119, July 2007.

[BMA2] *BMA220 digital, triaxial acceleration sensor.* Bosch, Reutlingen, Germany.

[Bowm 06] D. E. Bowman. "ASGE/SAGES working group on Natural Orifice Translumenal Endoscopic Surgery, White Paper October 2005". *Gastrointestinal Endoscopy, ISSN 0016-5107*, Vol. 63, No. 2, pp. 199–203, February 2006.

[Bozz 06] P. Bozzini. "Lichtleiter, eine Erfindung zur Anschauung innerer Teile und Krankheiten, nebst der Abbildung". *Journal der practischen Arzneykunde und Wundarzneykunde, ISSN 0930-2794*, Vol. 24, No. 204, pp. 107–124, 1806.

[Brad 00] G. Bradski. "The OpenCV Library". *Dr. Dobbï£¡s journal of software tools, ISSN 1044-789X*, November 2000.

[Brad 08] G. Bradski and A. Kaehler. *Learning OpenCV: Computer Vision with the OpenCV Library, ISBN 978-0-596-51613-0.* O'Reilly, Cambridge, MA, October 2008.

[Brah 08] A. Brahme, P. Nyman, and B. Skattc. "4D laser camera for accurate patient positioning, collision avoidance, image fusion and adaptive approaches during diagnostic and therapeutic procedures". *Medical Physics, ISSN 0094-2405*, Vol. 35, No. 5, pp. 1670–1681, May 2008.

[Cane 08] *Canesta 101 - introduction to 3D vision in CMOS.* Canesta Inc., Sunnyvale, CA, March 2008.

[Cao 00] C. G. Cao and P. Milgram. "Disorientation in minimal access surgery: a case study". In: *Proc. International Ergonomics Association / Human Factors and Ergonomics Society (IEA/HFES'00)*, pp. 169–172, San Diego, California, USA, August 2000.

[Carm 08] M. Carmichael. "Scar-free surgery". *The Boston Globe, ISSN 0743-1791*, January 2008.

[Chat 05] D. Chatenever, D. Mattsson-Boze, and M. R. Amling. "Image orientation for endoscopic video displays". United States Patent US 20050020883 A1, January 2005.

[Chat 06] D. Chatenever, D. Mattsson-Boze, and M. R. Amling. “Image orientation for endoscopic video displays”. United States Patent US 7037258 B2, May 2006.

[Chat 07] D. Chatenever, D. Mattsson-Boze, and M. R. Amling. “Image orientation for endoscopic video displays”. United States Patent US 7211042 B2, May 2007.

[Chiu 08] P. Chiu, J. Lau, E. Ng, C. Lam, M. Hui, K. To, J. Sung, and S. Chung. “Closure of a gastrotomy after transgastric tubal ligation by using the Eagle Claw VII: a survival experiment in a porcine model (with video)”. *Gastrointestinal Endoscopy, ISSN 0016-5107*, Vol. 68, No. 3, pp. 554–559, September 2008.

[Davi 92] C. J. Davis. “A history of endoscopic surgery”. *Surgical Laparoscopy, Endoscopy & Percutaneous Techniques, ISSN 1530-4515*, Vol. 2, No. 1, pp. 16–23, March 1992.

[Degu 96] K. Deguchi, T. Sasano, H. Arai, and H. Yoshikawa. “3D shape reconstruction from endoscope image sequences by the factorization method”. *IEICE Transactions on Information and Systems, ISSN 0916-8532*, Vol. 79, No. 9, pp. 1329–1336, August 1996.

[Deli 07a] S. von Delius, H. Feußner, D. Wilhelm, A. Karagianni, J. Henke, R. M. Schmid, and A. Meining. “Transgastric in vivo histology in the peritoneal cavity using miniprobe-based confocal fluorescence microscopy in an acute porcine model”. *Endoscopy, ISSN 0013-726X*, Vol. 39, No. 5, pp. 407–411, May 2007.

[Deli 07b] S. von Delius, W. Huber, H. Feußner, D. Wilhelm, A. Karagianni, J. Henke, A. Preissel, A. Schneider, R. M. Schmid, and A. Meining. “Effect of pneumoperitoneum on hemodynamics and inspiratory pressures during natural orifice transluminal endoscopic surgery (NOTES): An experimental, controlled study in an acute porcine model”. *Endoscopy, ISSN 0013-726X*, Vol. 39, No. 10, pp. 854–859, October 2007.

[Denn 83] J. E. Dennis and R. B. Schnabel. *Numerical Methods for Unconstrained Optimization and Nonlinear Equations.* Prentice Hall, New Jersey, 1983.

[DIN 90] DIN 9300-1. “Aerospace; concepts, quantities and symbols for flight dynamics; aircraft motion relative to the air; ISO 1151-1:1988 modified”. Deutsches Institut für Normung e.V. (German National Standard), October 1990.

[Doro 99] R. Dorobantu. “Simulation des Verhaltens einer low-cost Strapdown IMU unter Laborbedingungen”. Tech. Rep. 6, January 1999.

[Dubo 01] E. Dubois. “A projection method to generate anaglyph stereo images”. In: *Proc. International Conference on Acoustics, Speech, and Signal Processing (ICASSP'01), ISBN 0-7803-7041-4*, pp. 1661–1664, IEEE, Salt Lake City, UT , USA, May 2001.

[Dunk 08] R. J. Dunki-Jacobs, F. B. Metting, and S. Luanava. “Rotation compensation and image stabilization system”. United States Patent US 20080159653 A1, July 2008.

[Eile 10] H. Eilers, S. Tauscher, P. N. Meier, and T. Ortmaier. “Navigation Support for Flexible Endoscopy Based on Inertial Sensors”. *Endoskopie heute, ISSN 0933-811X*, Vol. 23, No. 1, pp. 50–52, March 2010.

[Fere 07] C. Feretis, D. Kalantzopoulos, P. Koulouris, C. Kolettas, F. Archontovasilis, S. Chandakas, H. Patsea, A. Pantazopoulou, M. Sideris, A. Papalois, K. Simopoulos, and E. Leandros. "Endoscopic transgastric procedures in anesthetized pigs: technical challenges, complications, and survival". *Endoscopy, ISSN 0013-726X*, Vol. 39, No. 5, pp. 394–400, May 2007.

[Feue 07] M. Feuerstein, T. Mussack, S. M. Heining, and N. Navab. "Registration-free laparoscope augmentation for intra-operative liver resection planning". In: K. R. Cleary and M. I. Miga, Eds., *Proc. SPIE Medical Imaging 2007: Visualization and Image-Guided Procedures (SPIE'07), ISBN 978-081-9466-27-3*, pp. 650915.1–650915.8, San Diego, CA, USA, February 2007.

[Feus 03] H. Feußner. "The operating room of the future - A view from Europe". *Seminars in Laparoscopic Surgery, ISSN 1071-5517*, Vol. 10, No. 3, pp. 149–156, September 2003.

[Feus 09] H. Feußner, D. Wilhelm, A. Meining, A. Schneider, A. Fiolka, S. Can, and H. Friess. "NOTES Technical Aspects - Hype or Hope?". *Surgical technology international, ISSN 1090-3941*, Vol. 18, pp. 26–35, April 2009.

[Fisc 08] R. Fischer. "3-D-Oberflächeninspektion in Echtzeit mit SPARC". *Pressemitteilung Informationsdienst Wissenschaft*, January 28 2008.

[Fong 06] D. G. Fong, R. D. Pai, D. S. Fishman, M. Ryou, and C. C. Thompson. "Transcolonic hepatic wedge resection in a porcine model". *Gastrointestinal Endoscopy, ISSN 0016-5107*, Vol. 63, No. 5, p. AB102, 2006.

[FOTO 10] *FOTONIC C70. Robust and reliable real vision.* Fotonic, Stockholm, Sweden, 2010.

[Fran 07] C. Frangou. "Hype, theories on NOTES abound, but where it is all headed is anyone's bet". *Gastroenterology & Endoscopy News, ISSN 0883-8348*, Vol. 58, No. 7, pp. 24–30, July 2007.

[Frit 04] A. Fritscher-Ravens, C. A. Mosse, D. Mukherjee, E. Yazaki, P. O. Park, T. Mills, and P. Swain. "Transgastric gastropexy and hiatal hernia repair for GERD under EUS control: a porcine model". *Gastrointestinal Endoscopy, ISSN 0016-5107*, Vol. 59, No. 1, pp. 89–95, January 2004.

[Frit 06] A. Fritscher-Ravens, C. A. Mosse, K. Ikeda, and P. Swain. "Endoscopic transgastric lymphadenectomy by using EUS for selection and guidance". *Gastrointestinal Endoscopy, ISSN 0016-5107*, Vol. 63, No. 2, pp. 302–306, February 2006.

[Frit 07a] A. Fritscher-Ravens. "Transgastric endoscopy - a new fashion, a new excitement!". *Endoscopy, ISSN 0013-726X*, Vol. 39, No. 2, pp. 161–167, February 2007.

[Frit 07b] A. Fritscher-Ravens, A. Ghanbari, C. A. Mosse, P. Swain, P. Köhler, and K. Patel. "Transesophageal endoscopic ultrasound-guided access to the heart". *Endoscopy, ISSN 0013-726X*, Vol. 39, No. 5, pp. 385–389, May 2007.

[Frit 07c] A. Fritscher-Ravens, K. Patel, A. Ghanbari, E. Kahle, A. von Herbay, T. Fritscher, H. Niemann, and P. Koehler. "Natural orifice transluminal endoscopic surgery (NOTES) in the mediastinum: long-term survival animal experiments in transesophageal access, including minor surgical procedures". *Endoscopy, ISSN 0013-726X*, Vol. 39, No. 10, pp. 870–875, October 2007.

[Fuch 08] K. Fuchs and W. Breithaupt. "NOTES als Zukunftsmodel fï£¡r die Adipositaschirurgie". *Der Chirurg, ISSN 0009-4722*, Vol. 79, No. 9, pp. 837–842, September 2008.

[Funk 07] N. Funk and Y.-H. Yang. "Using a Raster Display for Photometric Stereo". In: *Proc. 4th Canadian Conference on Computer and Robot Vision (CRV'07), ISBN 0-7695-2786-8*, pp. 201–207, Montreal, Canada, May 2007.

[Gaud 80] M. W. I. Gauderer, J. L. Ponsky, and R. J. Izant Jr. "Gastrostomy without laparotomy: a percutaneous endoscopic technique". *Journal of Pediatric Surgery, ISSN 0022-3468*, Vol. 15, No. 6, pp. 872–875, December 1980.

[Gee 07] D. Gee and D. Rattner. "New directions in Natural Orifice Transluminal Endoscopic Surgery". *US Surgery, Touch Briefings, ISSN 1754-5536*, pp. 29–30, 2007.

[Gida 06] S. A. Giday, S. V. Kantsevoy, and A. N. Kalloo. "Principle and history of Natural Orifice Translumenal Endoscopic Surgery (NOTES) [abstract]". *Minimally Invasive Therapy & Allied Technologies, ISSN 1364-5706*, Vol. 15, No. 6, pp. 373–377, December 2006.

[Gida 10] S. A. Giday, X. Dray, P. Magno, J. M. Buscaglia, E. J. Shin, V. C. Surti, L. Assumpcao, M. R. Marohn, D. Ruben, A. Zhigalin, L. J. Pipitone, and S. V. Kantsevoy. "Infection during natural orifice transluminal endoscopic surgery: a randomized, controlled study in a live porcine model". *Gastrointestinal Endoscopy, ISSN 0016-5107*, Vol. 71, No. 4, pp. 812–816, April 2010.

[Gilb 09] J. Gilbert. "The EndoAssist robotic camera holder as an aid to the introduction of laparoscopic colorectal surgery". *Annals of The Royal College of Surgeons of England, ISSN 0035-8843*, Vol. 91, No. 5, pp. 389–393, July 2009.

[Gill 08] S. Gillen, A. Schneider, A. Fiolka, S. von Delius, A. Meining, and H. Feußner. "The 'ELITE': construct validation of a new training system for NOTES". *Gastrointestinal Endoscopy, ISSN 0016-5107*, Vol. 67, No. 5, p. AB117, April 2008.

[Gokt 04] S. B. Gokturk, H. Yalcin, and C. Bamji. "A Time-of-Flight depth sensor - system description, issues and solutions". In: *Proc. Conference on Computer Vision and Pattern Recognition Workshop (CVPRW'04), ISBN 0-7695-2158-4*, p. 35, IEEE Computer Society, Washington, DC, USA, July 2004.

[Gow 98] J. G. Gow. "Harold Hopkins and optical systems for urology - an appreciation". *Urology, ISSN 0090-4295*, Vol. 52, No. 1, pp. 152–157, July 1998.

[Gree 02] D. Green, R. Ibach, and J. Fablanowski. "Image orientation for endoscopic video displays". United States Patent US 6471637 B1, October 2002.

[Guti 10a] J. Gutierrez Boronat, J. Jahn, A. Schneider, and K. Hoeller. "[DE] EIN ENDOSKOP UND EINE BILDAUFNAHMEVORRICHTUNG [EN] ENDOSCOPE AND IMAGING DEVICE [FR] ENDOSCOPE ET DISPOSITIF DE PRISE DE VUES". International Patent WO 2010105946 A1, September 2010.

[Guti 10b] J. Gutierrez Boronat, J. Jahn, A. Schneider, and K. Hoeller. "Ein Endoskop und eine Bildaufnahmevorrichtung". German Patent DE 102009013761 A1, September 2010.

[Hage 07] F. Hagenmüller, M. Immenroth, T. Berg, K. Bally, and S. Rasche. "Das Konzept der narbenlosen Eingriffe (scarless surgery)". *Der Chirurg, ISSN 0009-4722*, Vol. 78, No. 6, pp. 525–530, June 2007.

[Harr 05] A. Harrell and B. Heniford. "Minimally invasive abdominal surgery: lux et veritas past, present, and future". *The American Journal of Surgery, ISSN 0002-9610*, Vol. 190, No. 2, pp. 239–243, August 2005.

[Hart 07a] F. Härtl, K. Höller, S. Beller, and H. Feußner. "Current status of the use of medical robots in Germany, Austria and Switzerland". In: J. Hornegger, E. W. Mayr, S. Schookin, H. Feußner, N. Navab, Y. V. Gulyaev, K. Höller, and V. Ganzha, Eds., *Proc. 3rd Russian-Bavarian Conference on Bio-Medical Engineering (RBC'07), ISBN 3-921713-33-1*, pp. 2–4, Erlangen, Germany, July 2007.

[Hart 07b] R. S. B. K. Hartley. "Parameter-Free Radial Distortion Correction with Center of Distortion Estimation". *IEEE Transactions on Pattern Analysis and Machine Intelligence, ISSN 0162-8828*, Vol. 29, No. 8, pp. 1309–1321, August 2007.

[Hase 02] K. Hasegawa, K. Noda, and Y. Sato. "Electronic endoscope system for shape measurement". In: *Proc. 16th International Conference on Pattern Recognition (ICPR'02), ISBN 0-7695-1695-X*, p. 20761, IEEE Computer Society, Quebec City, Canada, August 2002.

[Hawe 07] R. H. Hawes. "Advanced endoscopy and endosurgical procedures: do we need a new subspecialty?". *Gastrointestinal Endoscopy Clinics of North America, ISSN 1052-5157*, Vol. 17, No. 3, pp. 635–639, July 2007.

[Hein 01] H. Heinol. *Untersuchung und Entwicklung von modulationslaufzeitbasierten 3D-Sichtsystemen.* PhD thesis, Department of Electrical Engineering and Computer Science at University of Siegen, 2001.

[Herr 99] D. M. Herron, J. C. Lantis II, J. Maykel, C. Basu, and S. D. Schwaitzberg. "The 3-D monitor and head-mounted display". *Surgical Endoscopy, ISSN 0930-2794*, Vol. 13, No. 8, pp. 751–755, January 1999.

[Hirs 61] B. I. Hirschowitz. "Endoscopic examination of the stomach and duodenal cap with the fiberscope". *Lancet*, Vol. 277, No. 7186, pp. 1074–1078, May 1961.

[Ho 07] K. Ho, S. L. Phee, B. J. SO, and S. S. Chung. "Robotic manipulator for Natural Orifice Transluminal Endoscopic Surgery". *Gastrointestinal Endoscopy, ISSN 0016-5107*, Vol. 65, No. 5, p. AB110, April 2007.

[Hoch 05] J. Hochberger and W. Lamade. "Transgastric surgery in the abdomen: the dawn of a new era?". *Gastrointestinal Endoscopy, ISSN 0016-5107*, Vol. 62, No. 2, pp. 293–296, August 2005.

[Hoeg 05] H. D. Hoeg, E. L. Hale, and N. J. Schara. "Endoscope with variable direction of view module". United States Patent US 20050177026 A1, August 2005.

[Hold 99] J. Holden, J. Flach, and Y. Donchin. "Perceptual-motor coordination in an endoscopic surgery simulation". *Surgical Endoscopy, ISSN 0930-2794*, Vol. 13, No. 2, pp. 127–132, February 1999.

[Holl 05] K. Höller. "Characterisation and modeling of an inertial sensor for navigation of autonomous systems". Diploma Thesis, Fraunhofer Institute for Integrated Circuits IIS and Friedrich-Alexander University Erlangen-Nuremberg, October 2005.

[Holl 08a] K. Höller, M. Petrunina, J. Penne, A. Schneider, D. Wilhelm, H. Feußner, and J. Hornegger. "Taking endoscopy to a higher dimension: Computer Aided 3-D NOTES". In: R. Bauernschmitt, Y. Chaplygin, H. Feußner, Y. Gulyaev, J. Hornegger, E. Mayr, N. Navab, S. Schookin, S. Selishchev, and S. Umnyashkin, Eds., *Proc. 4th Russian-Bavarian Conference on Bio-Medical Engineering (RBC'08), ISBN 978-5-7256-0506-8*, pp. 33–37, MIET, Zelenograd, Moscow, Russia, July 2008.

[Holl 08b] K. Höller, C. Schaller, D. Tacke, F. Höpfl, and J. Hornegger. "Contributions of Time-of-Flight cameras for biomedical applications". In: H. Malberg, T. Sander-Thï£¡mmes, N. Wessel, and W. Wolf, Eds., *Proc. DGBMT-Workshop Biosignalverarbeitung (BMT'08), ISBN 978-3-9810021-7-1*, pp. 180–183, Deutsche Gesellschaft für Biomedizinische Technik, Potsdam, Germany, July 2008.

[Holl 08c] K. Höller, A. Schneider, J. Jahn, J. Guttiérrez, T. Wittenberg, J. Hornegger, and H. Feußner. "Enhanced Endoscopic Engineering". In: J. Hornegger, K. Höller, P. Ritt, A. Borsdorf, and H.-P. Niedermeier, Eds., *Proc. Pattern Recognition in Medical and Health Engineering '08, ISBN 3-921713-34-X*, pp. 61–63, Pattern Recognition Lab, FAU Erlangen-Nuremberg, Wildbad Kreuth, Germany, July 2008.

[Holl 09a] K. Höller, J. Penne, A. Schneider, J. Jahn, H. Girgis, J. Guttiérrez, T. Wittenberg, H. Feußner, and J. Hornegger. "Suppression of shock based errors with gravity related endoscopic image rectification". In: H. Feußner, R. Bauernschmitt, N. Navab, J. Hornegger, E. Mayr, S. Schookin, Y. Gulyaev, Y. Chaplygin, and S. Selishchev, Eds., *Proc. 5th Russian-Bavarian Conference on Bio-Medical Engineering (RBC'09), ISBN 978-3-00-029049-7*, pp. 43–47, Munich, Germany, July 2009.

[Holl 09b] K. Höller, J. Penne, A. Schneider, J. Jahn, J. Guttiérrez, T. Wittenberg, H. Feußner, and J. Hornegger. "Endoscopic orientation correction". In: G.-Z. Yang, D. J. Hawkes, D. Rueckert, J. A. Noble, and C. J. Taylor, Eds., *Proc. 12th International Conference on Medical Image Computing and Computer-Assisted Intervention (MICCAI'09), ISBN 978-3-642-04267-6*, pp. 459–466, London, UK, September 2009.

[Holl 09c] K. Höller, A. Schneider, J. Jahn, J. Guttiérrez, T. Wittenberg, J. Hornegger, and H. Feußner. "Clinical evaluation of ENDOrientation: gravity related rectification for endoscopic images". In: P. Zinterhof,

S. Lončarič, A. Uhl, and A. Carini, Eds., *Proc. 6th International Symposium on Image and Signal Processing and Analysis (ISPA'09), ISBN 978-953-184-134-4*, pp. 713–717, IEEE Computer Society, Salzburg, Austria, September 2009.

[Holl 10a] K. Höller, S. Hempel, A. Schneider, J. Jahn, J. Guttiérrez, T. Wittenberg, J. Hornegger, and H. Feußner. "Rectification of Endoscopic Images by Gravity". In: J. Hornegger, K. Höller, M. Spiegel, and H.-P. Niedermeier, Eds., *Proc. Pattern Recognition in Medical and Health Engineering '10, ISBN 978-3-00-031916-7*, pp. 105–107, Pattern Recognition Lab, FAU Erlangen-Nuremberg, Kloster Banz, Germany, April 2010.

[Holl 10b] K. Höller, A. Schneider, J. Jahn, J. Gutierrez, T. Wittenberg, A. Meining, S. von Delius, J. Hornegger, and H. Feußner. "Orientation of endoscopic images: rectification by gravity". *Biomedizinische Technik / Biomedical Engineering, ISSN 0013-5585*, Vol. 55, No. 4, pp. 211–217, August 2010.

[Holl 10c] K. Höller, A. Schneider, J. Jahn, J. Gutierrez, T. Wittenberg, H. Feussner, and J. Hornegger. "Spatial orientation in translumenal surgery". *Minimally Invasive Therapy & Allied Technologies, ISSN 1364-5706*, Vol. 19, No. 5, pp. 262–273, October 2010.

[Holl 10d] K. Höller, A. Schneider, J. Jahn, J. Gutierrez, T. Wittenberg, H. Feußner, and J. Hornegger. "Endoscopic image rectification using gravity". *International Journal for Computer Assisted Radiology and Surgery, ISSN 1861-6410*, Vol. 5 (Suppl 1), No. 4, pp. S247–S248, August 2010.

[Hopk 54] H. Hopkins and N. Kapany. "A flexible fiberscope using static scanning". Vol. 173, No. 4392, pp. 39–41, January 1954.

[Horn 07] J. Hornegger, E. W. Mayr, S. Schookin, H. Feußner, N. Navab, Y. V. Gulyaev, K. Höller, and V. Ganzha, Eds. *Proc. 3rd Russian-Bavarian Conference on Bio-Medical Engineering (RBC'07), ISBN 3-921713-33-1*, Erlangen, Germany, July 2007.

[Horn 08] J. Hornegger, K. Höller, P. Ritt, A. Borsdorf, and H.-P. Niedermeier, Eds. *Proceedings of the Cooperation Seminar on Pattern Recognition in Medical and Health Engineering 2008*, Pattern Recognition Lab, FAU Erlangen-Nuremberg, Wildbad Kreuth, Germany, July 2008.

[Horn 10] J. Hornegger, K. Höller, M. Spiegel, and H.-P. Niedermeier, Eds. *Proceedings of the Cooperation Seminar on Pattern Recognition in Medical and Health Engineering 2010*, Pattern Recognition Lab, FAU Erlangen-Nuremberg, Kloster Banz, Germany, April 2010.

[Humm 02] J. Hummel, M. Figl, C. Kollmann, H. Bergmann, and W. Birkfellner. "Evaluation of a miniature electromagnetic position tracker". *Medical Physics, ISSN 0094-2405*, Vol. 29, No. 10, pp. 2205–2212, October 2002.

[Jaga 05] S. B. Jagannath, S. V. Kantsevoy, C. A. Vaughn, S. S. C. Chung, P. B. Cotton, C. J. Gostout, R. H. Hawes, P. J. Pasricha, D. G. Scorpio, C. A. Magee, L. J. Pipitone, and A. N. Kalloo. "Peroral transgastric endoscopic ligation of fallopian tubes with long-term survival in a porcine model". *Gastrointestinal Endoscopy, ISSN 0016-5107*, Vol. 62, No. 3, pp. 449–53, March 2005.

[Kall 04] A. N. Kalloo, V. K. Singh, S. B. Jagannath, H. Niiyama, S. L. Hill, C. A. Vaughn, C. A. Magee, and S. V. Kantsevoy. "Flexible transgastric peritoneoscopy: a novel approach to diagnostic and therapeutic interventions in the peritoneal cavity". *Gastrointestinal Endoscopy, ISSN 0016-5107*, Vol. 60, No. 1, pp. 114–117, July 2004.

[Kall 07a] A. Kalloo. "Natural Orifice Transluminal Endoscopic Surgery (NOTES)". *Journal of Gastroenterology and Hepatology, ISSN 1440-1746*, Vol. 3, No. 3, pp. 183–184, March 2007.

[Kall 07b] A. N. Kalloo and S. A. Giday. "Natural Orifice Translumenal Endoscopic Surgery - a clinical review". *Gastroenterology & Endoscopy News, ISSN 0883-8348*, pp. 1–6, July 2007.

[Kant 05] S. V. Kantsevoy, S. B. Jagannath, H. Niiyama, S. S. C. Chung, P. B. Cotton, C. J. Gostout, R. H. Hawes, P. J. Pasricha, C. A. Magee, C. A. Vaughn, D. Barlow, H. Shimonaka, and A. N. Kalloo. "Endoscopic gastrojejunostomy with survival in a porcine model". *Gastrointestinal Endoscopy, ISSN 0016-5107*, Vol. 62, No. 2, pp. 287–292, August 2005.

[Kant 06] S. V. Kantsevoy, B. Hu, S. B. Jagannath, C. A. Vaughn, D. M. Beitler, S. S. C. Chung, P. B. Cotton, C. J. Gostout, R. H. Hawes, P. J. Pasricha, C. A. Magee, L. J. Pipitone, M. A. Talamini, and A. N. Kalloo. "Per-oral transgastric endoscopic splenectomy: is it possible?". *Surgical Endoscopy, ISSN 0930-2794*, Vol. 20, No. 3, pp. 522–525, March 2006.

[Kant 07] S. V. Kantsevoy, B. Hu, S. B. Jagannath, C. A. Vaughn, D. M. Beitler, S. S. C. Chung, P. B. Cotton, C. J. Gostout, R. H. Hawes, P. J. Pasricha, C. A. Magee, L. J. Pipitone, M. A. Talamini, and A. N. Kalloo. "A novel safe approach to the peritoneal cavity for per-oral transgastric endoscopic procedures". *Gastrointestinal Endoscopy, ISSN 0016-5107*, Vol. 65, No. 3, pp. 497–500, March 2007.

[Kara 94] H. Karasawa, H. Tsujitani, Y. Kawase, A. Shiga, T. Kubota, A. Taguchi, H. Mizuno, K. Yoshino, S. Tanizawa, S. Yamashita, T. Ishikawa, and I. Kanamori. "Electronic endoscope apparatus". Japanese Patent JP 6269403 A, September 1994.

[Kawa 02] T. Kawai. "3D displays and applications". *Displays, ISSN 0141-9382*, Vol. 23, No. 1-2, pp. 49–56, April 2002.

[Kaza 07] P. Kazanzides. *Robotics in surgery: history, current and future applications*, Chap. Robots for Orthopaedic Joint Reconstruction, pp. 61–94. Nova Science Publishers, 2007.

[Kaza 08] P. Kazanzides, G. Fichtinger, G. Hager, A. Okamura, L. Whitcomb, and R. Taylor. "Surgical and interventional robotics: core concepts, technology, and design (part I)". *IEEE Robotics and Automation Magazine, ISSN 1070-9932*, Vol. 15, No. 2, pp. 122–130, June 2008.

[Kilg 96] M. J. Kilgard. *The OpenGL utility toolkit (GLUT) programming interface API version 3.* Silicon Graphics, Inc., 1996.

[Ko 06] C. W. Ko and A. N. Kalloo. "Per-oral transgastric abdominal surgery". *Journal of Digestive Diseases, ISSN 1751-2980*, Vol. 7, No. 2, pp. 67–70, May 2006.

[Koch 07] M. L. Kochman and C. P. Swain. "Deconstruction of the endoscope". *Gastrointestinal Endoscopy, ISSN 0016-5107*, Vol. 65, No. 4, pp. 677–678, April 2007.

[Kopp 01] D. Koppel, Y.-F. Wang, and H. Lee. "Automated image rectification in video-endoscopy". In: W. J. Niessen and M. A. Viergever, Eds., *Proc. 4th International Conference on Medical Image Computing and Computer-Assisted Intervention (MICCAI'01), ISBN 3-540-42697-3*, pp. 1412–1414, Utrecht, The Netherlands, October 2001.

[Kopp 04] D. Koppel, Y. Wang, and H. Lee. "Image-based rendering and modeling in video-endoscopy". In: *Proc. 2nd International Symposium on Biomedical Imaging: From Nano to Macro (ISBI'04)*, pp. 272–279, IEEE Computer Society, Arlington, VA, USA, April 2004.

[Kopp 05] D. Koppel, Y.-F. Wang, and H. Lee. "Robust and real-time image stabilization and rectification". In: *Proc. 7th Workshop on Application of Computer Vision (WACV/MOTION'05), ISBN 0-7695-2271-8-1*, pp. 350–355, IEEE Computer Society, Breckenridge, CO, USA, January 2005.

[Krug 06] S. Krüger, J. Penne, J. Hornegger, W. Hohenberger, and T. Horbach. "A novel approach to 3-D Endoscopy in minimally invasive surgery". In: T. Lenarz and H. K. Matthies, Eds., *Abstract-Band 5. Jahrestagung der Deutschen Gesellschaft fï£¡r Computer- und Roboterassistierte Chirurgie (CURAC'06)*, p. A124, Hannover, Germany, October 2006.

[L808 09] *L808P200 Product Specification Sheet*. Thorlabs, Newton, NJ, 2009.

[Lama 06] W. Lamade and J. Hochberger. "Transgastric surgery: avoiding pitfalls in the development of a new technique". *Gastrointestinal Endoscopy, ISSN 0016-5107*, Vol. 63, No. 4, pp. 698–700, April 2006.

[Lang 00] R. Lange. *3D Time-of-Flight distance measurement with custom solid-state image sensors in CMOS/CCD-technology*. PhD thesis, Department of Electrical Engineering and Computer Science at University of Siegen, 2000.

[Lang 99] R. Lange, P. Seitz, and R. Schwarte. "Time-of-flight Entfernungskamera in CMOS/CCD- Technik mit pixelintegrierten optischen Lock-in-Verstärkern". In: *Berichtsband 70 zur Fachtagung Optische Formerfassung, ISBN 3-931381-30-7*, pp. 271–280, VDI-VDE, Stuttgart, Germany, October 1999.

[Lima 07] E. Lima, C. Rolanda, J. M. Pego, T. Henriques-Coelho, D. Silva, L. Osorio, I. Moreira, J. L. Carvalho, and J. Correia-Pinto. "Third-generation nephrectomy by Natural Orifice Transluminal Endoscopic Surgery". *The Journal of Urology, ISSN 0022-5347*, Vol. 178, No. 6, pp. 2648–2654, December 2007.

[Lity 98] G. S. Litynski. "Erich Mühe and the rejection of laparoscopic cholecystectomy (1985): a surgeon ahead of his time". *Journal of the Society of Laparoendoscopic Surgeons, ISSN 1086-8089*, Vol. 2, No. 4, pp. 341–346, October-December 1998.

[Lott 98] J. Lötters, J. Schipper, P. Veltink, W. Olthuis, and P. Bergveld. "Procedure for in-use calibration of triaxial accelerometers in medical applications". *Sensors and Actuators A: Physical, ISSN 0924-4247*, Vol. 68, No. 1-3, pp. 221–228, June 1998.

[Luan 01] X. Luan. *Experimental investigation of photonic mixer device and development of TOF 3D ranging systems based on PMD technology.* PhD thesis, Department of Electrical Engineering and Computer Science at University of Siegen, 2001.

[Magn 07] P. Magno, S. A. Giday, X. Dray, S. S. Chung, P. B. Cotton, C. Gostout, R. H. Hawes, A. N. Kalloo, P. J. Pasricha, J. J.White, L. Assumpcao, M. R. Marohn, K. L. Gabrielson, and S. V. Kantsevoy. “A new stapler-based full-thickness transgastric access closure: results from an animal pilot trial”. *Endoscopy, ISSN 0013-726X*, Vol. 39, No. 10, pp. 876–880, October 2007.

[Mais 08] J. Maiss, J. Hochberger, and D. Schwab. “Hemoclips: which is the pick of the bunch”. *Gastrointestinal Endoscopy, ISSN 0016-5107*, Vol. 67, No. 1, pp. 40–43, January 2008.

[Mali 06] A. Malik, J. D. Mellinger, J. W. Hazey, B. J. Dunkin, and B. V. M. Jr. “Endoluminal and transluminal surgery: current status and future possibilities”. *Surgical Endoscopy, ISSN 0930-2794*, Vol. 20, No. 8, pp. 1179–1192, August 2006.

[Matt 00] D. Mattsson-Boze and D. Chatenever. “Image orientation for endoscopic video displays”. United States Patent US 6097423 A, August 2000.

[McGe 06] M. F. McGee, M. J. Rosen, J. Marks, R. P. Onders, A. Chak, A. Faulx, V. K. Chen, and J. Ponsky. “A primer on Natural Orifice Transluminal Endoscopic Surgery: building a new paradigm”. *Surgical Innovation, ISSN 1553-3506*, Vol. 13, No. 2, p. 86, June 2006.

[McGe 07] M. F. McGee, M. J. Rosen, J. Marks, A. Chak, R. Onders, A. Faulx, A. Ignagni, S. Schomisch, and J. Ponsky. “A reliable method for monitoring intraabdominal pressure during natural orifice translumenal endoscopic surgery”. *Surgical Endoscopy, ISSN 0930-2794*, Vol. 21, No. 4, pp. 672–676, April 2007.

[Mein 07] A. Meining, D. Wilhelm, M. Burian, M. Dundoulakis, A. Schneider, S. von Delius, and H. Feußner. “Development, standardization, and evaluation of NOTES cholecystectomy using a transsigmoid approach in the porcine model: an acute feasibility study”. *Endoscopy, ISSN 0013-726X*, Vol. 39, No. 10, pp. 860–864, October 2007.

[Merr 06] B. F. Merrifield, M. S. Wagh, and C. C. Thompson. “Peroral transgastric organ resection in the abdomen: feasibility study in pigs”. *Gastrointestinal Endoscopy, ISSN 0016-5107*, Vol. 63, No. 4, pp. 693–977, April 2006.

[MESA 06] *MESA Imaging SwissRanger SR-3000 manual.* CSEM MESA Imaging AG, Zurich, Swiss, 2006.

[MESA 09] *MESA Imaging SR-4000 data sheet.* MESA Imaging AG, Zurich, Swiss, 2009.

[Miga 09] M. I. Miga and K. H. Wong, Eds. *Medical Imaging 2009: Visualization, Image-Guided Procedures, and Modeling (SPIE’09), ISBN 978-081-9475-12-1*, Lake Buena Vista, FL, USA, February 2009.

[Milg 99] P. Milgram and H. Colquhoun. *Mixed reality - merging real and virtual worlds, ISBN 978-3540656234*, Chap. A taxonomy of real and virtual world display integration, pp. 5–30. Springer, Berlin, Heidelberg, New York, 1999.

[Miro 09] D. Mirota, R. Taylor, M. Ishii, and G. Hager. "Direct endoscopic video registration for sinus surgery". In: M. I. Miga and K. H. Wong, Eds., *Proc. Medical Imaging 2009: Visualization, Image-Guided Procedures, and Modeling (SPIE'09), ISBN 978-081-9475-12-1*, p. 72612K, Lake Buena Vista, FL, USA, February 2009.

[Morg 07] C. B. Morgenthal, W. O. Richards, B. J. Dunkin, K. A. Forde, G. Vitale, and E. Lin. "The role of the surgeon in the evolution of flexible endoscopy". *Surgical Endoscopy, ISSN 0930-2794*, Vol. 21, No. 6, pp. 838–853, June 2007.

[Muhe 92] E. Mühe. "Long-term follow-up after laparoscopic cholecystectomy". *Endoscopy, ISSN 0013-726X*, Vol. 24, No. 9, pp. 754–758, November 1992.

[Nava 01] N. Navab. "Medical & industrial Augmented Reality: challenges for real-time vision, computer graphics and mobile computing". In: B. Radig and S. Florczyk, Eds., *Proc. 23rd DAGM-Symposium on Pattern Recognition (DAGM'01), ISBN 3-540-42596-9*, pp. 443–452, Munich, Germany, September 2001.

[Nava 07] N. Navab, M. Feuerstein, and C. Bichlmeier. "Laparoscopic virtual mirror - new interaction paradigm for monitor based Augmented Reality". In: *Proc. Virtual Reality Conference (VR'07), ISBN 1-4244-0906-3*, pp. 43–50, IEEE Computer Society, Charlotte, NC, USA, March 2007.

[Neud 02] J. Neudecker, S. Sauerland, E. Neugebauer, R. Bergamaschi, H. J. Bonjer, A. Cuschieri, K.-H. Fuchs, C. Jacobi, F. W. Jansen, A.-M. Koivusalo, A. Lacy, M. J. McMahon, B. Millat, and W. Schwenk. "The European Association for Endoscopic Surgery clinical practice guideline on the pneumoperitoneum for laparoscopic surgery". *Surgical Endoscopy, ISSN 0930-2794*, Vol. 16, No. 7, pp. 1121–1143, July 2002.

[Numm 05] K. Numminen, O. Sipilä, and H. Mäkisalo. "Preoperative hepatic 3D models: Virtual liver resection using three-dimensional imaging technique". *European Journal of Radiology 0720-048X*, Vol. 56, No. 2, pp. 179–184, November 2005.

[Oban 03] M. A. Obando and J. H. Payne. "The future application of the robotic arm (Automatic Endoscopic System for Optimal Positioning or AESOP) with voice recognition in sinus endoscopic surgery". *Operative Techniques in Otolaryngology-Head and Neck Surgery, ISSN 1043-1810*, Vol. 14, No. 1, pp. 55–57, March 2003.

[Oggi 05] T. Oggier, B. Bï£¡ttgen, and F. Lustenberger. "SwissRanger SR3000 and first experiences based on miniaturized 3D-ToF cameras". Tech. Rep., Fachhochschule Rapperswil, Switzerland, Switzerland, 2005.

[Okat 96] T. Okatani and K. Deguchi. "Reconstructing Shape from Shading with a point light source at the projection center: shape reconstruction from an endoscope image". In: *Proc. 13th International Conference on Pattern Recognition (ICPR'96)*, pp. 830–834, IEEE Computer Society, Vienna, Austria, August 1996.

[Olbr 05] B. Olbrich, J. Traub, S. Wiesner, A. Wiechert, H. Feußner, and N. Navab. "Respiratory motion analysis: towards gated augmentation of the liver". In: H. U. Lempke, K. Inamura, K. Doi, M. W. Vannier, and A. G. Farman, Eds., *Proc. Computer Assisted Radiology and Surgery (CARS'05), ISSN 1861-6410*, pp. 248–253, Berlin, Germany, June 2005.

[Onde 07] R. Onders, M. F. McGee, J. Marks, A. Chak, R. Schilz, M. J. Rosen, A. Ignagni, A. Faulx, M. J. Elmo, S. Schomisch, and J. Ponsky. "Diaphragm pacing with Natural Orifice Transluminal Endoscopic Surgery: potential for difficult-to-wean intensive care unit patients". *Surgical Endoscopy, ISSN 0930-2794*, Vol. 21, No. 3, pp. 475–479, March 2007.

[OSRA 05] *OSRAM SPL2F81-2S Laserdiode im TO-220 Gehï£¡use mit FC-Faseranschluss 1.5 W cw.* OSRAM Opto Semiconductors, Regensburg, Germany, 2005.

[Pai 06] R. D. Pai, D. G. Fong, M. E. Bundga, R. D. Odze, D. W. Rattner, and C. C. Thompson. "Transcolonic endoscopic cholecystectomy: a NOTES survival study in a porcine model (with video)". *Gastrointestinal Endoscopy, ISSN 0016-5107*, Vol. 64, No. 3, pp. 428–434, September 2006.

[Park 05] P. O. Park, M. Bergstrom, K. Ikeda, A. Fritscher-Ravens, and P. Swain. "Experimental studies of transgastric gallbladder surgery: cholecystectomy and cholecystogastric anastomosis". *Gastrointestinal Endoscopy, ISSN 0016-5107*, Vol. 61, No. 4, pp. 601–606, April 2005.

[Pelo 93] M. A. Pelosi, N. Kadar, and M. A. Pelosi III. "The electronic video operative laparoscope". *The Journal of the American Association of Gynecologic Laparoscopists, ISSN 1074-3804*, Vol. 1, No. 1, pp. 54–57, November 1993.

[Penn 06] J. Penne, O. Jesorsky, M. Winter, T. Horbach, S. Krüger, W. Hohenberger, and J. Hornegger. "A novel approach for 3-D video-endoscopy". In: *Proc. 2rd Russian-Bavarian Conference on Biomedical Engineering (RBC'06)*, pp. [CD–ROM], Moscow, Russia, June 2006.

[Penn 07a] J. Penne, K. Höller, D. Wilhelm, H. Feußner, and J. Hornegger. "Photorealistic 3-D surface reconstructions using ToF cameras". In: J. Hornegger, E. W. Mayr, S. Schookin, H. Feußner, N. Navab, Y. V. Gulyaev, K. Höller, and V. Ganzha, Eds., *Proc. 3rd Russian-Bavarian Conference on Bio-Medical Engineering (RBC'07), ISBN 3-921713-33-1*, pp. 233–240, Erlangen, Germany, July 2007.

[Penn 07b] J. Penne, K. Höller, S. Krüger, and H. Feußner. "NOTES-3D: endoscopes learn to see 3-D - basic algorithms for a novel endoscope". In: A. Ranchordas, H. Araújo, and J. Vitrià, Eds., *Proc. 2nd International Conference on Computer Vision Theory and Applications (VISAPP'07), ISBN 978-972-8865-75-7*, pp. 134–142, Barcelona, Spain, March 2007.

[Penn 09] J. Penne, K. Höller, M. Stürmer, T. Schrauder, A. Schneider, R. Engelbrecht, H. Feußner, B. Schmauß, and J. Hornegger. "Time-of-Flight 3-D endoscopy". In: G.-Z. Yang, D. J. Hawkes, D. Rueckert, J. A. Noble, and C. J. Taylor, Eds., *Proc. 12th International Conference on Medical Image Computing and Computer-Assisted Intervention (MICCAI'09), ISBN 978-3-642-04267-6*, pp. 467–474, London, UK, September 2009.

[Perr 07] S. Perretta, S. Sereno, A. Forgione, B. Dallemagne, D. Coumaros, C. Boosfeld, C. Moll, and J. Marescaux. "A new method to close the gastrotomy by using a cardiac septal occluder: long-term survival study in a porcine model". *Gastrointestinal Endoscopy, ISSN 0016-5107*, Vol. 66, No. 4, pp. 809–813, October 2007.

[PMDv 05a] *PMD[vision] 19k 3D video range camera.* PMDTechnologies GmbH, Siegen, Germany, 2005.

[PMDv 05b] *PMD[vision] 3k-S 3D video range camera.* PMDTechnologies GmbH, Siegen, Germany, 2005.

[PMDv 09a] *PMD[vision] CamCube 2.0 High resolution 3D video camera.* PMDTechnologies GmbH, Siegen, Germany, 2009.

[PMDv 09b] *PMD[vision] CamCube 3D video range camera.* PMDTechnologies GmbH, Siegen, Germany, 2009.

[PMDv 10] *PMD[vision] CamCube 3.0 High resolution 3D video camera.* PMDTechnologies GmbH, Siegen, Germany, 2010.

[Pons 05] J. L. Ponsky. "Gastroenterologists as surgeons: what they need to know". *Gastrointestinal Endoscopy, ISSN 0016-5107*, Vol. 61, No. 3, p. 454, March 2005.

[Pons 06] J. L. Ponsky. "Endoluminal surgery: past, present and future". *Surgical Endoscopy, ISSN 0930-2794*, Vol. 20, No. 2, pp. S500–S502, April 2006.

[Rao 05] V. Rao, M. Tandan, S. Lakhtakia, R. Banerjee, and N. Reddy. "Per oral transgastric non anatomical segmental liver resection using flexible endoscope". *Gastrointestinal Endoscopy, ISSN 0016-5107*, Vol. 61, No. 5, p. AB237, April 2005.

[Ratt 06a] D. Rattner and R. H. Hawes. "NOTES: Gathering momentum". *Gastrointestinal Endoscopy, ISSN 0016-5107*, Vol. 63, No. 6, pp. 838–839, May 2006.

[Ratt 06b] D. Rattner and A. Kalloo. "ASGE/SAGES Working Group on Natural Orifice Translumenal Endoscopic Surgery: White Paper October 2005". *Surgical Endoscopy, ISSN 0930-2794*, Vol. 20, No. 2, pp. 329–333, February 2006.

[Ratt 06c] D. Rattner and A. Kalloo. "ASGE/SAGES Working Group on Natural Orifice Translumenal Endoscopic Surgery: White Paper October 2005". *Gastrointestinal Endoscopy, ISSN 0016-5107*, Vol. 63, No. 2, pp. 199–203, February 2006.

[Redd 07] N. Reddy and G. V. Rao. "Transgastric approach to the peritoneal cavity: Are we on the right track?". *Gastrointestinal Endoscopy, ISSN 0016-5107*, Vol. 65, No. 3, pp. 501–502, March 2007.

[Rich 05] W. O. Richards and D. W. Rattner. "Endoluminal and transluminal surgery - No longer if, but when". *Surgical Endoscopy, ISSN 0930-2794*, Vol. 19, No. 4, pp. 461–463, April 2005.

[Ritt 07a] P. Ritt. "Vermessung und Optimierung einer PMD-Kamera für den Einsatz in der minimal-invasiven Chirurgie". Diploma thesis, Pattern Recognition Lab, FAU Erlangen-Nuremberg, November 2007.

[Ritt 07b] P. Ritt, K. Höller, J. Penne, A. Schneider, J. Hornegger, and H. Feußner. "Auto-gain approach for use with Time-of-Flight examination in Minimally Invasive Surgery". In: J. Hornegger, E. W. Mayr, S. Schookin, H. Feußner, N. Navab, Y. V. Gulyaev, K. Höller, and V. Ganzha, Eds., *Proc. 3rd Russian-Bavarian Conference on Bio-Medical Engineering (RBC'07), ISBN 3-921713-33-1*, pp. 227–232, Erlangen, Germany, July 2007.

[Rola 07] C. Rolanda, E. Lima, J. M. Pego, T. Henriques-Coelho, D. Silva, I. Moreira, G. Macedo, J. L. Carvalho, and J. Correia-Pinto. “Third-generation cholecystectomy by natural orifices: transgastric and transvesical combined approach (with video)”. *Gastrointestinal Endoscopy, ISSN 0016-5107*, Vol. 65, No. 1, pp. 111–117, January 2007.

[Ryou 07a] M. Ryou, D. G. Fong, R. D. Pai, A. Tavakkolizadeh, D. W. Rattner, and C. C. Thompson. “Dual-port distal pancreatectomy using a prototype endoscope and endoscopic stapler: a natural orifice transluminal endoscopic surgery (NOTES) survival study in a porcine model”. *Endoscopy, ISSN 0013-726X*, Vol. 39, No. 10, pp. 881–887, October 2007.

[Ryou 07b] M. Ryou, R. Pai, J. Sauer, D. Rattner, and C. Thompson. “Evaluating an optimal gastric closure method for transgastric surgery”. *Surgical Endoscopy, ISSN 0930-2794*, Vol. 21, No. 4, pp. 677–680, April 2007.

[Sano 81] R. A. Sanowski, R. A. Kozarek, and E. K. Partyka. “Evaluation of a flexible endoscope for laparoscopy [abstract]”. *The American Journal of Gastroenterology, ISSN 0002-9270*, Vol. 76, No. 5, pp. 416–419, November 1981.

[Sata 93] R. M. Satava. “3-D vision technology applied to advanced minimally invasive surgery systems”. *Surgical Endoscopy, ISSN 0930-2794*, Vol. 7, pp. 429–431, 1993.

[Scha 05] N. J. Schara, H. D. Hoeg, and E. L. Hale. “Gravity referenced endoscopic image orientation”. United States Patent US 20050154260 A1, July 2005.

[Scha 06] N. J. Schara, H. D. Hoeg, and E. L. Hale. “Gravity referenced endoscopic image orientation”. United States Patent US 7134992 B2, November 2006.

[Scha 08] C. Schaller, J. Penne, and J. Hornegger. “Time-of-Flight sensor for respiratory motion gating”. *Medical Physics, ISSN 0094-2405*, Vol. 35, No. 7, pp. 3090–3093, July 2008.

[Scha 09] C. Schaller, A. Adelt, J. Penne, and J. Hornegger. “Time-of-Flight sensor for patient positioning”. In: M. I. Miga and K. H. Wong, Eds., *Proc. Medical Imaging 2009: Visualization, Image-Guided Procedures, and Modeling (SPIE’09), ISBN 978-081-9475-12-1*, pp. 726110.1–726110.8, Lake Buena Vista, FL, USA, February 2009.

[Schr 08] T. Schrauder. “Entwicklung einer Treiberschaltung fi£¡r schnell modulierte Leistungslaserdioden zur Optimierung von Lichtlaufzeit-Kameras”. Term paper, Chair for Microwave Engineering and High Frequency Technology, FAU Erlangen-Nuremberg, December 2008.

[Schw 99] R. Schwarte, H. Heinol, B. Buxbaum, T. Ringbeck, Z. Xu, and K. Hartmann. *Handbook of Computer Vision and Applications*, Chap. Principles of three dimensional imaging techniques. Vol. 1, The Academic Press, 1999.

[Scla 06] G. M. Sclabas, P. Swain, and L. L. Swanstrom. “Endoluminal methods for gastrotomy closure in Natural Orifice TransEnteric Surgery (NOTES)”. *Surgical Innovation, ISSN 1553-3506*, Vol. 13, No. 1, pp. 23–30, March 2006.

[Scot 07a] D. Scott, S.-j. Tang, R. Fernandez, R. Bergs, M. Goova, I. Zeltser, F. Kehdy, and J. Cadeddu. "Completely transvaginal NOTES cholecystectomy using magnetically anchored instruments". *Surgical Endoscopy, ISSN 0930-2794*, Vol. 21, No. 12, pp. 2308–2316, December 2007.

[Scot 07b] D. J. Scott, S.-J. Tang, M. T. Goova, R. Bergs, D. C. Hogg, F. J. Kehdy, J. A. Cadeddu, and R. Fernandez. "Short-term survival outcomes following transvaginal NOTES cholecystectomy using magnetically anchored instruments". *Gastrointestinal Endoscopy, ISSN 0016-5107*, Vol. 65, No. 5, p. 566, April 2007.

[Seif 00] H. Seifert, T. Wehrmann, T. Schmitt, S. Zeuzem, and W. F. Caspary. "Retroperitoneal endoscopic debridement for infected peripancreatic necrosis". *The Lancet, ISSN 0140-6736*, Vol. 356, No. 9230, pp. 653–5, August 2000.

[Semm 83a] K. Semm. "Endoscopic apendectomy". *Endoscopy, ISSN 0013-726X*, Vol. 15, No. 2, pp. 59–64, March 1983.

[Semm 83b] K. Semm. "Endoscopic intraabdominal surgery in gynecology". *Wiener klinische Wochenschrift, ISSN 0043-5325*, Vol. 95, No. 11, pp. 353–67, May 1983.

[Sepp 07] Y. Seppenwoolde, R. Berbeco, S. Nishioka, and B. Heijmen. "Accuracy of tumor motion compensation algorithm from a robotic respiratory tracking system: a simulation study". *Medical Physics, ISSN 0094-2405*, Vol. 34, No. 7, pp. 2774–2784, July 2007.

[Shah 02] J. Shah. "Endoscopy through the ages". *British Journal of Urology International, ISSN 2042-2997*, Vol. 89, No. 7, pp. 645–652, May 2002.

[Shib 02] T. Shibata. "Head mounted display". *Displays, ISSN 0141-9382*, Vol. 23, No. 1-2, pp. 57–64, April 2002.

[Shih 07] S. P. Shih, S. V. Kantsevoy, A. N. Kalloo, P. Magno, S. A. Giday, C.-W. Ko, N. V. Isakovich, O. Meireles, E. J. Hanly, and M. R. Marohn. "Hybrid minimally invasive surgery - a bridge between laparoscopic and translumenal surgery". *Surgical Endoscopy, ISSN 0930-2794*, Vol. 21, No. 8, pp. 1450–1453, August 2007.

[Sole 08] L. Soler, S. Nicolau, J. B. Fasquel, V. Agnus, A. Charnoz, A. Hostettler, J. Moreau, C. Forest, D. Mutter, and J. Marescaux. "Virtual reality and augmented reality applied to laparoscopic and notes procedures". In: *Proc. 5th International Symposium on Biomedical Imaging: From Nano to Macro (ISBI'08)*, pp. 1399–1402, IEEE Computer Society, Paris, France, May 2008.

[STM 08a] *STM AIS326DQ MEMS inertial sensor 3-axis, low g accelerometer with digital output.* STMicroelectronics, 2008.

[STM 08b] *STM LIS331DL MEMS motion sensor 3-axis smart digital output nano accelerometer.* STMicroelectronics, 2008.

[STM 09] *STM LIS331DLH MEMS digital output motion sensor ultra low-power high performance 3-axes nano accelerometer.* STMicroelectronics, 2009.

[Stoy 05] D. Stoyanov, A. Darzi, and G.-Z. Yang. "A practical approach towards accurate dense 3D depth recovery for robotic laparoscopic surgery.". *Computer Aided Surgery, ISSN 1092-9088*, Vol. 4, No. 10, June 2005.

[Stoy 08] D. Stoyanov, G. P. Mylonas, M. Lerotic, A. J. Chung, and G.-Z. Yang. "Intra-operative visualizations: perceptual fidelity and human factors". *Journal of Display Technology, ISSN 1551-319X*, Vol. 4, No. 4, pp. 491–501, December 2008.

[Swai 07a] C. P. Swain. "A justification for NOTES - Natural Orifice Translumenal EndoSurgery". *Gastrointestinal Endoscopy, ISSN 0016-5107*, Vol. 65, No. 3, pp. 514–516, March 2007.

[Swai 07b] P. Swain and L. L. Swanstrom. "The development and testing of a new platform for endoscopic surgery featuring off axis visualization". *Gastrointestinal Endoscopy, ISSN 0016-5107*, Vol. 65, No. 5, p. AB291, April 2007.

[Swan 05] L. L. Swanstrom, R. Kozarek, P. J. Pasricha, S. Gross, D. Birkett, P.-O. Park, V. Saadat, R. Ewers, and P. Swain. "Development of a new access device for transgastric surgery". *Journal of Gastrointestinal Surgery, ISSN 1091-255X*, Vol. 9, No. 8, pp. 1129–1136, November 2005.

[Swan 08] L. L. Swanstrom, Y. Khajanchee, and M. A. Abbas. "Natural Orifice Transluminal Endoscopic Surgery: the future of gastrointestinal surgery". *The Permanente Journal, ISSN 1552-5767*, Vol. 12, No. 2, pp. 42–47, spring 2008.

[Swan 09] L. L. Swanstrom, E. Volckmann, E. Hungness, and N. J. Soper. "Patient attitudes and expectations regarding natural orifice translumenal endoscopic surgery". *Surgical Endoscopy, ISSN 0930-2794*, Vol. 23, No. 7, pp. 1519–1525, July 2009.

[Tack 08] D. Tacke. "Ankopplung einer optischen Lichtlaufzeit-Kamera an ein Endoskop zur Aufnahme dreidimensionaler Oberflächenbilder". Diploma thesis, Chair for Microwave Engineering and High Frequency Technology, FAU Erlangen-Nuremberg, March 2008.

[Tang 08] S.-J. Tang, R. Bergs, S. F. Jazrawi, C. O. Olukoga, J. Caddedu, R. Fernandez, and D. J. Scott. "Live video manipulator for endoscopy and NOTES". *Gastrointestinal Endoscopy, ISSN 0016-5107*, Vol. 68, No. 3, pp. 559–564, September 2008.

[Tart 06] S. Tarte, J. McClelland, S. Hughes, J. Blackall, D. Landau, and D. Hawkes. "A non-contact method for the acquisition of breathing signals that enable distinction between abdominal and thoracic breathing". *Radiotherapy & Oncology, ISSN 0167-8140*, Vol. 81, No. 1, p. S209, October 2006.

[Thor 01] T. Thormählen, H. Broszio, and P. N. Meier. "Three-dimensional endoscopy". In: *Proc. Falk Symposium No. 124, Medical Imaging in Gastroenterology and Hepatology, ISBN 0-7923-8774-0*, pp. 199–211, Hannover, Germany, September 2001.

[Titt 04] D. Titterton and J. Weston. *Strapdown inertial navigation technology*. IEE Radar, Sonar, Navigation and Avionics, Stevenage, UK, 2nd Ed., 2004.

[Toma 98] C. Tomasi and R. Manduchi. "Bilateral filtering for gray and color images". In: *Proc. 6th International Conference on Computer Vision (ICCV'98), ISBN 81-7319-221-9*, pp. 839–846, IEEE Computer Society, Bombay, India, January 1998.

[Tsai 87] R. Y. Tsai. "A versatile camera calibration technique for high-accuracy 3-D machine vision metrology using off-the-shelf TV Cameras and Lenses". Vol. Ra-3(3), No. 4, pp. 323–344, August 1987.

[Voer 07] R. P. Voermans, M. I. van Berge Henegouwen, and P. Fockens. "Natural Orifice Transluminal Endoscopic Surgery (NOTES)". *Endoscopy, ISSN 0013-726X*, Vol. 39, No. 11, pp. 1013–1017, November 2007.

[Vogt 04] F. Vogt, S. Krüger, T. Zinsser, T. Maier, H. Niemann, W. Hohenberger, and C. H. Schick. "Fusion von Lichtfeldern und CT-Daten für minimal-invasive Operationen". In: T. Tolxdorff, J. Braun, H. Handels, A. Horsch, and H.-P. Meinzer, Eds., *Proc. 8th. Workshop Bildverarbeitung für die Medizin (BVM'04), ISBN 3-540-21059-8*, pp. 309–313, Berlin, Germany, March 2004.

[Vogt 05a] F. Vogt, S. Krüger, H. Niemann, W. Hohenberger, G. Greiner, and C. Schick. "Erweiterte Realität und 3-D Visualisierung für minimal-invasive Operationen durch Einsatz eines optischen Trackingsystems". In: H.-P. Meinzer, H. Handels, A. Horsch, and T. Tolxdorff, Eds., *Proc. 9th. Workshop Bildverarbeitung für die Medizin (BVM'05), ISBN 3-540-25052-2*, pp. 217–221, Heidelberg, Germany, March 2005.

[Vogt 05b] F. Vogt. *Augmented light field visualization and real-time image enhancement for computer assisted endoscopic surgery.* PhD thesis, Friedrich-Alexander-University Erlangen-Nuremberg, 2005.

[Volb 96] S. Volbracht, K. Shahrbabaki, G. Domik, and G. Fels. "Perspective viewing, anaglyph stereo or shutter glass stereo?". In: *Proc. Symposium on Visual Languages (VL'96), ISBN 0-8186-7508-X*, pp. 192–193, IEEE Computer Society, Boulder, CO, USA, September 1996.

[Vosb 07] K. G. Vosburgh and R. San Jose Estepar. "Natural Orifice Transluminal Endoscopic Surgery (NOTES): an opportunity for augmented reality guidance". *Studies in Health Technology and Informatics, ISSN 0926-9630*, Vol. 125, pp. 485–490, January 2007.

[Wagh 05] M. S. Wagh, B. F. Merrifield, and C. C. Thompson. "Endoscopic transgastric abdominal exploration and organ resection: initial experience in a porcine model". *Clinical Gastroenterology and Hepatology, ISSN 1542-3565*, Vol. 3, No. 9, pp. 892–896, September 2005.

[Wagh 06] M. S. Wagh, B. F. Merrifield, and C. C. Thompson. "Survival studies after endoscopic transgastric oophorectomy and tubectomy in a porcine model". *Gastrointestinal Endoscopy, ISSN 0016-5107*, Vol. 63, No. 3, pp. 473–478, March 2006.

[Wall 06] M. B. Wallace. "Take NOTES (Natural Orifice Transluminal Endoscopic Surgery)". *Gastroenterology, ISSN 0016-5085*, Vol. 131, No. 1, p. 39489, July 2006.

[Welc 02] G. Welch and E. Foxlin. "Motion tracking: no silver bullet, but a respectable arsenal". *IEEE computer graphics and applications, ISSN 0272-1716*, Vol. 22, No. 6, pp. 24–38, November 2002.

[Wenz 94] R. Wenzl, R. Lehner, N. Pateisky, P. Sevelda, P. Husslein, and U. Vry. "Three-dimensional video-endoscopy: clinical use in gynaecological laparoscopy". *The Lancet, ISSN 0140-6736*, Vol. 344, No. 8937, pp. 1621–1622, December 1994.

[West 04] J. B. West and C. R. Maurer, Jr. "Designing optically tracked instruments for image-guided surgery". *IEEE Transactions on Medical Imaging, ISSN 0278-0062*, Vol. 23, No. 5, pp. 533–545, May 2004.

[Wiit 08] B. E. Wiita and G. D. Witta. "Apparatus and method for stabilizing an image from an endoscopic camera". United States Patent US 20080108870 A1, May 2008.

[Wilh 07] D. Wilhelm, A. Meining, S. von Delius, A. Fiolka, S. Can, C. Hann von Weyhern, A. Schneider, and H. Feußner. "An innovative, safe and sterile sigmoid access (ISSA) for NOTES". *Endoscopy, ISSN 0013-726X*, Vol. 39, No. 5, pp. 401–406, May 2007.

[Wilh 08] D. Wilhelm, S. von Delius, M. Burian, A. Schneider, E. Frimberger, A. Meining, and H. Feußner. "Simultaneous use of laparoscopy and endoscopy for minimally invasive resection of gastric subepithelial masses - analysis of 93 interventions". *World Journal of Surgery, ISSN 0364-2313*, Vol. 32, No. 6, pp. 1021–1028, June 2008.

[Witt 06] T. Wittenberg, C. Winter, I. Scholz, S. Rupp, K. Bumm, M. Stamminger, and C. Nimsky. "3-D reconstruction of the sphenoidal sinus from monocular endoscopic views: first results". In: *Proc's Jahrestagung Biomedizinische Technik 2006 (BMT'06), ISSN 0939-4990*, Zürich, Switzerland, September 2006.

[Yang 09] G.-Z. Yang, D. J. Hawkes, D. Rueckert, J. A. Noble, and C. J. Taylor, Eds. *Medical Image Computing and Computer-Assisted Intervention - MICCAI 2009, 12th International Conference, London, UK, September 20-24, 2009, Proceedings, Part I*, London, UK, September 2009.

[Yeun 99] S. Y. Yeung, H. T. Tsui, and A. Yim. "Global Shape from Shading for an Endoscope Image". In: C. J. Taylor and A. C. F. Colchester, Eds., *Proc. 2nd International Conference on Medical Image Computing and Computer-Assisted Intervention (MICCAI'99), ISBN 3-540-66503-X*, Cambridge, UK, September 1999.

[Zhou 10] H. Zhou, J. Zhang, Q. Wang, and Z. Hu. "Transvaginal Natural Orifice Transluminal Endoscopic Surgery cholecystectomy: is it the best route?". *Annals of Surgery, ISSN 0003-4932*, Vol. 251, No. 3, pp. 578–579, March 2010.

[Zorr 08] R. Zorron, L. C. Maggioni, L. Pombo, A. L. Oliveira, G. L. Carvalho, and M. Filgueiras. "NOTES transvaginal cholecystectomy: preliminary clinical application". *Surgical Endoscopy, ISSN 0930-2794*, Vol. 22, No. 2, pp. 542–547, February 2008.

Kurt Höller
studied Electrical Engineering at the
Friedrich-Alexander-University Erlangen-Nürnberg
with a diploma thesis on inertial sensors for navigation
at the Fraunhofer Institute of Integrated Circuits IIS.

From 2005 to 2009, he was working on his dissertation
in Computer Science at the Pattern Recognition Lab LME
in Erlangen and the Research Group for Minimally invasive
Interdisciplinary Therapeutical Interventions MITI at
the TU München.

Since 2009, Kurt Höller is managing director of the
Central Institute of Healthcare Engineering ZiMT
at the FAU Erlangen-Nürnberg.